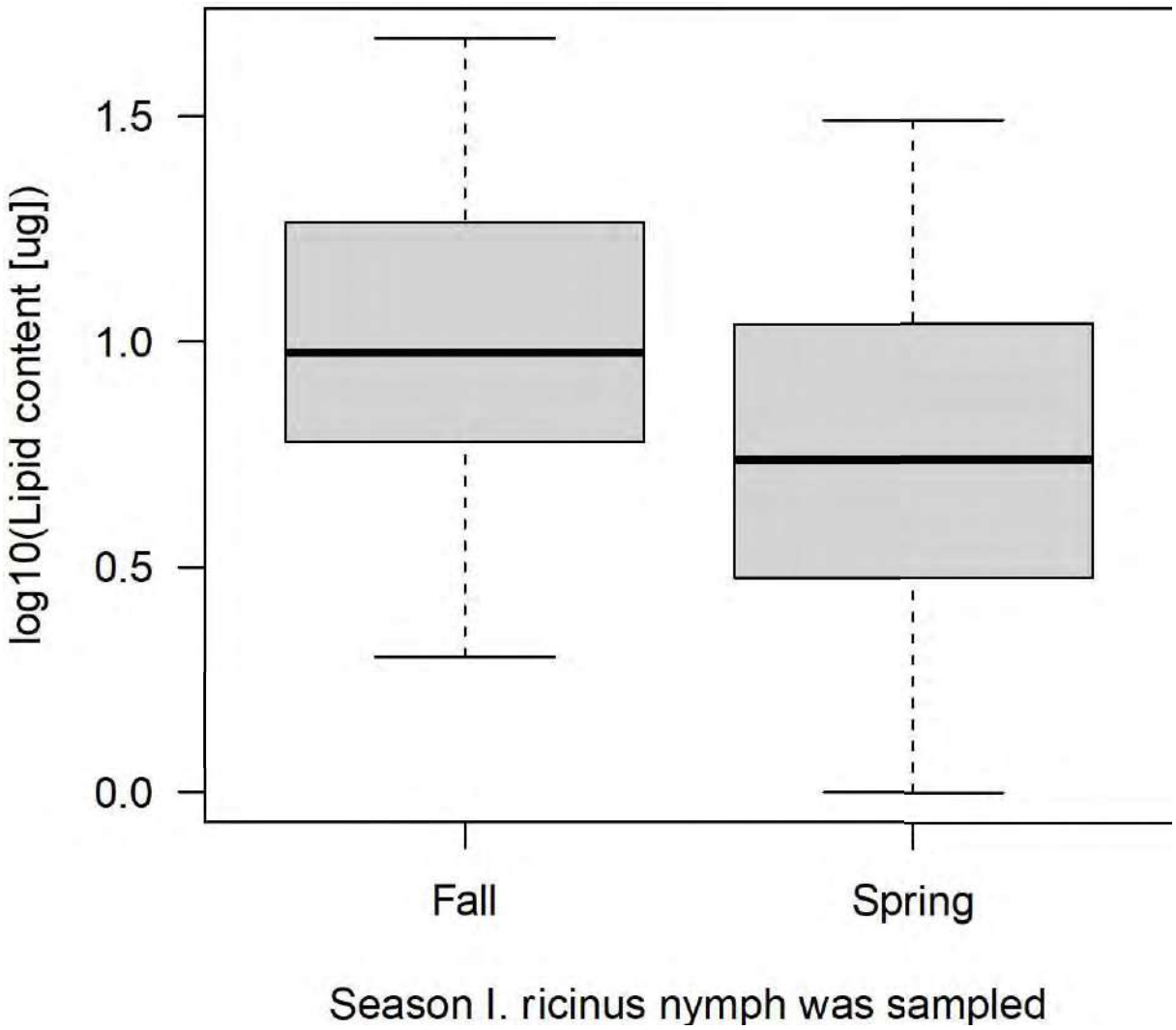

Figure 9. *I. ricinus* nymphs collected in the fall have a higher fat content compared to nymphs collected in the spring of the same calendar year. This result suggests that the fall nymphs are younger than the spring nymphs. The boxplot shows the medians (black line), the 25th and 75th percentiles (edges of the box), and the minimum and maximum values (whiskers).

7 Chapter 4

Experimental infections of mice and birds with *Borrelia afzelii* and *Borrelia garinii*

Cindy Bregnard[1*], Olivier Rais[2], Anouk Sarr[3], Kees van Oers[4], Peter Kraiczy[5], Ryan Rego[7], and Maarten J. Voordouw[1, 7]

[1] Laboratory of Ecology and Evolution of Parasites, Institute of Biology, University of Neuchâtel, Neuchâtel, Switzerland

[2] Laboratory of Ecology and Epidemiology of Parasites, Institute of Biology, University of Neuchâtel, Neuchâtel, Switzerland

[3] INVENesis LLC, Chemin de Belleroche 14, 2000 Neuchâtel, Switzerland

[4] Department of Animal Ecology, Netherlands Institute of Ecology (NIOO-KNAW), Wageningen, Netherlands

[5] Institute of Medical Microbiology and Infection Control, University Hospital of Frankfurt, Goethe University, Frankfurt, Germany

[6] Biology Centre, Institute of Parasitology, Czech Academy of Sciences, České Budějovice, Czechia

[7] Department of Veterinary Microbiology, Western College of Veterinary Medicine, University of Saskatchewan, Saskatoon, Canada

Experimental infections of mice and birds with *Borrelia afzelii* and *Borrelia garinii*.

Authors: Cindy Bregnard[1*], Olivier Rais[2], Anouk Sarr[3], Kees van Oers[4], Peter Kraiczy[5], Ryan Rego[7], and Maarten J. Voordouw[1, 7]

[1] Laboratory of Ecology and Evolution of Parasites, Institute of Biology, University of Neuchâtel, Neuchâtel, Switzerland

[2] Laboratory of Ecology and Epidemiology of Parasites, Institute of Biology, University of Neuchâtel, Neuchâtel, Switzerland

[3] INVENesis LLC, Chemin de Belleroche 14, 2000 Neuchâtel, Switzerland

[4] Department of Animal Ecology, Netherlands Institute of Ecology (NIOO-KNAW), Wageningen, Netherlands

[5] Institute of Medical Microbiology and Infection Control, University Hospital of Frankfurt, Goethe University, Frankfurt, Germany

[6] Biology Centre, Institute of Parasitology, Czech Academy of Sciences, České Budějovice, Czechia

[7] Department of Veterinary Microbiology, Western College of Veterinary Medicine, University of Saskatchewan, Saskatoon, Canada

ABSTRACT

Background: Tick-borne spirochete bacteria of the *Borrelia* burgdorferi sensu lato (sl) genospecies complex cause Lyme disease in humans. Several studies observed specific associations between *Borrelia* genospecies and vertebrate hosts. In Europe, *B. afzelii* and *B. garinii* use the same tick vector, *Ixodes ricinus*, but cycle in different hosts: rodents and birds, respectively. In vitro studies suggest that this host-specificity is mediated by the vertebrate complement system.

Methods: We used an experimental infection approach that includes combinations of *B. burgdorferi* sl genospecies and rodent and avian reservoir hosts to test the host-specificity hypothesis. Laboratory mice, canary finches, and great tits were infected via needle inoculation with different strains of *B. afzelii* and *B. garinii* to create *B. garinii*-infected nymphs. At 30 days post-infection, animals were infested with pathogen-free larval *I. ricinus* ticks to test if experimentally infected hosts with the wrong *Borrelia* genospecies can transmit viable spirochetes to larval *I. ricinus* ticks. The subsequent engorged larvae were allowed to moult into nymphs which were then tested for the spirochete load and viability using qPCR and culture.

Results: We found that 5 of the 48 animals that we exposed to *B. burgdorferi* sl exhibited a proper establishment of chronic infection, which led to the subsequent *B. burgdorferi* sl larvae – nymph transstadial transmission. Of the 5 mice, one was unexpectedly infected by the bird-associated genospecies, *B. garinii*. Surprisingly, none of the 28 birds exhibited any signs of infection.

Conclusion: Despite the existence of data supporting the complement-mediated host specificity hypothesis, there might be some permeability in the host barrier provided by the host complement system.

KEYWORDS: Host-specificity, *Borrelia afzelii*, *Borrelia garinii*, *Ixodes ricinus*, complement system, bird, rodent, experimental infection

INTRODUCTION

Lyme borreliosis is the most common vector-borne disease in the northern hemisphere [1, 2]. The causative agents of Lyme borreliosis are tick-borne spirochete bacteria that belong to the *Borrelia burgdorferi* sensu lato (sl) complex, which comprises 19 genospecies [3, 4]. The three genospecies responsible for most human cases of Lyme borreliosis are *Borrelia burgdorferi* sensu stricto (ss), *B. afzelii*, and *B. garinii* [5-7]. In Europe, *B. afzelii* and *B. garinii* use the same tick vector, the sheep tick (*Ixodes ricinus*), but cycle in different vertebrate hosts; *B. afzelii* is adapted to small mammals (e.g., rodents and insectivores), whereas *B. garinii* is adapted to birds [8-10].

Early evidence for the host specificity of these two genospecies came from field studies where ticks sampled from rodent hosts were consistently infected with *B. afzelii* [11-15] whereas ticks sampled from avian hosts were consistently infected with *B. garinii* and also *B. valaisiana* [16-20]. Controlled studies demonstrated that rodent hosts could be chronically infected with *B. afzelii* and transmit this pathogen to feeding *I. ricinus* ticks [14, 21-23]. Conversely, that avian hosts could be chronically infected with *B. garinii* and transmit this pathogen back to feeding *I. ricinus* ticks [24-26]. The observation that *B. afzelii* and *B. garinii* are often sympatric, but that co-infections in *I. ricinus* ticks are relatively rare was interpreted as further evidence that these two genospecies circulate in separate populations of vertebrate hosts[27-29].

One possible mechanism underlying the host-specificity of the *B. burgdorferi* sl genospecies is the vertebrate complement system [8, 30]. The complement system is part of the innate immune system of vertebrate hosts that consists of more than 30 components that circulate in the blood. Upon activation, these components trigger a biochemical cascade that eventually produce a membrane attack complex that punctures the cell wall of bacterial pathogens [8, 31-33]. The complement-mediated lysis of a particular *B. burgdorferi* sl genospecies have been shown to depend on its resistance and/or sensitivity to the blood serum complement of a given vertebrate host [30, 32, 34, 35]. For example, *B. afzelii* was found to be sensitive to bird complement but resistant to rodent complement, which makes rodents appropriate hosts for this genospecies [30]. In additions, rodent complement resistance of *B. afzelii* mirrors the high transmission success of this genospecies by different species of rodents [13, 36, 37] In contrast, *B. garinii* was sensitive to rodent complement but resistant to bird complement, which makes birds appropriate hosts for this genospecies [30]. Again, high transmission competence of *B. garinii* by birds parallels the bird complement resistance of this genospecies [25].

The aim of this study was to better understand the host-specificity using an experimental infection approach that includes different combinations of *B. burgdorferi* sl genospecies and rodent and avian reservoir hosts. The purpose of the present study was to create *I. ricinus* nymphs that were infected with different strains of *B. afzelii* or *B. garinii*. The best method to create such nymphs is to culture the strains of interests in BSK-H medium and needle-inoculate a dose of spirochetes into appropriate vertebrate hosts. Once the infection has developed inside the host, the host is infested with *I. ricinus* larvae which acquire the *B. burgdorferi* sl pathogens during their larval blood meal. The engorged larvae moult into nymphs, which are tested for their *B. burgdorferi* sl infection status. In the present study, we needle-inoculated laboratory mice (*Mus musculus*) and canary finches (*Serina canaria*) with different strains of *B. afzelii* and *B. garinii* and we also inoculated great tits (*Parus major*) with different strains of *B. garinii*. All vertebrate hosts were subsequently infested with *I. ricinus* larvae, and the engorged larvae were allowed to moult into nymphs. With respect to *B. afzelii*, our predictions were that *B. afzelii* strains would establish infection in mice but not in birds and that only mice would transmit *B. afzelii* to immature *I. ricinus* ticks. Conversely, with respect to *B. garinii*, our predictions were that *B. garinii* strains would establish infection in birds but not in mice and that only birds would transmit *B. garinii* to immature *I. ricinus* ticks.

METHODS

Vertebrate hosts and *I. ricinus* ticks

Four-week-old, pathogen-free, female BALB/c mice (*Mus musculus*) were purchased from Envigo (Horst, Netherlands). One-year-old, pathogen-free, male canaries (*Serinus canaria* forma domestica) were purchased from a pet shop (Oisellerie de la Tour, Switzerland). Two-year-old, pathogen-free, male and female great tits (*Parus major*) were obtained from a laboratory colony at the Netherlands Institute of Ecology (NIOO-KNAW). All animals were kept in cages at the animal care facility of the University of Neuchâtel under controlled temperature (20 °C) and light conditions (12 h light from 6:00 to 18:00 and 12 h dark from 18:00 to 6:00). Animals were allowed to adjust to their surroundings for 10–23 days before the start of the study (mice: 10 days; canaries: 14 days; great tits: 23 days). All animals were given food and water *ad libitum*. Animals were initially housed in groups (mice: 4–5; canaries: 5–6; great tits: 1), but were housed individually after infection to avoid any direct pathogen transmission between animals. Animals were euthanized at 50–65 days after entering the animal care facility (mice: 50 days; canaries: 54 days; great tits: 65 days). *Ixodes ricinus* ticks were

obtained from our pathogen-free, laboratory colony that has been maintained for over 33 years at the Institute of Biology, University of Neuchâtel.

The commission that is part of the 'Service de la Consommation et des Affaires Vétérinaires (SCAV)' of Canton Vaud, Switzerland evaluated and approved the ethics of this study. The Veterinary Service of the Canton of Neuchâtel, Switzerland issued the animal experimentation permit used in this study (NE05a-2016).

Isolates of *Borrelia afzelii and Borrelia garinii*

Isolates of *B. afzelii* (n = 8) and *B. garinii* (n = 10) were selected from the collection of *B. burgdorferi* sl isolates at the University of Neuchâtel. Most of these isolates (17/18) had been cultured from *I. ricinus* ticks, one isolate was cultured from a bank vole (Table 1). We had previously used 454-sequencing of the *ospC* gene to determine whether these isolates were clonal or consisted of multiple strains [38]. Isolates were selected based on the following criteria: they contained a single *ospC* major group allele (oMG) and they had vigorous growth in BSK-H medium. All isolates were genotyped with respect to their multi-locus sequence type (MLST) and their oMG, and are thus hereafter referred to as strains. The genotype and origin of these strains are shown in Table 1.

The 8 *B. afzelii* strains used in this study include: NE1857, NE1827, NE4556, NE4049, NE4832, NE4558, NE4779, and Fin-Jyv-A3. The 10 *B. garinii* strains used in this study include: NE5135, NE4554, NE1845, NE4891, NE1883, NE5245, NE1879, NE5158, NE4907, and NE5308. We had recently used *B. afzelii* strains NE4049 and Fin-Jyv-A3 in experimental infections with BALB/c mice [39, 40]. To our knowledge, the other 16 strains had not been used in any experimental infection studies.

Study design

The experimental infections of the vertebrate hosts were conducted in two temporal blocks. In May 2016, each of 10 mice and 10 canaries were experimentally infected with one of the 8 *B. afzelii* strains (strains NE1857 and NE4049 were duplicated). In September 2016, each of 10 mice and 10 canaries were experimentally infected with one of the 10 *B. garinii* strains. As we were not sure that canaries were a competent host for *B. garinii*, we also infected each of 8 great tits with one of the 8 *B. garinii* strains (strains NE5245 and NE1879 were excluded). A total of 48 animals were experimentally infected in this study: 20 mice, 20 canaries, and 8 great tits. Animals were infected via subcutaneous inoculation with ~3 million spirochetes (n = 20 cultures, geometric mean = 2.98×10^6, CI = 2.06×10^6–4.31×10^6) suspended in 100 µl of BSK-H

medium (see Additional file 1). For each temporal block, 1 mouse and 1 canary were used as negative controls and were inoculated with 100 µl of BSK-H medium. Thus, a total of 52 animals were used in this study: 48 experimentally infected and 4 negative controls. At 14 days and 28 days post-infection (PI), each host was infested with ~100 pathogen-free larval ticks from multiple adult tick females our laboratory colony of *I. ricinus* using previously described infestation protocols [22, 37, 41]. At 42 days PI, great tits were infested for a third time with 100 pathogen-free larvae. Blood-engorged larvae were placed in individual Eppendorf tubes and allowed to moult into nymphs. The Eppendorf tubes (containing the ticks) were kept in a sealed Tupperware container that contained a layer of water to ensure high humidity. The Tupperware containers were stored under the same temperature and light conditions as the animals. Between 40–42 days PI, each host was euthanized, exsanguinated, dissected, and frozen at –20 °C for future analysis.

Body mass of vertebrate hosts

To test whether vertebrate hosts experienced fluctuations in body mass during the experimental infection and tick infestation, we weighed the host body mass over the course of the study. For block 1, we weighed the hosts on days 0, 14, and 28 PI, and on the date of euthanasia (22 hosts x 4 measurements per host = 88 measurements). For block 2, we weighed the hosts on days 0, 7, 14, 21, 28, 35, 42, 49 PI (day 49 PI was for great tits only), and on the date of euthanasia (30 hosts x 4, 7, or 8 measurements per host = 212 measurements).

Body mass of immature *I. ricinus* ticks

To test whether there was an effect of host species on the body mass of immature *I. ricinus* ticks, we weighed a subset of blood-engorged larvae and unfed nymphs at 4 weeks after the larva-to-nymph moult using a Mettler M3 microbalance. For block 1, we weighed 5 unfed 4-week-old nymphs for each combination of animal and infestation (22 hosts x 2 infestations per host x 5 nymphs per infestation = 220 nymphs). For block 2, we weighed 10 engorged larvae for each combination of animal and infestation (30 hosts x 2 infestations per host x 10 engorged larvae per infestation = 600 engorged larvae) and 5 unfed 4-week-old nymphs for each combination of animal and infestation (30 hosts x 2 infestations per host x 5 nymphs per infestation = 300 nymphs). The immature ticks were subsequently frozen at –20 °C until DNA extraction.

Molecular analysis

***DNA extractions of the host organs*:** We collected 9 organs from each mouse including the ear, bladder, brain, spleen, liver, skin, kidney, heart, and joint. We collected 7 organs from each bird including the brain, spleen, liver, skin, kidney, heart, and joint. A total of 408 organs were collected for a total of 52 hosts; 198 organs from 22 mice, 154 organs from 22 canaries, and 56 organs from 8 great tits. Each host organ was cut into two halves; one half was used to detect *B. burgdorferi* sl using qPCR, and the other half was used to detect *B. burgdorferi* sl using culture (see below). We obtained 20–25 mg of tissue for each organ, except the spleen for which we obtained 10 mg. The total DNA was extracted using the DNeasy 96 Blood & Tissue Kit (QIAGEN, # 69582) according to the manufacturer's instructions. The DNA of each sample was eluted in 100 µl of deionized autoclaved water, the DNA concentration was measured using a Nanodrop 2000 (Thermo Fisher), and the DNA extraction was frozen at –20 °C until qPCR.

***DNA extractions of the xenodiagnostic I. ricinus ticks*:** For each host, 10 xenodiagnostic unfed 4-week-old *I. ricinus* nymphs (5 nymphs per infestation) were tested for infection with *B. burgdorferi* sl and to estimate the host-to-tick transmission. The nymphs were homogenized following a previously described protocol [22]. Briefly, ticks were placed in a 5 µl droplet of deionized water at the bottom of a cryovial with a 1.4 mm bead before being crushed twice at 30 Hz for 45 seconds, using a TissueLyser Adapter Set 2 x 24 (QIAGEN®). The total DNA was extracted using the DNeasy 96 Blood & Tissue Kit (QIAGEN, # 69582) according to the manufacturer's instructions. The DNA of each sample was eluted in 65 µl of deionized autoclaved water, the DNA concentration was measured using a Nanodrop 2000 (Thermo Fisher), and the DNA extraction was frozen at –20 °C until qPCR.

***Quantitative PCR to detect B. burgdorferi sl*:** A quantitative PCR (qPCR) amplifying a 132-base pair fragment of the *flagellin* gene was used to detect *B. burgdorferi* sl following a previously described protocol [22, 42]. Each qPCR reaction had a total reaction volume of 20 µL and contained 10 µL of Master Mix Vial (FastStart Essential DNA Probes Master, Roche Applied Science), 0.4 µM of Primer FlaF1, 0.4 µM of Primer FlaR1, 0.2 µM of Flaprobe 1, and 3 µL of template for each host organ or 5 µL of template for each tick. The thermocycling conditions were as follows: a preincubation step at 95 °C for 10 min followed by 50 cycles at 95 °C for 10 sec, 60 °C for 30 sec, and 37 °C for 30 sec, before a final elongation step at 72 °C for 10 min. The qPCR was performed using a LightCycler® 96 Real-Time PCR System (Roche Applied Science). Each 96-well plate contained 6 negative controls and 6 positive controls. We

used a previously established standard curve to transform the Cq values into spirochete loads. To determine the repeatability of the sample Cq values, we repeated the qPCR for 22 DNA extractions (in two different plates). The repeatability of the Cq values was 99.8%, which is very high ($F_{22, 21} = 1833$, $p < 0.001$).

Detection of antibodies against B. burgdorferi sl: A blood sample was taken from each host at day 0 PI and at the date of euthanasia to test whether it had developed antibodies against *B. burgdorferi* sl. A total of 104 serum samples were screened using an enzyme-linked immunosorbent assay (ELISA). For the mice, we used anti-mouse IgG horseradish peroxidase conjugate for secondary antibody. For the birds, we used anti-chicken IgY horseradish peroxidase conjugate for secondary antibody. Positive and negative controls came from a previous study and were serum samples from laboratory mice that had been experimentally infected with *B. afzelii* or not. Controls for the background absorbance consisted of wells filled with phosphate-buffered saline (PBS) solution. The 104 serum samples were randomly assigned to one of two 96-well commercial ELISA plates (Virion; SERION ELISA). Each ELISA plate contained 62–64 host serum samples, 3–4 positive controls, 2–3 negative controls, and 2–4 background absorbance controls. To determine the repeatability of the absorbance values, we repeated the ELISA for 22 serum samples (in two different plates). The repeatability of the absorbance values was 95.7%, which is very high ($F_{20, 19} = 45.49$, $p < 0.001$).

***Culture of B. burgdorferi sl in BSK-H medium*:** To confirm the viability of the spirochetes, we cultured *B. burgdorferi* spirochetes from host organs and from the xenodiagnostic unfed 4-week-old nymphs. Each host organ was cut into two halves; one half was used to detect *B. burgdorferi* sl using qPCR (see above), and the other half was incubated in 1 ml of BSK-H medium at 34 °C. Similarly, for each combination of host and infestation, 3 unfed 4-week-old nymphs were cut in half lengthwise using micro scissors and incubated in 1 ml of BSK-H medium at 34 °C. The cultures were checked for live spirochetes after 14 days and 30 days using a dark-field microscope.

Plasmid content of the strains of *B. burgdorferi* sl: To determine whether the *B. afzelii* and *B. garinii* strains contained all the necessary plasmids to complete their life cycle, we tested the following 9 plasmids for each strain via PCR: lp 17, lp 28-2, lp 28-3, lp 28-8, lp 38, lp 54, cp 32-10, *adeC*, and *pncA*. Total genomic DNA was prepared from approximately 8 ml of *Borrelia* culture using the Wizard genomic DNA kit (Promega, Madison, WI). The total plasmid contents of the strains were compared using primers specific for plasmids based on the complete genome

sequence of PKo and ACA-1 [43]. In addition, primers specific for the genes *pncA* and *adeC* were used to confirm their presence [43].

Statistical analysis

As expected, negative control animals were found to be uninfected in our study. Thus, they are only included in the statistical analyses when specified.

***Detection of antibodies against B. burgdorferi* sl:** *B. burgdorferi* sl-specific antibody responses of the vertebrate hosts were analysed separately for blocks 1 and block 2. The sample sizes for the block 1 mice, block 2 mice, block 1 canaries, block 2 canaries, and block 2 great tits were 13, 13, 14, 14, and 8, respectively. Antibody responses were log10-transformed to improve the normality of the residuals. The threshold value between a positive and a negative antibody response was determined as the mean antibody response of the uninfected host plus three standard deviations of the uninfected host. We used Welch's *t*-test to determine whether the classification of the infection status was correct.

***Body mass of vertebrate hosts*:** In block 1, 10 mice and 10 canaries (20 animals) were inoculated with different strains of *B. afzelii*; in block 2, 10 mice, 10 canaries, and 8 great tits (28 animals) were inoculated with different strains of *B. garinii*. The weights of the hosts were analysed separately for the two blocks because they differed in host species and the number of times the animals were weighed (i.e., the blocks were not orthogonal). We used linear mixed effects models (LMMs) with normal errors to model the host body weight as a function of the fixed factors time (4 levels for block 1: days 0, 14, 28, and 35 PI; 8 levels for block 2: days 0, 7, 14, 21, 28, 35, 42, and 49 PI) and host species (2 levels for block 1: mouse, canary; 3 levels for block 2: mouse, canary, great tit). Host body weights were log10-transformed to improve the normality of the residuals. Host identification number was included as a random factor.

***Body mass of the engorged larvae*:** The weights of the immature ticks were analysed separately for the two blocks because they were not orthogonal with respect to host species and tick stage. In addition, the two blocks differed with respect to the *B. burgdorferi* sl species, adult female *I. ricinus* ticks that produced the larvae, and the timing and methodology of the block. We had weighed 220 unfed nymphs for block 1 and 572 engorged larvae and 300 unfed nymphs for block 2. We used LMMs with normal errors to model the engorged larval weight or the unfed nymphal weight as a function of the fixed factors infestation (2 levels: infestation 1 at 14 days PI and infestation 2 at 28 days PI) and host species (2 levels for block 1: mouse, canary; 3 levels

for block 2: mouse, canary, great tit). Immature tick weights were log10-transformed to improve the normality of the residuals. Host identification number was included as a random factor.

RESULTS

Experimental infections of vertebrate hosts with *B. burgdorferi* sl

In block 1, 4 of 10 mice (M7, M8, M9, M10) became infected with strains of *B. afzelii* (NE4049, Fin-Jyv-A3, NE4049, NE1857). In block 2, 1 of 10 mice (M22) became infected with one strain of *B. garinii* (NE5135). None of the birds became infected with *B. burgdorferi* sl following the experimental isolations. For the 5 mice that we consider infected, proof of infection was demonstrated by the qPCR-based detection of *B. burgdorferi* sl DNA in mouse tissues and in the xenodiagnostic nymphs that fed on these hosts as larvae. We showed the viability of *B. burgdorferi* sl by culturing live spirochetes from mouse tissues and xenodiagnostic nymphs.

Antibodies against B. burgdorferi sl in the vertebrate hosts

Mice were defined as having seroconverted if they had a log10-transformed antibody response greater than 3.60 (mean + 3 standard deviations = 3.26 + 0.34). By this criterion, most of the mice (17/20) seroconverted following the inoculation with either *B. afzelii* in block 1 or *B. garinii* in block 2. The mice that became infected with strains of *B. afzelii* (M7, M8, M9, and M10) or *B. garinii* (M22) had the stronger IgG responses against *B. burgdorferi* sl (Figure 9).

Birds were defined as having seroconverted if they had a log10-transformed antibody response greater than 3.26 (mean + 3 standard deviation = 2.93 + 0.33). By this criterion, very few birds (3/28) seroconverted following the inoculation with either *B. afzelii* in block 1 or *B. garinii* in block 2 (Figure 10).

The prevalence of *B. burgdorferi* sl in host organs

In block 1, 4 of 10 mice contained *B. afzelii*-infected tissues (16/36), whereas 6 of 10 mice did not produce any infected tissues (0/54; Table 2). Mice M7, M8, M9, and M10 were infected with *B. afzelii* strains NE4049, Fin-Jyv-A3, NE4049, and NE1857 and the tissue samples that tested positive were 4 ears, 4 bladders, 3 hearts, 3 joints, and 2 skin biopsies (Table 2). None of the 10 canaries produced any *B. afzelii*-infected tissues (0/90; Table 2).

In block 2, 1 of 10 mice produced *B. garinii*-infected tissues (2/9), whereas 9 of 10 mice did not produce any infected nymphs (0/81). Mouse M22 was infected with *B. garinii* strain NE5135 and the tissue samples that infected with *B. garinii* were 1 ear and 1 joint (Table 2).

None of the 10 canaries and 8 great tits produced any *B. garinii*-infected tissues (0/126; Table 2).

The *B. burgdorferi* sl spirochete load in host organs

Organs were defined as infected when they had a spirochete load > 2.44 (Cq value ≤ 40). For the subset of infected tissue samples, we compared the mean spirochete load (units are number of spirochetes per mg of DNA) among the 5 mouse organs. The mean spirochete number per mg of organ DNA was highest in the heart, followed by joint, ear, skin, and bladder for the subset of infected mice (Table 3).

Culture of *B. burgdorferi* sl from host organs

In block 1, only 3 of 90 tissue samples from the 10 mice contained live *B. afzelii* spirochetes. Three mice (M8, M9, and M10) infected with *B. afzelii* strains Fin-Jyv-A3, NE4049, and NE1857 had tissue samples (skin, ear, and ear) that produced live spirochetes. None of the 70 tissue samples from the 10 canaries produced live *B. afzelii* spirochetes.

In block 2, only 1 of 90 tissue samples from the 10 mice contained live *B. garinii* spirochetes. Mouse M22 infected with *B. garinii* strain NE5135 had an ear culture that produced live spirochetes. None of the 70 and 56 tissue samples from the 10 canaries and 8 great tits, respectively, produced live *B. garinii* spirochetes.

The prevalence of *B. burgdorferi* sl in *I. ricinus* nymphs

In block 1, 4 of 10 mice produced *B. afzelii*-infected nymphs (25/40), whereas 6 of 10 mice did not produce any infected nymphs (0/60). Mice M7, M8, M9, and M10 were infected with *B. afzelii* strains NE4049, Fin-Jyv-A3, NE4049, and NE1857 and the percentage of infected nymphs was 80.0% (8/10), 90.0% (9/10), 50.0% (5/10), and 30.0% (3/10), respectively (Table 4). None of the 10 canaries produced any *B. afzelii*-infected nymphs (0/100; Table 4).

In block 2, 1 of 10 mice produced *B. garinii*-infected nymphs (4/10), whereas 9 of 10 mice did not produce any infected nymphs (0/90). Mouse M22 was infected with *B. garinii* strain NE5135 and the percentage of infected ticks was 40.0% (4/10; Table 5). None of the 10 canaries produced any *B. garinii*-infected nymphs (0/100; Table 5) and none of the 8 great tits produced any *B. garinii*-infected nymphs (0/80; Table 5).

The *B. burgdorferi* sl spirochete load in *I. ricinus* nymphs

Unfed 4-week-old nymphs were defined as infected when they had a spirochete load > 2.44 (Cq value ≤ 40). The spirochete load of *B. burgdorferi* sl in the unfed 4-week-old *I. ricinus* nymphs differed among the strains. The nymphal spirochete load of *B. garinii* strain NE5135 was intermediate compared to the 4 *B. afzelii* strains (Table 6).

Culture of *B. burgdorferi* sl from *I. ricinus* nymphs

In block 1, only 10 of 120 unfed nymphs that had fed as larvae on the 10 mice contained live *B. afzelii* spirochetes. Four mice (M7, M8, M9, and M10) infected with *B. afzelii* strains NE4049, Fin-Jyv-A3, NE4049, and NE1857 produced live *B. afzelii* spirochetes for 1, 5, 3, and 1 nymph, respectively. None of the nymphs that had fed as larvae on the 10 canaries produced live *B. afzelii* spirochetes (Table 7).

In block 2, only 2 of 186 unfed nymphs that had fed as larvae on the 10 mice contained live *B. garinii* spirochetes. Mouse M22 infected with *B. garinii* strain NE5135 produced live spirochetes for 2 nymphs (Table 8). None of the nymphs that had fed as larvae on the 10 canaries or 8 great tits produced live *B. garinii* spirochetes (Table 8).

Plasmid content of the strains of *B. burgdorferi* sl

Of the 9 tested plasmids, strain NE4049 contained all 9 critical plasmids. Strains NE1857 and Fin-Jyv-A3 contained 7 and 6 critical plasmids, respectively. These 3 strains were thus able to established infection in mice. All other strains only contained between 2 and 4 critical plasmids and were thus unable to establish infection in mice or birds. Surprisingly, strain NE5135 contained only 3 of the 9 critical plasmids but was able to establish infection in mice.

Body mass of vertebrate hosts

We weighed 52 hosts. Of the 52 hosts, 20, 20, and 8 were infected mice, infected canaries, and infected great tits, respectively. Of the 52 hosts, 2 and 2 were uninfected control mice and uninfected control canaries, respectively. Of the 52 hosts, 22 and 30 were sampled from block 1 and block 2, respectively. For block 1, we weighed a total of 22 hosts on 4 different occasions (days 0, 14, 28, and 35 PI). For block 2, we weighed a total of 22 and 8 hosts on 7 (days 0, 7, 14, 21, 28, 35, and 42 PI) and 8 different occasions (days 0, 7, 14, 21, 28, 35, 42, and 49 PI), respectively.

For block 1, the interaction between the host species and day had a significant effect on host weight (LMM: $\chi^2 = 33.290$, df = 3, $p < 0.001$). We therefore tested the effect of time on

host weight separately for each host species. For the mice, body weight increased between d0 and d14 (mean ± standard deviation: 0.032 ± 0.010), and between d14 and d28 (mean ± standard deviation: 0.011 ± 0.006), but it decreased between d28 and d35 (mean ± standard deviation: -0.004 ± 0.012; Figure 1). Mice were heavier on days 14, 28, and 35 PI than on day 0, and these differences were significant (Figure 1, Table 9). Thus, the mice did not lose weight following the inoculation with *B. afzelii* or the first infestation, but they did lose weight following the second larval infestation. For the canaries, body weight decreased between d0 and d14 (mean ± standard deviation: -0.003 ± 0.017), but it increased between d14 and d28 (mean ± standard deviation: 0.001 ± 0.011), and between the d28 and d35 (mean ± standard deviation: 0.013 ± 0.023; Figure 2). Thus, the canaries lost weight following the inoculation with *B. afzelii*, but regained it during the period of the first and second larval infestations (Figure 2, Table 9).

For the block 2, the interaction between the host species and day had a significant effect on host weight (LMM: $\chi^2 = 165.30$, df = 12, $p < 0.001$). We therefore tested the effect of time on host weight separately for each host species. For the mice, body weight increased between d0 and d7 (mean ± standard deviation: 0.008 ± 0.010), between d7 and d14 (mean ± standard deviation: 0.015 ± 0.012), d14 and d21 (mean ± standard deviation: 0.003 ± 0.010), d21 and d28 (mean ± standard deviation: 0.016 ± 0.009), and d28 and d35 (mean ± standard deviation: 0.008 ± 0.010), but it decreased between d35 and d42 (mean ± standard deviation: -0.004 ± 0.005; Figure 3). Mice were heavier on days 7, 14, 21, 28, 35, 42 days PI than at 0 day PI, and these differences were significant (Figure 3, Table 10). Thus, the mice did not lose weight following the inoculation with *B. garinii* or the first infestation, but they did lose weight one week following the second larval infestation. For the canaries, body weight decreased between d0 and d7 (mean ± standard deviation: -0.009 ± 0.014), d7 and d14 (mean ± standard deviation: -0.012 ± 0.012), d14 and d21 (mean ± standard deviation: -0.011 ± 0.027), and d21 and d28 (mean ± standard deviation: -0.008 ± 0.014), but it increased between d28 and d35 (mean ± standard deviation: 0.003 ± 0.020), and d35 and d42 (mean ± standard deviation: 0.020 ± 0.016; Figure 4). Thus, the canaries lost weight following the inoculation with *B. garinii* and the first larval infestation, but regained it during the period of the second larval infestation (Figure 4, Table 10). For the great tits, body weight increased d0 and d7 (mean ± standard deviation: 0.009 ± 0.009), but decreased between d7 and d14 (mean ± standard deviation: -0.025 ± 0.004), d14 and d21 (mean ± standard deviation: -0.002 ± 0.013), and d21 and d28 (mean ± standard deviation: -0.002 ± 0.012), and increased again between d28 and d35 (mean ± standard deviation: 0.010 ± 0.009), d35 and d42 (mean ± standard deviation: 0.012 ± 0.008), and d42 and d49 (mean ± standard deviation: 0.005 ± 0.013; Figure 5). Thus, the great tits gain weight

following the inoculation with *B. garinii* but lost it during the period of the first larval infestation, and regained it during the period of the second larval infestation (Figure 5, Table 10).

Collection of engorged larvae from vertebrate hosts

We collected engorged larvae from 48 infected hosts. Of the 48 hosts, 20, 20, and 8 were infected mice, infected canaries, and infected tits, respectively. At 14 days and 28 days PI (and 42 days PI for the great tits only), each host was infested with ~100 pathogen-free larval ticks from multiple adult tick females of our laboratory colony of *I. ricinus*.

For the block 1, the numbers of engorged larvae collected from the mice were 631 (mean ± standard deviation = 63.1 ± 20.3) and 596 (mean ± standard deviation = 59.6 ± 21.75) for the first and second infestation, respectively (Table 11). The numbers of engorged larvae collected from the canaries were 682 (mean ± standard deviation = 68.2 ± 24.4) and 980 (mean ± standard deviation = 98.0 ± 17.37) for the first and second infestation, respectively (Table 11).

For the block 2, the numbers of engorged larvae collected from the mice were 308 (mean ± standard deviation = 30.8 ± 25.34) and 423 (mean ± standard deviation = 42.3 ± 12.88) for the first and second infestation, respectively (Table 11). The numbers of engorged larvae collected from the canaries were 677 (mean ± standard deviation = 67.7 ± 15.62) and 1129 (mean ± standard deviation = 112.9 ± 25.9) for the first and second infestation, respectively (Table 11). The numbers of engorged larvae collected from the great tits were 643 (mean ± standard deviation = 80.38 ± 27.72), 611 (mean ± standard deviation = 76.38 ± 29.43), and 342 (mean ± standard deviation = 42.75 ± 18.43) for the first, second, and third infestation, respectively (Table 11).

Body mass of the unfed *I. ricinus* nymphs in block 1

For the unfed nymphal weight of block 1, the interaction between the host species and infestation was significant (LMM: $\chi^2 = 7.365$, df = 1, p = 0.007). We therefore tested the effect of infestation on the unfed nymphal weight separately for each host species. For the canaries, the unfed nymphal weight for the second infestation was significantly higher than the first infestation (contrast = 0.022, SE = 0.009, p = 0.049; Figure 6; Table 12). For the mice, the unfed nymphal weight was not significantly different between the first and second infestation (contrast = -0.025, SE = 0.013, p = 0.093; Figure 6; Table 12).

We tested the effect of host species on nymphal weight for each infestation. For the first and second infestation, the unfed nymphal weight differences between mice and canaries were

not significant (first infestation: contrast = -0.026, SE = 0.014, p = 0.072; second infestation: contrast = 0.020, SE = 0.015, p = 0.201; Figure 6; Table 13).

Body mass of the engorged *I. ricinus* larvae in block 2

For the engorged larval weight, the interaction between the host species and infestation was significant (LMM: χ^2 = 13.248, df = 2, p = 0.001). We therefore tested the effect of infestation on engorged larval weight separately for each host species. The mean engorged larval weight was not significantly different between the first and second infestation for the mice (contrast = 0.012, SE = 0.008, p = 0.171; Figure 7; Table 12) or the canaries (contrast = -0.008, SE = 0.009, p = 0.351; Figure 7; Table 12). For the great tits, the engorged larval weight for the second infestation was significantly lower than the first infestation (contrast = -0.033, SE = 0.007, p = 0.002; Figure 7; Table 12).

We tested the effect of host species on engorged larval weight for each infestation. For the first infestation, the engorged larval weight of the mice was significantly higher than the canaries (contrast = 0.022, SE = 0.008, p = 0.006; Figure 7; Table 13) but significantly lower than the great tits (contrast = -0.031, SE = 0.008, p = 0.001; Figure 7; Table 13), while the engorged larval weight of the great tits were significantly higher than the canaries (contrast = 0.053, SE = 0.008, p < 0.001; Figure 7; Table 13). For the second infestation, the engorged larval weight of the mice was significantly higher than the canaries (contrast = 0.043, SE = 0.009, p < 0.001; Figure 7; Table 13), but not different from the great tits (contrast = -0.014, SE = 0.009, p = 0.144; Figure 7; Table 13), while the engorged larval weight of the great tits was significantly higher than the canaries (contrast = 0.029, SE = 0.009, p = 0.005; Figure 7; Table 13).

Body mass of the *I. ricinus* nymphs in block 2 (Table 12)

For the unfed nymphal weight of block 2, the interaction between the infestation and host was highly significant (LMM: χ^2 = 21.168, df = 2, p < 0.001). We therefore tested the effect of infestation on nymphal weight separately for each host species. For the mice, the unfed nymphal weight was not significantly different between the first and second infestation (contrast = 0.032, SE = 0.017, p = 0.083; Figure 8; Table 12). For the canaries, the unfed nymphal weight for the second infestation was significantly lower than the first infestation (contrast = -0.028, SE = 0.012, p = 0.034; Figure 8; Table 12). For the great tits, the unfed nymphal weight for the second infestation was significantly lower than the first infestation (contrast = -0.070, SE = 0.008, p < 0.001; Figure 8; Table 12).

We tested the effect of host species on nymphal weight for each infestation. For the first infestation, the unfed nymphal weight of the mice was significantly lower than the canaries (contrast = -0.041, SE = 0.019, p = 0.043; Figure 8; Table 13) and great tits (contrast = -0.081, SE = 0.021, p = 0.001; Figure 8; Table 13), but the unfed nymphal weight differences between canaries and great tits were not significant (contrast = 0.040, SE = 0.021, p = 0.072; Figure 8; Table 13). For the second infestation, the unfed nymphal weight differences were not significant between mice and canaries (contrast = -0.020, SE = 0.013, p = 0.133; Figure 8; Table 13), mice and great tits (contrast = -0.022, SE = 0.014, p = 0.132; Figure 8; Table 13), and canaries and great tits (contrast = -0.001, SE = 0.014, p = 0.898; Figure 8; Table 13).

DISCUSSION

Success of infection experiment: One disappointing result was that none of the birds became infected with *B. garinii*. We expected that the canary would be a good host for *B. garinii* because previous studies had shown that this bird species can host *B. burgdorferi* ss, which is less of a bird specialist than *B. garinii* [44]. We expected that the great tit would be a good host for *B. garinii* as numerous studies have shown that this species can be experimentally infected with *B. garinii* [25, 45, 46]. We had a more success with our experimental infections of mice with strains of *B. afzelii*. Four of 10 mice became infected with 3 different *B. afzelii* strains of NE4049 (2x), Fin-Jyv-A3, and NE1857. We have previously infected BALB/c mice with strains NE4049 and Fin-Jyv-A3 [39, 40, 47], so we expected these two strains to work. It was disappointing that of the 6 new strains of *B. afzelii* tested here for the first time, only one (NE1857) managed to establish infection in the BALB/c mice. A previous study had experienced much higher infection success in BALB/c mice using *B. afzelii* strains from the same collection [48]. All the hosts were inoculated with a large infectious dose (3 million spirochetes) and they did appear to develop a weak antibody response to the *B. burgdorferi* sl pathogens. These results suggest that our hosts were exposed, but that most of the *B. burgdorferi* sl strains failed to establish a proper infection and were cleared by the host immune system. In summary, we had unexpectedly low success with infecting the appropriate rodent and avian reservoir hosts with strains of *B. afzelii* and *B. garinii*.

B. burgdorferi sl pathogens contain many plasmids that contain the genes that are necessary to complete the life cycle in both the vertebrate host and the tick vector [49]. For example, linear plasmids lp25 and lp28 are important for infectivity in the host and required for survival in the tick [50]. It is well known that during repeated serial passage *B. burgdorferi* sl strains can lose their plasmids and hence their infectiousness to the vertebrate host or the tick

vector. At the start of the study, we had not been concerned about plasmid loss because all of the *B. burgdorferi* sl strains used in this study had undergone limited passage before being stored at –80 °C. Following the disappointing results, we examined the plasmid profiles and discovered that many of our strains were missing critical plasmids (Table 14). NE4049, which established infection in mice, was the only strain that contained all 9 plasmids. The two other strains that established infection mice, NE1857 and Fin-Jyv-A3, contained 7 and 6 of the 9 critical plasmids. The *B. garinii* strains only contained between 2 and 4 plasmids and all were missing the critical L17 and L28 plasmids. This result suggests that the majority of our strains were not infectious before the start of the study. We are not sure why our *B. burgdorferi* sl strains were so deficient in plasmids. One potential explanation is an inadequate long-term storage protocol. Strains were frozen without glycerol and were stored for many years without ever being re-cultured. Over the years, freezers failed, and strains thawed before being refrozen again. One surprising result of the study was that *B. garinii* strain NE5135 was able to establish infection and achieve transmission to xenodiagnostic ticks, despite the fact that this strain was missing all the critical L17 and L28 plasmids and contained only 3 of the 9 critical plasmids.

***Borrelia garinii* can infect rodents:** An interesting result is our demonstration that one of our *B. garinii* strains (NE5135) was able to establish infection and achieve transmission to feeding ticks in a mouse but not birds. This result was unexpected as this genospecies is normally associated with avian hosts [16, 51]. Such host associations were attributed to the differential sensitivity of each genospecies to the complement system of the vertebrate host [8, 28, 30, 34, 35]. Previous studies have shown that bird-associated genospecies can establish infection in rodents. Studies in England demonstrated that 19% of trapped rodents harboured *B. garinii* in diverse organs and that this genospecies was the more commonly detected in introduced grey squirrels [52, 53]. Other studies in France showed that introduced Siberian chipmunks and European red squirrels were infected with *B. garinii* [54, 55]. There are surprisingly few experimental infection studies investigating whether rodents can be experimentally infected with *B. garinii*; most of these studies unknowingly used the closely related but rodent-adapted *B. bavariensis* [56-58]. In contrast, there are numerous experimental infection studies that have shown that birds can be infected with *B. garinii* and *B. valaisiana*, but not *B. afzelii*. For example, an experimental infection study on pheasants showed that they could transmit *B. garinii* and *B. burgdorferi* ss but not *B. afzelii* to xenodiagnostic *I. ricinus* ticks [26]. Experimental infection studies on common blackbirds (*Turdus merula*) and great tits (*Parus major*) have also shown that these species can amplify bird-associated genospecies like *B.*

garinii and *B. valaisiana*, but not rodent-associated species like *B. afzelii* [59]. There is a large amount of evidence that supports the hypothesis that *B. afzelii* is adapted to small mammals and that *B. garinii* is adapted to birds. Our modest study merely shows that from time to time, specialist genospecies can sometimes establish infection in atypical hosts.

Fluctuation of the host weight: The trajectory of host body mass over the course of the infection differed among the three host species. Mice continued to gain body weight after the inoculation with the *B. burgdorferi* sl strains. The mice were young at the start of the experiment (4 weeks old) and still in their active growth phase. In contrast, the birds were mature (canaries were one year old and the great tits were two years old) and were no longer growing. The birds exhibited weight loss in the weeks following the inoculation with the *B. burgdorferi* sl strains, but most birds had regained this weight by the end of the study. Even though the *B. burgdorferi* sl strains were not infectious for the birds, the inoculation of 3 million spirochetes probably triggered a strong immune response, which may have caused the weight loss in the birds. This result contradicts previous studies which found that birds experimentally infected with *B. burgdorferi* sl via injection or tick bite exhibited no weight loss or increased body mass [44]. Another explanation for the weight loss is that tick blood feeding might exert a cost on birds. A reduction in body mass could be due to the increased allocation of resources to compensate for blood loss, to repair tissue lesions, and to mount an immune response. We estimate that an infestation with 100 *I. ricinus* larvae removes about 260 µl of blood [60], which, if the blood volume accounts for ~8% of the body mass in a great tit [61], represents a loss of ~17% of the total blood volume. Several studies on birds have found that the presence and intensity of infestation by *I. ricinus* ticks can have negative effects on body mass and general health [62, 63].

Great tits show resistance against larval ticks: An interesting result is that the weight of *I. ricinus* larvae that had fed on great tits decreased from the first to the second infestation. Similarly, nymphs that had fed as larvae on canaries inoculated with *B. burgdorferi* sl in block 2 were able to acquire more blood during the second infestation than the first infestation. This suggests that birds might be able to develop an immune response that gives them acquired resistance against *I. ricinus* larvae. Studies have demonstrated evidence of acquired resistance in different host species but particularly in rodents, where larval weight decreased with successive infestation [64-66]. In contrast, previous studies on birds have found no evidence for the development of acquired resistance against *I. ricinus* ticks [67, 68]. However, these

trends are somewhat difficult to interpret given the fact that what was true for canaries in block 2, did not for canaries in block 1, and that the infestation densities seem to differ substantially between the first and second infestation. Thus, a second explanation for the smaller engorged larval volume on the second infestation for the birds in block 2 is that high larval density might reduce feeding efficacy.

Conclusion: The success of our experimentally infecting rodent and avian hosts with strains of *B. afzelii* and *B. garinii* was unexpectedly low. The few strains that were successful had been recently used in other experimental infection studies. Subsequent investigation found that most *B. burgdorferi* sl strains were missing the plasmids critical for establishing infection in the vertebrate host. We believe that the inevitable freeze-thaw cycles associated with long-term storage at -80 °C played a role in the loss of plasmids and infectiousness of the *B. burgdorferi* sl strains. One interesting result was that a single strain of *B. garinii* was able to establish infection in a BALB/c mouse and be transmitted to feeding *I. ricinus* ticks.

Acknowledgements

We would like to thank Alfonso Rojas for his help with the inoculation of the birds with the strains of *B. burgdorferi* sl. This study was part of the PhD thesis of Cindy Bregnard.

Competing interests

The authors declare that they have no competing interests.

Funding

This study was supported by a grant from the Swiss National Science Foundation (SNSF) to Maarten Voordouw (FN 31003A_141153).

Authors' contributions

CB and MJV designed the study, analysed the data, and wrote the manuscript. CB performed the experimental infections. OR cultured the strains of *B. burgdorferi* sl and provided the *I. ricinus* larvae. CB and AS performed the molecular work and managed the data. All authors read and approved the final version of the manuscript.

REFERENCES

1. Mysterud A, Stigum V, Seland I, Herland A, Easterday WR, Jore S, et al. Tick abundance, pathogen prevalence, and disease incidence in two contrasting regions at the northern distribution range of Europe. Parasit Vectors. 2018;11:309.
2. Kilpatrick A, Dobson A, Levi T, Salkeld D, Swei A, S. Ginsberg H, et al. Lyme disease ecology in a changing world: consensus, uncertainty and critical gaps for improving control. Philos Trans R Soc Lond, B, Biol Sc. 2017;372:20160117.
3. Rudenko N, Golovchenko M, Grubhoffer L, Oliver Jr JH. Updates on *Borrelia burgdorferi* sensu lato complex with respect to public health. Ticks Tick Borne Dis. 2011;2:123-8.
4. Pritt BS, Mead PS, Johnson DKH, Neitzel DF, Respicio-Kingry LB, Davis JP, et al. Identification of a novel pathogenic *Borrelia* species causing Lyme borreliosis with unusually high spirochaetaemia: a descriptive study. Lancet Infect Dis. 2016;16:556-64.
5. Johnson RC, Schmid GP, Hyde FW, Steigerwalt AG, Brenner DJ. *Borrelia burgdorferi* sp. nov.: etiologic agent of Lyme disease. Int J Syst Evol Microbiol. 1984;34:496-7.
6. Baranton G, Postic D, Saint Girons I, Boerlin P, Piffaretti JC, Assous M, et al. Delineation of *Borrelia burgdorferi* sensu stricto, *Borrelia garinii* sp. nov., and group VS461 associated with Lyme borreliosis. Int J Syst Bacteriol. 1992;42:378-83.
7. Canica MM, Nato F, du Merle L, Mazie JC, Baranton G, Postic D. Monoclonal antibodies for identification of *Borrelia afzelii* sp. nov. associated with late cutaneous manifestations of Lyme borreliosis. Scand J Infect Dis. 1993;25:441-8.
8. Kurtenbach K, De Michelis S, Etti S, Schäfer SM, Sewell H-S, Brade V, et al. Host association of *Borrelia burgdorferi* sensu lato – the key role of host complement. Trends Microbiol. 2002;10:74-9.
9. Mannelli A, Bertolotti L, Gern L, Gray J. Ecology of *Borrelia burgdorferi* sensu lato in Europe: transmission dynamics in multi-host systems, influence of molecular processes and effects of climate change. FEMS Microbiol Rev. 2012;36:837-61.
10. Movila A, Ion T, Dubinina H, Uspenskaia I, Alekseev A. Zoonotic peculiarities of *Borrelia burgdorferi* s.l.: vectors competence and vertebrate host specificity. In: A Karami, editor Lyme disease INTECH. 2012:1-26.
11. Hu CM, Humair P-F, Wallich R, Gern L. *Apodemus* sp. rodents, reservoir hosts for *Borrelia afzelii* in an endemic area in Switzerland. Zentralbl Bakteriol. 1997;285:558-64.

12. Humair P-F, Gern L. Relationship between *Borrelia burgdorferi* sensu lato species, red squirrels (*Sciurus vulgaris*) and *Ixodes ricinus* in enzootic areas in Switzerland. Acta Trop. 1998;69:213-27.
13. Humair P-F, Peter O, Wallich R, Gern L. Strain variation of Lyme disease spirochetes isolated from *Ixodes ricinus* ticks and rodents collected in two endemic areas in Switzerland. J Med Entomol. 1995;32:433-8.
14. Humair PF, Rais O, Gern L. Transmission of *Borrelia afzelii* from *Apodemus* mice and *Clethrionomys* voles to *Ixodes ricinus* ticks: differential transmission pattern and overwintering maintenance. Parasitology. 1999;118:33-42.
15. Hanincová K, Schäfer SM, Etti S, Sewell HS, Taragelová V, Ziak D, et al. Association of *Borrelia afzelii* with rodents in Europe. Parasitology. 2003;126:11-20.
16. Hanincová K, Taragelová V, Koci J, Schäfer SM, Hails R, Ullmann AJ, et al. Association of *Borrelia garinii* and *B. valaisiana* with songbirds in Slovakia. Appl Environ Microbiol. 2003;69:2825-30.
17. Taragel'ová V, Koči J, Hanincová K, Kurtenbach K, Derdáková M, Ogden NH, et al. Blackbirds and song thrushes constitute a key reservoir of *Borrelia garinii*, the causative agent of Borreliosis in Central Europe. Appl Environ Microbiol. 2008;74:1289-93.
18. Mannelli A, Nebbia P, Tramuta C, Grego E, Tomassone L, Ainardi R, et al. *Borrelia burgdorferi* sensu lato infection in larval *Ixodes ricinus* (Acari: Ixodidae) feeding on blackbirds in northwestern Italy. J Med Entomol. 2005;42:168-75.
19. Dubska L, Literak I, Kocianova E, Taragelova V, Sychra O. Differential role of passerine birds in distribution of *Borrelia* spirochetes, based on data from ticks collected from birds during the postbreeding migration period in central Europe. Appl Environ Microbiol. 2009;75:596-602.
20. Norte AC, Ramos JA, Gern L, Núncio MS, Lopes de Carvalho I. Birds as reservoirs for *Borrelia burgdorferi* s.l. in western Europe: circulation of *B. turdi* and other genospecies in bird–tick cycles in Portugal. Environ Microbiol. 2013;15:386-97.
21. Gern L, Siegenthaler M, Hu CM, Leuba-Garcia S, Humair PF, Moret J. *Borrelia burgdorferi* in rodents (*Apodemus flavicollis* and *A. sylvaticus*): duration and enhancement of infectivity for *Ixodes ricinus* ticks. Eur J Epidemiol. 1994;10:75-80.
22. Jacquet M, Durand J, Rais O, Voordouw MJ. Cross-reactive acquired immunity influences transmission success of the Lyme disease pathogen, *Borrelia afzelii*. Infect, Genet Evol. 2015;36:131-40.

23. Tälleklint L, Jaenson TGT. Is the small mammal (*Clethrionomys glareolus*) or the tick vector (*Ixodes ricinus*) the primary overwintering reservoir for the Lyme borreliosis spirochete in Sweden? J Wildl Dis. 1995;31:537-40.
24. Norte AC, Lopes de Carvalho I, Núncio MS, Ramos JA, Gern L. Blackbirds *Turdus merula* as competent reservoirs for *Borrelia turdi* and *Borrelia valaisiana* in Portugal: evidence from a xenodiagnostic experiment. Environmental Microbiology Reports. 2013;5:604-7.
25. Heylen D, Matthysen E, Fonville M, Sprong H. Songbirds as general transmitters but selective amplifiers of *Borrelia burgdorferi* sensu lato genotypes in *Ixodes rinicus* ticks. Environ Microbiol. 2014;16:2859-68.
26. Kurtenbach K, Schäfer SM, Sewell H-S, Peacey M, Hoodless A, Nuttall PA, et al. Differential survival of Lyme borreliosis spirochetes in ticks that feed on birds. Infect Immun. 2002;70:5893-5.
27. Herrmann C, Gern L, Voordouw MJ. Species co-occurrence patterns among Lyme borreliosis pathogens in the tick vector *Ixodes ricinus*. Appl Environ Microbiol. 2013;79:7273-80.
28. Kurtenbach K, De Michelis S, Sewell H-S, Etti S, Schäfer SM, Hails R, et al. Distinct combinations of *Borrelia burgdorferi* sensu lato genospecies found in individual questing ticks from Europe. Appl Environ Microbiol. 2001;67:4926-9.
29. Rauter C, Hartung T. Prevalence of *Borrelia burgdorferi* sensu lato genospecies in *Ixodes ricinus* ticks in Europe: a metaanalysis. Appl Environ Microbiol. 2005;71:7203-16.
30. Kurtenbach K, Sewell H-S, Ogden NH, Randolph SE, Nuttall PA. Serum complement sensitivity as a key factor in Lyme disease ecology. Infect Immun. 1998;66:1248-51.
31. Kraiczy P, Skerka C, Kirschfink M, Zipfel PF, Brade V. Mechanism of complement resistance of pathogenic *Borrelia burgdorferi* isolates. Int Immunopharmacol. 2001;1:393-401.
32. Lin Y-P, Diuk-Wasser M, Stevenson B, Kraiczy P. Complement evasion contributes to Lyme borreliae–host associations. Trends Parasitol. 2020;36.
33. Müller-Eberhard HJ. Molecular organization and function of the complement system. Annu Rev Biochem. 1988;57:321-47.
34. Lane RS, Quistad GB. Borreliacidal factor in the blood of the Western fence lizard (*Sceloporus occidentalis*). The Journal of Parasitology. 1998;84:29-34.

35. Bhide MR, Travnicek M, Levkutova M, Curlik J, Revajova V, Levkut M. Sensitivity of *Borrelia* genospecies to serum complement from different animals and human: a host-pathogen relationship. FEMS Immunol Med Microbiol. 2005;43:165-72.
36. Craine NG, Nuttall PA, Marriott AC, Randolph SE. Role of grey squirrels and pheasants in the transmission of *Borrelia burgdorferi* sensu lato, the Lyme disease spirochaete, in the U.K. Folia Parasitol (Praha). 1997;44:155-60.
37. Jacquet M, Margos G, Fingerle V, Voordouw MJ. Comparison of the lifetime host-to-tick transmission between two strains of the Lyme disease pathogen *Borrelia afzelii*. Parasites & vectors. 2016;9:1-8.
38. Durand J, Jacquet M, Paillard L, Rais O, Gern L, Voordouw MJ. Cross-immunity and community structure of a multiple-strain pathogen in the tick vector. Appl Environ Microbiol. 2015;81:7740-52.
39. Genné Vizcardo D, Rossel M, Sarr A, Battilotti F, Rais O, Rego R, et al. Competition between strains of *Borrelia afzelii* in the host tissues and consequences for transmission to ticks. The ISME Journal. 2021.
40. Genné Vizcardo D, Sarr A, Rais O, Voordouw M. Competition between strains of *Borrelia afzelii* in immature *Ixodes ricinus* ticks is not affected by season. Frontiers in Cellular and Infection Microbiology. 2019;9:431.
41. Jacquet M, Durand J, Rais O, Voordouw MJ. Strain-specific antibodies reduce co-feeding transmission of the Lyme disease pathogen, *Borrelia afzelii*. Environ Microbiol. 2016;18:833-45.
42. Schwaiger M, Peter O, Cassinotti P. Routine diagnosis of *Borrelia burgdorferi* (sensu lato) infections using a real-time PCR assay. Clin Microbiol Infect. 2001;7:461-9.
43. Honeder S, Drskova E, Danklmaier A, Vavruskova Z, Martin S, Grubhoffer L. Now you see me: transfomration of infectious *Borrelia afzelii* with fluorescent reporters. *Submitted: Pathogens*. 2020.
44. Olsen B, Gylfe Å, Bergström S. Canary finches (*Serinus canaria*) as an avian infection model for Lyme borreliosis. Microb Pathog. 1996;20:319-24.
45. Heylen D, Tijsse E, Fonville M, Matthysen E, Sprong H. Transmission dynamics of *Borrelia burgdorferi* s.l. in a bird tick community. Environ Microbiol. 2013;15:663-73.
46. Heylen D, Fonville M, van Leeuwen AD, Sprong H. Co-infections and transmission dynamics in a tick-borne bacterium community exposed to songbirds. Environ Microbiol. 2016;18:988-96.

47. Gomez-Chamorro A, Heinrich V, Sarr A, Roethlisberger O, Genné D, Bregnard C, et al. Maternal antibodies provide strain-specific protection against infection with the Lyme disease pathogen in bank voles. Appl Environ Microbiol. 2019:AEM.01887-19.
48. Tonetti N, Voordouw MJ, Durand J, Monnier S, Gern L. Genetic variation in transmission success of the Lyme borreliosis pathogen *Borrelia afzelii*. Ticks and tick-borne diseases. 2015;6:334-43.
49. Jewett MW, Byram R, Bestor A, Tilly K, Lawrence K, Burtnick MN, et al. Genetic basis for retention of a critical virulence plasmid of *Borrelia burgdorferi*. Mol Microbiol. 2007;66:975-90.
50. Grimm D, Eggers CH, Caimano MJ, Tilly K, Stewart PE, Elias AF, et al. Experimental assessment of the roles of linear plasmids lp25 and lp28-1 of *Borrelia burgdorferi* throughout the infectious cycle. Infect Immun. 2004;72:5938-46.
51. Comstedt P, Jakobsson T, Bergström S. Global ecology and epidemiology of *Borrelia garinii* spirochetes. Infect Ecol Epidemiol. 2011;1:10.3402/iee.v1i0.9545.
52. Kurtenbach K, Peacey M, Rijpkema SG, Hoodless AN, Nuttall PA, Randolph SE. Differential transmission of the genospecies of *Borrelia burgdorferi* sensu lato by game birds and small rodents in England. Appl Environ Microbiol. 1998;64:1169-74.
53. Millins C, Magierecka A, Gilbert L, Edoff A, Brereton A, Kilbride E, et al. An invasive mammal (the gray squirrel, *Sciurus carolinensis*) commonly hosts diverse and atypical genotypes of the zoonotic pathogen *Borrelia burgdorferi* sensu Lato. Appl Environ Microbiol. 2015;81:4236-45.
54. Marsot M, Sigaud M, Chapuis JL, Ferquel E, Cornet M, Vourc'h G. Introduced Siberian chipmunks (Tamias sibiricus barberi) harbor more-diverse *Borrelia burgdorferi* sensu lato genospecies than native bank voles (*Myodes glareolus*). Appl Environ Microbiol. 2011;77:5716-21.
55. Pisanu B, Chapuis JL, Dozières A, Basset F, Poux V, Vourc'h G. High prevalence of *Borrelia burgdorferi* s.l. in the European red squirrel *Sciurus vulgaris* in France. Ticks Tick Borne Dis. 2014;5:1-6.
56. Hovius JW, Li X, Ramamoorthi N, Van Dam AP, Barthold SW, Van Der Poll T, et al. Coinfection with *Borrelia burgdorferi* sensu stricto and *Borrelia garinii* alters the course of murine Lyme borreliosis. FEMS Immunology & Medical Microbiology. 2007;49:224-34.

57. Sato Y, Nakao M. Transmission of the Lyme disease spirochete, *Borrelia garinii*, between infected and uninfected immature *Ixodes persulcatus* during cofeeding on mice. The Journal of parasitology. 1997;83:547-50.
58. Hu CM, Wilske B, Fingerle V, Lobet Y, Gern L. Transmission of *Borrelia garinii* OspA serotype 4 to BALB/c mice by *Ixodes ricinus* ticks collected in the field. J Clin Microbiol. 2001;39:1169-71.
59. Heylen DJA, Sprong H, Krawczyk A, Van Houtte N, Genné D, Gomez-Chamorro A, et al. Inefficient co-feeding transmission of *Borrelia afzelii* in two common European songbirds. Scientific Reports. 2017;7:39596.
60. Tälleklint L, Jaenson TG. Infestation of mammals by *Ixodes ricinus* ticks (Acari: Ixodidae) in south-central Sweden. Experimental & applied acarology. 1997;21:755-71.
61. Lubjuhn T, Brün J, Winkel W, Muth S. Effects of blood sampling in great tits. J Field Ornithol. 1998;69:595-602.
62. Norte AC, Lobato DNC, Braga EM, Antonini Y, Lacorte G, Gonçalves M, et al. Do ticks and *Borrelia burgdorferi* s.l. constitute a burden to birds? Parasitol Res. 2013;112:1903-12.
63. Heylen DJA, Matthysen E. Effect of tick parasitism on the health status of a passerine bird. Funct Ecol. 2008;22:1099-107.
64. Randolph SE. Population regulation in ticks: the role of acquired resistance in natural and unnatural hosts. Parasitology. 1979;79:141-56.
65. Fielden LJ, Rechav Y, Bryson NR. Acquired immunity to larvae of *Amblyomma marmoreum* and *A.hebraeum* by tortoises, guinea-pigs and guinea-fowl. Med Vet Entomol. 1992;6:251-4.
66. Dizij A, Kurtenbach K. *Clethrionomys glareolus*, but not *Apodemus flavicollis*, acquires resistance to *Ixodes ricinus* L., the main European vector of *Borrelia burgdorferi*. Parasite Immunol. 1995;17:177-83.
67. Heylen DJ, Madder M, Matthysen E. Lack of resistance against the tick *Ixodes ricinus* in two related passerine bird species. Int J Parasitol. 2010;40:183-91.
68. Van Oosten AR, Heylen DJA, Elst J, Philtjens S, Matthysen E. An experimental test to compare potential and realised specificity in ticks with different ecologies. Evol Ecol. 2016;30:487-501.

Table 1. Information on the strains of *B. afzelii* and *B. garinii* used in this study. Shown are the *B. burgdorferi* sl genospecies, strain ID, region of origin, source of isolate, year of isolation, purity, multi-locus sequence type (MLST), the *ospC* major group (oMG), and nick name.

Genospecies	Strain ID	Origin	Source	Year	Purity	MLST	oMG	Nick name
B. afzelii	NE1857	Neuchatel, CH	*I. ricinus* tick	2005	84.0	327	A1	A1
B. afzelii	NE1827	Neuchatel, CH	*I. ricinus* tick	2005	99.8	20	A2	A2
B. afzelii	NE4556	Neuchatel, CH	*I. ricinus* tick	2005	82.2	347	A9	A9
B. afzelii	NE4049	Neuchatel, CH	*I. ricinus* tick	NA	NA	679	A10	A10
B. afzelii	NE4832	Neuchatel, CH	*I. ricinus* tick	2007	95.4	354	A11	A11
B. afzelii	NE4558	Neuchatel, CH	*I. ricinus* tick	2005	99.9	72	A14	A14a
B. afzelii	NE4779	Neuchatel, CH	*I. ricinus* tick	2007	99.5	72	A14	A14b
B. afzelii	Fin-Jyv-A3	Jyvaskyla, FI	Bank vole	2014	NA	676	A3	A3
B. garinii	NE5135	Neuchatel, CH	*I. ricinus* tick	2009	100.0	246	G2	G2
B. garinii	NE4554	Neuchatel, CH	*I. ricinus* tick	2005	99.8	244	G6	G6a
B. garinii	NE1845	Neuchatel, CH	*I. ricinus* tick	2005	99.8	244	G6	G6b
B. garinii	NE4891	Neuchatel, CH	*I. ricinus* tick	2007	99.8	180	G8	G8a
B. garinii	NE1883	Neuchatel, CH	*I. ricinus* tick	2005	99.7	87	G8	G8b
B. garinii	NE5245	Neuchatel, CH	*I. ricinus* tick	2010	99.7	82	G9	G9a
B. garinii	NE1879	Neuchatel, CH	*I. ricinus* tick	2005	98.7	82	G9	G9b
B. garinii	NE5158	Neuchatel, CH	*I. ricinus* tick	2009	99.8	82	G9	G9c
B. garinii	NE4907	Neuchatel, CH	*I. ricinus* tick	2007	99.6	88	G14	G14a
B. garinii	NE5308	Neuchatel, CH	*I. ricinus* tick	2010	100.0	90	G14	G14b

CH: Switzerland, FI: Finland

Table 2. The spirochete load of *B. afzelii* and *B. garinii* in the organs of the five infected mice. The spirochete load has units of the number of spirochetes per mg of DNA. Shown are the block, mouse ID, *B. burgdorferi* sl genospecies, organ, and number of spirochetes per mg of organ DNA.

Block	ID	Genospecies	Organ	Spirochetes/mg of DNA
1	M7	*B. afzelii*	Ear	1249.9
1	M8	*B. afzelii*	Ear	1210.3
1	M9	*B. afzelii*	Ear	912.1
1	M10	*B. afzelii*	Ear	40.1
1	M7	*B. afzelii*	Joint	1535.3
1	M8	*B. afzelii*	Joint	357.8
1	M10	*B. afzelii*	Joint	139.8
1	M7	*B. afzelii*	Bladder	308.7
1	M8	*B. afzelii*	Bladder	25.6
1	M9	*B. afzelii*	Bladder	101.2
1	M10	*B. afzelii*	Bladder	237.1
1	M7	*B. afzelii*	Heart	811.1
1	M8	*B. afzelii*	Heart	950.8
1	M9	*B. afzelii*	Heart	1239.1
1	M7	*B. afzelii*	Skin	478.1
1	M9	*B. afzelii*	Skin	98.4
2	M22	*B. garinii*	Ear	106.2
2	M22	*B. garinii*	Joint	428.0

Table 3. The spirochete load in the mouse organs. The spirochete load is measured as the number of spirochetes per mg of DNA. The sample size (N) refers to the number of organs that were infected with *B. burgdorferi* sl. Shown are the host, organ, sample size, geometric mean spirochete load, and 95% confident intervals of the geometric mean spirochete load.

Host	Organ	N	Spirochete load	95% CI
Mouse	Bladder	4	117.34	19.70 – 698.90
Mouse	Ear	5	357.88	49.30 – 2597.90
Mouse	Heart	3	984.95	578.75 – 1676.27
Mouse	Joint	4	425.76	88.68 – 2044.18
Mouse	Skin	2	216.89	

Table 4. *B. afzelii* infection status of *I. ricinus* nymphs that fed as larvae on mice and canaries in block 1. Shown are the host species, host ID, host sex, strain name, number of larvae recovered from the first infestation (Infest 1 Larvae) and the second infestation (Infest 2 Larvae), number of flat nymphs tested positive divided by the total number of nymphs tested from the first infestation (Infest 1 Nymphs), and the second infestation (Infest 2 Nymphs).

Host species	ID	Sex	Strain ID	Infest 1 Larvae	Infest 2 Larvae	Infest 1 Nymphs	Infest 2 Nymphs
M. musculus	M1	F	NE1827	60	58	0/5	0/5
M. musculus	M2	F	NE1857	65	51	0/5	0/5
M. musculus	M3	F	NE4556	100	68	0/5	0/5
M. musculus	M4	F	NE4558	46	29	0/5	0/5
M. musculus	M5	F	NE4779	69	54	0/5	0/5
M. musculus	M6	F	NE4832	44	48	0/5	0/5
M. musculus	M7	F	NE4049	49	71	5/5	3/5
M. musculus	M8	F	Fin-Jyv-A3	69	65	4/5	5/5
M. musculus	M9	F	NE4049	38	42	5/5	0/5
M. musculus	M10	F	NE1857	91	110	3/5	0/5
S. canaria	C1	M	NE1827	105	103	0/5	0/5
S. canaria	C2	M	NE1857	80	90	0/5	0/5
S. canaria	C3	M	NE4556	84	102	0/5	0/5
S. canaria	C4	M	NE4558	75	104	0/5	0/5
S. canaria	C5	M	NE4779	77	77	0/5	0/5
S. canaria	C6	M	NE4832	58	61	0/5	0/5
S. canaria	C7	M	NE4049	38	114	0/5	0/5
S. canaria	C8	M	Fin-Jyv-A3	35	102	0/5	0/5
S. canaria	C9	M	NE4049	91	111	0/5	0/5
S. canaria	C10	M	NE1857	39	116	0/5	0/5

Table 5. *B. garinii* infection status of *I. ricinus* nymphs that fed as larvae on mice, canaries, and great tits in block 2. Shown are the host species, host ID, host sex, strain name, number of larvae recovered from the first infestation (Infest 1 Larvae) and the second infestation (Infest 2 Larvae), number of flat nymphs tested positive divided by the total number of nymphs tested from the first infestation (Infest 1 Nymphs), and the second infestation (Infest 2 Nymphs).

Host species	ID	Sex	Strain ID	Infest 1 Larvae	Infest 2 Larvae	Infest 1 Nymphs	Infest 2 Nymphs
M. musculus	M12	F	NE5308	55	50	0/5	0/5
M. musculus	M13	F	NE1883	62	38	0/5	0/5
M. musculus	M14	F	NE5158	80	65	0/5	0/5
M. musculus	M15	F	NE4907	15	20	0/5	0/5
M. musculus	M16	F	NE4891	18	55	0/5	0/5
M. musculus	M18	F	NE1845	21	33	0/5	0/5
M. musculus	M19	F	NE1879	22	40	0/5	0/5
M. musculus	M20	F	NE4554	15	45	0/5	0/5
M. musculus	M21	F	NE5245	3	31	0/2	0/8
M. musculus	M22	F	NE5135	17	46	2/5	2/5
S. canaria	C12	M	NE4907	53	146	0/5	0/5
S. canaria	C13	M	NE5158	45	99	0/5	0/5
S. canaria	C14	M	NE4891	84	115	0/5	0/5
S. canaria	C15	M	NE1883	56	124	0/5	0/5
S. canaria	C16	M	NE1879	65	96	0/5	0/5
S. canaria	C17	M	NE4554	73	160	0/5	0/5
S. canaria	C18	M	NE5245	90	113	0/5	0/5
S. canaria	C19	M	NE1845	66	113	0/5	0/5
S. canaria	C20	M	NE5135	57	73	0/5	0/5
S. canaria	C21	M	NE5308	88	90	0/5	0/5
P. major	G1	F	NE5135	61	115	0/5	0/5
P. major	G2	F	NE4891	107	72	0/5	0/5
P. major	G3	F	NE1883	65	116	0/5	0/5
P. major	G4	F	NE5158	101	59	0/5	0/5
P. major	G5	M	NE1845	121	80	0/5	0/5
P. major	G6	M	NE5308	83	84	0/5	0/5
P. major	G7	M	NE4554	67	55	0/5	0/5
P. major	G8	M	NE4907	38	30	0/5	0/5

Table 6. The spirochete load of *B. burgdorferi* sl in *I. ricinus* nymphs. The sample size (N) refers to the number of nymphs that were infected with *B. burgdorferi* sl. Shown are the block, *B. burgdorferi* sl genospecies, strain ID, Host ID, sample size, geometric mean spirochete load, and 95% confident intervals of the geometric mean spirochete load.

Block	Genospecies	Strain ID	Host ID	N	Mean	95% CI
1	*B. afzelii*	NE4049	M7	8	5960	2073–17136
1	*B. afzelii*	Fin-Jyv-A3	M8	9	1484	403–5456
1	*B. afzelii*	NE4049	M9	5	666	63–7072
1	*B. afzelii*	NE1857	M10	3	120	30–482
2	*B. garinii*	NE5135	M22	4	1057	402–2783

Table 7. Viability of *B. afzelii* spirochetes from cultures of *I. ricinus* nymphs that fed as larvae on mice and canaries in block 1. Shown are the host species, host ID, host sex, strain name, number of unfed nymphs with live spirochetes divided by the total number of nymphs tested from the first infestation (Infest 1), and the second infestation (Infest 2).

Host species	ID	Sex	Strain ID	Infest 1	Infest 2
M. musculus	M1	F	NE1827	0/6	0/6
M. musculus	M2	F	NE1857	0/6	0/6
M. musculus	M3	F	NE4556	0/6	0/6
M. musculus	M4	F	NE4558	0/6	0/6
M. musculus	M5	F	NE4779	0/6	0/6
M. musculus	M6	F	NE4832	0/6	0/6
M. musculus	M7	F	NE4049	1/6	0/6
M. musculus	M8	F	Fin-Jyv-A3	3/6	2/6
M. musculus	M9	F	NE4049	3/6	0/6
M. musculus	M10	F	NE1857	1/6	0/6
S. canaria	C1	M	NE1827	0/6	0/6
S. canaria	C2	M	NE1857	0/6	0/6
S. canaria	C3	M	NE4556	0/6	0/6
S. canaria	C4	M	NE4558	0/6	0/6
S. canaria	C5	M	NE4779	0/6	0/6
S. canaria	C6	M	NE4832	0/6	0/6
S. canaria	C7	M	NE4049	0/6	0/6
S. canaria	C8	M	Fin-Jyv-A3	0/6	0/6
S. canaria	C9	M	NE4049	0/6	0/6
S. canaria	C10	M	NE1857	0/6	0/6

Table 8. Viability of *B. garinii* spirochetes from cultures of *I. ricinus* nymphs that fed as larvae on mice, canaries, and great tits in block 2. Shown are the host species, host ID, host sex, strain name, number of unfed nymphs with live spirochetes divided by the total number of nymphs tested from the first infestation (Infest 1), and the second infestation (Infest 2).

Host species	ID	Sex	Strain ID	Infest 1	Infest 2
M. musculus	M12	F	NE5308	0/6	0/6
M. musculus	M13	F	NE1883	0/6	0/6
M. musculus	M14	F	NE5158	0/6	0/6
M. musculus	M15	F	NE4907	0/6	0/6
M. musculus	M16	F	NE4891	0/6	0/6
M. musculus	M18	F	NE1845	0/6	0/6
M. musculus	M19	F	NE1879	0/6	0/6
M. musculus	M20	F	NE4554	0/6	0/6
M. musculus	M21	F	NE5245	0/6	0/6
M. musculus	M22	F	NE5135	1/6	1/6
S. canaria	C12	M	NE4907	0/6	0/6
S. canaria	C13	M	NE5158	0/6	0/6
S. canaria	C14	M	NE4891	0/6	0/6
S. canaria	C15	M	NE1883	0/6	0/6
S. canaria	C16	M	NE1879	0/6	0/6
S. canaria	C17	M	NE4554	0/6	0/6
S. canaria	C18	M	NE5245	0/6	0/6
S. canaria	C19	M	NE1845	0/6	0/6
S. canaria	C20	M	NE5135	0/6	0/6
S. canaria	C21	M	NE5308	0/6	0/6
P. major	G1	F	NE5135	0/6	0/6
P. major	G2	F	NE4891	0/6	0/6
P. major	G3	F	NE1883	0/6	0/6
P. major	G4	F	NE5158	0/6	0/6
P. major	G5	M	NE1845	0/6	0/6
P. major	G6	M	NE5308	0/6	0/6
P. major	G7	M	NE4554	0/6	0/6
P. major	G8	M	NE4907	0/6	0/6

Table 9. Changes in body weight over time in block 1 for two host species: mice and canaries. The animals were infected with different strains of *B. afzelii* on day 0 and infested with *I. ricinus* larvae on days 14 and 28. Shown are the host species, parameter estimates, standard errors (s.e.), t-statistics (t), and p-values (p).

Host species	Parameters	Estimates	s.e.	t	p
M. musculus	(Intercept)	1.276	0.005	233.57	< 0.001
M. musculus	14 days PI	0.032	0.003	9.41	< 0.001
M. musculus	28 days PI	0.044	0.003	12.78	< 0.001
M. musculus	35 days PI	0.040	0.003	11.67	< 0.001
S. canaria	(Intercept)	1.321	0.011	120.65	< 0.001
S. canaria	14 days PI	-0.003	0.007	-0.46	0.653
S. canaria	28 days PI	-0.002	0.007	-0.29	0.775
S. canaria	35 days PI	0.011	0.007	1.62	0.116

Table 10. Changes in body weight over time in block 2 for three host species: mice, canaries, and great tits. The animals were infected with different strains of *B. garinii* on day 0 and infested with *I. ricinus* larvae on days 14 and 28. The great tits were also infested with *I. ricinus* larvae on day 42. Shown are the host species, parameter estimates, standard errors (s.e.), t-statistics (t), and p-values (p).

Host species	Parameters	Estimates	s.e.	t	p
M. musculus	(Intercept)	1.276	0.006	219.65	< 0.001
M. musculus	7 days PI	0.008	0.003	2.32	< 0.001
M. musculus	14 days PI	0.023	0.003	6.69	< 0.001
M. musculus	21 days PI	0.026	0.003	7.68	< 0.001
M. musculus	28 days PI	0.042	0.003	12.36	< 0.001
M. musculus	35 days PI	0.050	0.003	14.71	< 0.001
M. musculus	42 days PI	0.045	0.003	13.39	0.024
S. canaria	(Intercept)	1.322	0.025	53.04	< 0.001
S. canaria	7 days PI	-0.009	0.008	-1.23	0.007
S. canaria	14 days PI	-0.021	0.008	-2.80	< 0.001
S. canaria	21 days PI	-0.032	0.008	-4.23	< 0.001
S. canaria	28 days PI	-0.040	0.008	-5.23	< 0.001
S. canaria	35 days PI	-0.037	0.008	-4.82	0.028
S. canaria	42 days PI	-0.017	0.008	-2.25	0.224
P. major	(Intercept)	1.212	0.009	140.24	< 0.001
P. major	7 days PI	0.009	0.004	2.02	< 0.001
P. major	14 days PI	-0.016	0.004	-3.82	< 0.001
P. major	21 days PI	-0.018	0.004	-4.23	< 0.001
P. major	28 days PI	-0.020	0.004	-4.69	0.025
P. major	35 days PI	-0.010	0.004	-2.31	0.608
P. major	42 days PI	0.002	0.004	0.52	0.090
P. major	49 days PI	0.007	0.004	1.73	0.049

Table 11. Recovery of immature *I. ricinus* ticks from the vertebrate hosts. The sample size (N) refers to the number of hosts that were infected with *B. burgdorferi* sl. Shown are the block, host, infestation, sample size, total of larvae collected, mean larvae collected per animal (mean ± sd), and range.

Block	Host	Infestation	N	Total larvae	Larvae per animal	Range
1	Mouse	1	10	631	63.1 ± 20.3	38 – 100
1	Mouse	2	10	596	59.6 ± 21.75	29 – 110
1	Canary	1	10	682	68.2 ± 24.4	35 – 105
1	Canary	2	10	980	98.0 ± 17.37	61 – 116
2	Mouse	1	10	308	30.8 ± 25.34	3 – 80
2	Mouse	2	10	423	42.3 ± 12.88	20 – 65
2	Canary	1	10	677	67.7 ± 15.62	45 – 90
2	Canary	2	10	1129	112.9 ± 25.9	73 – 160
2	Great tit	1	8	643	80.38 ± 27.72	38 – 121
2	Great tit	2	8	611	76.38 ± 29.43	30 – 116
2	Great tit	3	8	342	42.75 ± 18.43	11 – 67

Table 12. Weights for immature *I. ricinus* ticks that fed on different host species during the first and second infestation. Shown are the block, tick stage, host, infestation, host sample size, tick sample size, mean weight, 95% confidence interval lower limit (LL95%), and 95% confidence interval upper limit (UL95%).

Block	Tick stage	Host	Infestation	N host	N ticks	Mean (ug)	LL95%	LL95%
1	nymph	Mouse	1	10	50	0.222	0.212	0.233
1	nymph	Mouse	2	10	50	0.220	0.210	0.231
1	nymph	Canary	1	10	50	0.220	0.210	0.230
1	nymph	Canary	2	10	50	0.218	0.208	0.228
2	larva	Mouse	1	10	92	0.554	0.540	0.567
2	larva	Mouse	2	10	100	0.542	0.529	0.556
2	larva	Canary	1	10	99	0.510	0.498	0.523
2	larva	Canary	2	10	99	0.500	0.488	0.512
2	larva	Great tit	1	8	78	0.564	0.549	0.580
2	larva	Great tit	2	8	80	0.553	0.538	0.568
2	nymph	Mouse	1	10	47	0.219	0.207	0.231
2	nymph	Mouse	2	10	53	0.208	0.197	0.220
2	nymph	Canary	1	10	50	0.223	0.211	0.235
2	nymph	Canary	2	10	50	0.212	0.201	0.224
2	nymph	Great tit	1	8	40	0.235	0.222	0.249
2	nymph	Great tit	2	8	40	0.224	0.211	0.237

Table 13. Mean difference in weight of engorged *I. ricinus* larvae between three host species for the first and second larval infestations. Shown are the infestation, host comparison, mean difference, 95% confidence interval lower limit (LL95%), 95% confidence interval upper limit (UL95%), and the p-value (p).

Block	Stage	Infestation	Host comparison	Mean difference	LL95%	UL95%	p
1	Nymph	1	M – C	-0.026	-0.003	0.055	0.072
1	Nymph	2	M – C	0.020	-0.051	0.016	0.201
2	Larva	1	M – C	0.022	0.004	0.041	0.017
2	Larva	1	M – G	-0.031	-0.051	-0.011	0.002
2	Larva	1	G – C	0.053	0.033	0.074	< 0.001
2	Larva	2	M – C	0.043	0.021	0.064	< 0.001
2	Larva	2	M – G	-0.014	-0.009	0.037	0.305
2	Larva	2	G – C	0.029	0.006	0.052	0.013
2	Nymph	1	M – C	-0.041	-0.089	0.007	0.104
2	Nymph	1	M – G	-0.081	0.028	0.133	0.002
2	Nymph	1	G – C	0.040	-0.013	0.092	0.166
2	Nymph	2	M – C	-0.020	-0.012	0.051	0.284
2	Nymph	2	M – G	-0.022	-0.056	0.013	0.283
2	Nymph	2	G – C	-0.002	-0.036	0.033	0.991

M = Mice, C = Canaries, G = Great tits

Table 14. Plasmid profiles for the 8 strains of *B. afzelii* and the 10 strains of *B. garinii*. PCR was used to determine the presence of the following 9 plasmids: lp17, lp 28-2, lp 28-3, lp 28-8, lp 38, lp 54, cp 32-10, *adeC*, *pncA*. The '+' and '-' symbols indicate whether a plasmid was present or absent for a given strain.

Genospecies	Strains ID	MLST	oMG	Plasmids	lp 17	lp 28-2	lp 28-3	lp 28-8	lp 38	lp 54	cp 32-10	*adeC*	*pncA*
B. afzelii	NE1857	327	A1	7	-	+	+	-	+	+	+	+	+
B. afzelii	NE1827	20	A2	3	-	-	-	-	+	+	-	+	-
B. afzelii	NE4556	347	A9	8	+	+	+	+	+	+	+	+	-
B. afzelii	NE4049	679	A10	9	+	+	+	+	+	+	+	+	+
B. afzelii	NE4832	354	A11	8	-	+	+	+	+	+	+	+	+
B. afzelii	NE4558	72	A14	5	-	-	-	-	+	+	+	+	+
B. afzelii	NE4779	72	A14	5	-	-	-	-	+	+	+	+	+
B. afzelii	Fin-JyV-A3	676	A3	6	-	-	-	+	+	+	+	+	+
B. garinii	NE5135	246	G2	3	-	-	-	-	+	-	-	+	+
B. garinii	NE4554	244	G6	4	-	-	-	-	+	+	-	+	+
B. garinii	NE1845	244	G6	4	-	-	-	-	+	+	-	+	+
B. garinii	NE4891	180	G8	4	-	-	-	-	+	+	-	+	+
B. garinii	NE1883	87	G8	4	-	-	-	-	+	+	-	+	+
B. garinii	NE5245	82	G9	4	-	-	-	-	+	+	-	+	+
B. garinii	NE1879	82	G9	3	-	-	-	-	+	-	-	+	+
B. garinii	NE5158	82	G9	4	-	-	-	-	+	+	-	+	+
B. garinii	NE4907	88	G14	4	-	-	-	-	+	+	-	+	+
B. garinii	NE5308	90	G14	2	-	-	-	-	+	-	-	+	-
	PC			9	+	+	+	+	+	+	+	+	+
	NC			0	-	-	-	-	-	-	-	-	-

PC = Positive control; NC = Negative control

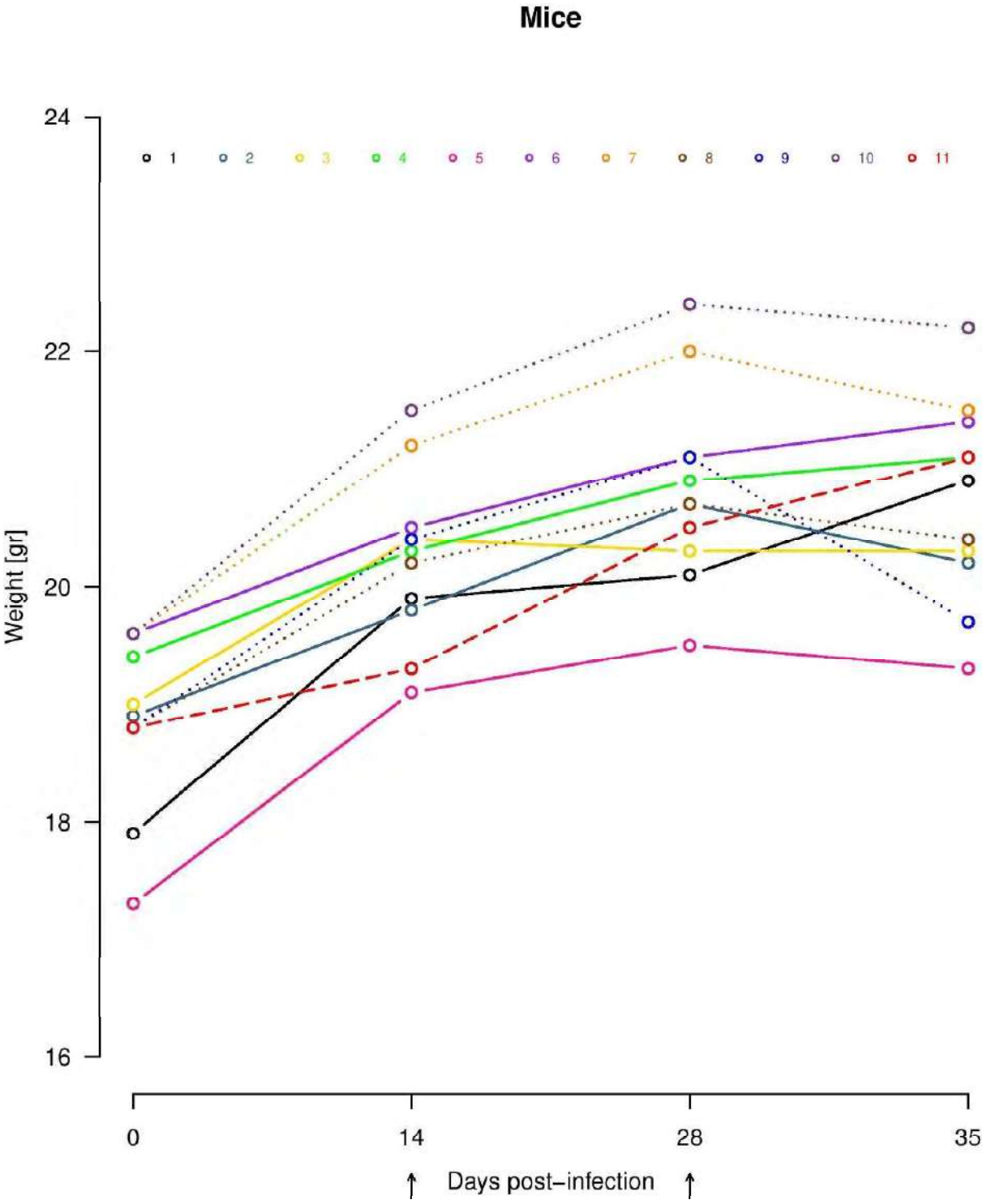

Figure 1. The weight of the mice increased over the course of block 1. The mice were infected with different strains of *B. afzelii* on day 0 and infested with *I. ricinus* larvae on days 14 and 28 (shown by the arrows). Following the infectious challenge with *B. afzelii*, 4 mice (M7, M8, M9, and M10) became infected (dotted lines), and 6 mice (M1, M2, M3, M4, M5, and M6) remained uninfected (solid lines). The control mouse (M11) was inoculated with BSK-H medium (red dashed line).

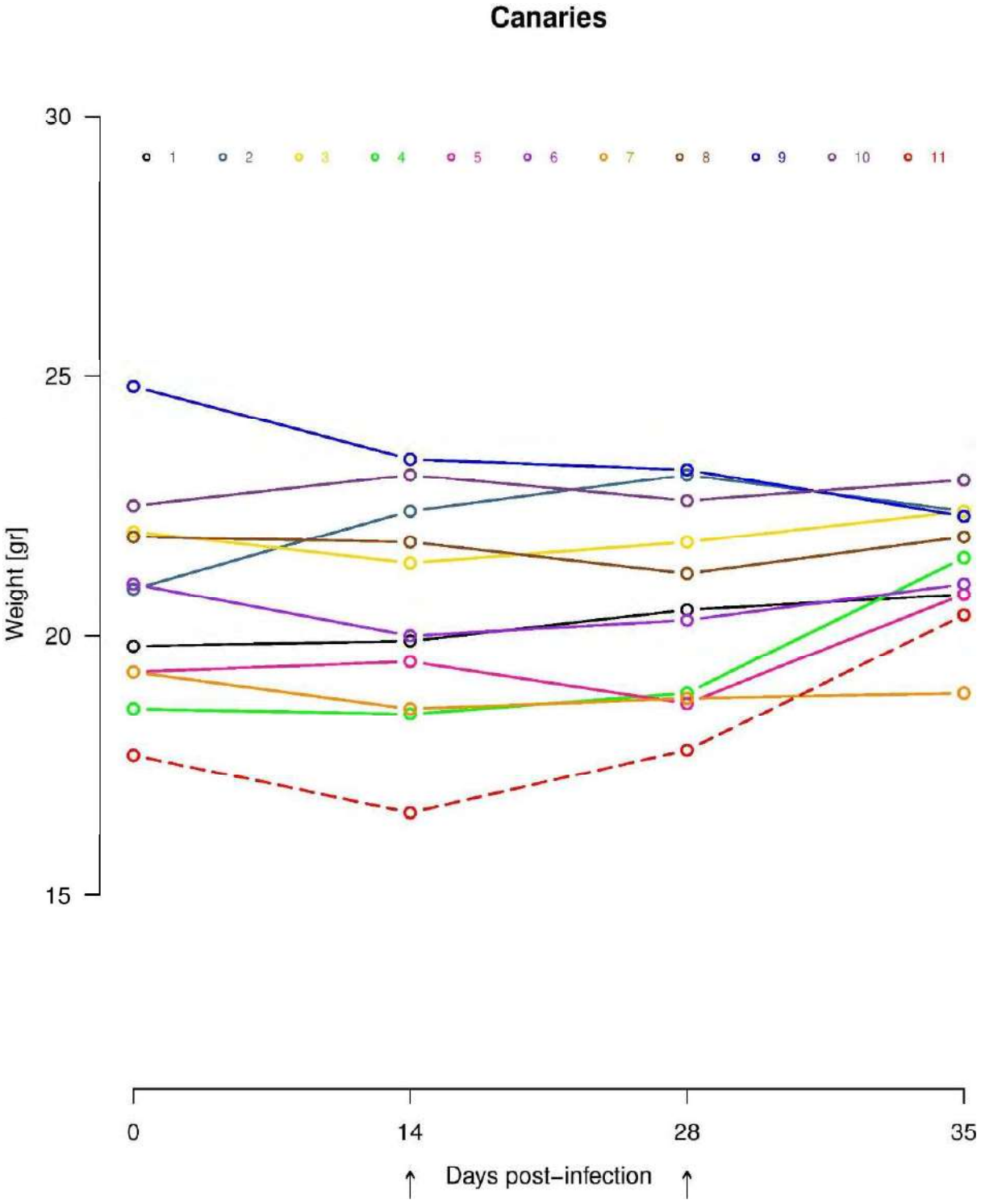

Figure 2. The weight of the canaries decreased over the course of block 1. The canaries were infected with different strains of *B. afzelii* on day 0 and infested with *I. ricinus* larvae on days 14 and 28 (shown by the arrows). Following the infectious challenge with *B. afzelii*, all 10 canaries (C1, C2, C3, C4, C5, C6, C7, C8, C9, and C10) remained uninfected (solid lines). The control canary (C11) was inoculated with BSK-H medium (red dashed line).

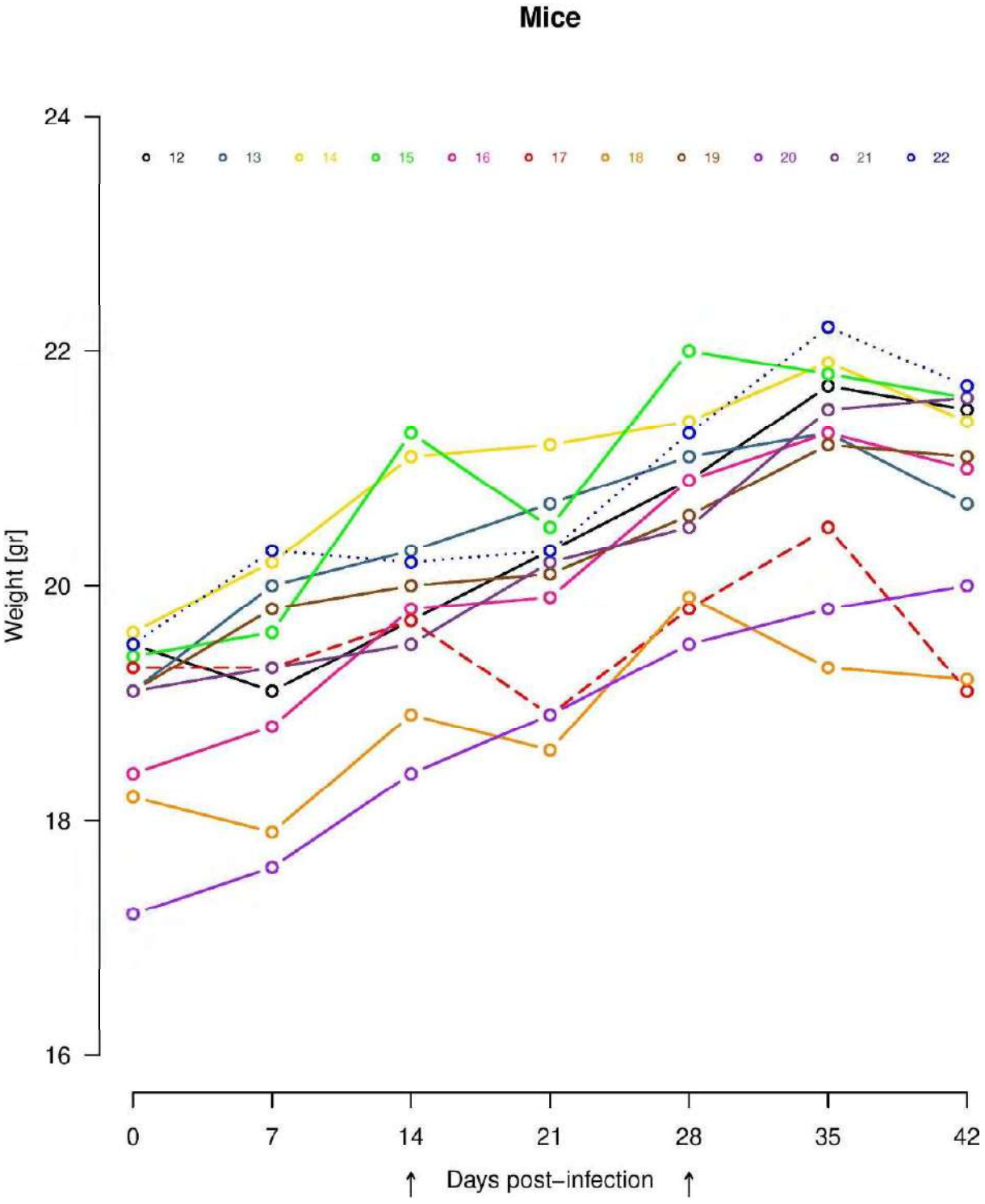

Figure 3. The weight of the mice increased over the course of block 2. The mice were infected with different strains of *B. garinii* on day 0 and infested with *I. ricinus* larvae on days 14 and 28 (shown by the arrows). Following the infectious challenge with *B. garinii*, 1 mouse (M22) became infected (dotted line), and 9 mice (M12, M13, M14, M15, M16, M18, M19, M20, and M21) remained uninfected (solid lines). The control mouse (M23) was inoculated with BSK-H medium (red dashed line).

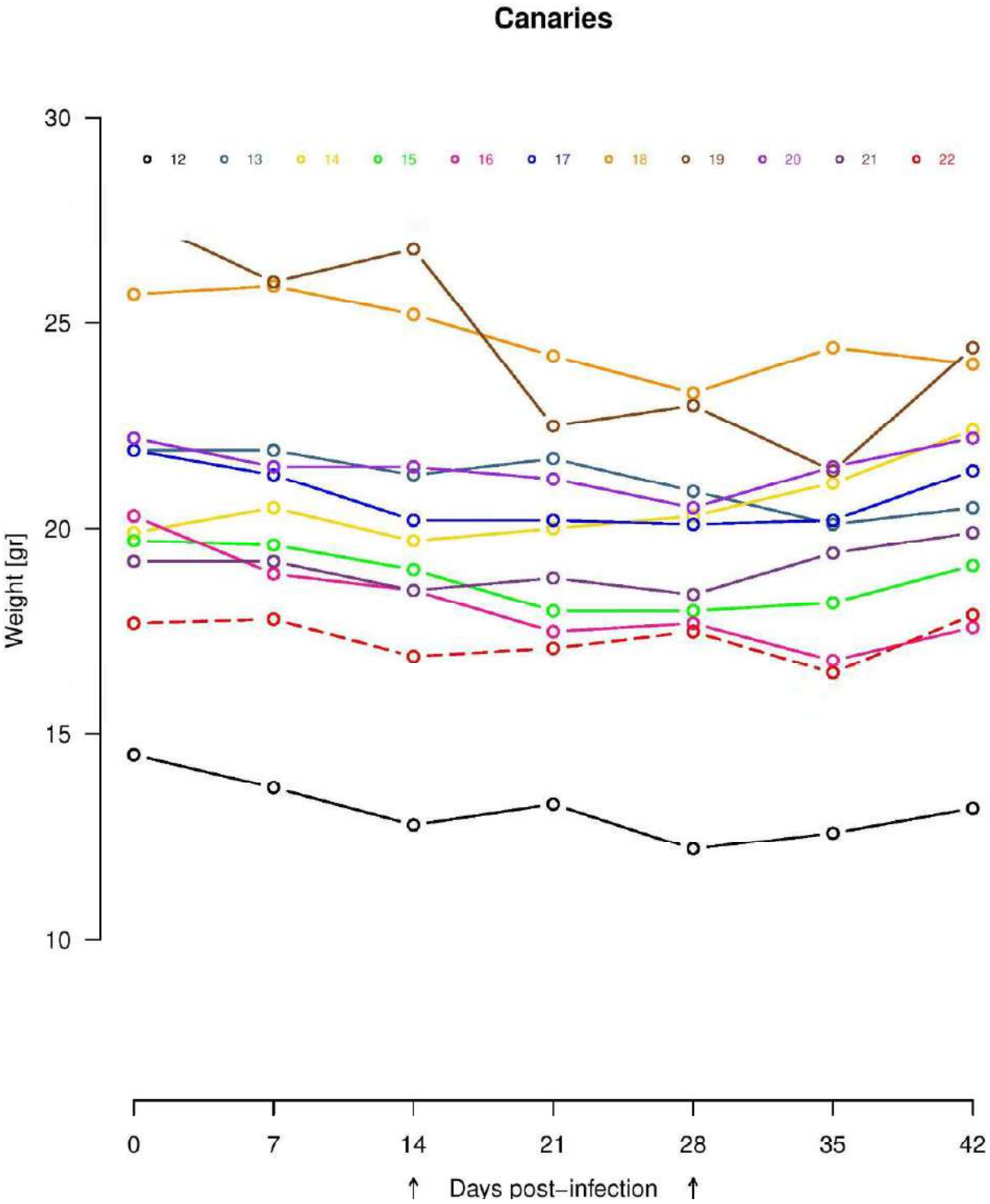

Figure 4. The weight of the canaries decreased over the course of block 2. The canaries were infected with different strains of *B. garinii* on day 0 and infested with *I. ricinus* larvae on days 14 and 28 (shown by the arrows). Following the infectious challenge with *B. garinii*, all 10 canaries (C12, C13, C14, C15, C16, C17, C18, C19, C20, and C21) remained uninfected (solid lines). The control canary (C22) was inoculated with BSK-H medium (red dashed line).

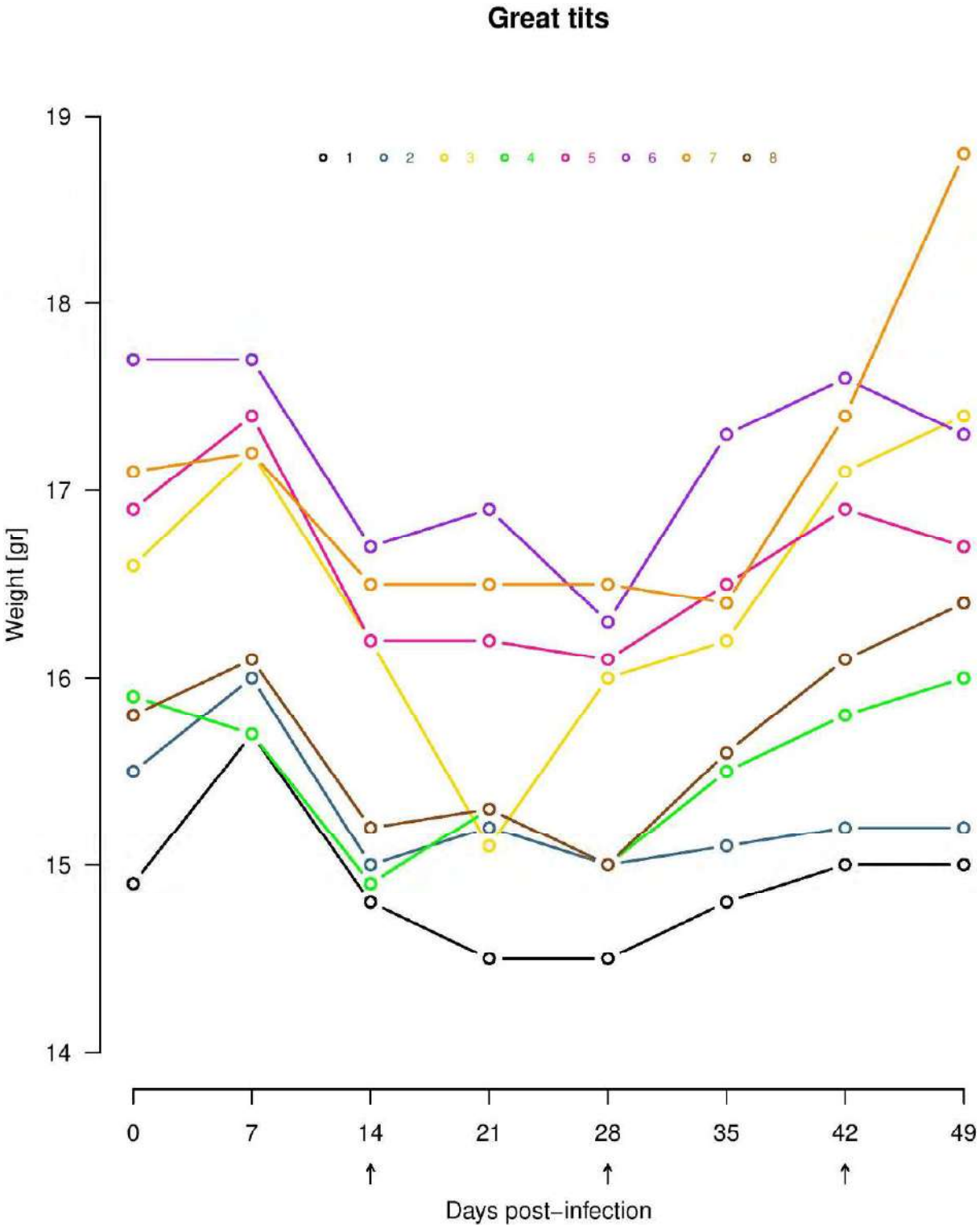

Figure 5. The weight of the great tits first decreased and then increased over the course of block 2. The great tits were infected with different strains of *B. garinii* on day 0 and infested with *I. ricinus* larvae on days 14, 28, and 42 (shown by the arrows). Following the infectious challenge with *B. garinii*, all 8 great tits (G1, G2, G3, G4, G5, G6, G7, and G8) remained uninfected (solid lines).

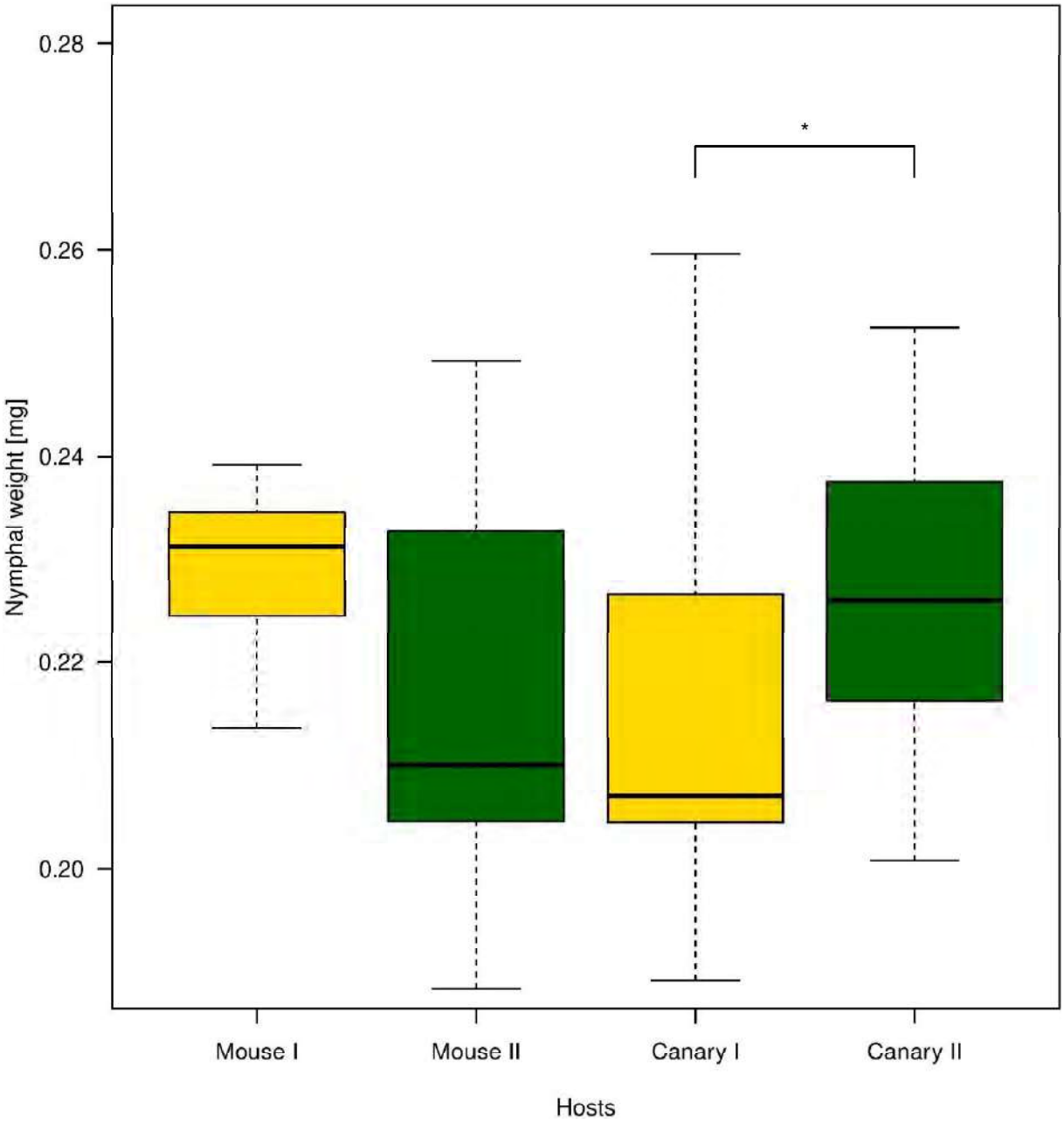

Figure 6. The weights of the unfed *I. ricinus* nymphs are shown for host species and infestation in block 1. The yellow and green boxes represent the first and second infestations, respectively. Shown are the medians (black lines), the upper and lower quartiles (edges of the box), the minimum and maximum values (whiskers), and the outliers (circles) for each combination of host and infestation.

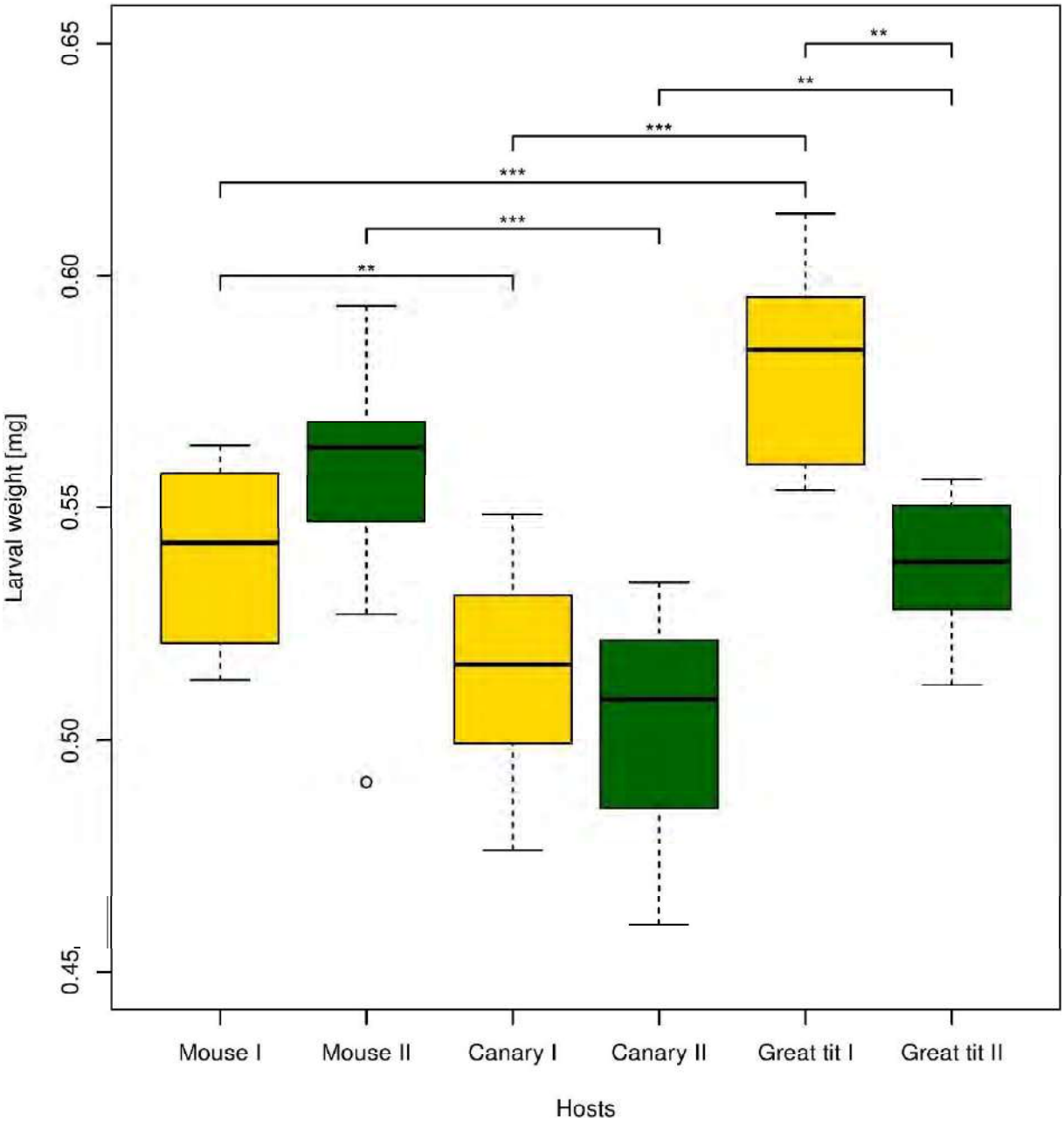

Figure 7. The weights of the engorged *I. ricinus* larvae depend on host species and infestation in block 2. The yellow and green boxes represent the first and second infestations, respectively. Shown are the medians (black lines), the upper and lower quartiles (edges of the box), the minimum and maximum values (whiskers), and the outliers (circles) for each combination of host and infestation.

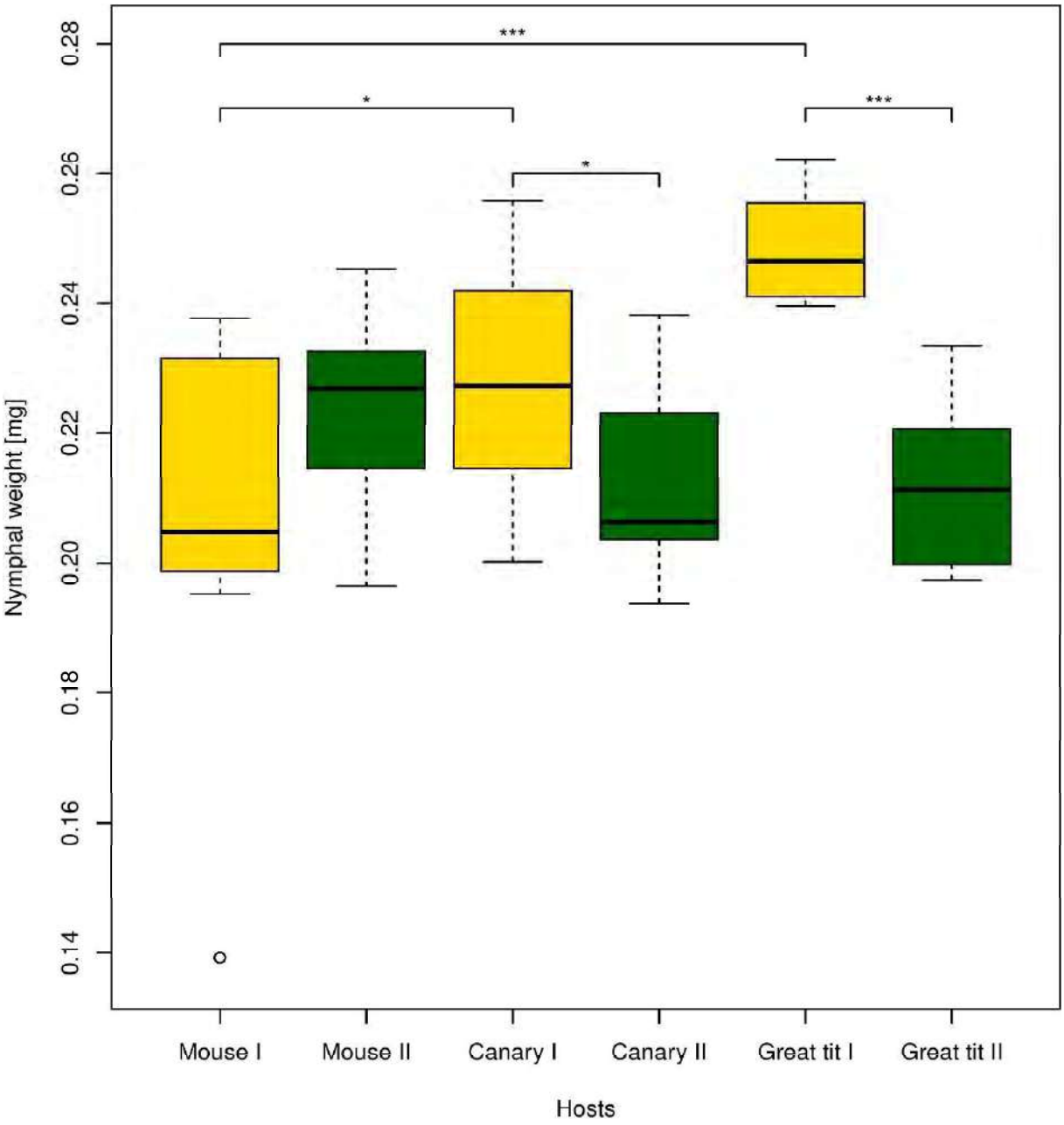

Figure 8. The weights of the unfed *I. ricinus* nymphs depend on host species and infestation in block 2. The yellow and green boxes represent the first and second infestations, respectively. Shown are the medians (black lines), the upper and lower quartiles (edges of the box), the minimum and maximum values (whiskers), and the outliers (circles) for each combination of host and infestation.

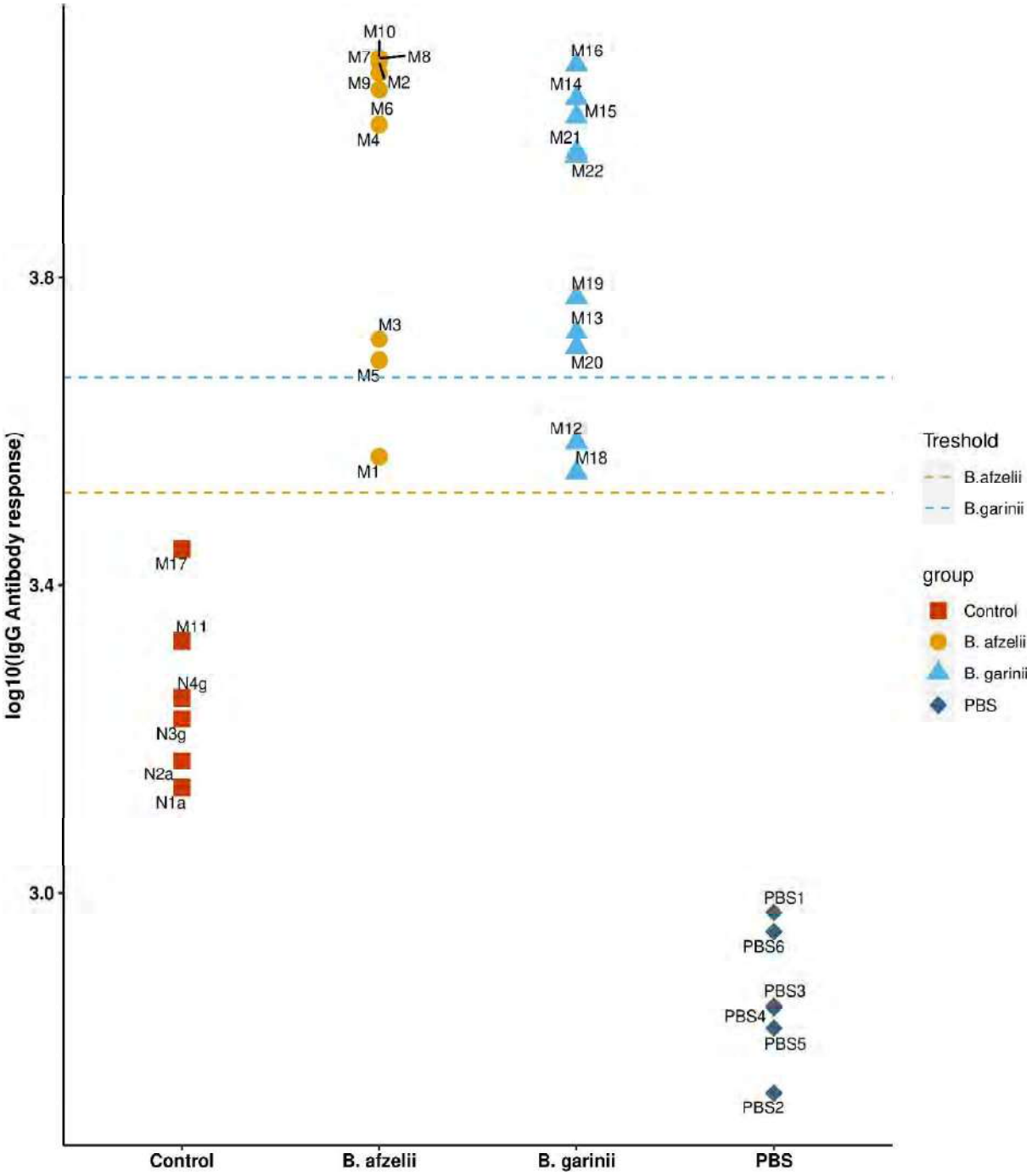

Figure 9. The log10-transformed *B. burgdorferi* sl-specific IgG antibody responses of the BALB/c mice that were inoculated with strains of *B. afzelii* or *B. garinii*. The control group contains 2 control BALB/c mice inoculated with BSK-H medium (M11, M17) and 4 uninfected BALB/c mice from another experiment (N1a, N2a, N3g, N4g). The 10 mice in the *B. afzelii* group were each inoculated with 8 different strains of *B. afzelii* (strains NE1857 and NE4049 were used twice). The 10 mice in the B. garinii group were each inoculated with 10 different strains of *B. garinii*. The PBS group shows the background absorbance in wells that were incubated with PBS instead of mouse serum (PBS1, PBS2, PBS3, PBS4, PBS5, PBS6). The

threshold value that determines whether a mouse was exposed to *B. burgdorferi* sl is shown by the horizontal line.

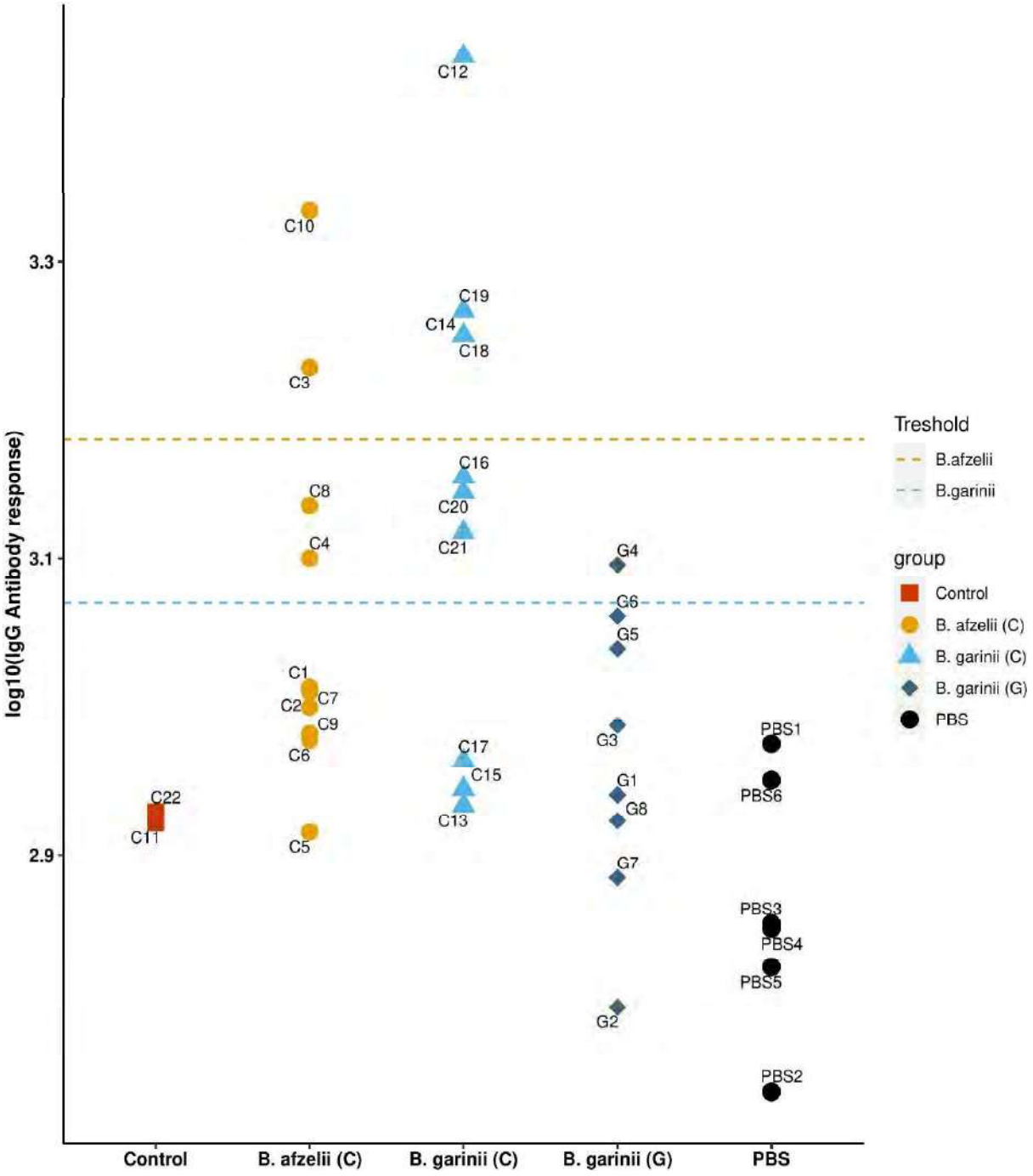

Figure 10. The log10-transformed *B. burgdorferi* sl-specific IgY antibody responses of the birds that were inoculated with strains of *B. afzelii* or *B. garinii*. The control group contains 2 control canaries injected with BSK-H medium (C11, C22). The 10 canaries in the *B. afzelii* group were each inoculated with 8 different strains of *B. afzelii* (strains NE1857 and NE4049 were used twice). The 10 canaries in the *B. garinii* group were each inoculated with 10 different strains of *B. garinii*. The 8 great tits in the *B. garinii* group were each inoculated with 8 different strains of *B. garinii* (strains NE5245 and NE1879 were excluded). The PBS group shows the background absorbance in wells that were incubated with PBS instead of bird serum (PBS1,

PBS2, PBS3, PBS4, PBS5, PBS6). The threshold value that determines whether a bird was exposed to *B. burgdorferi* sl is shown by the horizontal line.

8 General discussion

This PhD thesis allowed us to better understand the ecological factors that influence the seasonal and inter-annual abundance of *I. ricinus* ticks and their tick-borne pathogens on Chaumont Mountain, Switzerland. This work addresses three main subjects: (1) The effect of masting events on the population ecology of *I. ricinus* ticks, (2) the origin and dynamics of the bimodal phenology of *I. ricinus* ticks, and (3) the effect of climate on the questing behaviour and life history traits of *I. ricinus* ticks.

8.1 Effect of masting on the population ecology of I. ricinus ticks

Beech masting events were always found to be an extremely important factor for the population ecology of nymphal *I. ricinus* ticks on Chaumont Mountain. In Chapters 1 and 2, beech masting index drive the inter-annual variation in the DON and the DIN of *I. ricinus* nymphs with a 2-year time lag [227, 228]. In Chapter 3, different time lags of masting events drive the inter-annual variation in the densities of *I. ricinus* nymphs in the spring and fall of the same calendar year [229]. The importance of masting for the ecology of Lyme borreliosis was first discovered by Ostfeld and colleagues in the eastern USA where the blacklegged tick (Ixodes scapularis) is the tick vector [47, 120, 122]. These studies found that there was a 2-year time lag between inter-annual variation in the masting of oak trees (*Quercus rubra*, *Quercus prinus*, *Quercus alba*) and inter-annual variation in the DON of *I. scapularis* nymphs [47, 120, 122]. The chain of causality is as follows: mast seeding in year y increases the abundance of small mammals, deer, and larval ticks in year y + 1 [47, 107, 108, 111, 118-121, 130, 131]. Higher densities of larval ticks coincide with and feed on higher densities of small mammals in year y + 1, which in turn increases the abundance of nymphs in year y + 2 [47, 120, 122, 123, 133, 230, 231]. In Europe, there is a growing body of evidence that masting events of deciduous trees influence the density of rodents, which in turn influences the density of ticks, the density of ticks infected with tick-borne pathogens, and the incidence of tick-borne diseases in the human population. An 18-year study in central Europe found a strong correlation between rodent densities in year *y* and tick-borne diseases (Lyme disease and tick-borne encephalitis) in year *y* + 1, but did not demonstrate a direct link to ticks or tree seed production [232]. A 3-year study in the Netherlands artificially manipulate the rodent densities by either acorn addition or rodent removal in a natural habitat and found a strong correlation between mast seeding in year *y* and rodent densities in year *y* + 1, and between rodent densities in year *y* + 1 and the DIN in year *y*

+ 2, but this study did not find any correlation between mast seeding in year *y* and the DIN in year *y* + 2 [231]. The principle advantage of these manipulative studies is that they can control a particular factor to determine if such manipulation generates a significant change. By controlling extraneous influences, any change observed is presumed to be caused by the variable that has been manipulated (e.g., dissecting cause-and-effect). However, variation due to other factors may be important but remain excluded from the study, thus masking the importance of the phenomenon over time. For example, fluctuations in abundance of other vertebrate hosts affecting seasonal activity of both rodents and ticks that were not account for in the Dutch study might explain the lack of direct link between mast seeding and the DIN in year y + 2. A 10-year study in the Netherlands found that the mast scores of the common oak (*Quercus robur*) and beech (*Fagus sylvatica*) in year *y* had a negative effect on larvae, nymphs and adults in year *y* + 1 [74]. In this case, even though tree mast score increased host density, higher host density could result in higher rate at which ticks are removed from the vegetation and hence become unavailable for cloth dragging [233], which could potentially explain this counter-intuitive result. A 9-year study in Germany found a 2-year time lag between the masting of beech trees (*Fagus sylvatica*) and the DON, but did not measure the DIN [50]. A 7-year study in Poland found the expected 2-year time lag between mast seeding of oak trees (*Quercus robur*, *Quercus petraea*) and the incidence of Lyme borreliosis, but the causal link between tree seed production and nymphal abundance was not demonstrated [234]. In summary, numerous studies have shown the links between masting, rodent density, the density of ticks, the risk and incidence of tick-borne disease, although no study has shown all of the links. My PhD thesis has made an important contribution to this literature by demonstrating that masting events of deciduous trees are strongly associated with the inter-annual variation of the DON and DIN of *I. ricinus* tick in Europe, which in turn determines the human risk of tick-borne diseases two years later [234].

Masting by beech trees did not influence the NIP in our study, and this result is both in agreement and in conflict with previous studies [47, 120]. The effects of masting and rodent density on the NIP are complex and counterintuitive. Theoretical models have shown that the R_0 of tick-borne diseases depends on the ratio of nymphs to hosts [87] and on the aggregation of immature ticks on the same host, which ensures horizontal transmission from infected nymphs to uninfected larvae [88]. In the year following a masting event, the rodent host population is expected to increase dramatically, but the density of infected nymphs that will feed on those rodents was determined by the conditions in the previous year (i.e., the year of the masting event when rodent density was 'normal'). Field studies have shown that when the

rodent density increases relative to the density of immature ticks, the mean burden of ticks on rodent hosts decreases [101, 133, 235], which reduces horizontal transmission of *B. burgdorferi* between nymphs and larvae. Thus, masting in year y, will decrease the ratio of infected nymphs to hosts and the aggregation of immature ticks on infected hosts in year $y + 1$, and both effects are expected to reduce the NIP in year $y + 2$ when the DON is expected to increase dramatically. However, if the proportional increase in the DON is larger than the proportional decrease in the NIP, the DIN is still expected to increase 2 years after a masting event. In the present work, the relationship between masting and the DIN was much less strong than the relationship between masting and the DON. Obviously, it is possible that this relationship is biological reality but we believed, however, that it is caused by experimental error. A simple DNA extraction method is often used to extract *Borrelia* DNA from ticks by boiling them in ammonium hydroxide (NH_4OH). This extraction method was originally developed by Guy and Stanek [236]. According to a meta-analysis, this simple DNA extraction method is used in many reported papers [237]. However, this method is not adapted for long-term storage of DNA as the resultant extraction is supposed to be boiled with the tubes opened for a certain amount of time to allow the ammonia to evaporate. In contrast, commercial DNA extraction kits contain elution solutions that are optimized for long-term DNA storage. In the present work, *Borrelia* DNA was extracted following the simple extraction method and the resultant DNA extractions were stored in this poor DNA storage solution for an average of 2.4 years prior to detection of *B. burgdorferi* sl using RLB (some DNA extractions were stored for as long as 13.8 years prior to RLB). Consequently, we found that the time interval between the date of tick sampling and the RLB (e.g., RLB time lag) had a large negative effect on the NIP and by extension, a moderately negative effect on the DIN. We believe that the DNA in these crude DNA extractions degraded over time, which decreased the ability of the RLB to detect *B. burgdorferi* sl infection in the ticks. The sensitivity of the RLB is comparable to a widely used qPCR assay that can detect a variety of *B. burgdorferi* sl genospecies [238]. In this method, the variable spacer region between 2 repeated copies of the 23S and 5S ribosomal genes is amplified using conventional PCR. The resultant amplicon is then hybridized with genospecies-specific DNA probes, which can detect the multiple *B. burgdorferi* sl genospecies present in the tick. The sensitivity of the RLB blots was repeatedly tested over the course of the study by using the DNA from isolates of the six *B. burgdorferi* sl genospecies cultured in BSK media as positive controls. However, these isolates were grown up fresh from frozen stocks when needed, and they were therefore unable to detect the DNA degradation over time in the whole tick DNA extractions. For future studies, one solution to check for DNA degradation over time is to repeatedly test known

positive controls that are stored in the same freezers as the study samples over the duration of the study. Another solution is to process all the tick DNA extractions with respect to pathogen detection in a timely manner; for example, within a one-year window. We suspect that a second type of experimental error occurred with respect to the DNA extractions of the ticks. The NH_4OH solution has a shelf life of 2 years if not opened and stored at room temperature [239]. Olivier Rais who extracted the DNA purchased three different bottles of NH_4OH solution over the 15-year duration of the study period suggesting that DNA extractions in 9 of 15 years were done with expired tick lysis solution, which would have reduced the efficacy of DNA extraction. The fact that we felt that RLB data might not have been entirely reliable retain us from further exploring these data. For example, we expected that beech masting would increase food for rodents and that rodent-associated *Borrelia* genospecies (e.g., *B. afzelii*) should increase in the 2 years following a mast year, but this was not the case. In summary, these methodological errors reduced our ability to detect *B. burgdorferi* sl, and made it more difficult for our study to identify the ecological factors that drive inter-annual variation in the DIN and hence the risk of Lyme borreliosis.

Inter-annual variation in the densities of *I. ricinus* nymphs in the spring and fall of the same calendar year were best explained by different time lags of masting events on Chaumont Mountain (Chapter 3). Contrasting with our previous findings for the annual DON and DIN in Chapters 1 and 2, it suggests that the spring peak and the fall peak in year *y* represent different cohorts of ticks that were born in different calendar years. For the spring peak, the consensus is that it consists of larvae that obtained their blood meal the previous summer, moulted into nymphs, entered behavioural diapause, overwintered as unfed nymphs, and quested the following spring [18, 38, 151]. Because masting in year *y* increases the density of mice and larval feeding success in year $y + 1$, which in turn increases the DON in the spring of year $y + 2$, the expected 2-year time lag between beech masting and the spring nymphal was confirmed. Unexpected was our finding that inter-annual variation in the fall peak was best predicted by the beach masting index 1 year prior. This result provides strong evidence for the direct development hypothesis [38, 83, 143, 145, 151], which predicts a 1-year time lag between beech masting and the fall nymphal peak; masting in year *y* increases the density of mice and larval feeding success in year $y + 1$, the larvae moult into nymphs and quest in the same year that they obtained their larval blood meal, which increases the DON in the fall of year $y + 1$. In contrast, the developmental diapause hypothesis [18, 38, 151] predicts a 2-year time lag between beech masting and the fall nymphal peak; masting in year *y* increases the density of mice and larval feeding success in year $y + 1$, but larvae that obtain their blood meal in late summer have to

overwinter as engorged larvae, moult in the summer, and quest in the fall of year $y + 2$. A seminal review on diapause in *Ixodes* ticks suggested that both hypotheses could account for the fall nymphal peak, but this review appeared to favour the developmental diapause hypothesis over the direct development hypothesis [18]. In contrast, the analysis of our long-term data set in Chapter 3 (14 years) found strong evidence that the direct development hypothesis is the best explanation for the fall peak of *I. ricinus* nymphs.

The direct development hypothesis also implies that the fall nymphs are younger compared to the spring nymphs, which agrees with studies comparing the fat content between these two types of nymphs in our study area and elsewhere [38, 240]. Fat is a non-renewable source of energy derived from each blood meal that ticks use to quest for hosts and to maintain their water balance [21, 23, 25]. Because *I. ricinus* ticks feed once per life stage and have no other energy sources, their fat content can be used as a relative measure of their current age and future longevity [23, 38, 141]. Studies on field-collected *I. ricinus* nymphs in Neuchâtel and the UK have shown that fall nymphs have higher fat content than spring nymphs [38, 240]. This phenomenon can be explained by the direct development hypothesis; fall nymphs obtained their larval blood meal earlier that summer and their fat content is high because they are young (~3 months since the larval blood meal) with little time to burn their fat reserves. In contrast, spring nymphs obtained their larval meal the previous summer and their fat content is low because they are older (~9 months since the larval blood meal) with more time to burn their fat reserves. Thus, the finding that fall nymphs have higher fat reserves than spring nymphs is consistent with our discovery of different time lags (1 year and 2 years) between inter-annual variation in the beech masting and the fall and spring peak of nymphs, and both these results support the direct development hypothesis.

The local composition and abundance of vertebrate hosts greatly affects *Ixodes* tick populations and their tick-borne pathogens [241, 242], because all active tick stages must blood feed to graduate to the next stage in the life cycle [87, 88]. The three *Ixodes* tick stages feed on different types of vertebrate hosts; larvae and nymphs usually feed on small mammals and birds, whereas adult female ticks feed on ungulates [6, 14, 99, 242]. In the present work, we used the beech masting index as an indirect estimate of the abundance of small vertebrate hosts available to feed the larval ticks the following year. The cascading effects of masting on vertebrate hosts have been well documented in rodents [47, 111, 118-121]. However, many vertebrate host species respond to masting occurring in the fall, including carnivores, birds, ungulates and omnivores [117]. Following beech masting years, breeding densities of different species of passerine birds such as great tits (*Parus major*) and true thrushes (*Turdus* spp.) were found to

be significantly higher [117, 243]. In North-America, white-tailed deer (*Odocoileus virginianus*) were found to increase their home range to incorporate acorn-producing areas during masting [128] and which are known to be important host for *I. scapularis* adult female ticks [244]. Similarly, red deer (*Cervus elaphus*) and roe deer (*Capreolus capreolus*) are the most important hosts for the *I. ricinus* adult female ticks [245]. The role of masting in diet-switching and body condition of roe deer was established [246, 247]. However, the role of masting fruits in the recruitment of roe deer to masting areas still need to be assessed. Future studies should investigate whether other vertebrate hosts respond to masting and how this could impact the abundance of *Ixodes* ticks. Vertebrate hosts can also differ extensively in their ability to harbour and transmit *B. burgdorferi* sl infections to feeding *Ixodes* larval ticks [14, 91, 98-100]. Field studies on *I. ricinus* in Europe and on *I. scapularis* in North America have shown that the density of rodent reservoir hosts plays a critical role in determining larval feeding success, and hence the DON and the DIN in the following year [47, 120, 122, 123, 133, 230, 231]. Host blood meal analyses of unfed *I. ricinus* nymphs at our field site have shown that they obtain their larval blood meal from a variety of vertebrate hosts including rodents, birds, carnivores, and ungulates [95]. As discussed above, the abundance of several of these vertebrate hosts are higher following a masting year (e.g., rodents, passerine birds). Being more abundant in the environment, larval ticks are more likely to feed on rodents and passerine birds than other vertebrate hosts. Consequently, one might argue that rodent and passerine bird DNA would be more often detected in nymphal ticks the following year compared to vertebrate hosts that do not respond to masting. However, data on the vertebrate host community are the missing link in this work and would have undoubtedly enhanced the ability of our models to explain seasonal and inter-annual variation in the density of ticks and their associated tick-borne pathogens on Chaumont Mountain.

8.2 Origin and dynamics of the bimodal phenology of *I. ricinus* ticks

Given the importance of *I. ricinus* as a disease vector, forecasting the density of ticks questing for hosts is important for managing the risk of tick-borne diseases [50, 135-137, 227, 228, 248]. In Europe, there is much interest to determine which ecological factors influence the seasonal and inter-annual abundance of *I. ricinus* ticks [50, 227]. In Europe, a wide variety of countries reported a bimodal phenology for *I. ricinus* nymphs with a large spring peak followed by a smaller peak (Table 1). A unimodal phenology for *I. ricinus* nymphs has also been reported from diverse part of Europe but this pattern seems to occur at high elevations or northern latitudes (Table 1). The unimodal phenology occurs in places with a short cool summer, which

does not give larvae enough time to acquire a blood meal, moult into nymphs, and quest in the same calendar year [38, 249]. In contrast, the bimodal phenology occurs in places with a long warm summer, which accelerates the development of engorged larvae into unfed nymphs and causes a second peak of nymphal activity in the fall [38, 249]. The seasonal phenology of nymphal *I. ricinus* ticks at Chaumont Mountain was found to be bimodal, where a large peak in spring is followed by a smaller peak in fall. This bimodal phenology occurred at the three lower elevation sites, whereas a unimodal phenology with a single large peak in the spring occurred at the top elevation site. The unimodal phenology at the top elevation site is consistent with the direct development hypothesis. At the top elevation site, tick development rates are slower because of cooler temperatures; as a result, no nymphs undergo direct development (i.e., obtain their larval blood meal, moult into unfed nymphs and quest in the same calendar year), and there is no fall peak of nymphs.

Consistent with the differentiation between the bimodal phenology at low elevations and the unimodal phenology at the high elevations in Europe (Table 1), nymphs started questing earlier at the low elevation site compared to the higher elevation sites. The nymph peak in spring occurred in April for the low site whereas it occurred in May at the medium, high, and top elevation sites. This result is probably also true for the larvae. If larvae start questing earlier at the low site, they are more likely to obtain their blood meal earlier and thus have more time to moult into nymphs, which would increase the size of the fall peak. Conversely, if larvae start questing later at the higher elevation sites (e.g., medium, high, and top), they are less likely to obtain their blood meal and have thus less time to moult into nymphs, which would decrease (or even suppress) the size of the fall peak.

Generalized additive models (GAMs) is a modelling approach that allows the user to flexibly model non-linear relationships, using a generalized linear model in which the response variable depends linearly on unknown smoother functions of one or more explanatory variables. The smoother functions are non-parametric and can be used to fit any complex curve. The seasonal phenology of *I. ricinus* ticks follows a bimodal pattern, which make it a challenge for statistical modelling. In Chapters 1 and 2, we avoided this complexity by analysing the total DON and DIN for each year [227, 228] and the same approach was used in a 14-year study in Switzerland that is near our study site [48], in a 10-year study in the Netherlands [74], and in a 13-year study in North America [47]. An 8-year study in Germany used different intercepts for the spring, summer, fall, and winter to deal with the non-linear phenology of *I. ricinus* nymphs [248]. In Chapter 3, we demonstrated that the bimodal non-linear phenology of *I. ricinus* nymphs can be analysed with GAMs. The smoothed function of the calendar day provided an

excellent fit to the seasonal bimodal phenology of *I. ricinus* nymphs. The other explanatory variables (e.g., beech masting score and climate variables) were initially modelled with non-parametric smoothed functions because we did not want to assume a linear function, but were subsequently replaced with parametric functions (e.g., linear or quadratic). We did not want to use smoother functions for all of the explanatory variables because model interpretation is easier for simple parametric functions compared to complex non-parametric functions. In summary, we demonstrated that the bimodal non-linear phenology of *I. ricinus* ticks can be captured by GAMs using a combination of parametric and non-parametric functions of the explanatory variables of interest, and should be used in future studies.

8.3 Effect of climate on the questing behaviour and life history traits of *I. ricinus* ticks

Many theoretical models have predicted that *Ixodes* ticks will increase their distribution and abundance under global warming [43, 250-252]. In Canada and Scandinavia, *Ixodes* ticks have expanded their range towards northern latitudes [41-46]. However, few studies have investigated whether climate change is affecting the abundance of *Ixodes* ticks in areas where they are known to be endemic [47-54]. Such studies are rare because they require decades-long field studies for which it is difficult to obtain scientific funding. The original purpose of this work was to document how climate change is influencing endemic *I. ricinus* tick population abundance across an altitudinal gradient. Our first expectation is that tick abundance would be increasing and more severely at higher elevations due to global warming. Consistent with the first expectation, the abundance of *I. ricinus* nymphs almost doubled from 2004 to 2018 on Chaumont Mountain [227]. This result is a rare demonstration that the abundance of *Ixodes* ticks has increased in a Lyme disease-endemic area. A 15-year study at the Bois de l'Hopital site in Neuchâtel, Switzerland, which is very close to the location of our study sites, found a significant decrease in the abundance of *I. ricinus* nymphs [48]. In that study, questing nymph density increase in spring was strongly limited by an upper threshold of a saturation deficit. This upper limit was exceeded more than a month earlier in 2014 than it was at the beginning of the study in 2000. As a consequence, the duration of favourable period for questing nymph activity is reduced, which may limit their survival, and thus negatively impact nymph abundance over time. In contrast, a 10-year study in the Netherlands found an increase in the abundance of *I. ricinus* larvae and adults, but climate did not have significant effects on the total tick abundance [74]. Similarly, Chapter 1 found no direct links between climate change and the observed doubling in tick abundance. Relative humidity was the climate variable that had the greatest impact on and negatively influenced the DON, but there was no evidence that

it had decreased over the 15-year study period. Conversely, the temperature increased significantly over the 15-year duration of the study (i.e., evidence of directional climate change), and while temperature had a significant and positive effect on the DON, models that contained temperature had low support in our model selection approach. In summary, despite finding a significant increase in temperature and ticks over the 15-year study period, the evidence for a causal link between the two is weak.

Theoretical models of climate change models also predict that warming temperatures will favour the expansion of ticks into colder areas [252, 253]. In Europe, *I. ricinus* populations have shifted their distribution towards higher altitudes [66-72]. Another expectation was that tick abundance would increase more dramatically at the higher elevations. In contrast, we found that the nymphal tick abundance was inversely related to the altitudinal gradient, and that it actually decreased most dramatically at the top elevation site (81.0% over time). One potential explanation is that leisure activities and the number of human visitors have increased on Chaumont Mountain over the last 20 years, with the construction of an outdoor adventure park, which includes a zip line and outdoor laser games, and mountain biking trails [254, 255]. The top elevation site is closest to the zip line park and the start of the mountain biking trails (a distance of 25 m) and is expected to be the most affected, whereas the high, medium, and low elevation sites are much further away (770, 1500, and 2600 m, respectively). The alteration of the forest habitat and subsequent human disturbance caused by the construction and maintenance of these recreational areas since the early 2000's may have reduced the habitat suitability for ticks. Habitat modifications such as clearing bushes along forest trails reduce the abundance of ticks [256-258]. A larger human footprint may also have reduced the abundance of vertebrate hosts by scaring them away. Tick abundance depends on the abundance of large mammals such as deer [6, 132, 259, 260], which are important for feeding adult female ticks. In summary, a plausible explanation for the five-fold decrease in tick abundance at the top elevation site on Chaumont Mountain is that the construction of the outdoor adventure park reduced the habitat quality for ticks and their vertebrate hosts. An interesting alternative explanation is that repeated tick sampling over a period of 15 years decreased the tick population at the top site [83]. Field studies typically assume that dragging removes a small fraction of the available tick population, but this assumption may not be true in habitats where tick density is already low. A study in the United-States sampled nymphal *I. pacificus* ticks on 17 occasions in the same area over a period of 3 weeks [261]. They estimated that the first drag removed 5.9% of the population of nymphs. Likewise, they reported that they had removed 50% of the nymphal population after 13 drags and that only 3 or 4 drags were sufficient to

remove 50% of the adult population. Capture efficiency likely differs between species but if these statistics are similar for *I. ricinus* ticks, it suggests that a substantial percentage (~30%) of the nymphs was being removed at each elevation site from March to August during our study (and perhaps even more for the adult tick population). While the very marked decrease over time at the top elevation might be due to external human disturbance or repeated tick sampling, this result is not without precedent and other studies at this study location have found a negative relationship between tick abundance and altitude [73, 143]. A mechanistic explanation for this phenomenon is the relationship between temperature and tick development rates [36, 77]. At higher and colder elevations, eggs and larvae have much slower development rates, which ultimately reduces the number of larvae that graduate to the nymphal stage [34, 38, 253, 262]. Given the lack of evidence that directional climate change was influencing the directional changes in the DON at the four elevation site, the focus of this work changed especially when we discovered that beech masting and differences in climate between the four elevation sites were important at explaining the variation in tick questing behaviour and tick life history traits (development, survival, reproduction). Consequently, Chapter 3 became much more focused on other aspects of tick ecology.

Ixodes ticks spend ~98% of their time in the environment (e.g., more than a year for *I. ricinus* ticks) [6, 10] and are therefore exposed to seasonal changes in abiotic variables such as temperature, relative humidity, and precipitation. This work found that temperature, relative humidity, and saturation deficit influence the ecology of *I. ricinus* ticks on Chaumont Mountain.

Temperature in the present year (annual or daily) was always found to have a positive effect on the life history traits and questing behaviour of the DON and DIN. In Chapter 1, the field-collected mean annual temperature in the present year had a positive effect on the annual DON [227]. In Chapter 2, the field-collected mean annual temperature in the present year had a positive effect on the DIN [228]. While long-term climate measurements (e.g., annual or seasonal) are more likely to influence tick life history traits (survival, development, and reproduction) and therefore the abundance of ticks, Chapter 3 found that the field-collected temperature on the day of tick sampling had a positive effect on the DON and thus assumed that short-term weather events reflect true variation in tick questing behaviour. Accordingly, temperature on day of sampling did not influence the overall nymphal abundance but increased the fraction of nymphs questing for hosts, which increases the number of questing nymphs captured by our drag sampling. This result agrees with other studies in Europe, where the density of *I. ricinus* ticks was positively correlated with daily temperatures recorded during tick sampling [81, 82, 263, 264]. Altogether, these studies suggest that for any given date, warmer

temperatures increase the proportion of nymphs questing for hosts (i.e., increased nymphal activity levels), which in turn, increase the number of questing nymphs captured by drag sampling. *Ixodes* ticks are known to vary their questing activity in response to their immediate climate conditions. *Ixodes* ticks become active above a minimum threshold temperature of 7.0°C, and questing activity increases with temperature up to a maximum value of 24°C [83] to 30°C (Chapter 3). *Ixodes* ticks are sensitive to desiccation during questing [6], and they make repeated return trips to the litter layer where they can rehydrate and maintain their water balance [20, 22, 37]. For this reason, ticks are also prone to quest under cool and humid conditions (i.e., low SD) [49, 54] and thus reduce their questing activity in hot and dry conditions (i.e., high SD) [23, 83, 84, 265, 266]. The observation that the DON plateaued at ~30°C in Chapter 3 suggests that the *I. ricinus* nymphs at our study site avoid questing at hot (and presumably dry) conditions.

Relative humidity (RH) in the present year (annual or seasonal) was always the most important climate variable for the ecology of *I. ricinus* but its effect (negative or positive) differed among the three studies. In Chapter 1, the field-collected mean annual RH in the present year had a negative effect on the annual DON [227]. In Chapter 2, the weather station mean annual RH in the present year had a negative effect on the DIN [228]. In Chapter 3, the summer RH in the present year had a positive effect on the DON. In accordance with this result, the general wisdom is that *Ixodes* ticks require a high percentage of relative humidity to maintain a stable water balance for increasing their survival [21, 37], which is known to increase with relative humidity [6, 36, 79]. However, a negative relationship between moisture and the abundance of *I. ricinus* nymphs is not without precedent in Europe [81, 82, 263, 264, 267]. One explanation is that humid environments are favourable for the development of entomopathogenic fungi, which can cause high mortality in *Ixodes* ticks [39, 80]. An alternative explanation is that high levels of rainfall inhibit host-seeking activity or cause flooding that reduces tick survival [36, 47]. Both of the explanations seem to support the negative relationships found between the DON and relative humidity in Chapters 1 and 2. The biological reason of the discrepancy between our results for the effect of relative humidity remain uncertain.

Saturation deficit (SD) in the present year (annual or seasonal) had an influence on the DON. It is a combination of temperature and relative humidity and measures the drying power of the atmosphere. In Chapter 1, the field-collected mean annual SD in the present year had a positive effect on the annual DON [227]. In Chapter 3, the relationship between the summer SD in the present year and the DON differed among the four elevation sites. The relationship

was positive linear for the low and high elevation sites, and it was negative quadratic for the medium and top elevation sites. These observations are broadly consistent with the direct development hypothesis, under which the summer SD is expected to have different effects on the spring and fall nymphs. With respect to the spring nymphs, increasing the SD is initially expected to increase the nymphal questing activity (the positive effects of higher temperatures outweigh the negative effects of lower relative humidity). However, the risk of desiccation and death both increase with high SD [84, 268], and at a certain threshold SD value, questing activity and survival will both start to decrease for the spring nymphs (the negative effects of lower relative humidity outweigh the positive effects of higher temperatures). Thus, for the spring nymphs we expect a negative quadratic relationship between SD_{S0} and the DON, as observed at the medium and top elevation sites. With respect to the fall nymphs, a hot and dry summer (high SD) accelerates tick developmental rates, which under the direct development hypothesis, would increase the size of the fall nymphal peak of that calendar year [38, 83, 143, 145, 151].

Finally, our understanding of how climate variables are influencing tick questing behaviour and tick life history traits remain uncertain. First, we have repeatedly encountered the difficulty that capturing questing ticks is a very imperfect way of estimating the tick density. This estimate confounds tick abundance with tick questing behaviour, which both can be influenced by climate. When ticks are not collected in the field, it is difficult to know if it is because their abundance is low or because they are not questing on that particular day. One might thus argue that tick abundance remains the same over the time but the proportion of ticks that are questing is changing. This is obvious in the winter time when ticks are present but not available for sampling (e.g., diapause). One way to separate these issues would be to use quasi-natural conditions, where the total abundance of ticks in the environment is known and the proportion of questing ticks can be observed. In Germany, field plots were used to follow the host seeking activity of *I. ricinus* [139]. Sometimes, as much as 70 – 90% of the existing unfed nymphs and adults were observed questing at the same time (Olaf Kahl, personal communication, October 01, 2021). Although the latter observation supports that most of the ticks quests at the same time and thus are likely to be collected during dragging, some remaining ticks were not observed and suggest that the abundance of questing nymphs, as measured by dragging, only partially measures tick abundance. Another strategy to avoid confound tic abundance and tick questing behaviour would be to use manipulative or laboratory studies which would allow to use controlled conditions of climate and observed significant change in tick questing behaviour and/or tick life history traits. For example, laboratory studies have

clearly shown that temperature and relative humidity are important for *Ixodes* ticks development rates [37, 77, 269, 270]. However, such effects were not always clearly observed in nature. Again, field studies offer to observe, analyse, and describe tick abundance together with a complete set of factors, biotic and abiotic, that surround and influence the biota and its habitat. The principal advantage of field studies is that they represent a greater variety of conditions and environments that ticks experience in their natural habitat. As suggested above, this advantage can be misleading, the lack of control and the impossibility of precisely characterizing the field environment may make it very difficult to reproduce results found in laboratory studies. Second, the temporal window over which these climate variables operate to influence the vital rates of tick population is a great unknown. For example, the DON in the spring might depend on the climate conditions of the previous winter (e.g., overwinter survival of nymphs), or on the climate conditions of the previous summer, which would influence the rates at which larvae obtain and digest their blood meals, and moult into nymphs. Chapters 1 and 2 found that annual climate variables (e.g., mean annual relative humidity and mean annual precipitation) were important for explaining the inter-annual variation in the DON or DIN [227, 228]. In contrast, Chapter 3 compares climate variables operating at different temporal scales (i.e., annual versus seasonal) and found that seasonal climate variables were much more important than the annual climate variables at explaining the variation in the DON. Many steps in the tick life cycle happen over shorter time scales; for example, engorged larvae take ~ 6 to 8 weeks to moult into nymphs at room temperature [271]. Thus, the life history traits of tick populations may depend on climate variables that are operating over shorter temporal windows (e.g., seasons rather than years). Researchers have addressed this issue by investigating a wide variety of durations and time lags. For example, a 14-year study in Switzerland considered daily means and moving averages (5, 10, 17 or 30 days) to take into account different time periods for determining nymph activity [48]. A 8-year study in Germany used cross correlation maps to explore month-to-month correlation between the DON and climate variables, as well as time-lagged and interval-averaged correlations by considering a second time lag [248]. A 2-year study in five European countries examined time-lagged and interval-aggregated monthly and yearly means to test the associations between the abundance of host-seeking *I. ricinus* nymphs and climate [272]. As it was demonstrated in at least one of these studies, we could have tried to used finer temporal scales (e.g., weeks or days) but for simplicity, we decided not to. Instead, we believe that seasonal means are more informative than annual means at our field site and that it might be relevant to consider more than one temporal window in future ecological studies analysing tick ecology.

9 Conclusion

This PhD thesis demonstrated that masting events by deciduous trees is a critical driver of the seasonal and inter-annual abundance of *I. ricinus* ticks, and hence the risk of tick-borne disease. The abundance of *I. ricinus* nymphs almost doubled over 15 years at our study location in Switzerland, but we found no direct association between this doubling of nymphal tick abundance and climate change. However, there could be indirect effects if climate change is increasing the frequency of masting events and thereby increasing the abundance of reservoir hosts and ticks. This work is the first long-term study in Europe to provide evidence that seed production by deciduous trees influences the density of nymphs infected with *B. burgdorferi*. This work provides new information on the bimodal phenology of *I. ricinus* ticks, particularly that the direct development hypothesis is the best explanation for the spring and fall peaks of *I. ricinus* nymphs. In conclusion, public health officials should be aware that mast years are an important time-lagged predictor of tick abundance and the incidence of tick-borne diseases.

10 References

1. Guglielmone A, Robbins R, Apanaskevich D, Petney T, Estrada-Peña A, Horak I, et al. The Argasidae, Ixodidae and Nuttalliellidae (Acari: Ixodida) of the world: a list of valid species names. Zootaxa. 2010;2528:1-28.
2. de la Fuente J, Estrada-Peña A, Venzal J, Kocan K, Sonenshine D. Overview: ticks as vectors of pathogens that cause disease in humans and animals. Front Biosci. 2008;13:6938-46.
3. Dantas-Torres F, Chomel BB, Otranto D. Ticks and tick-borne diseases: a one health perspective. Trends Parasitol. 2012;28:437-46.
4. Jongejan F, Uilenberg G. The global importance of ticks. Parasitology. 2005;129:3-14.
5. Hubálek Z. Epidemiology of Lyme borreliosis. 2009.
6. Gray JS. Review The ecology of ticks transmitting Lyme borreliosis. Exp Appl Acarol. 1998;22:249-58.
7. Piesman J, Gern L. Lyme borreliosis in Europe and North America. Parasitology. 2004;129:S191-S220.
8. Eisen L. Vector competence studies with hard ticks and *Borrelia burgdorferi* sensu lato spirochetes: a review. Ticks Tick Borne Dis. 2020;11:101359.
9. Kahl O, Gern L, Eisen L, Lane RS. Ecological research on *Borrelia burgdorferi* sensu lato: terminology and some methodological pitfalls. 2002. p. 29-46.
10. Stanek G, Wormser GP, Gray J, Strle F. Lyme borreliosis. Lancet. 2012;379:461-73.
11. Gray JS. Mating and behavioural diapause in *Ixodes ricinus* L. Experimental & Applied Acarology. 1987;3:61-71.
12. Graf J. Copulation, nutrition et ponte chez *Ixodes ricinus* L. (Ixodoidea: Ixodidae)-2e partie. Bull Soc ent Suisse. 1978;51:241-53.
13. Kocan KM, de la Fuente J, Coburn LA. Insights into the development of *Ixodes scapularis*: a resource for research on a medically important tick species. Parasites & Vectors. 2015;8:592.
14. Gern L, Estrada-Peña A, Frandsen F, Gray JS, Jaenson TGT, Jongejan F, et al. European reservoir hosts of *Borrelia burgdorferi* sensu lato. Zentralblatt für Bakteriologie. 1998;287:196-204.
15. Schotthoefer AM, Frost HM. Ecology and epidemiology of Lyme borreliosis. Clinics in laboratory medicine. 2015;35:723-43.

16. Heylen D, Tijsse E, Fonville M, Matthysen E, Sprong H. Transmission dynamics of *Borrelia burgdorferi* s.l. in a bird tick community. Environ Microbiol. 2013;15:663-73.
17. Gern L, Humair PF. Ecology of *Borrelia burgdorferi* sensu lato in Europe. In: Gray JS, Kahl O, Lane RS, Stanek G, editors Lyme Borreliosis: biology, epidemiology and control Wallinford: CABI International. 2002:149-74.
18. Gray JS, Kahl O, S. Lane R, Levin M, Tsao J. Diapause in ticks of the medically important *Ixodes ricinus* species complex. Ticks Tick Borne Dis. 2016;7:992-1003.
19. Chrdle A, Chmelík V, Ruzek D. Tick-borne encephalitis: what travelers should know when visiting an endemic country. Human Vaccines & Immunotherapeutics. 2016;12.
20. Lees AD. The water balance in *Ixodes ricinus* L. and certain other species of ticks. Parasitology. 1946;37:1-20.
21. Knülle W, Rudolph D. Humidity relationships and water balance of ticks. vol. 1; 1982.
22. Mejlon HA, Jaenson TGT. Questing behaviour of *Ixodes ricinus* ticks (Acari: Ixodidae). Exp Appl Acarol. 1997;21:747-54.
23. Randolph SE, Storey K. Impact of microclimate on immature tick-rodent host interactions (Acari: Ixodidae): implications for parasite transmission. J Med Entomol. 1999;36:741-8.
24. Gray J, Kahl O, Zintl A. What do we still need to know about *Ixodes ricinus*? Ticks Tick Borne Dis. 2021;12:101682.
25. Herrmann C, Gern L. Search for blood or water is influenced by *Borrelia burgdorferi* in *Ixodes ricinus*. Parasit Vectors. 2015;8:6.
26. Gregson JD. Observations on the movement of fluids in the vicinity of the mouthparts of naturally feeding *Dermacentor andersoni* Stiles. Parasitology. 1967;57:1-8.
27. Brossard M, Wikel SK. Tick immunobiology. Parasitology. 2004;129 Suppl:S161-76.
28. Francischetti IMB, Sa-Nunes A, Mans BJ, Santos IM, Ribeiro JMC. The role of saliva in tick feeding. Front Biosci (Landmark Ed). 2009;14:2051-88.
29. Ribeiro JMC, Alarcon-Chaidez F, B. Francischetti IM, Mans BJ, Mather TN, Valenzuela JG, et al. An annotated catalog of salivary gland transcripts from *Ixodes scapularis* ticks. Insect Biochem Mol Biol. 2006;36:111-29.
30. Šimo L, Kazimirova M, Richardson J, Bonnet SI. The essential role of tick salivary glands and saliva in tick feeding and pathogen transmission. Frontiers in Cellular and Infection Microbiology. 2017;7.
31. Ramamoorthi N, Narasimhan S, Pal U, Bao F, Yang XF, Fish D, et al. The Lyme disease agent exploits a tick protein to infect the mammalian host. Nature. 2005;436:573-7.

32. Macháčková M, Oborník M, Kopecký J. Effect of salivary gland extract from *Ixodes ricinus* ticks on the proliferation of *Borrelia burgdorferi* sensu stricto in vivo. Folia Parasitol. 2006;53:153-8.
33. Zeidner NS, Schneider BS, Nuncio MS, Gern L, Piesman J. Coinoculation of *Borrelia* spp. with tick salivary gland lysate enhances spirochete load in mice and is tick species-specific. J Parasitol. 2002;88:1276-8.
34. Randolph SE. Tick ecology: processes and patterns behind the epidemiological risk posed by ixodid ticks as vectors. Parasitology. 2004;129:37-65.
35. Eisen RJ, Eisen L, Beard CB. County-scale distribution of *Ixodes scapularis* and *Ixodes pacificus* (Acari: Ixodidae) in the continental United States. J Med Entomol. 2016;53:349-86.
36. Kilpatrick A, Dobson A, Levi T, Salkeld D, Swei A, S. Ginsberg H, et al. Lyme disease ecology in a changing world: consensus, uncertainty and critical gaps for improving control. Philos Trans R Soc Lond, B, Biol Sc. 2017;372:20160117.
37. MacLeod J. *Ixodes ricinus* in relation to its physical environment: II. The factors governing survival and activity. Parasitology. 1935;27:123-44.
38. Randolph SE, Green RM, Hoodless AN, Peacey MF. An empirical quantitative framework for the seasonal population dynamics of the tick *Ixodes ricinus*. Int J Parasitol. 2002;32:979-89.
39. Benjamin MA, Zhioua E, Ostfeld RS. Laboratory and field evaluation of the entomopathogenic fungus *Metarhizium anisopliae* (Deuteromycetes) for controlling questing adult *Ixodes scapularis* (Acari: Ixodidae). J Med Entomol. 2002;39:723-8.
40. Estrada-Peña A, Ayllón N, de la Fuente J. Impact of climate trends on tick-borne pathogen transmission. Frontiers in physiology. 2012;3:64.
41. Lindgren E, Tälleklint L, Polfeldt T. Impact of climatic change on the northern latitude limit and population density of the disease-transmitting European tick *Ixodes ricinus*. Environ Health Perspect. 2000;108:119-23.
42. Tälleklint L, Jaenson TGT. Increasing geographical distribution and density of *Ixodes ricinus* (Acari: Ixodidae) in central and northern Sweden. J Med Entomol. 1998;35:521-6.
43. Ogden NH, Maarouf A, Barker IK, Bigras-Poulin M, Lindsay LR, Morshed MG, et al. Climate change and the potential for range expansion of the Lyme disease vector *Ixodes scapularis* in Canada. Int J Parasitol. 2006;36:63-70.

44. Brownstein JS, Holford TR, Fish D. Effect of climate change on Lyme disease risk in North America. EcoHealth. 2005;2:38-46.
45. Jaenson TGT, Jaenson DG, Eisen L, Petersson E, Lindgren E. Changes in the geographical distribution and abundance of the tick *Ixodes ricinus* during the past 30 years in Sweden. Parasit Vectors. 2012;5:8.
46. Tokarevich NK, Tronin AA, Blinova OV, Buzinov RV, Boltenkov VP, Yurasova ED, et al. The impact of climate change on the expansion of *Ixodes persulcatus* habitat and the incidence of tick-borne encephalitis in the north of European Russia. Global health action. 2011;4:8448.
47. Ostfeld RS, Canham CD, Oggenfuss K, Winchcombe RJ, Keesing F. Climate, deer, rodents, and acorns as determinants of variation in Lyme-disease risk. PLoS Biol. 2006;4:e145.
48. Hauser G, Rais O, Morán Cadenas F, Gonseth Y, Bouzelboudjen M, Gern L. Influence of climatic factors on *Ixodes ricinus* nymph abundance and phenology over a long-term monthly observation in Switzerland (2000–2014). Parasit Vectors. 2018;11:289.
49. Schulze TL, Jordan RA, Schulze CJ, Hung RW. Precipitation and temperature as predictors of the local abundance of *Ixodes scapularis* (Acari: Ixodidae) nymphs. J Med Entomol. 2009;46:1025-9.
50. Brugger K, Walter M, Chitimia-Dobler L, Dobler G, Rubel F. Forecasting next season's *Ixodes ricinus* nymphal density: the example of southern Germany 2018. Exp Appl Acarol. 2018;75:281-8.
51. Daniel M, Malý M, Danielová V, Kříž B, Nuttall P. Abiotic predictors and annual seasonal dynamics of *Ixodes ricinus*, the major disease vector of central Europe. Parasit Vectors. 2015;8:478.
52. Berger KA, Ginsberg HS, Dugas KD, Hamel LH, Mather TN. Adverse moisture events predict seasonal abundance of Lyme disease vector ticks (*Ixodes scapularis*). Parasit Vectors. 2014;7:181.
53. Hayes LE, Scott JA, Stafford KC. Influences of weather on *Ixodes scapularis* nymphal densities at long-term study sites in Connecticut. Ticks Tick Borne Dis. 2015;6:258-66.
54. Burtis JC, Sullivan P, Levi T, Oggenfuss K, Fahey TJ, Ostfeld RS. The impact of temperature and precipitation on blacklegged tick activity and Lyme disease incidence in endemic and emerging regions. Parasit Vectors. 2016;9:606.

55. van Duijvendijk G, Coipan C, Wagemakers A, Fonville M, Ersöz J, Oei A, et al. Larvae of *Ixodes ricinus* transmit *Borrelia afzelii* and *B. miyamotoi* to vertebrate hosts. Parasit Vectors. 2016;9:97.
56. Rollend L, Fish D, Childs JE. Transovarial transmission of *Borrelia* spirochetes by *Ixodes scapularis*: a summary of the literature and recent observations. Ticks Tick Borne Dis. 2013;4:46-51.
57. Matuschka FR, Schinkel TW, Klug B, Spielman A, Richter D. Failure of *Ixodes* ticks to inherit *Borrelia afzelii* infection. Appl Environ Microbiol. 1998;64:3089-91.
58. Ostfeld RS. Lyme disease: the ecology of a complex system. OUP USA; 2011.
59. Barbour AG, Fish D. The biological and social phenomenon of Lyme disease. Science. 1993;260:1610-6.
60. Stafford KC, 3rd, Cartter ML, Magnarelli LA, Ertel SH, Mshar PA. Temporal correlations between tick abundance and prevalence of ticks infected with *Borrelia burgdorferi* and increasing incidence of Lyme disease. J Clin Microbiol. 1998;36:1240-4.
61. Ostfeld RS, Keesing F, Schauber EM, Schmidt KA. Ecological context of Lyme disease: biodiversity, habitat fragmentation, and risk of infection. Conservation Medicine: Ecological Health In Practice. 2002:207-19.
62. Diuk-Wasser MA, Hoen AG, Cislo P, Brinkerhoff R, Hamer SA, Rowland M, et al. Human risk of infection with *Borrelia burgdorferi*, the Lyme disease agent, in eastern United States. Am J Trop Med Hyg. 2012;86:320-7.
63. Medlock J, Leach S. Impact of climate change on vector-borne disease in the UK. Lancet. 2015;15:159-99.
64. Gage KL, Burkot TR, Eisen RJ, Hayes EB. Climate and vectorborne diseases. Am J Prev Med. 2008;35:436-50.
65. Mills JN, Gage KL, Khan AS. Potential influence of climate change on vector-borne and zoonotic diseases: a review and proposed research plan. Environ Health Perspect. 2010;118:1507-14.
66. Materna J, Daniel M, Metelka L, Harčarik J. The vertical distribution, density and the development of the tick Ixodes ricinus in mountain areas influenced by climate changes (The Krkonoše Mts., Czech Republic). Int J Med Microbiol. 2008;298:25-37.
67. Burri C, Morán Cadenas F, Douet V, Moret J, Gern L. *Ixodes ricinus* density and infection prevalence of *Borrelia burgdorferi* sensu lato along a north-facing altitudinal gradient in the Rhône Valley (Switzerland). Vector Borne Zoonotic Dis. 2007;7:50-8.

68. Gern L, Morán Cadenas F, Burri C. Influence of some climatic factors on *Ixodes ricinus* ticks studied along altitudinal gradients in two geographic regions in Switzerland. Int J Med Microbiol. 2008;298:55-9.
69. Danielová V, Rudenko N, Daniel M, Holubová J, Materna J, Golovchenko M, et al. Extension of *Ixodes ricinus* ticks and agents of tick-borne diseases to mountain areas in the Czech Republic. Int J Med Microbiol. 2006;296:48-53.
70. Daniel M, Danielová V, Kříž B, Jirsa A, Nožička J. Shift of the tick *Ixodes ricinus* and tick-borne encephalitis to higher altitudes in Central Europe. European Journal of Clinical Microbiology and Infectious Diseases. 2003;22:327-8.
71. Jouda F, Perret J-L, Gern L. Density of questing *Ixodes ricinus* nymphs and adults infected by *Borrelia burgdorferi* sensu lato in Switzerland: spatio-temporal pattern at a regional scale. vol. 4; 2004.
72. Gilbert L. Altitudinal patterns of tick and host abundance: a potential role for climate change in regulating tick-borne diseases? Oecologia. 2010;162:217-25.
73. Morán Cadenas F, Rais O, Jouda F, Douet V, Humair PF, Moret J, et al. Phenology of *Ixodes ricinus* and infection with *Borrelia burgdorferi* sensu lato along a north- and south-facing altitudinal gradient on Chaumont Mountain, Switzerland. J Med Entomol. 2007;44:683-93.
74. Hartemink N, van Vliet A, Sprong H, Jacobs F, Garcia-Marti I, Zurita-Milla R, et al. Temporal-spatial variation in questing tick activity in the Netherlands: The effect of climatic and habitat factors. Vector Borne Zoonotic Dis. 2019;19:494-505.
75. Parham PE, Waldock J, Christophides GK, Hemming D, Agusto F, Evans KJ, et al. Climate, environmental and socio-economic change: weighing up the balance in vector-borne disease transmission. Philos Trans R Soc Lond, B, Biol Sc. 2015;370:20130551.
76. Süss J, Klaus C, Gerstengarbe FW, Werner PC. What makes ticks tick? Climate change, ticks, and tick-borne diseases. J Travel Med. 2008;15:39-45.
77. Ogden NH, Lindsay LR, Beauchamp G, Charron D, Maarouf A, O'Callaghan CJ, et al. Investigation of relationships between temperature and developmental rates of tick *Ixodes scapularis* (Acari: Ixodidae) in the laboratory and field. J Med Entomol. 2004;41:622-33.
78. Gray JS, Dautel H, Estrada-Peña A, Kahl O, Lindgren E. Effects of climate change on ticks and tick-borne diseases in europe. Interdiscip Perspect Infect Dis. 2009;2009:593232.

79. Rodgers SE, Zolnik CP, Mather TN. Duration of exposure to suboptimal atmospheric moisture affects nymphal blacklegged tick survival. J Med Entomol. 2007;44:372-5.
80. Hartelt K, Wurst E, Collatz J, Zimmermann G, Kleespies RG, Oehme RM, et al. Biological control of the tick *Ixodes ricinus* with entomopathogenic fungi and nematodes: Preliminary results from laboratory experiments. Int J Med Microbiol. 2008;298:314-20.
81. Hubálek Z, Halouzka J, Juricova Z. Host-seeking activity of ixodid ticks in relation to weather variables. J Vector Ecol. 2003;28:159-65.
82. Schwarz A, Maier WA, Kistemann T, Kampen H. Analysis of the distribution of the tick *Ixodes ricinus* L. (Acari: Ixodidae) in a nature reserve of western Germany using Geographic Information Systems. Int J Hyg Environ Health. 2009;212:87-96.
83. Perret JL, Guigoz E, Rais O, Gern L. Influence of saturation deficit and temperature on *Ixodes ricinus* tick questing activity in a Lyme borreliosis-endemic area (Switzerland). Parasitol Res. 2000;86:554-7.
84. Perret J-L, Rais O, Gern L. Influence of climate on the proportion of *Ixodes ricinus* nymphs and adults questing in a tick population. J Med Entomol. 2004;41:361-5.
85. Estrada-Peña A, Martinez JM, Acedo CS, Quilez J, Cacho ED. Phenology of the tick, *Ixodes ricinus*, in its southern distribution range (central Spain). Med Vet Entomol. 2004;18:387-97.
86. Perret J-L. Computer-assisted laboratory observations and field studies of the host-finding behaviour of the tick *Ixodes ricinus* (Acarina: Ixodidae): ecological implications of climate and light. PhD dissertation, University of Neuchâtel, Switzerland. 2003.
87. Randolph SE. Ticks are not insects: consequences of contrasting vector biology for transmission potential. Parasitol Today. 1998;14:186-92.
88. Ogden NH, Tsao JI. Biodiversity and Lyme disease: dilution or amplification? Epidemics. 2009;1:196-206.
89. Jaenson TG, Tälleklint L. Incompetence of roe deer as reservoirs of the Lyme borreliosis spirochete. J Med Entomol. 1992;29:813-7.
90. Telford SR, 3rd, Mather TN, Moore SI, Wilson ML, Spielman A. Incompetence of deer as reservoirs of the Lyme disease spirochete. Am J Trop Med Hyg. 1988;39:105-9.
91. LoGiudice K, Ostfeld RS, Schmidt KA, Keesing F. The ecology of infectious disease: effects of host diversity and community composition on Lyme disease risk. PNAS. 2003;100:567-71.

92. Keesing F, Brunner J, Duerr S, Killilea M, LoGiudice K, Schmidt K, et al. Hosts as ecological traps for the vector of Lyme disease. Proceedings of the Royal Society B: Biological Sciences. 2009;276:3911-9.
93. Brunner JL, LoGiudice K, Ostfeld RS. Estimating reservoir competence of *Borrelia burgdorferi* hosts: prevalence and infectivity, sensitivity, and specificity. J Med Entomol. 2008;45:139-47.
94. Humair P-F, Douet V, Cadenas FM, Schouls LM, Pol IVD, Gern L. Molecular identification of bloodmeal source in *Ixodes ricinus* ticks using 12S rDNA as a genetic marker. J Med Entomol. 2007;44:869-80.
95. Morán Cadenas F, Rais O, Humair PF, Douet V, Moret J, Gern L. Identification of host bloodmeal source and *Borrelia burgdorferi* sensu lato in field-collected *Ixodes ricinus* ticks in Chaumont (Switzerland). J Med Entomol. 2007;44:1109-17.
96. Pichon B, Rogers M, Egan D, Gray J. Blood-meal analysis for the identification of reservoir hosts of tick-borne pathogens in Ireland. Vector Borne Zoonotic Dis. 2005;5:172-80.
97. Scott MC, Harmon JR, Tsao JI, Jones CJ, Hickling GJ. Reverse line blot probe design and polymerase chain reaction optimization for bloodmeal analysis of ticks from the eastern United States. J Med Entomol. 2012;49:697-709.
98. Tälleklint L, Jaenson T. Transmission of *Borrelia burgdorferi* s.l. from mammal reservoirs to the primary vector of Lyme borreliosis, *Ixodes ricinus* (Acari: Ixodidae), in Sweden. J Med Entomol. 1994;31:880-6.
99. Hofmeester T, Coipan E, Van Wieren S, Prins H, Takken W, Sprong H. Few vertebrate species dominate the *Borrelia burgdorferi* sl life cycle. Environ Res Lett. 2016;11:043001.
100. LoGiudice K, Duerr ST, Newhouse MJ, Schmidt KA, Killilea ME, Ostfeld RS. Impact of host community composition on Lyme disease risk. Ecology. 2008;89:2841-9.
101. Brunner JL, Ostfeld RS. Multiple causes of variable tick burdens on small-mammal hosts. Ecology. 2008;89:2259-72.
102. Mather TN, Wilson ML, Moore SI, Ribeiro JM, Spielman A. Comparing the relative potential of rodents as reservoirs of the Lyme disease spirochete (Borrelia burgdorferi). Am J Epidemiol. 1989;130:143-50.
103. Hanincová K, Schäfer SM, Etti S, Sewell HS, Taragelová V, Ziak D, et al. Association of *Borrelia afzelii* with rodents in Europe. Parasitology. 2003;126:11-20.

104. Harrison A, Scantlebury M, Montgomery WI. Body mass and sex-biased parasitism in wood mice *Apodemus sylvaticus*. Oikos. 2010;119:1099-104.
105. Kiffner C, Vor T, Hagedorn P, Niedrig M, Rühe F. Factors affecting patterns of tick parasitism on forest rodents in tick-borne encephalitis risk areas, Germany. Parasitol Res. 2011;108:323-35.
106. Perkins SE, Cattadori IM, Tagliapietra V, Rizzoli AP, Hudson PJ. Empirical evidence for key hosts in persistence of a tick-borne disease. Int J Parasitol. 2003;33:909-17.
107. Jensen TS. Seed production and outbreaks of non-cyclic rodent populations in deciduous forests. Oecologia. 1982;54:184-92.
108. Pucek Z, Jędrzejewski W, Jędrzejewska B, Pucek M. Rodent population dynamics in a primeval deciduous forest (Białowieża National Park) in relation to weather, seed crop, and predation. Acta Theriologica. 1993;38:199-232.
109. Zwolak R, Bogdziewicz M, Rychlik L. Beech masting modifies the response of rodents to forest management. For Ecol Manage. 2016;359:268-76.
110. Randolph SE. Population regulation in ticks: the role of acquired resistance in natural and unnatural hosts. Parasitology. 1979;79:141-56.
111. Clotfelter E, Pedersen A, Cranford J, Ram N, Snajdr E, Nolan V, et al. Acorn mast drives long-term dynamics of rodent and songbird populations. Oecologia. 2008;154:493-503.
112. Schnurr JL, Ostfeld RS, Canham CD. Direct and indirect effects of masting on rodent populations and tree seed survival. Oikos. 2002;96:402-10.
113. Drobyshev I, Niklasson M, Mazerolle MJ, Bergeron Y. Reconstruction of a 253-year long mast record of European beech reveals its association with large scale temperature variability and no long-term trend in mast frequencies. Agric For Meteorol. 2014;192:9-17.
114. Drobyshev I, Övergaard R, Saygin I, Niklasson M, Hickler T, Karlsson M, et al. Masting behaviour and dendrochronology of European beech (*Fagus sylvatica* L.) in southern Sweden. For Ecol Manag. 2010;259:2160-71.
115. Piovesan G, Adams JM. Masting behaviour in beech: linking reproduction and climatic variation. Can J Bot. 2001;79:1039-47.
116. Övergaard R, Gemmel P, Karlsson M. Effects of weather conditions on mast year frequency in beech (*Fagus sylvatica* L.) in Sweden. Forestry. 2007;80:555-65.
117. Bogdziewicz M, Zwolak R, Crone EE. How do vertebrates respond to mast seeding? Oikos. 2016;125:300-7.

118. Wolff JO. Population fluctuations of mast-eating rodents are correlated with production of acorns. J Mammal. 1996;77:850-6.
119. Ostfeld RS, Jones CG, Wolff JO. Of mice and mast. Bioscience. 1996;46:323-30.
120. Ostfeld RS, Schauber EM, Canham CD, Keesing F, Jones CG, Wolff JO. Effects of acorn production and mouse abundance on abundance and *Borrelia burgdorferi* infection prevalence of nymphal *Ixodes scapularis* ticks. Vector Borne Zoonotic Dis. 2001;1:55-63.
121. Jones CG, Ostfeld RS, Richard MP, Schauber EM, Wolff JO. Chain reactions linking acorns to gypsy moth outbreaks and Lyme disease risk. Science. 1998;279:1023-6.
122. Ostfeld RS, Levi T, Keesing F, Oggenfuss K, Canham CD. Tick-borne disease risk in a forest food web. Ecology. 2018;99:1562-73.
123. Schauber EM, Ostfeld RS, Evans J, Andrew S. What is the best predictor of annual Lyme disease incidence: weather, mice, or acorns? Ecol Appl. 2005;15:575-86.
124. Pearse IS, Koenig WD, Kelly D. Mechanisms of mast seeding: resources, weather, cues, and selection. New Phytol. 2016;212:546-62.
125. Schmidt W. Temporal variation in beech masting (*Fagus sylvatica* L.) in a limestone beech forest (1981-2004). Allgemeine Forst und Jagdzeitung. 2006;177:9-19.
126. Bogdziewicz M, Kelly D, Thomas PA, Lageard JG, Hacket-Pain A. Climate warming disrupts mast seeding and its fitness benefits in European beech. Nature Plants. 2020;6:88-94.
127. Clement J, Vercauteren J, Verstraeten WW, Ducoffre G, Barrios JM, Vandamme AM, et al. Relating increasing hantavirus incidences to the changing climate: the mast connection. Int J Health Geogr. 2009;8:1.
128. McShea WJ, Schwede G: Variable acorn crops: responses of white-tailed deer and other mast consumers. 1993.
129. Watts CHS. The regulation of wood mouse (*Apodemus sylvaticus*) numbers in Wytham Woods, Berkshire. J Anim Ecol. 1969;38:285-304.
130. McShea WJ. The influence of acorn crops on annual variation in rodent and bird populations. Ecology. 2000;81:228-38.
131. Ostfeld RS, Keesing F. Pulsed resources and community dynamics of consumers in terrestrial ecosystems. Trends Ecol Evol. 2000;15:232-7.
132. Gray JS, Kahl O, Janetzki C, Stein J. Studies on the ecology of Lyme disease in a deer forest in County Galway, Ireland. J Med Entomol. 1992;29:915-20.

133. Perez G, Bastian S, Agoulon A, Bouju A, Durand A, Faille F, et al. Effect of landscape features on the relationship between *Ixodes ricinus* ticks and their small mammal hosts. Parasit Vectors. 2016;9:20.
134. Lindquist L, Vapalahti O. Tick-borne encephalitis. The Lancet. 2008;371:1861-71.
135. Rubel F, Walter M, Vogelgesang JR, Brugger K. Tick-borne encephalitis (TBE) cases are not random: explaining trend, low- and high-frequency oscillations based on the Austrian TBE time series. BMC Infect Dis. 2020;20:448.
136. Rubel F, Brugger K. Tick-borne encephalitis incidence forecasts for Austria, Germany, and Switzerland. Ticks Tick Borne Dis. 2020;11:101437.
137. Rubel F, Brugger K. Operational TBE incidence forecasts for Austria, Germany, and Switzerland 2019–2021. Ticks Tick Borne Dis. 2021;12:101579.
138. Dantas-Torres F, Otranto D. Seasonal dynamics of *Ixodes ricinus* on ground level and higher vegetation in a preserved wooded area in southern Europe. Vet Parasitol. 2013;192:253-8.
139. Dautel H, Dippel C, Kämmer D, Werkhausen A, Kahl O. Winter activity of *Ixodes ricinus* in a Berlin forest. Int J Med Microbiol. 2008;298:50-4.
140. Gray JS. The development and seasonal activity of the tick *Ixodes ricinus*: a vector of Lyme borreliosis. Rev MedVet Entomol. 1991;79:323-33.
141. Steele G, Randolph S. An experimental evaluation of conventional control measures against the sheep tick, *Ixodes ricinus* (L.) (Acari: Ixodidae). I. A unimodal seasonal activity pattern. Bull Entomol Res. 1985;75.
142. Tälleklint L, Jaenson TG. Seasonal variations in density of questing *Ixodes ricinus* (Acari: Ixodidae) nymphs and prevalence of infection with *B. burgdorferi* s.l. in south central Sweden. J Med Entomol. 1996;33:592-7.
143. Jouda F, Perret JL, Gern L. *Ixodes ricinus* density, and distribution and prevalence of *Borrelia burgdorferi* sensu lato infection along an altitudinal gradient. J Med Entomol. 2004;41:162-9.
144. Gray JS. Studies on the dynamics of active populations of the sheep tick, *Ixodes ricinus* L. in Co. Wicklow, Ireland. Acarologia. 1984;25:167-78.
145. Korenberg EI. Seasonal population dynamics of *Ixodes* ticks and tick-borne encephalitis virus. Exp Appl Acarol. 2000;24:665-81.
146. Sormunen JJ, Klemola T, Vesterinen EJ, Vuorinen I, Hytönen J, Hänninen J, et al. Assessing the abundance, seasonal questing activity, and *Borrelia* and tick-borne

encephalitis virus (TBEV) prevalence of *Ixodes ricinus* ticks in a Lyme borreliosis endemic area in southwest Finland. Ticks Tick Borne Dis. 2016;7:208-15.

147. Cayol C, Koskela E, Mappes T, Siukkola A, Kallio ER. Temporal dynamics of the tick *Ixodes ricinus* in northern Europe: epidemiological implications. Parasit Vectors. 2017;10:1-11.

148. Borde JP, Kaier K, Hehn P, Matzarakis A, Frey S, Bestehorn M, et al. The complex interplay of climate, TBEV vector dynamics and TBEV infection rates in ticks—Monitoring a natural TBEV focus in Germany, 2009–2018. PLOS ONE. 2021;16:e0244668.

149. Belozerov V. Diapause and quiescence as two main kinds of dormancy and their significance in life cycles of mites and ticks (Chelicerata: Arachnida: Acari). Part 2. Parasitiformes. Acarina. 2009;17:3-32.

150. Belozerov V. Diapause and biological rhythms in ticks. In: Obenchain FD, Galun R, editors. Physiology of Ticks: Pergamon; 1982. p. 469-500.

151. Gray J. The development and questing activity of *Ixodes ricinus* (L.) (Acari: Ixodidae) under field conditions in Ireland. Bull Entomol Res. 1982;72:263-70.

152. Knap N, Durmiši E, Saksida A, Korva M, Petrovec M, Avšič-Županc T. Influence of climatic factors on dynamics of questing *Ixodes ricinus* ticks in Slovenia. Vet Parasitol. 2009;164:275-81.

153. Gray JS. The fecundity of *Ixodes ricinus* (L.) (Acarina: Ixodidae) and the mortality of its developmental stages under field conditions. Bull Entomol Res. 1981;71:533-42.

154. Furness RW, Furness EN. *Ixodes ricinus* parasitism of birds increases at higher winter temperatures. Journal of Vector Ecology. 2018;43:59-62.

155. Sykes RA, Makiello P. An estimate of Lyme borreliosis incidence in Western Europe. Journal of Public Health. 2017;39:74-81.

156. Centers for Disease Control and Prevention: National Center for Emerging and Zoonotic Infectious Diseases (NCEZID), Division of Vector-Borne Diseases (DVBD). (2019). Accessed January 13 2021.

157. Rosenberg R, Lindsey N, Fischer M, Gregory C, Hinckley A, Mead P, et al. Vital signs : trends in reported vectorborne disease cases — United States and territories, 2004–2016. MMWR Morbidity and Mortality Weekly Report. 2018;67:1-6.

158. Hinckley AF, Connally NP, Meek JI, Johnson BJ, Kemperman MM, Feldman KA, et al. Lyme disease testing by large commercial laboratories in the United States. Clinical

infectious diseases : an official publication of the Infectious Diseases Society of America. 2014;59:676-81.

159. Steere AC, Malawista SE, Snydman DR, Shope RE, Andiman WA, Ross MR, et al. An epidemic of oligoarticular arthritis in children and adults in three Connecticut communities. Arthritis & Rheumatism: Official Journal of the American College of Rheumatology. 1977;20:7-17.

160. Burgdorfer W, Barbour AG, Hayes SF, Benach JL, Grunwaldt E, Davis JP. Lyme disease-a tick-borne spirochetosis? Science. 1982;216:1317-9.

161. Burgdorfer W, Keirans JE: Ticks and Lyme disease in the United States. American College of Physicians; 1983.

162. Hyde FW, Johnson RC. Genetic relationship of Lyme disease spirochetes to *Borrelia*, *Treponema*, and *Leptospira* spp. J Clin Microbiol. 1984;20:151-4.

163. Steere AC, Coburn J, Glickstein L. The emergence of Lyme disease. The Journal of clinical investigation. 2004;113:1093-101.

164. Steere AC, Bartenhagen NH, Craft JE, Hutchinson GJ, Newman JH, Rahn DW, et al. The early clinical manifestations of Lyme disease. Annals of Internal Medicine. 1983;99:76-82.

165. Stanek G, Strle F. Lyme borreliosis–from tick bite to diagnosis and treatment. FEMS Microbiol Rev. 2018;42:233-58.

166. Margos G, Fedorova N, Becker NS, Kleinjan JE, Marosevic D, Krebs S, et al. *Borrelia maritima* sp. nov., a novel species of the *Borrelia burgdorferi* sensu lato complex, occupying a basal position to North American species. Int J Syst Evol Microbiol. 2020;70:849-56.

167. Rudenko N, Golovchenko M, Grubhoffer L, Oliver Jr JH. Updates on *Borrelia burgdorferi* sensu lato complex with respect to public health. Ticks Tick Borne Dis. 2011;2:123-8.

168. Stanek G: Lyme borreliosis, ticks and *Borrelia* species. Springer; 2018.

169. Baranton G, De Martino SJ. *Borrelia burgdorferi* sensu lato diversity and its influence on pathogenicity in humans. Lyme borreliosis. vol. 37: Karger Publishers; 2009. p. 1-17.

170. Walter L, Sürth V, Röttgerding F, Zipfel PF, Fritz-Wolf K, Kraiczy P. Elucidating the immune evasion mechanisms of *Borrelia mayonii*, the causative agent of Lyme disease. Frontiers in immunology. 2019;10:2722.

171. van Dam AP, Kuiper H, Vos K, Widjojokusumo A, de Jongh BM, Spanjaard L, et al. Different genospecies of *Borrelia burgdorferi* are associated with distinct clinical manifestations of Lyme borreliosis. Clin Infect Dis. 1993;17:708-17.
172. De Silva AM, Fikrig E. Growth and migration of *Borrelia burgdorferi* in *Ixodes* ticks during blood feeding. Am J Trop Med Hyg. 1995;53:397-404.
173. Kahl O, Janetzki-Mittmann C, Gray J, Jonas R, Stein J, De Boer R. Risk of infection with *Borrelia burgdorferi* sensu lato for a host in relation to the duration of nymphal *Ixodes ricinus* feeding and the method of tick removal. Zentralblatt für Bakteriologie. 1998;287:41-52.
174. Crippa M, Rais O, Gern L. Investigations on the mode and dynamics of transmission and infectivity of *Borrelia burgdorferi* sensu stricto and *Borrelia afzelii* in *Ixodes ricinus* ticks. Vector-Borne and Zoonotic Diseases. 2002;2:3-9.
175. Schwan TG, Piesman J, Golde WT, Dolan MC, Rosa PA. Induction of an outer surface protein on *Borrelia burgdorferi* during tick feeding. Proceedings of the national academy of sciences. 1995;92:2909-13.
176. Pal U, Li X, Wang T, Montgomery RR, Ramamoorthi N, Desilva AM, et al. TROSPA, an *Ixodes scapularis* receptor for *Borrelia burgdorferi*. Cell. 2004;119:457-68.
177. Grimm D, Tilly K, Byram R, Stewart PE, Krum JG, Bueschel DM, et al. Outer-surface protein C of the Lyme disease spirochete: a protein induced in ticks for infection of mammals. Proceedings of the National Academy of Sciences. 2004;101:3142-7.
178. Tilly K, Rosa PA, Stewart PE. Biology of infection with *Borrelia burgdorferi*. Infectious disease clinics of North America. 2008;22:217-34.
179. Singh SK, Girschick HJ. Molecular survival strategies of the Lyme disease spirochete *Borrelia burgdorferi*. Lancet Infect Dis. 2004;4:575-83.
180. Hovius JW, van Dam AP, Fikrig E. Tick–host–pathogen interactions in Lyme borreliosis. Trends Parasitol. 2007;23:434-8.
181. de Silva AM, Tyson KR, Pal U. Molecular characterization of the tick-Borrelia interface. Front Biosci. 2009;14:3051-63.
182. Kindt TJ, Goldsby RA, Osborne BA, Kuby J. Kuby immunology. Macmillan; 2007.
183. Müller-Eberhard HJ. Molecular organization and function of the complement system. Annu Rev Biochem. 1988;57:321-47.
184. Barlow PN. Chapter 30 - Factor H and Factor H-like Protein 1. In: Barnum S, Schein T, editors. The Complement FactsBook (Second Edition): Academic Press; 2018. p. 317-27.

185. Józsi M. Factor H family proteins in complement evasion of microorganisms. Frontiers in Immunology. 2017;8.
186. Kraiczy P, Skerka C, Kirschfink M, Zipfel PF, Brade V. Mechanism of complement resistance of pathogenic *Borrelia burgdorferi* isolates. Int Immunopharmacol. 2001;1:393-401.
187. Kurtenbach K, De Michelis S, Etti S, Schäfer SM, Sewell H-S, Brade V, et al. Host association of *Borrelia burgdorferi* sensu lato – the key role of host complement. Trends Microbiol. 2002;10:74-9.
188. Lin Y-P, Diuk-Wasser M, Stevenson B, Kraiczy P. Complement evasion contributes to Lyme borreliae–host associations. Trends Parasitol. 2020;36.
189. Alitalo A, Meri T, Lankinen H, Seppälä I, Lahdenne P, Hefty PS, et al. Complement inhibitor factor H binding to Lyme disease spirochetes is mediated by inducible expression of multiple plasmid-encoded outer surface protein E paralogs. The Journal of Immunology. 2002;169:3847-53.
190. Brooks CS, Vuppala SR, Jett AM, Alitalo A, Meri S, Akins DR. Complement regulator-acquiring surface protein 1 imparts resistance to human serum in Borrelia burgdorferi. The Journal of Immunology. 2005;175:3299-308.
191. Hellwage J, Meri T, Heikkilä T, Alitalo A, Panelius J, Lahdenne P, et al. The complement regulator factor H binds to the surface protein OspE of *Borrelia burgdorferi*. J Biol Chem. 2001;276:8427-35.
192. Kenedy MR, Akins DR. The OspE-related proteins inhibit complement deposition and enhance serum resistance of *Borrelia burgdorferi*, the lyme disease spirochete. Infect Immun. 2011;79:1451-7.
193. Kraiczy P, Hartmann K, Hellwage J, Skerka C, Kirschfink M, Brade V, et al. Immunological characterization of the complement regulator factor H-binding CRASP and Erp proteins of *Borrelia burgdorferi*. International Journal of Medical Microbiology Supplements. 2004;293:152-7.
194. Kraiczy P, Hellwage J, Skerka C, Kirschfink M, Brade V, Zipfel PF, et al. Immune evasion of *Borrelia burgdorferi*: mapping of a complement-inhibitor factor H-binding site of BbCRASP-3, a novel member of the Erp protein family. Eur J Immunol. 2003;33:697-707.
195. McDowell JV, Wolfgang J, Tran E, Metts MS, Hamilton D, Marconi RT. Comprehensive analysis of the factor H binding capabilities of *Borrelia* species

associated with Lyme disease: delineation of two distinct classes of factor H binding proteins. Infect Immun. 2003;71:3597-602.

196. Siegel C, Hallström T, Skerka C, Eberhardt H, Uzonyi B, Beckhaus T, et al. Complement factor H-related proteins CFHR2 and CFHR5 represent novel ligands for the infection-associated CRASP proteins of *Borrelia burgdorferi*. PloS ONE. 2010;5:e13519.

197. Wallich R, Pattathu J, Kitiratschky V, Brenner C, Zipfel PF, Brade V, et al. Identification and functional characterization of complement regulator-acquiring surface protein 1 of the Lyme disease spirochetes *Borrelia afzelii* and *Borrelia garinii*. Infect Immun. 2005;73:2351-9.

198. Kraiczy P, Skerka C, Brade V, Zipfel PF. Further characterization of complement regulator-acquiring surface proteins of *Borrelia burgdorferi*. Infect Immun. 2001;69:7800-9.

199. Kraiczy P, Skerka C, Kirschfink M, Brade V, Zipfel PF. Immune evasion of *Borrelia burgdorferi* by acquisition of human complement regulators FHL-1/reconectin and Factor H. Eur J Immunol. 2001;31:1674-84.

200. Humair P-F, Gern L. Relationship between *Borrelia burgdorferi* sensu lato species, red squirrels (*Sciurus vulgaris*) and *Ixodes ricinus* in enzootic areas in Switzerland. Acta Trop. 1998;69:213-27.

201. Humair P-F, Peter O, Wallich R, Gern L. Strain variation of Lyme disease spirochetes isolated from *Ixodes ricinus* ticks and rodents collected in two endemic areas in Switzerland. J Med Entomol. 1995;32:433-8.

202. Humair PF, Rais O, Gern L. Transmission of *Borrelia afzelii* from *Apodemus* mice and *Clethrionomys* voles to *Ixodes ricinus* ticks: differential transmission pattern and overwintering maintenance. Parasitology. 1999;118:33-42.

203. Dubska L, Literak I, Kocianova E, Taragelova V, Sverakova V, Sychra O, et al. Synanthropic birds Influence the distribution of Borrelia species: analysis of *Ixodes ricinus* ticks feeding on passerine birds. Appl Environ Microbiol. 2011;77:1115-7.

204. Dubska L, Literak I, Kocianova E, Taragelova V, Sychra O. Differential role of passerine birds in distribution of *Borrelia* spirochetes, based on data from ticks collected from birds during the postbreeding migration period in central Europe. Appl Environ Microbiol. 2009;75:596-602.

205. Hanincová K, Taragelová V, Koci J, Schäfer SM, Hails R, Ullmann AJ, et al. Association of *Borrelia garinii* and *B. valaisiana* with songbirds in Slovakia. Appl Environ Microbiol. 2003;69:2825-30.

206. Taragel'ová V, Koči J, Hanincová K, Kurtenbach K, Derdáková M, Ogden NH, et al. Blackbirds and song thrushes constitute a key reservoir of *Borrelia garinii*, the causative agent of Borreliosis in Central Europe. Appl Environ Microbiol. 2008;74:1289-93.

207. Mannelli A, Nebbia P, Tramuta C, Grego E, Tomassone L, Ainardi R, et al. *Borrelia burgdorferi* sensu lato infection in larval *Ixodes ricinus* (Acari: Ixodidae) feeding on blackbirds in northwestern Italy. J Med Entomol. 2005;42:168-75.

208. Norte AC, Ramos JA, Gern L, Núncio MS, Lopes de Carvalho I. Birds as reservoirs for *Borrelia burgdorferi* s.l. in western Europe: circulation of *B. turdi* and other genospecies in bird–tick cycles in Portugal. Environ Microbiol. 2013;15:386-97.

209. Michalik J, Wodecka B, Skoracki M, Sikora B, Stańczak J. Prevalence of avian-associated *Borrelia burgdorferi* s.l. genospecies in *Ixodes ricinus* ticks collected from blackbirds (*Turdus merula*) and song thrushes (*T. philomelos*). Int J Med Microbiol. 2008;298:129-38.

210. James MC, Furness RW, Bowman AS, Forbes KJ, Gilbert L. The importance of passerine birds as tick hosts and in the transmission of *Borrelia burgdorferi*, the agent of Lyme disease: a case study from Scotland. Ibis. 2011;153:293-302.

211. Comstedt P, Bergström S, Olsen B, Garpmo U, Marjavaara L, Mejlon H, et al. Migratory passerine birds as reservoirs of Lyme borreliosis in Europe. Emerg Infect Dis. 2006;12:1087-95.

212. Kipp S, Goedecke A, Dorn W, Wilske B, Fingerle V. Role of birds in Thuringia, Germany, in the natural cycle of *Borrelia burgdorferi* sensu lato, the Lyme disease spirochaete. Int J Med Microbiol. 2006;296:125-8.

213. Hasle G, Bjune GA, Midthjell L, Røed KH, Leinaas HP. Transport of Ixodes ricinus infected with Borrelia species to Norway by northward-migrating passerine birds. Ticks and Tick-borne Diseases. 2011;2:37-43.

214. Junttila J, Peltomaa M, Soini H, Marjamäki M, Viljanen MK. Prevalence of *Borrelia burgdorferi* in *Ixodes ricinus* ticks in urban recreational areas of Helsinki. J Clin Microbiol. 1999;37:1361-5.

215. Kirstein F, Rijpkema S, Molkenboer M, Gray J. The distribution and prevalence of *B. burgdorferi* genomospecies in *Ixodes ricinus* ticks in Ireland. Eur J Epidemiol. 1997;13:67-72.

216. Kurtenbach K, Peacey M, Rijpkema SG, Hoodless AN, Nuttall PA, Randolph SE. Differential transmission of the genospecies of *Borrelia burgdorferi* sensu lato by game birds and small rodents in England. Appl Environ Microbiol. 1998;64:1169-74.

217. Schouls LM, Van De Pol I, Rijpkema SG, Schot CS. Detection and identification of *Ehrlichia*, *Borrelia burgdorferi* sensu lato, and *Bartonella* species in Dutch *Ixodes ricinus* ticks. J Clin Microbiol. 1999;37:2215-22.

218. Kurtenbach K, De Michelis S, Sewell H-S, Etti S, Schäfer SM, Hails R, et al. Distinct combinations of *Borrelia burgdorferi* sensu lato genospecies found in individual questing ticks from Europe. Appl Environ Microbiol. 2001;67:4926-9.

219. Kurtenbach K, Schäfer SM, Sewell H-S, Peacey M, Hoodless A, Nuttall PA, et al. Differential survival of Lyme borreliosis spirochetes in ticks that feed on birds. Infect Immun. 2002;70:5893-5.

220. Kurtenbach K, Sewell H-S, Ogden NH, Randolph SE, Nuttall PA. Serum complement sensitivity as a key factor in Lyme disease ecology. Infect Immun. 1998;66:1248-51.

221. Papatheodorou V, Brossard M. C3 levels in the sera of rabbits infested and reinfested with *Ixodes ricinus* L. and in midguts of fed ticks. Exp Appl Acarol. 1987;3:53-9.

222. Heylen DJA, Sprong H, Krawczyk A, Van Houtte N, Genné D, Gomez-Chamorro A, et al. Inefficient co-feeding transmission of *Borrelia afzelii* in two common European songbirds. Scientific Reports. 2017;7:39596.

223. Franke J, Hildebrandt A, Dorn W. Exploring gaps in our knowledge on Lyme borreliosis spirochaetes – Updates on complex heterogeneity, ecology, and pathogenicity. Ticks Tick Borne Dis. 2013;4:11-25.

224. Hu CM, Wilske B, Fingerle V, Lobet Y, Gern L. Transmission of *Borrelia garinii* OspA serotype 4 to BALB/c mice by *Ixodes ricinus* ticks collected in the field. J Clin Microbiol. 2001;39:1169-71.

225. Huegli D, Hu CM, Humair P-F, Wilske B, Gern L. *Apodemus* species mice are reservoir hosts of *Borrelia garinii* OspA serotype 4 in Switzerland. J Clin Microbiol. 2002;40:4735-7.

226. Margos G, Vollmer SA, Cornet M, Garnier M, Fingerle V, Wilske B, et al. A new borrelia species defined by multilocus sequence analysis of housekeeping genes. Appl Environ Microbiol. 2009;75:5410-6.

227. Bregnard C, Rais O, Voordouw MJ. Climate and tree seed production predict the abundance of the European Lyme disease vector over a 15-year period. Parasit Vectors. 2020;13:408.

228. Bregnard C, Rais O, Voordouw MJ. Masting by beech trees predicts the risk of Lyme disease. Parasit Vectors. 2021;14:168.
229. Bregnard C, Rais O, Herrmann C, Kahl O, Brugger K, Voordouw MJ. Beech tree masting explains the inter-annual variation in the fall and spring peaks of *Ixodes ricinus* ticks with different time lags. bioRxiv. 2021:2021.04.20.440690.
230. Hofmeester TR, Jansen PA, Wijnen HJ, Coipan EC, Fonville M, Prins HHT, et al. Cascading effects of predator activity on tick-borne disease risk. Proc Royal Soc B. 2017;284.
231. Krawczyk AI, van Duijvendijk GLA, Swart A, Heylen D, Jaarsma RI, Jacobs FHH, et al. Effect of rodent density on tick and tick-borne pathogen populations: consequences for infectious disease risk. Parasit Vectors. 2020;13:34.
232. Tkadlec E, Václavík T, Široký P. Rodent host abundance and climate variability as predictors of tickborne disease risk 1 year in advance. Emerg Infect Dis. 2019;25:1738.
233. Dobson ADM. History and complexity in tick-host dynamics: discrepancies between 'real' and 'visible' tick populations. Parasites & Vectors. 2014;7:231.
234. Bogdziewicz M, Szymkowiak J. Oak acorn crop and Google search volume predict Lyme disease risk in temperate Europe. Basic Appl Ecol. 2016;17:300-7.
235. Schmidt K, Ostfeld RS, Schauber EM. Infestation of *Peromyscus leucopus* and *Tamias striatus* by *Ixodes scapularis* (Acari: Ixodidae) in relation to the abundance of hosts and parasites. J Med Entomol. 1999;36:749-57.
236. Guy EC, Stanek G. Detection of *Borrelia burgdorferi* in patients with Lyme disease by the polymerase chain reaction. J Clin Pathol. 1991;44:610-1.
237. Rauter C, Hartung T. Prevalence of *Borrelia burgdorferi* sensu lato genospecies in *Ixodes ricinus* ticks in Europe: a metaanalysis. Appl Environ Microbiol. 2005;71:7203-16.
238. Berret J, Voordouw MJ. Lyme disease bacterium does not affect attraction to rodent odour in the tick vector. Parasit Vectors. 2015;8:249.
239. Sigma-Aldrich: *Ammonium Hydroxide*. Safety data sheet number 338818. Sigma-aldrich: St. Louis, MO, December 24, 2019. https://www.sigmaaldrich.com (2019). Accessed September 21 2020.
240. Herrmann C, Voordouw MJ, Gern L. *Ixodes ricinus* ticks infected with the causative agent of Lyme disease, *Borrelia burgdorferi* sensu lato, have higher energy reserves. Int J Parasitol. 2013;43:477-83.

241. Pfäffle M, Littwin N, Muders SV, Petney TN. The ecology of tick-borne diseases. Int J Parasitol. 2013;43:1059-77.
242. Mannelli A, Bertolotti L, Gern L, Gray J. Ecology of *Borrelia burgdorferi* sensu lato in Europe: transmission dynamics in multi-host systems, influence of molecular processes and effects of climate change. FEMS Microbiol Rev. 2012;36:837-61.
243. Perdeck A, Visser M, Balen J. Great tit *Parus major* survival, and the beech-crop cycle. Ardea. 2000;88:99-108.
244. Main AJ, Sprance HE, Kloter KO, Brown SE. *Ixodes Dammini* (Acari: Ixodidae) on white-tailed deer (*Odocoileus Virginianus*) in Connecticut. J Med Entomol. 1981;18:487-92.
245. Vor T, Kiffner C, Hagedorn P, Niedrig M, Rühe F. Tick burden on European roe deer (*Capreolus capreolus*). Exp Appl Acarol. 2010;51:405-17.
246. Kjellander P, Gaillard J-M, Hewison A. Density-dependent responses of fawn cohort body mass in two contrasting roe deer populations. Oecologia. 2006;146:521-30.
247. Abbas F, Morellet N, Hewison AJM, Merlet J, Cargnelutti B, Lourtet B, et al. Landscape fragmentation generates spatial variation of diet composition and quality in a generalist herbivore. Oecologia. 2011;167:401-11.
248. Brugger K, Walter M, Chitimia-Dobler L, Dobler G, Rubel F. Seasonal cycles of the TBE and Lyme borreliosis vector *Ixodes ricinus* modelled with time-lagged and interval-averaged predictors. Exp Appl Acarol. 2017;73:439-50.
249. Kurtenbach K, Hanincová K, Tsao JI, Margos G, Fish D, Ogden NH. Fundamental processes in the evolutionary ecology of Lyme borreliosis. Nature Reviews Microbiology. 2006;4:660-9.
250. Ogden NH, St-Onge L, Barker IK, Brazeau S, Bigras-Poulin M, Charron DF, et al. Risk maps for range expansion of the Lyme disease vector, *Ixodes scapularis*, in Canada now and with climate change. Int J Health Geogr. 2008;7:24.
251. Alkishe AA, Peterson AT, Samy AM. Climate change influences on the potential geographic distribution of the disease vector tick *Ixodes ricinus*. PloS ONE. 2017;12:e0189092.
252. Li S, Gilbert L, Harrison PA, Rounsevell MDA. Modelling the seasonality of Lyme disease risk and the potential impacts of a warming climate within the heterogeneous landscapes of Scotland. J R Soc Interface. 2016;13:20160140.

253. Ogden NH, Bigras-Poulin M, O'Callaghan CJ, Barker IK, Lindsay LR, Maarouf A, et al. A dynamic population model to investigate effects of climate on geographic range and seasonality of the tick *Ixodes scapularis*. Int J Parasitol. 2005;35:375-89.

254. BikeAttitude: BikeAttitude, The World of Freeride. www.neuchbikepark.ch (2003). Accessed October 28 2019.

255. Neuchâtel LVd: Fête de Chaumont. www.neuchatelville.ch (2011). Accessed October 28 2019.

256. Wilson ML. Reduced abundance of adult *Ixodes dammini* (Acari: Ixodidae) following destruction of vegetation. J Econ Entomol. 1986;79:693-6.

257. Schulze TL, Jordan RA, Hung RW. Suppression of subadult *Ixodes scapularis* (Acari: Ixodidae) following removal of leaf litter. J Med Entomol. 1995;32:730-3.

258. Tack W, Madder M, Baeten L, Vanhellemont M, Verheyen K. Shrub clearing adversely affects the abundance of Ixodes ricinus ticks. Exp Appl Acarol. 2013;60:411-20.

259. Medlock JM, Pietzsch ME, Rice NVP, Jones L, Kerrod E, Avenell D, et al. Investigation of ecological and environmental determinants for the presence of questing *Ixodes ricinus* (Acari: Ixodidae) on Gower, South Wales. J Med Entomol. 2014;45:314-25.

260. Gilbert L, Maffey GL, Ramsay SL, Hester AJ. The effect of deer management on the abundance of *Ixodes ricinus* in Scotland. Ecol Appl. 2012;22:658-67.

261. Tälleklint-Eisen L, Lane RS. Efficiency of drag sampling for estimating population sizes of *Ixodes pacificus* (Acari: Ixodidae) nymphs in leaf litter. J Med Entomol. 2000;37:484-7.

262. Eisen RJ, Eisen L, Ogden NH, Beard CB. Linkages of weather and climate with *Ixodes scapularis* and *Ixodes pacificus* (Acari: Ixodidae), enzootic transmission of *Borrelia burgdorferi*, and Lyme disease in North America. J Med Entomol. 2016;53:250-61.

263. Kiewra D, Kryza M, Szymanowski M. Influence of selected meteorological variables on the questing activity of *Ixodes ricinus* ticks in Lower Silesia, SW Poland. J Vector Ecol. 2014;39:138-45.

264. Li S, Heyman P, Cochez C, Simons L, Vanwambeke SO. A multi-level analysis of the relationship between environmental factors and questing *Ixodes ricinus* dynamics in Belgium. Parasit Vectors. 2012;5:149.

265. Herrmann C, Gern L. Do the level of energy reserves, hydration status and *Borrelia* infection influence walking by *Ixodes ricinus* (Acari: Ixodidae) ticks? Parasitology. 2012;139:330-7.

266. Perret JL, Guerin PM, Diehl PA, Vlimant M, Gern L. Darkness induces mobility, and saturation deficit limits questing duration, in the tick *Ixodes ricinus*. J Exp Biol. 2003;206:1809-15.
267. James M, Bowman A, Forbes K, Lewis F, McLeod J, Gilbert L. Environmental determinants of *Ixodes ricinus* ticks and the incidence of *Borrelia burgdorferi* sensu lato, the agent of Lyme borreliosis, in Scotland. Parasitology. 2012;140:1-10.
268. Tagliapietra V, Rosà R, Arnoldi D, Cagnacci F, Capelli G, Montarsi F, et al. Saturation deficit and deer density affect questing activity and local abundance of *Ixodes ricinus* (Acari, Ixodidae) in Italy. Vet Parasitol. 2011;183:114-24.
269. Herrmann C, Gern L. Survival of *Ixodes ricinus* (Acari: Ixodidae) under challenging conditions of temperature and humidity is influenced by *Borrelia burgdorferi* sensu lato infection. J Med Entomol. 2010;47:1196-204.
270. Herrmann C, Gern L. Survival of *Ixodes ricinus* (Acari: Ixodidae) nymphs under cold conditions is negatively influenced by frequent temperature variations. Ticks Tick Borne Dis. 2013;4:445-51.
271. Hurry G, Maluenda E, Sarr A, Belli A, Hamilton P, Duron O, et al. Infection with *Borrelia afzelii* reduces moulting time of *Ixodes ricinus* ticks. 2021.
272. Rosà R, Andreo V, Tagliapietra V, Baráková I, Arnoldi D, Hauffe HC, et al. Effect of climate and land use on the spatio-temporal variability of tick-borne bacteria in Europe. Int J Env Res Public Health. 2018;15:732.

11 Acknowledgements

First, I would like to very much thank my supervisor Maarten Voordouw for the continuous support of my PhD study and related research, for his patience, kindness, motivation, immense knowledge, and hospitality in a country where I experienced the coldest temperature of my life. His guidance helped me in all the time of research and writing of this thesis. I could not have imagined having a better advisor and mentor.

Besides my supervisor, I would like to thank the rest of my thesis committee: Prof. Jacob Koella, Prof. Pilar Junier, Prof. Olaf Kahl, and Prof. Alexander Mathis for accepting to be part of my PhD thesis defence committee.

My sincere thanks also go to Prof. Lise Gern who provided me access to the data and financial support. I would like to acknowledge Oliver Rais (Pitou) for his wonderful contribution to this project by collecting over 40'000 ticks. Without their precious support and work it would not have been possible to conduct this research.

I thank my fellow labmates, Dr. Dolores Genné, Dr. Andrea Gómez-Chamorro, Anouk Sarr and Marika De Fabritis, Océane Courbat for the stimulating discussions, essential help and advices throughout my project, and for all the fun and tremendous laughs we have had in the last five years.

I would like to thank all the related people to the lab for their valuable support as well as happy distractions to rest my mind outside of my research: Mélisande Aellen, Ophélie Gning, Alessandro Belli, Alida Kropf, Sandra Le Bissonnais, Tiago Gonçalves, Dr. Alfonso Rojas Mora, Dr. Gaël Hauser, Dr. Kevin Thiévent, Dr. Giacomo Zilio, Dr. Jonas Durand, Elodie Maluenda, Jérémy Berret, Liselore Roelfstra.

Beaucoup de choses se sont déroulées pendant ces cinq dernières années : bonnes et mauvaises. J'ai été extrêmement chanceuse d'avoir été entourée par des amis et une famille sur qui j'ai toujours peu compter et qui ont toujours su être présents dans les moments où il le fallait : à Christian Livi, Yolanda Ventura, Julien Jacot, Mathieu Rubi, Sabine Jacot, Alberto (dont je ne me rappelle jamais le nom de famille), Noemy Renevey, merci du fond du cœur. A ma famille,

Møøøm, le vieux Halibut, Rummi, Manu, et le p’tit T-Rex, merci de votre soutien et amour inconditionnels. Je vous aime !

Questa tesi non sarebbe mai stata possibile senza la mia ragazza, Robi, che c'è sempre per me, che mi ha spinto quando ne avevo bisogno, che mi ha sempre sostenuto, che mi ha permesso di superarmi e superare ogni passo per finire, e soprattutto non si è mai fermata di amarmi. Amore, ti amo tanto tantissimo !

Thank you ! Merci ! Grazie !

12 Appendixes

Additional file – Chapter 1

Climate and tree seed production predict the abundance of the European Lyme disease vector over a 15-year period

Cindy Bregnard, Olivier Rais, and Maarten J. Voordouw

Table of Contents

SECTION 1 - Validation of the field-collected temperature data 229
SECTION 2 - Validation of the field-collected relative humidity data 237
SECTION 3 – Interpolation of the climap-net climate data 245
SECTION 4 – full statistical analysis of the cumulative nymph abundance (cnd) for the four elevation sites 247
SECTION 5 – Full statistical analysis of the cumulative adult abundance (cad) for the four elevation sites 261
SECTION 6 – Full model selection table, support of each individual explanatory variable, and model-averaged parameter estimates of the nymph abundance for the three lowest elevation sites 273
SECTION 7 – Assumptions of the linear models for the best models from the aic-based model selection approach of the nymph and adult abundance for the three lowest elevation sites 283
SECTION 8 – Parameter estimates of the top model in the model selection table of the nymph abundance for the three lowest elevation sites 285
SECTION 9 – Time lag between the nymph abundance and beech masting 287
SECTION 10 – Climate change over the 15-year study period 295
SECTION 11 – Analysis of cnd using generalized linear models with negative binomial errors 311

SECTION 1 - Validation of the field-collected temperature data

Methods – Correlation between field-collected and Climap-net data: To validate our field-collected temperature data, we compared it to the Climap-net data that we obtained from two weather stations that are close to our four elevation sites and that are located at 485 m ASL in Neuchâtel and at 1136 m ASL in Chaumont. We used Pearson's correlation tests to show that the mean daily temperature was correlated between the field-collected data and each of the two weather stations. We also used a paired samples t-test to determine the difference in the mean daily temperature between our field-collected data and each of the two weather stations.

Results – Correlation between field-collected data and Climap-net data: Across all four elevation sites, the mean daily temperature for the field-collected data and the Neuchâtel weather station was positively correlated (Pearson's $r = 0.907$, $n = 597$, $p < 0.001$; Figure S1; Table S1). The daily mean temperature from the field-collected data was 13% higher than the Neuchâtel weather station data (mean difference ± standard error: 2.0 ± 0.01°C), and this difference was significant (Paired sample t-test: $df = 596$, $t = -17.181$, $p < 0.001$). Taking each elevation site independently, the mean daily temperature was positively correlated between the field-collected data and the Neuchâtel weather station (Figure S2; Table S1). The absolute difference in mean daily temperature between the field-collected data and the Neuchâtel weather station increased from the top site (0.3 °C) to the low elevation site (3.9 °C; Table S2). Across all four elevation sites, the mean daily temperature for the field-collected data and the Chaumont weather station was positively correlated (Pearson's $r = 0.914$, $n = 597$, $p < 0.001$; Figure S1; Table S1). The daily mean temperature from the field-collected data was 34% higher than the Chaumont weather station data (mean difference ± standard error: 5.4 ± 0.11°C), and this difference was significant (Paired sample t-test: $df = 596$, $t = -47.908$, $p < 0.001$). Taking each elevation site independently, the mean daily temperature was positively correlated between the field-collected data and the Chaumont weather station (Figure S3; Table S1). The absolute difference in mean daily temperature between the field-collected data and the Chaumont weather station increased from the top site (3.0 °C) to the low elevation site (7.1 °C; Table S3). In summary, the strong correlations between the mean daily temperature for field-collected data and each of the two weather stations validate the use of our field-collected temperature data.

Table S1. The correlation in the daily mean temperature between the field-collected data and the Climap-net data is shown for each of the four elevation sites and the two weather stations. The four sites were located on the south side of Chaumont Mountain. The two weather stations in Neuchâtel and Chaumont were located at 485 m ASL and 1136 m ASL, respectively. The mean daily temperature for the field-collected data and the two weather stations were measured at 60 cm above ground and 200 cm above ground, respectively. Shown are Pearson's correlation coefficient (r), the sample size (n), and the statistical significance of the correlation (p).

	Neuchâtel[b]			Chaumont[c]		
Site	r	n	p	r	n	p
Top	0.907	142	< 0.001	0.939	142	< 0.001
High	0.924	147	< 0.001	0.949	147	< 0.001
Medium	0.946	154	< 0.001	0.954	154	< 0.001
Low	0.950	154	< 0.001	0.928	154	< 0.001
All[a]	0.907	597	< 0.001	0.914	597	< 0.001

[a] The daily mean temperatures were positively correlated between the field-collected data and the Climap-net data from both weather stations.

[b] The mean daily temperature from the field-collected data was 13% higher than the Climap-net data from the Neuchâtel weather station (mean difference ± standard error: 2.0 ± 0.01 °C), and this difference was significant (Paired sample t-test: df = 596, t = -17.181, p < 0.001).

[c] The mean daily temperature from the field-collected data was 34% higher than the Climap-net data from the Chaumont weather station (mean difference ± standard error: 5.4 ± 0.11 °C), and this difference was significant (Paired sample t-test: df = 596, t = -47.908, p < 0.001).

Table S2. Comparison of the mean daily temperature between the field-collected data and the Climap-net data from the Neuchâtel weather station is shown for each of the four elevation sites. The mean difference in temperature is calculated as the field-collected mean minus the Neuchâtel Climap-net mean. Shown are the mean temperatures for the two sources of data and the results of the paired sample t-test for each of the four elevation sites.

Site	Source	Mean (°C)	Diff (°C)	s.e. (°C)	t	df	p
Top	Field-collected	13.9	-0.3	0.28	1.282	141	0.202
	Neuchâtel Climap-net	14.2					
High	Field-collected	15.7	1.7	0.19	-8.093	146	< 0.001
	Neuchâtel Climap-net	14.0					
Medium	Field-collected	16.1	2.7	0.13	-14.622	153	< 0.001
	Neuchâtel Climap-net	13.4					
Low	Field-collected	17.2	3.9	0.23	-20.387	153	< 0.001
	Neuchâtel Climap-net	13.3					

Table S3. Comparison of the mean daily temperature between the field-collected data and the Climap-net data from the Chaumont weather station is shown for each of the four elevation sites. The mean difference in temperature is calculated as the field-collected mean minus the Chaumont Climap-net mean. Shown are the mean temperatures for the two sources of data and the results of the paired sample t-test for each of the four elevation sites.

Site	Source	Mean	Diff	s.e.	t	df	p
Top	Field-collected	13.9	3.0	0.15	-17.853	141	< 0.001
	Chaumont Climap-net	10.9					
High	Field-collected	15.7	5.0	0.12	-31.278	146	< 0.001
	Chaumont Climap-net	10.7					
Medium	Field-collected	16.1	6.0	0.24	-34.903	153	< 0.001
	Chaumont Climap-net	10.1					
Low	Field-collected	17.1	7.1	0.21	-31.332	153	< 0.001
	Chaumont Climap-net	10.0					

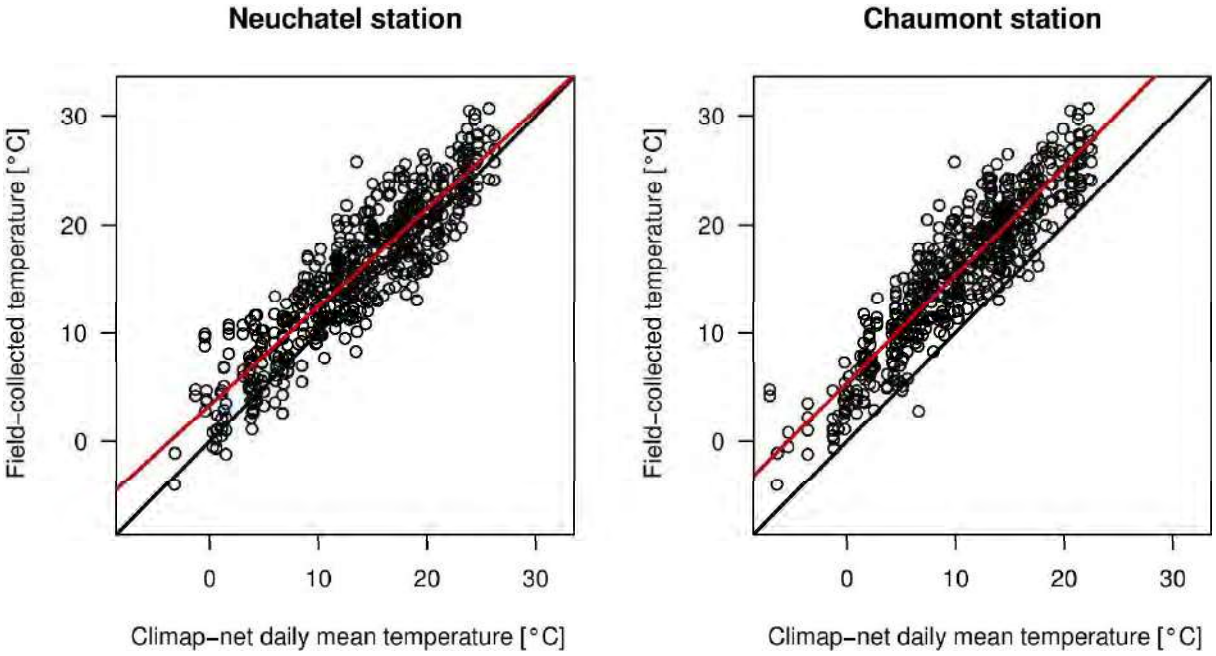

Figure S1. Linear regression of the mean daily temperature between the field-collected data and the Climap-net temperature data is shown for each of two weather stations: Neuchâtel (left panel) and Chaumont (right panel). The field-collected temperature data were sampled at four different elevation sites on Chaumont Mountain: low, medium, high, and top elevation site with an altitude of 620, 740, 900, and 1073, m ASL, respectively. The two weather stations in Neuchâtel and Chaumont were located at 485 m ASL and 1136 m ASL, respectively. The mean daily temperature for the field-collected data and the two weather stations were measured at 60 cm above ground and 200 cm above ground, respectively. The black line represents the 1:1 slope, whereas the red line represents the line of best fit from the linear regression.

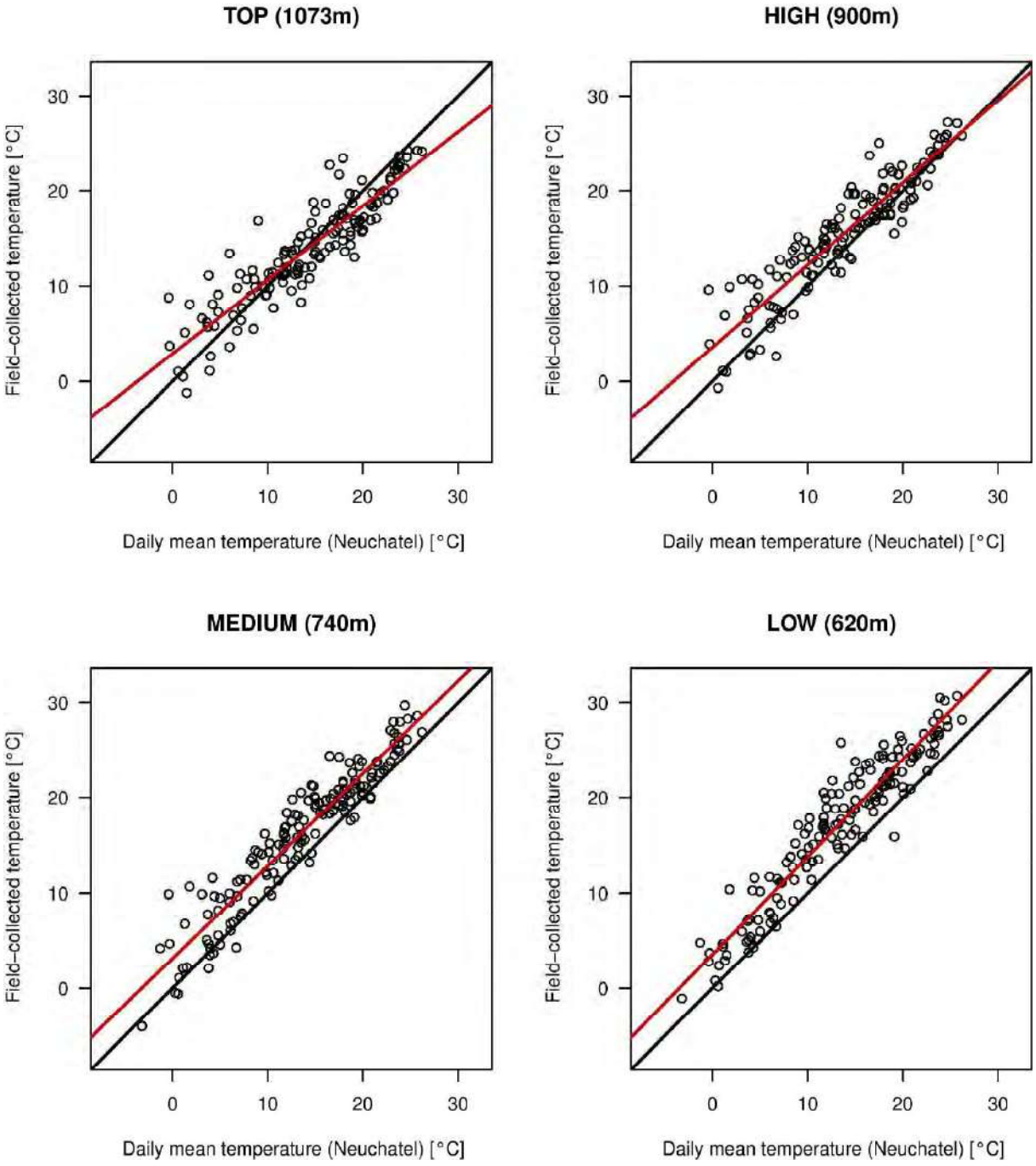

Figure S2. Linear regression of the mean daily temperature between the field-collected data and Climap-net temperature data from the Neuchâtel weather station is shown for each site. The field-collected temperature data were sampled at four different elevation sites on Chaumont Mountain: low, medium, high, and top elevation site with an altitude of 620, 740, 900, and 1073, m ASL, respectively. The weather station in Neuchâtel was located at 485 m ASL. The mean daily temperature for the field-collected data and the weather station were measured at 60 cm above ground and 200 cm above ground, respectively. The black line represents the 1:1 slope, whereas the red line represents the line of best fit from the linear regression.

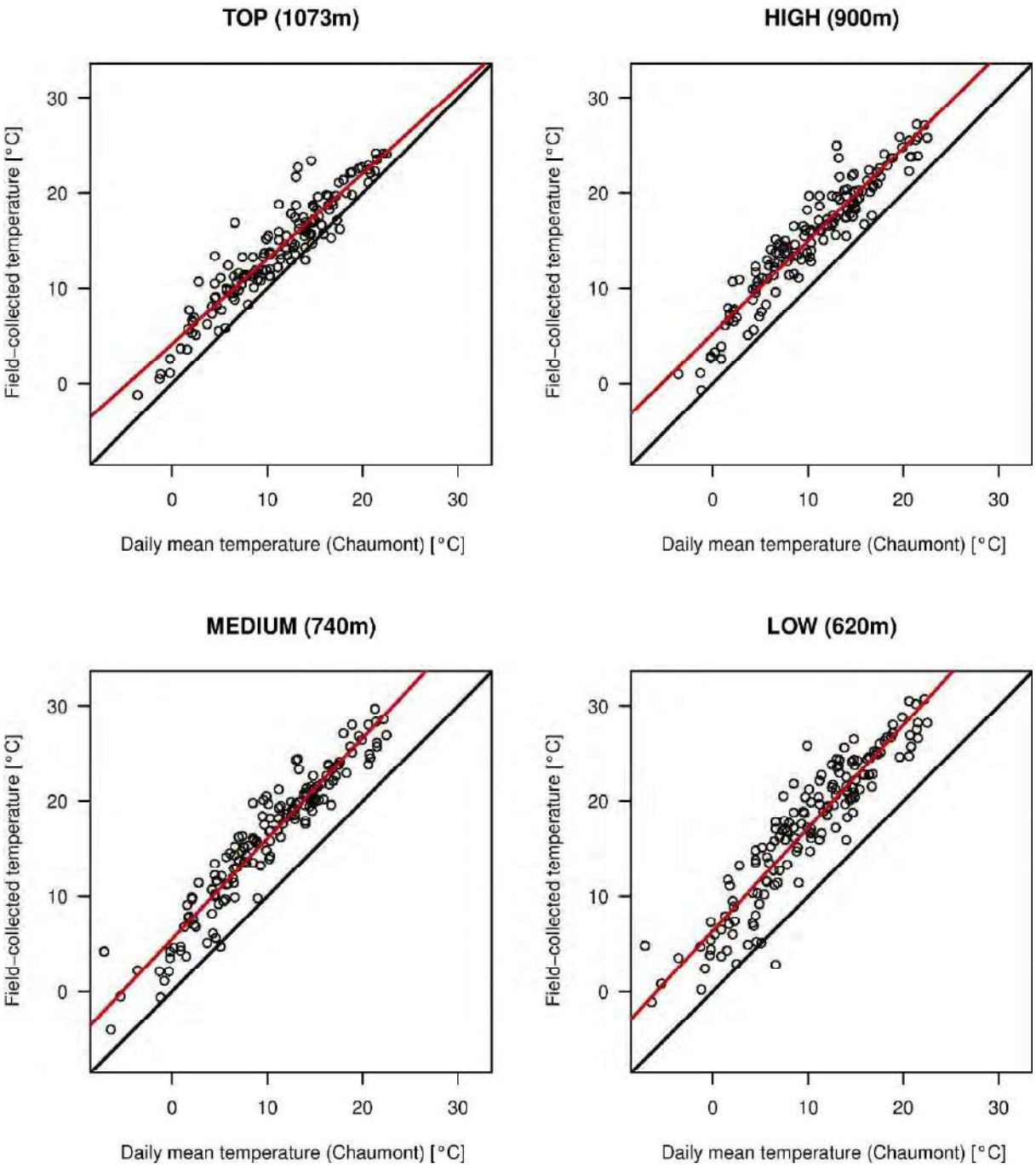

Figure S3. Linear regression of the mean daily temperature between the field-collected data and Climap-net temperature data from the Chaumont weather station is shown for each site. The field-collected temperature data were sampled at four different elevation sites on Chaumont Mountain: low, medium, high, and top elevation site with an altitude of 620, 740, 900, and 1073, m ASL, respectively. The weather station in Chaumont was located at 1136 m ASL. The mean daily temperature for the field-collected data and the weather station were measured at 60 cm above ground and 200 cm above ground, respectively. The black line represents the 1:1 slope, whereas the red line represents the line of best fit from the linear regression.

SECTION 2 - Validation of the field-collected relative humidity data

Methods – Correlation between field-collected and Climap-net data: To validate our field-collected relative humidity data, we compared it to the Climap-net data that we obtained from two weather stations that are close to our four elevation sites and that are located at 485 m ASL in Neuchâtel and at 1136 m ASL in Chaumont. We used Pearson's correlation tests to show that the mean daily relative humidity was correlated between the field-collected data and each of the two weather stations. We also used a paired samples t-test to determine the difference in the mean daily relative humidity between our field-collected data and each of the two weather stations.

Results – Correlation between field-collected data and Climap-net data: Across all four elevation sites, the mean daily relative humidity for the field-collected data and the Neuchâtel weather station was positively correlated (Pearson's $r = 0.597$, $n = 571$, $p < 0.001$; Figure S4; Table S4). The daily mean relative humidity from the field-collected data was 8% lower than the Neuchâtel weather station data (mean difference ± standard error: -5.1 ± 0.41%), and this difference was significant (Paired sample t-test: $df = 570$, $t = 9.523$, $p < 0.001$). Taking each elevation site independently, the mean daily relative humidity was positively correlated between the field-collected data and the Neuchâtel weather station (Figure S5; Table S4). The absolute difference in mean daily relative humidity between the field-collected data and the Neuchâtel weather station increased from the top site (0.1%) to the low elevation site (9.1%; Table S5). Across all four elevation sites, the mean daily relative humidity for the field-collected data and the Chaumont weather station was positively correlated (Pearson's $r = 0.623$, $n = 571$, $p < 0.001$; Figure S4; Table S4). The daily mean relative humidity from the field-collected data was 10% lower than the Chaumont weather station data (mean difference ± standard error: -6.4 ± 0.38%), and this difference was significant (Paired sample t-test: $df = 570$, $t = 11.937$, $p < 0.001$). Taking each elevation site independently, the mean daily relative humidity was positively correlated between the field-collected data and the Chaumont weather station (Figure S6; Table S4). The absolute difference in mean daily relative humidity between the field-collected data and the Chaumont weather station increased from the top site (1.2%) to the low elevation site (10.4%; Table S6). In summary, the strong correlations between the mean daily relative humidity for field-collected data and each of the two weather stations validate the use of our field-collected relative humidity data.

Table S4. The correlation in the daily mean relative humidity between the field-collected data and the Climap-net data is shown for each of the four elevation sites and the two weather stations. The four sites were located on the south side of Chaumont Mountain. The two weather stations in Neuchâtel and Chaumont were located at 485 m ASL and 1136 m ASL, respectively. The mean daily relative humidity for the field-collected data and the two weather stations were measured at 60 cm above ground and 200 cm above ground, respectively. Shown are Pearson's correlation coefficient (r), the sample size (n), and the statistical significance of the correlation (p).

	Neuchâtel[b]			Chaumont[c]		
Site	r	n	P	r	n	p
Top	0.376	135	< 0.001	0.639	135	< 0.001
High	0.516	141	< 0.001	0.665	141	< 0.001
Medium	0.704	148	< 0.001	0.665	148	< 0.001
Low	0.800	147	< 0.001	0.603	147	< 0.001
All[a]	0.597	571	< 0.001	0.623	571	< 0.001

[a] The daily mean relative humidity was positively correlated between the field-collected data and the Climap-net data from both weather stations.

[b] The daily mean relative humidity from the field-collected data was 8% lower than the Climap-net data from the Neuchâtel weather station (mean difference ± standard error: -5.1 ± 0.41%), and this difference was significant (Paired sample t-test: df = 570, t = 9.523, p < 0.001).

[c] The daily mean relative humidity from the field-collected data was 10% lower than the Climap-net data from the Chaumont weather station (mean difference ± standard error: -6.4 ± 0.38%), and this difference was significant (Paired sample t-test: df = 570, t = 11.937, p < 0.001).

Table S5. Comparison of the mean daily relative humidity between the field-collected data and the Climap-net data from the Neuchâtel weather station is shown for each of the four elevation sites. The mean difference in relative humidity is calculated as the field-collected mean minus the Neuchâtel Climap-net mean. Shown are the mean relative humidity for the two sources of data and the results of the paired sample t-test for each of the four elevation sites.

Site	Source	Mean	Diff	s.e.	t	df	p
Top	Field-collected	68.1	-0.1	0.71	0.069	134	0.945
	Neuchâtel Climap-net	68.2					
High	Field-collected	64.1	-4.2	0.60	3.715	140	< 0.001
	Neuchâtel Climap-net	68.3					
Medium	Field-collected	61.5	-7.2	0.80	7.657	147	< 0.001
	Neuchâtel Climap-net	68.7					
Low	Field-collected	59.6	-9.1	0.96	10.668	146	< 0.001
	Neuchâtel Climap-net	68.7					

Table S6. Comparison of the mean daily relative humidity between the field-collected data and the Climap-net data from the Chaumont weather station is shown for each of the four elevation sites. The mean difference in relative humidity is calculated as the field-collected mean minus the Chaumont Climap-net mean. Shown are the mean relative humidity for the two sources of data and the results of the paired sample t-test for each of the four elevation sites.

Site	Source	Mean	Diff	s.e.	t	df	p
Top	Field-collected	68.1	-1.2	0.66	1.168	134	0.245
	Chaumont Climap-net	69.3					
High	Field-collected	64.1	-5.3	0.50	5.525	140	< 0.001
	Chaumont Climap-net	69.4					
Medium	Field-collected	61.5	-8.5	0.73	8.421	147	< 0.001
	Chaumont Climap-net	70.0					
Low	Field-collected	59.6	-10.4	0.91	8.967	146	< 0.001
	Chaumont Climap-net	70.0					

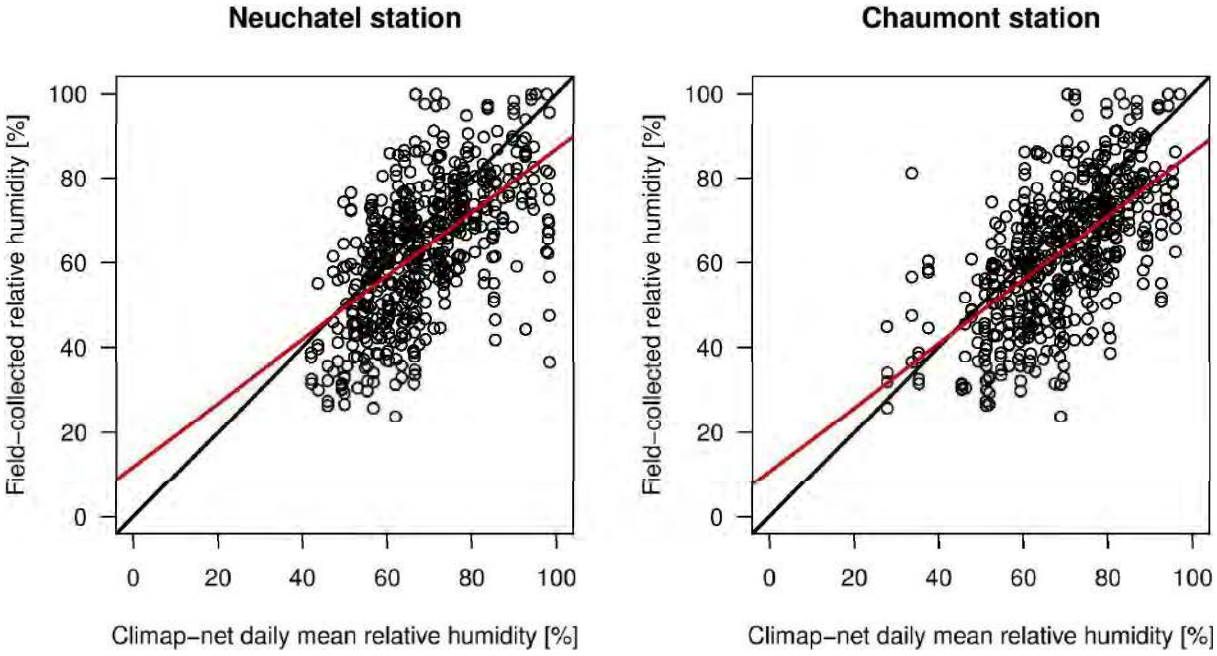

Figure S4. Linear regression of the mean daily relative humidity between the field-collected data and the Climap-net relative humidity data is shown for each of two weather stations: Neuchâtel (left panel) and Chaumont (right panel). The field-collected relative humidity data were sampled at four different elevation sites on Chaumont Mountain: low, medium, high, and top elevation site with an altitude of 620, 740, 900, and 1073, m ASL, respectively. The two weather stations in Neuchâtel and Chaumont were located at 485 m ASL and 1136 m ASL, respectively. The mean daily relative humidity for the field-collected data and the two weather stations were measured at 60 cm above ground and 200 cm above ground, respectively. The black line represents the 1:1 slope, whereas the red line represents the line of best fit from the linear regression.

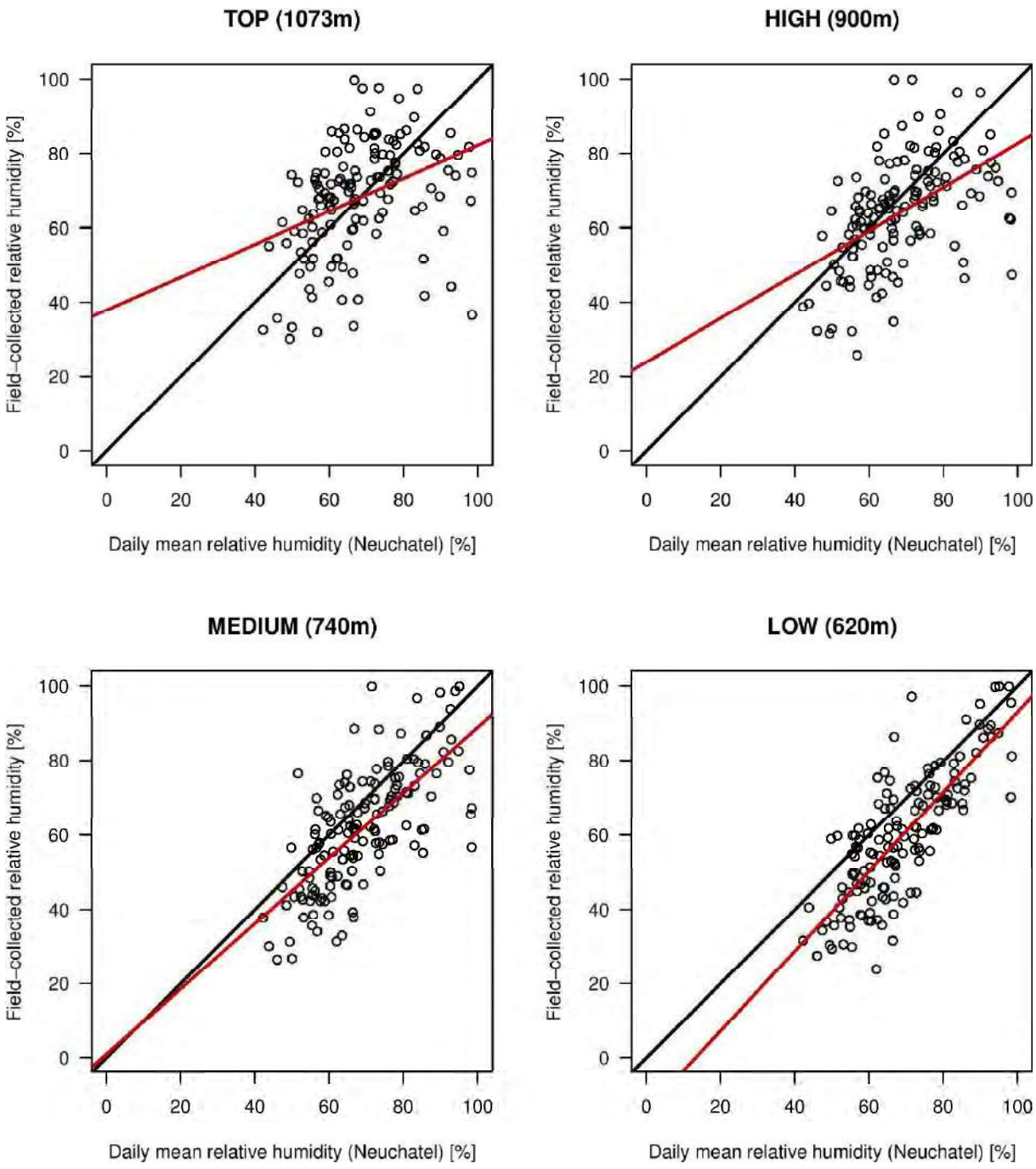

Figure S5. Linear regression of the mean daily relative humidity between the field-collected data and Climap-net relative humidity data from the Neuchâtel weather station is shown for each site. The field-collected relative humidity data were sampled at four different elevation sites on Chaumont Mountain: low, medium, high, and top elevation site with an altitude of 620, 740, 900, and 1073, m ASL, respectively. The weather station in Neuchâtel was located at 485 m ASL. The mean daily relative humidity for the field-collected data and the weather station were measured at 60 cm above ground and 200 cm above ground, respectively. The black line represents the 1:1 slope, whereas the red line represents the line of best fit from the linear regression.

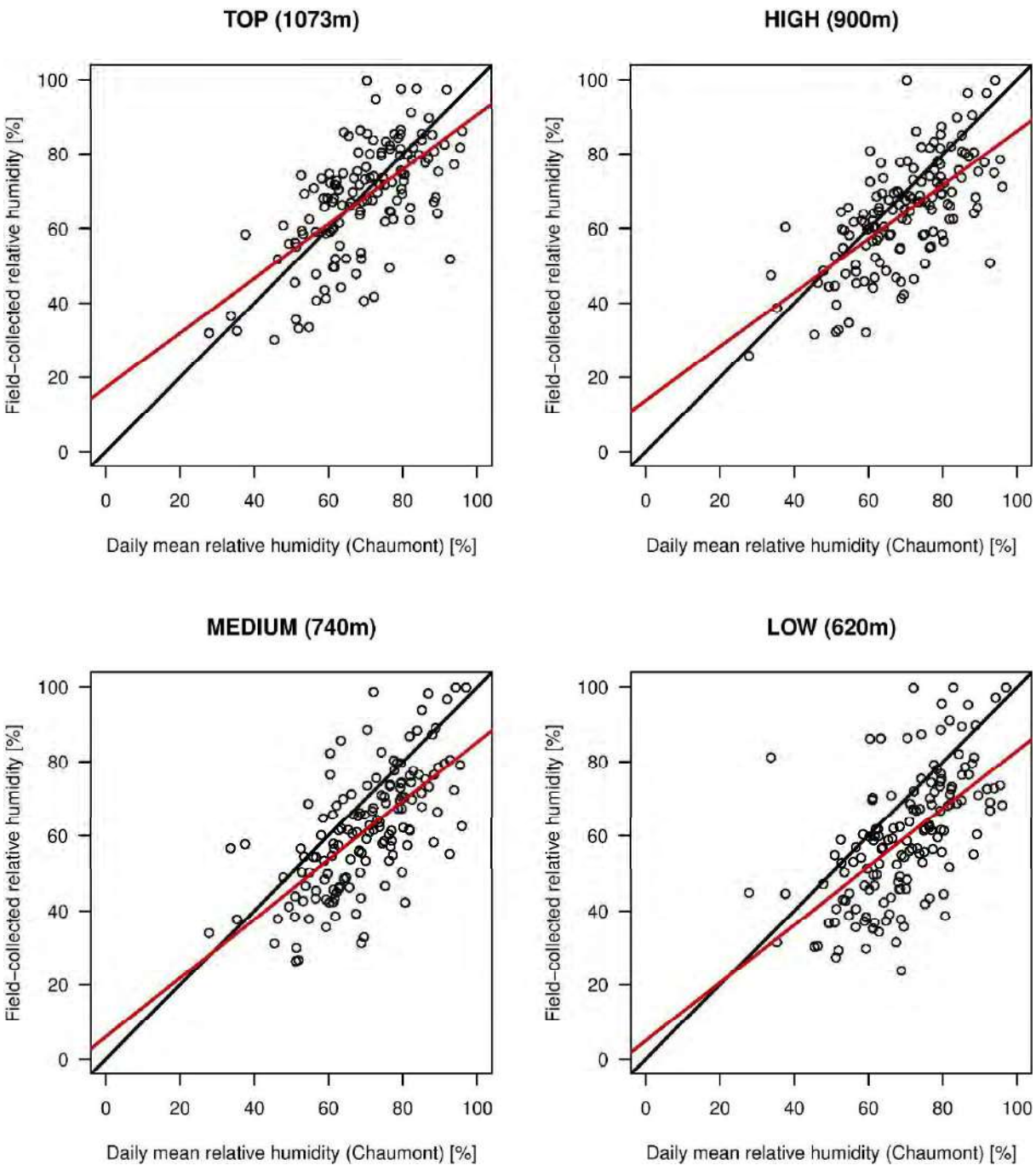

Figure S6. Linear regression of the mean daily relative humidity between the field-collected data and Climap-net relative humidity data from the Chaumont weather station is shown for each site. The field-collected relative humidity data were sampled at four different elevation sites on Chaumont Mountain: low, medium, high, and top elevation site with an altitude of 620, 740, 900, and 1073, m ASL, respectively. The weather station in Chaumont was located at 1136 m ASL. The mean daily relative humidity for the field-collected data and the weather station were measured at 60 cm above ground and 200 cm above ground, respectively. The black line represents the 1:1 slope, whereas the red line represents the line of best fit from the linear regression.

SECTION 3 – Interpolation of the Climap-net climate data

Methods: Climap-net data were obtained from two weather stations that are close to our four elevation sites and that are located at 485 m ASL in Neuchâtel and at 1136 m ASL in Chaumont. To create a climate profile that was specific for each of the four elevation sites, we interpolated the values between the two weather stations using the relative elevation distance of each elevation site to the two weather stations. For example, the total elevation distance between the Neuchâtel and Chaumont weather stations is 651 meters, and the elevation distance between the top site and the Neuchâtel weather station is 620 meters, which represents 95.2% of the elevation distance. Thus, the climate at the top site is expected to be more similar to the Chaumont weather station (95.2%) compared to the Neuchâtel weather station (4.8%), whereas the reverse would be true for the low site. For each elevation site, the mean daily temperature, relative humidity, saturation deficit, and precipitation were calculated based on the interpolating percentages (Table S7).

Table S7. Climap-net data interpolation. Shown are the site, elevation, elevation distance with the Neuchâtel weather station (Dist 1), elevation distance between Neuchâtel and Chaumont weather station (Dist 2), the interpolating percentage from the Neuchâtel weather station (Neuchâtel), and the interpolating percentage from the Chaumont weather station (Chaumont).

Site	Elevation	Dist 1	Dist 2	Neuchâtel	Chaumont
Top	1073	620	651	4.80%	95.20%
High	900	447	651	31.30%	68.70%
Medium	740	287	651	55.90%	44.10%
Low	620	167	651	74.30%	25.70%

SECTION 4 – Full statistical analysis of the cumulative nymph abundance (CND) for the four elevation sites

Background: In the main manuscript, we restricted the analysis to the cumulative nymph density (CND) at the low, medium, and high elevation sites. For simplicity, we did not include analyses of the cumulative adult tick abundance (CAD). We excluded the top site from the analysis of the CND because we believe that the construction of an adventure park caused the top site to have very different tick population dynamics over time compared to the other three elevation sites. In this section, we analyze the CND for all four sites. With respect to the CND, we show that the most important results remain the same. These results are that the CND increased over time at the three lower elevations, that CND is positive related to beech seed production two years prior, and that it is negatively related with elevation and relative humidity.

Methods: We used a model selection approach based on the Akaike information criterion (AIC) to find the most parsimonious model. Models were ranked according to their AIC values and the Akaike weights were calculated for each model. We used the Akaike weights to calculate the model-averaged parameter estimates and their 95% confidence intervals (CIs). The support for a given explanatory variable of interest was calculated as the sum of the Akaike weights of all the models in the set that included that particular explanatory variable. The support for a given explanatory variable ranged from low (0.0%) to high (100%).

Results – Variation in CND among elevation sites: We used a one-way ANOVA to compare the mean CND between the four elevations (i.e. this analysis ignores year). The CND was significantly different between the four elevation sites ($F_{4, 52} = 5180.0$, $p < 0.001$; Figure S7). The mean CND (and 95% CI) for the low, medium, high, and top elevations were as follows: 21311 (95% CI = 16465–27584), 18127 (95% CI = 14005–23463), 10854 (95% CI =8385–14048), 2421 (95% CI = 1871–3134). In summary, the mean nymph density was inversely related to the altitudinal gradient and it was highest at the low elevation and lowest at the top elevation (Figure S7).

Results – Effects of the abiotic and biotic variables on the variation in the annual estimates of cumulative nymphal density (CND): For the CND, the best six models had a combined support of 95.0% (Table S8). The other 46 models had a combined support of 5% (Table S8). The best six models all contained the explanatory variables of elevation site, year, the site:year

interaction, and beech tree mast score, but they differed with respect to the identity of the climate variable. The best model had 57.0% of the support, explained 91.6% of the variation in the CND, and contained the explanatory variables of elevation site (partial r^2 = 65.6%), year (partial r^2 = 9.1%), the site:year interaction (partial r^2 = 8.8%), beech tree mast score from 2 years prior (partial r^2 = 6.9%), and the field-collected relative humidity from the same year (partial r^2 = 1.4%) (Table S8). For the individual explanatory variables, there was strong support for the explanatory variables of site (100.0%), year (100.0%), site:year interaction (100.0%), beech tree mast score from 2 years prior (100.0%), and moderate support for the field-collected relative humidity from the same year (56.7%), the field-collected saturation deficit from the same year (22.8%; Table S9), and the field-collected temperature from the same year (9.6%; Table S9). None of the other explanatory variables had a support > 2.0% (Table S9).

We calculated the model-averaged parameter estimates to make robust inferences about the relationships between the explanatory variables and the CND (Table S10). We calculated the effect sizes with respect to the following baseline: the site was low elevation, the year was 2004, the beech tree mast was 1, and the field-collected relative humidity from the same year was 50.0%.

The CND was different between the four elevation sites, but this difference was not significant (Figures S7 and S8). The CND at the low elevation was 1.3% higher than the medium elevation (Medium – Low contrast = 0.001, 95% CI = -0.223 – 0.224; Table S10). The CND at the low elevation was 31.5% higher than the high elevation (High – Low = -0.153, 95% CI = -0.383 – 0.076; Table S10). The CND at the low elevation was 49.0% higher than the top elevation (Top – Low = -0.216, 95% CI = -0.460 – 0.028; Table S10). In summary, the CND was inversely related to altitude; it was highest at the low elevation and lowest at the top elevation (Figure S7 and Figure S8).

The site:year interaction indicated that the change in the CND over time differed between the four elevation sites (Figures S7 and S8, Table S10). Over the 15-year period (2004 – 2018), the CND increased by 123.1% at the low site (slope = 0.025, 95% CI = 0.008 – 0.042), increased by 82.8% at the medium site (Medium – Low contrast of the slope = -0.006, 95% CI = -0.030 – 0.018), increased by 55.3% at the high site (High – Low contrast of the slope = -0.011, 95% CI = -0.035 – 0.012), and decreased by 80.8% at the top site (Top – Low contrast of the slope = -0.076, 95% CI = -0.100 – -0.052). In summary, the CND increased over time at the low, medium, and high elevations but decreased at the top elevation (Figures S7 and S8, Table S10).

The covariate beech mast score 2 years prior had a strong positive effect on the CND (0.059 per class, 95% CI = 0.039 – 0.079; Figure S7, Table S10). Increasing the beech mast score from 1 (poor mast) to 5 (full mast) increased the CND by 72.5% at each of the four elevation sites on Chaumont Mountain (Figure S8).

Over the 15-year study period, beech trees produced 6 years of good or full mast scores (2004, 2006, 2009, 2011, 2014, and 2016), where high CND years were expected to occur two years later (2006, 2008, 2011, 2013, 2016, and 2018, respectively). At the low, medium, high, and top site, these 6 good mast years produced 3 (2016, 2018, and 2006), 4 (2006, 2013, 2018, and 2016), 4 (2018, 2006, 2016, and 2011), and 2 (2006 and 2011) of the 6 highest CND values two years later (Figure S7).

The slope of the field-collected relative humidity from the same year was negative (-0.057 per standard deviation; Table S10) and the 95% CI did not overlap zero (-0.096 – -0.019), indicating that the CND decreased with the field-collected relative humidity in the same year. Increasing the field-collected relative humidity from 50.0% to 75.0% decreased the CND from the same year by 38.2% at each of the four elevation sites on Chaumont Mountain (Figure S8; Table S10). Temperature had a positive effect on the CND (slope = 0.059 per standard deviation, 95% CI = 0.009 – 0.109; Table S10) and saturation deficit had a positive effect on the CND (slope = 0.063 per standard deviation, 95% CI = 0.016 – 0.111; Table S10). In summary, our study found that years with higher temperatures and lower relative humidity have higher annual estimates of the CND compared to years with lower temperatures and high relative humidity. According to our model selection table, the level of support for relative humidity (56.7% in Table S9) is 5.9 times higher than that of temperature (9.6% in Table S9). As expected, the saturation deficit has an intermediate level of support (22.8% in Table S9) because it is calculated using both the temperature and relative humidity.

In summary, the CND increased significantly over time at the three lower elevations and decreased at the top elevation. The CND increased with beech tree seed production two years earlier while it decreased significantly with the field-collected relative humidity in the same year (Table S10).

Discussion – removal of the top elevation in the main manuscript: We expected that tick abundance would increase more dramatically at the higher elevation sites. In contrast, we found that the CND actually decreased by 81.0% over time at the top elevation. One potential explanation is the construction of recreation facilities near the top of Chaumont Mountain with negative consequences for tick ecology (especially at our top site). Construction of a network

of mountain bike trails occurred from 2006 to 2010 and construction of an adventure park, which includes a zip line and outdoor laser games, started in 2011. These recreation facilities have greatly increased the number of human visitors to the top of Chaumont Mountain [1, 2]. The top elevation site was the most affected because it is closest to the adventure park and the start of the mountain biking trails (a distance of 25 m), whereas the other elevation sites are much further away (770, 1500, and 2600 m, respectively; Figure S9). The alteration of the forest caused by the construction and maintenance of these recreational areas since the early 2000's may have reduced the habitat suitability for ticks. Habitat modifications such as clearing bushes along forest trails have been shown to reduce the abundance of ticks [3]. A larger human footprint may also have reduced the abundance of vertebrate hosts by scaring them away. In summary, a plausible explanation for the 81.0% decrease in nymph abundance at the top elevation site on Chaumont Mountain is that the construction of the outdoor adventure park reduced the habitat quality for ticks and their vertebrate hosts. An interesting alternative explanation is that our monthly tick sampling over a period of 15 years decreased the nymphal tick abundance at the top site. Field studies typically assume that dragging removes a small fraction of the tick population, but this assumption may not be true in habitats where tick density is already low. For this reason, we restricted our analysis in the main manuscript to the three lower elevation sites.

Table S8. Model selection results are shown for the linear models with normal errors of the log10-transformed CND response variable. The explanatory variables were elevation site, year, tree masting variables obtained from MASTREE, and the climate variables obtained from the Climap-net and collected in the field. Shown for each model are the model rank (Rank), model structure (see below for explanation of explanatory variables), model degrees of freedom (Df), log-likelihood (logLik), Akaike information criterion (AIC), difference in the AIC value from the top model (ΔAIC), model weight (Weight1), cumulative weight (Weight2), and adjusted r-squared (r^2).

Rank	Model structure	Df	logLik	AIC	ΔAIC	Weight1	Weight2	r^2
1	CND ~ S+Y+S:Y+B+RH2	11	43.2	-58.3	0.0	57.0	57.0	91.6
2	CND ~ S+Y+S:Y+B+SD2	11	42.3	-56.5	1.8	23.0	80.0	91.4
3	CND ~ S+Y+S:Y+B+T2	11	41.4	-54.8	3.5	10.0	90.0	91.1
4	CND ~ S+Y+S:Y+B+$SD2_{y-1}$	11	39.8	-51.5	6.8	2.0	92.0	90.6
5	CND ~ S+Y+S:Y+B	10	38.2	-51.5	6.8	2.0	94.0	90.2
6	CND ~ S+Y+S:Y+B+$RH2_{y-1}$	11	39.4	-50.9	7.5	1.0	95.0	90.5
7	CND ~ S+Y+S:Y+B+T1	11	39.2	-50.5	7.9	1.0	96.0	90.4
8	CND ~ S+Y+S:Y+B+PR	11	39.1	-50.2	8.1	1.0	97.0	90.3
9	CND ~ S+Y+S:Y+B+PR_{y-1}	11	38.6	-49.2	9.2	1.0	98.0	90.2
10	CND ~ S+Y+S:Y+B+SD1	11	38.5	-48.9	9.4	1.0	99.0	90.1
11	CND ~ S+Y+S:B+B+S:Y	13	41.8	-48.9	9.5	1.0	100.0	90.8
12	CND ~ S+Y+S:Y+B+$T2_{y-1}$	11	38.4	-48.7	9.6	0.0	100.0	90.1
13	CND ~ S+Y+S:Y+B+$SD1_{y-1}$	11	38.3	-48.6	9.7	0.0	100.0	90.1
14	CND ~ S+Y+S:Y+B+$RH1_{y-1}$	11	38.3	-48.5	9.8	0.0	100.0	90.0
15	CND ~ S+Y+S:Y+B+$T1_{y-1}$	11	38.2	-48.4	9.9	0.0	100.0	90.0
16	CND ~ S+Y+S:Y+B+RH1	11	38.2	-48.4	9.9	0.0	100.0	90.0
17	CND ~ S+B+$T1_{y-1}$+S:$T1_{y-1}$	10	27.4	-29.9	28.5	0.0	100.0	85.6
18	CND ~ S+B+T1+S:T1	10	27.3	-29.7	28.7	0.0	100.0	85.6
19	CND ~ S+B	6	19.3	-24.9	33.4	0.0	100.0	82.3
20	CND ~ S+Y+S:Y	9	22.6	-23.3	35.1	0.0	100.0	83.3
21	CND ~ S+B+SD1+S:SD1	10	24.0	-23.2	35.1	0.0	100.0	83.8
22	CND ~ S+Y+B+RH2	8	20.7	-22.4	35.9	0.0	100.0	82.5
23	CND ~ S+Y+B	7	19.3	-22.3	36.0	0.0	100.0	82.0
24	CND ~ S+B+$SD1_{y-1}$+S:$SD1_{y-1}$	10	23.5	-22.1	36.2	0.0	100.0	83.5
25	CND ~ S+Y+B+SD2	8	20.5	-21.9	36.4	0.0	100.0	82.4
26	CND ~ S+Y+B+T2	8	20.3	-21.5	36.8	0.0	100.0	82.3
27	CND ~ S+Y+B+PR	8	20.1	-21.1	37.3	0.0	100.0	82.1
28	CND ~ S+B+RH2+S:RH2	10	22.8	-20.6	37.7	0.0	100.0	83.1
29	CND ~ S+Y+B+T1	8	19.7	-20.4	37.9	0.0	100.0	81.9
30	CND ~ S+B+S:B	9	21.2	-20.4	37.9	0.0	100.0	82.4

31	CND ~ S+Y+B+$RH1_{y-1}$	8	19.6	-20.2	38.1	0.0	100.0	81.8
32	CND ~ S+Y+B+$RH2_{y-1}$	8	19.6	-20.1	38.2	0.0	100.0	81.8
33	CND ~ S+Y+B+$SD2_{y-1}$	8	19.6	-20.1	38.2	0.0	100.0	81.8
34	CND ~ S+Y+B+SD1	8	19.5	-20.0	38.4	0.0	100.0	81.7
35	CND ~ S+Y+B+PR_{y-1}	8	19.4	-19.7	38.6	0.0	100.0	81.7
36	CND ~ S+Y+B+$T2_{y-1}$	8	19.4	-19.7	38.6	0.0	100.0	81.7
37	CND ~ S+Y+B+$T1_{y-1}$	8	19.4	-19.7	38.7	0.0	100.0	81.7
38	CND ~ S+Y+B+$SD1_{y-1}$	8	19.3	-19.6	38.7	0.0	100.0	81.6
39	CND ~ S+Y+B+RH1	8	19.3	-19.6	38.8	0.0	100.0	81.6
40	CND ~ S+B+SD2+S:SD2	10	21.9	-19.0	39.4	0.0	100.0	82.5
41	CND ~ S+B+PR_{y-1}+S:PR_{y-1}	10	21.7	-18.5	39.9	0.0	100.0	82.4
42	CND ~ S+B+T2+S:T2	10	21.6	-18.2	40.1	0.0	100.0	82.3
43	CND ~ S+Y+B+S:B	10	21.2	-17.5	40.9	0.0	100.0	82.1
44	CND ~ S+B+PR+S:PR	10	21.1	-17.4	41.0	0.0	100.0	82.0
45	CND ~ S+B+$RH1_{y-1}$+S:$RH1_{y-1}$	10	20.4	-15.8	42.5	0.0	100.0	81.5
46	CND ~ S+B+$RH2_{y-1}$+S:$RH2_{y-1}$	10	20.2	-15.5	42.8	0.0	100.0	81.4
47	CND ~ S+B+RH1+S:RH1	10	20.1	-15.4	43.0	0.0	100.0	81.4
48	CND ~ S+B+$SD2_{y-1}$+S:$SD2_{y-1}$	10	19.8	-14.7	43.6	0.0	100.0	81.2
49	CND ~ S+B+$T2_{y-1}$+S:$T2_{y-1}$	10	19.4	-14.0	44.4	0.0	100.0	80.9
50	CND ~ S+Y	6	10.3	-6.9	51.5	0.0	100.0	75.6
51	CND ~ B	3	-29.5	65.6	123.9	0.0	100.0	4.5
52	CND ~ P	3	-31.0	68.6	126.9	0.0	100.0	0.0

The acronyms for the explanatory variables are as follows: S = site, Y = year, B = beech tree mast score, P = spruce tree mast score, T1 = temperature from the Climap-net data, $T1_{y-1}$ = temperature in year y-1 from the Climap-net data, RH1 = relative humidity from the Climap-net data, $RH1_{y-1}$ = relative humidity in year y-1 from the Climap-net data, SD1 = saturation deficit from the Climap-net data, $SD1_{y-1}$ = saturation deficit in year y-1 from the Climap-net data, PR = precipitation from the Climap-net data, and PR_{y-1} = precipitation in year y-1 from the Climap-net data, T2 = temperature from the field-collected data, $T2_{y-1}$ = temperature in year y-1 from the field-collected data, RH2 = relative humidity from the field-collected data, $RH2_{y-1}$ = relative humidity in year y-1 from the field-collected data, SD2 = saturation deficit from the field-collected data, $SD2_{y-1}$ = saturation deficit in year y-1 from the field-collected data.

Table S9. The support for each individual explanatory variable is shown for the CND. This support is calculated as the sum of the Akaike weights for all the models in the set that include that particular explanatory variable.

Rank	Explanatory variable of interest	Support (%)
1	Site	100.0
2	Beech tree mast score	100.0
3	Year	100.0
4	Site:Year	100.0
5	RH2	56.7
6	SD2	22.8
7	T2	9.6
8	SD2y-1	1.9
9	RH2y-1	1.4
10	T1	1.1
11	PR	1.0
12	PRy-1	< 1.0
13	SD1	< 1.0
14	T2y-1	< 1.0
15	SD1y-1	< 1.0
16	RH1y-1	< 1.0
17	T1y-1	< 1.0
18	RH1	< 1.0
19	Site:T1y-1	< 1.0
20	Site:T1	< 1.0
21	Site:SD1	< 1.0
22	Site:SD1y-1	< 1.0
23	Site:RH2	< 1.0
24	Site:SD2	< 1.0
25	Site:PRy-1	< 1.0
26	Site:T2	< 1.0
27	Site:PR	< 1.0
28	Site:RH1y-1	< 1.0
29	Site:RH2y-1	< 1.0
30	Site:RH1	< 1.0
31	Site:SD2y-1	< 1.0
32	Site:T2y-1	< 1.0
33	Spruce tree mast score	< 1.0
34	Site:Beech tree mast score	< 1.0

The acronyms for the explanatory variables are as follows: T1 = temperature from the Climap-net data, $T1_{y-1}$ = temperature in year y-1 from the Climap-net data, RH1 = relative humidity

from the Climap-net data, $RH1_{y-1}$ = relative humidity in year y-1 from the Climap-net data, SD1 = saturation deficit from the Climap-net data, $SD1_{y-1}$ = saturation deficit in year y-1 from the Climap-net data, PR = precipitation from the Climap-net data, and PR_{y-1} = precipitation in year y-1 from the Climap-net data, T2 = temperature from the field-collected data, $T2_{y-1}$ = temperature in year y-1 from the field-collected data, RH2 = relative humidity from the field-collected data, $RH2_{y-1}$ = relative humidity in year y-1 from the field-collected data, SD2 = saturation deficit from the field-collected data, $SD2_{y-1}$ = saturation deficit in year y-1 from the field-collected data.

Table S10. Model-averaged parameter estimates are shown for the linear models of the log10-transformed CND response variable. Shown are the parameter types, the parameter names, the parameter estimates, and the 95% confidence limits (LL = lower limit and UL = upper limit). Estimate 1 is averaged over all the models in the set. Estimate 2 is averaged over the subset of models with a cumulative support of 95%. The 95% confidence limits are for estimate 2. Statistically significant parameter estimates are shown in bold-face type.

Type	Name	Estimate 1	Estimate 2	95% LL	95% UL
Intercept	Low site	3.919	3.919	3.747	4.090
Contrast 1	Medium site	0.001	0.001	-0.223	0.224
Contrast 2	High site	-0.153	-0.153	-0.383	0.076
Contrast 3	Top site	-0.216	-0.216	-0.460	0.028
Slope 1	Year	0.025	0.025	0.008	0.042
Slope 2	Beech tree mast score	0.059	0.059	0.039	0.079
Slope 3	Spruce tree mast score	0.000	0.034	-0.055	0.124
Slope 4	T1	0.001	0.054	-0.029	0.138
Slope 5	RH1	0.000	-0.003	-0.051	0.045
Slope 6	SD1	0.000	0.021	-0.043	0.085
Slope 7	PR	0.000	0.025	-0.016	0.065
Slope 8	$T1_{y-1}$	0.000	-0.008	-0.095	0.079
Slope 9	$RH1_{y-1}$	0.000	0.009	-0.051	0.068
Slope 10	$SD1_{y-1}$	0.000	0.017	-0.058	0.092
Slope 11	PR_{y-1}	0.000	-0.017	-0.061	0.026
Slope 12	T2	0.006	0.059	0.009	0.109
Slope 13	RH2	-0.033	-0.057	-0.096	-0.019
Slope 14	SD2	0.014	0.063	0.016	0.111
Slope 15	$T2_{y-1}$	0.000	0.014	-0.041	0.069
Slope 16	$RH2_{y-1}$	0.000	-0.032	-0.077	0.013
Slope 17	$SD2_{y-1}$	0.001	0.045	-0.011	0.101
Contrast 4	Medium site:Year	-0.006	-0.006	-0.030	0.018
Contrast 5	High site:Year	-0.011	-0.011	-0.035	0.012
Contrast 6	Top site:Year	-0.076	-0.076	-0.100	-0.052
Contrast 7	Medium site:Beech mast score	0.000	0.016	-0.041	0.073
Contrast 8	High site: Beech mast score	0.000	0.053	-0.004	0.110
Contrast 9	Top site: Beech mast score	0.000	-0.012	-0.068	0.045
Contrast 10	Medium site:T1	0.000	-0.079	-0.322	0.163
Contrast 11	High site:T1	0.000	-0.072	-0.310	0.166
Contrast 12	Top site:T1	0.000	-0.395	-0.628	-0.162
Contrast 13	Medium site:RH1	0.000	0.074	-0.112	0.261
Contrast 14	High site:RH1	0.000	0.002	-0.183	0.188

Contrast 15	Top site:RH1	0.000	0.080	-0.100	0.260
Contrast 16	Medium site:SD1	0.000	-0.065	-0.253	0.124
Contrast 17	High site:SD1	0.000	0.005	-0.192	0.201
Contrast 18	Top site:SD1	0.000	-0.264	-0.469	-0.060
Contrast 19	Medium site:PR	0.000	0.050	-0.095	0.195
Contrast 20	High site:PR	0.000	-0.017	-0.163	0.128
Contrast 21	Top site:PR	0.000	0.071	-0.073	0.214
Contrast 22	Medium site:$T1_{y-1}$	0.000	-0.136	-0.395	0.122
Contrast 23	High site:$T1_{y-1}$	0.000	-0.178	-0.431	0.074
Contrast 24	Top site:$T1_{y-1}$	0.000	-0.458	-0.705	-0.212
Contrast 25	Medium site:$RH1_{y-1}$	0.000	0.014	-0.194	0.222
Contrast 26	High site:$RH1_{y-1}$	0.000	-0.040	-0.246	0.166
Contrast 27	Top site:$RH1_{y-1}$	0.000	0.067	-0.132	0.266
Contrast 28	Medium site:$SD1_{y-1}$	0.000	-0.038	-0.264	0.187
Contrast 29	High site:$SD1_{y-1}$	0.000	-0.008	-0.241	0.224
Contrast 30	Top site:$SD1_{y-1}$	0.000	-0.290	-0.528	-0.052
Contrast 31	Medium site:PR_{y-1}	0.000	-0.001	-0.150	0.147
Contrast 32	High site:PR_{y-1}	0.000	-0.002	-0.151	0.146
Contrast 33	Top site:PR_{y-1}	0.000	0.118	-0.029	0.265
Contrast 34	Medium site:T2	0.000	-0.060	-0.274	0.154
Contrast 35	High site:T2	0.000	0.050	-0.162	0.262
Contrast 36	Top site:T2	0.000	-0.073	-0.285	0.138
Contrast 37	Medium site:RH2	0.000	-0.052	-0.198	0.094
Contrast 38	High site:RH2	0.000	-0.104	-0.262	0.053
Contrast 39	Top site:RH2	0.000	0.038	-0.123	0.199
Contrast 40	Medium site:SD2	0.000	0.046	-0.117	0.208
Contrast 41	High site:SD2	0.000	0.145	-0.039	0.330
Contrast 42	Top site:SD2	0.000	0.041	-0.175	0.256
Contrast 43	Medium site:$T2_{y-1}$	0.000	0.014	-0.215	0.242
Contrast 44	High site:$T2_{y-1}$	0.000	0.014	-0.213	0.241
Contrast 45	Top site:$T2_{y-1}$	0.000	-0.008	-0.235	0.219
Contrast 46	Medium site:$RH2_{y-1}$	0.000	0.016	-0.136	0.168
Contrast 47	High site:$RH2_{y-1}$	0.000	-0.056	-0.219	0.107
Contrast 48	Top site:$RH2_{y-1}$	0.000	0.021	-0.144	0.185
Contrast 49	Medium site:$SD2_{y-1}$	0.000	0.004	-0.167	0.174
Contrast 50	High site:$SD2_{y-1}$	0.000	0.053	-0.138	0.243
Contrast 51	Top site:$SD2_{y-1}$	0.000	0.044	-0.172	0.261

The acronyms for the explanatory variables are as follows: T1 = temperature from the Climap-net data, $T1_{y-1}$ = temperature in year y-1 from the Climap-net data, RH1 = relative humidity from the Climap-net data, $RH1_{y-1}$ = relative humidity in year y-1 from the Climap-net data, SD1

= saturation deficit from the Climap-net data, $SD1_{y-1}$ = saturation deficit in year y-1 from the Climap-net data, PR = precipitation from the Climap-net data, and PR_{y-1} = precipitation in year y-1 from the Climap-net data, T2 = temperature from the field-collected data, $T2_{y-1}$ = temperature in year y-1 from the field-collected data, RH2 = relative humidity from the field-collected data, $RH2_{y-1}$ = relative humidity in year y-1 from the field-collected data, SD2 = saturation deficit from the field-collected data, $SD2_{y-1}$ = saturation deficit in year y-1 from the field-collected data.

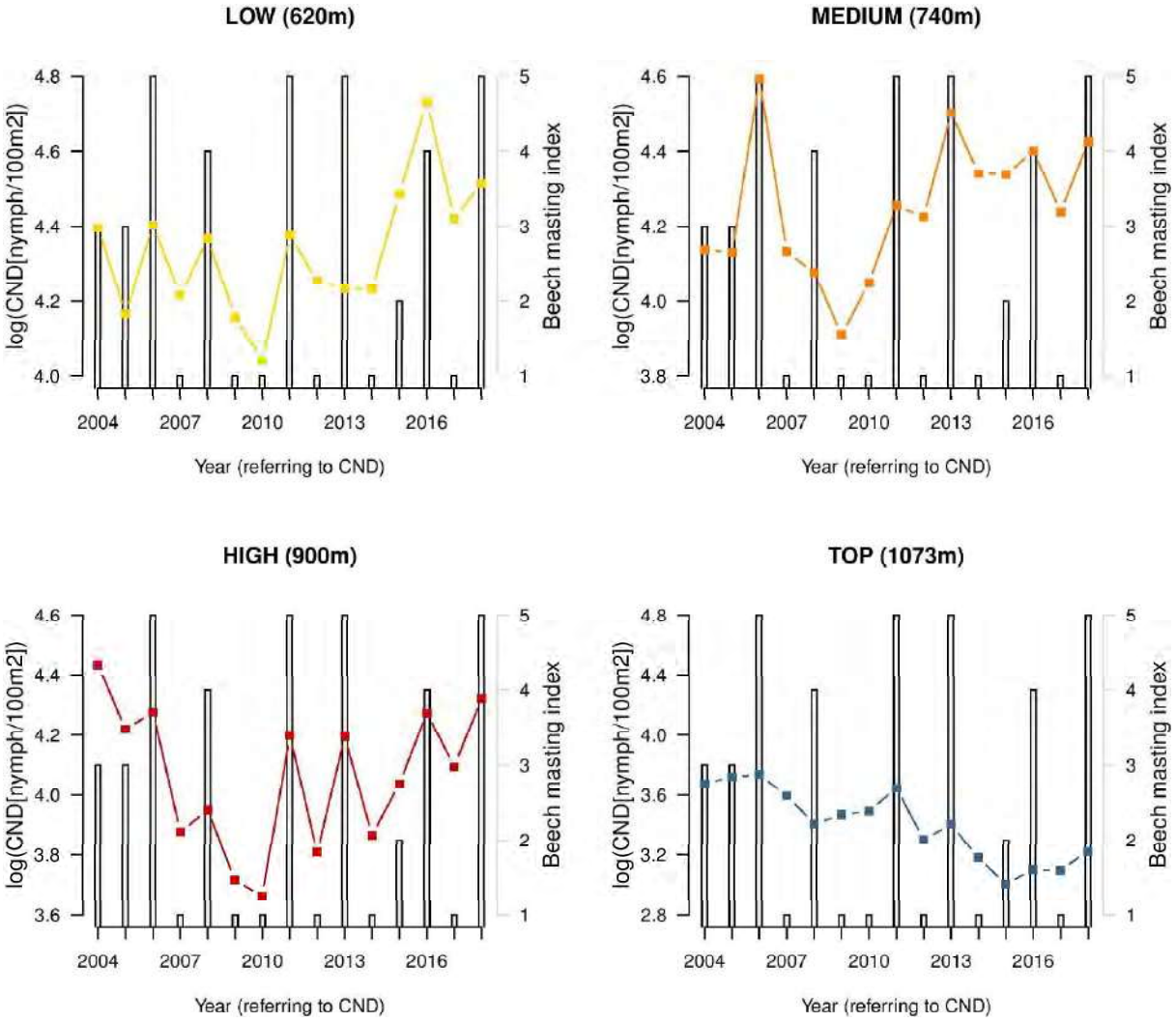

Figure S7. The log10-transformed cumulative nymphal density (CND; points and solid lines) and the beech tree mast score (grey bars) are shown over time for each of the four elevations on Chaumont Mountain. The CND increased significantly over the 15-year study period (2004–2018) at the low, medium, and high elevation sites, but it decreased significantly at the top elevation. Years of high seed production by beech trees cause high CND two years later. The CND is the total number of questing *I. ricinus* nymphs sampled by the dragging method each year. Beech tree mast score ranges from 1 to 5 (class 1 = very poor, 2 = poor, 3 = moderate, 4 = good, and class 5 = full mast year).

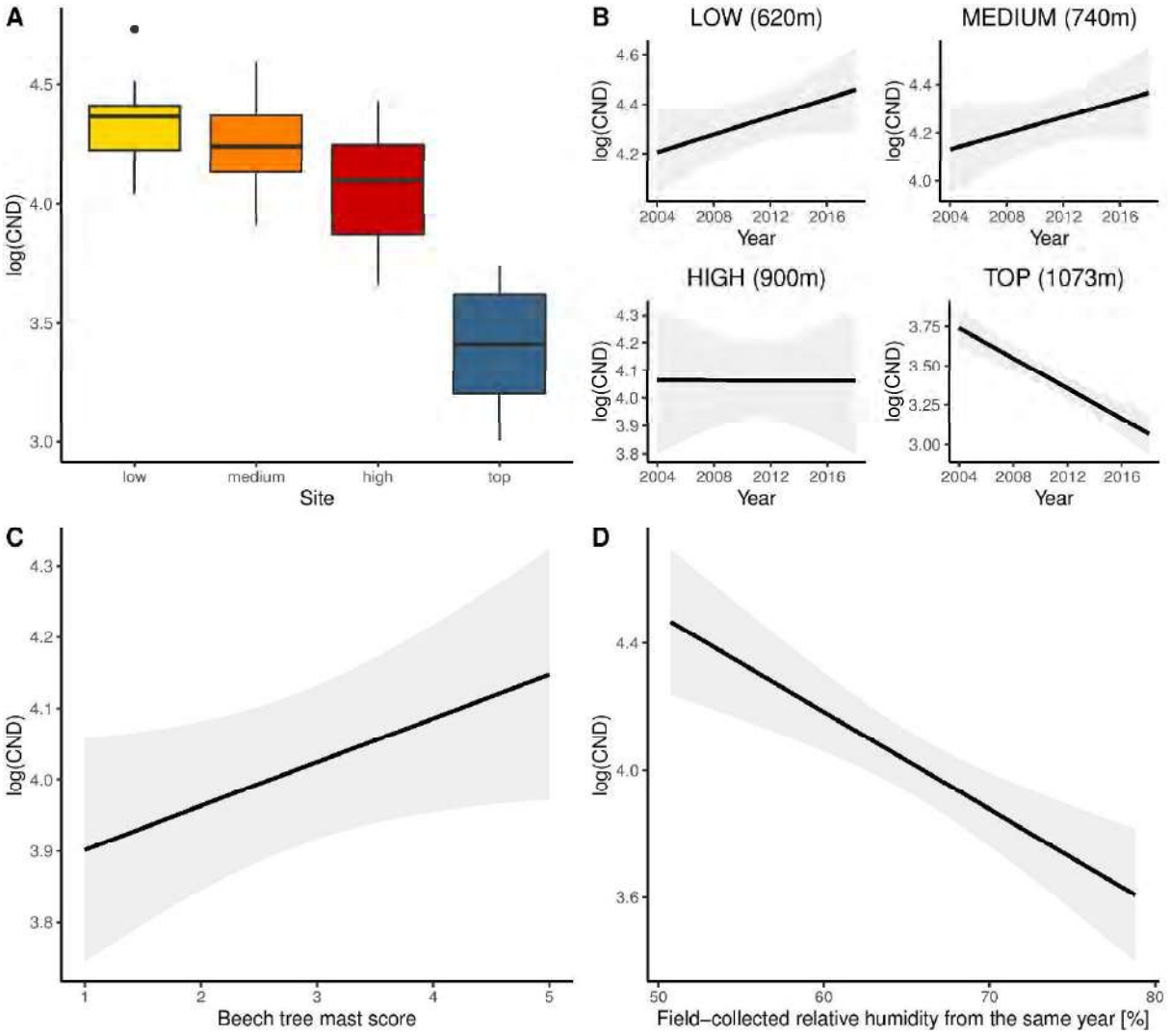

Figure S8. Effect sizes of the explanatory variables (elevation, year, site:year interaction, beech mast score 2 years prior, and mean annual relative humidity in the same year) on the log10-transformed cumulative nymphal density (CND). The parameter estimates used to calculate the effect sizes were taken from the model-averaged in Table S10 (A) Effect of elevation on the CND. The CND at the low elevation was 1.3% higher than the medium elevation, 31.5% higher than the high elevation, and 49.0% higher than the top elevation (partial r^2 = 65.6%). (B) Effect of year (e.g. time) on the CND. The CND increased by 123.1% at the low elevation, 82.8% at the medium elevation, and 55.3% at the high elevation, but decreased by 80.8% at the top elevation (partial r^2 = 8.8%). (C) Effect of beech mast score on the CND. Increasing the beech mast score from 1 (poor mast) to 5 (full mast) increased the CND by 72.5% (partial r^2 = 6.9%). (D) Effect of the mean annual field-collected relative humidity on the CND in the same year. Increasing the field-collected relative humidity from 50.0% to 75.0% decreased the CND by 38.2% (partial r^2 = 1.4%).

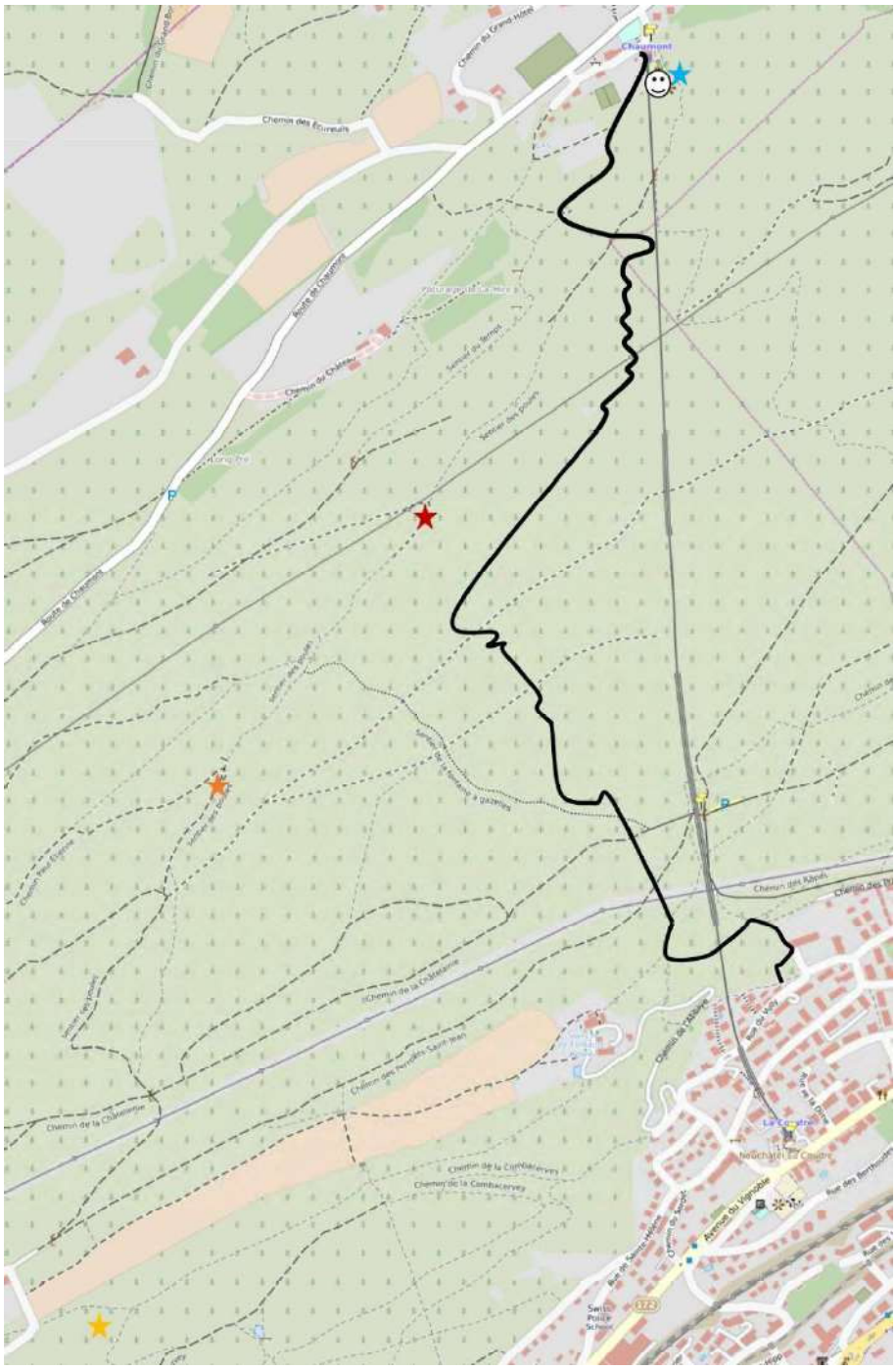

Figure S9. Map of the four elevation sites on Chaumont Mountain, canton Neuchâtel, Switzerland. The stars represent the 4 different elevation sites: low elevation site (yellow star), medium elevation site (orange) star, high elevation site (red star), and top elevation site (blue star). The smiley face indicates the location of the outdoor adventure park, and the solid black line represent the mountain biking trail.

SECTION 5 – Full statistical analysis of the cumulative adult abundance (CAD) for the four elevation sites

Background: In the main manuscript, we restricted the analysis to the cumulative nymph density (CND) at the low, medium, and high elevation sites. For simplicity, we did not include analyses of the cumulative adult tick abundance (CAD). We excluded the top site from the analysis of the CND because we believe that the construction of an adventure park caused the top site to have very different tick population dynamics over time compared to the other three elevation sites. In this section, we analyze the CAD for all four sites.

Methods: We used a model selection approach based on the Akaike information criterion (AIC) to find the most parsimonious model. Models were ranked according to their AIC values and the Akaike weights were calculated for each model. We used the Akaike weights to calculate the model-averaged parameter estimates and their 95% confidence intervals (CIs). The support for a given explanatory variable of interest was calculated as the sum of the Akaike weights of all the models in the set that included that particular explanatory variable. The support for a given explanatory variable ranged from low (0.0%) to high (100%).

Results – Variation in CAD among elevation sites: We used a one-way ANOVA to compare the mean CAD between the four elevations (i.e. this analysis ignores year). The CAD was significantly different between the four elevation sites ($F_{4, 52} = 1785.2$, $p < 0.001$; Figure S10). The mean CAD (and 95% CI) for the low, medium, high, and top elevations were as follows: 2718 (95% CI = 1861–3970), 5689 (95% CI = 3895–8309), 3368 (95% CI = 2306–4919), and 1281 (95% CI =877–1871). In summary, the mean adult density was highest in the medium and high elevations and lowest at the low and top elevations (Figure S10). The ratios of nymphs to adult ticks at the low, medium, high, and top elevations were as follows: 7.84, 3.19, 3.22, and 1.89.

Results – Effects of the abiotic and biotic variables on the variation in the annual estimates of cumulative adult density (CAD): For the CAD, the best fourteen models had a combined support of 95.0% (Table S11). The other 38 models had a combined support of 5% (Table S11). The best fourteen models all contained the explanatory variables of elevation site, year, the site:year interaction, and beech tree mast score, but they differed with respect to the identity of the climate variable. The best model had 14.0% of the support, explained 64.6% of the variation

in the CAD, and contained the explanatory variables of site (partial r^2 = 47.7%), year (partial r^2 = 10.6%), the site:year interaction (partial r^2 = 9.8%), and beech tree mast score from 2 years prior (partial r^2 = 21.0%) (Table S11). For the individual explanatory variables, there was strong support for the main effects of site (100.0%), beech tree mast score from 2 years prior (100.0%), year (99.1%), and the site:year interaction (98.2%;Table S12). None of the other explanatory variables had a support > 13.0% (Table S12).

We calculated the model-averaged parameter estimates to make robust inferences about the relationships between the explanatory variables and the CAD (Table S13). We also calculated the effect sizes with respect to the following baseline: the site was low elevation, the year was 2004, and the beech tree mast score was 1.

The CAD was different between the four elevation sites (Figures S10 and S11, Table S13). The CAD at the medium site was 256.6% higher than the low site (Medium – Low contrast = 0.583, 95% CI = 0.177 – 0.990). The CAD at the high site was 224.6% higher than the low site (High – Low contrast = 0.567, 95% CI = 0.134 – 1.001). The CAD at the top site was 108.0% higher than the low site (High – Low contrast = 0.404, 95% CI = -0.094 – 0.903). In summary, the CAD was highest at the medium and high site and lowest at the low and top site (Figures S10 and S11, Table S13).

The site:year interaction indicated that the change in the CAD over time differed between the four elevation sites (Figures S10 and S11, Table S13). Over the 15-year period (2004 – 2018), the CAD increased by 280.3% at the low site (slope = 0.041, 95% CI = 0.010 – 0.073), increased by 38.9% at the medium site (Medium – Low contrast of the slope = -0.031, 95% CI = -0.074 – 0.011), decreased by 37.7% at the high site (High – Low contrast of the slope = -0.056, 95% CI = -0.099 – -0.014), and decreased by 76.5% at the top site (Top – Low contrast of the slope = -0.086, 95% CI = -0.129 – -0.044). In summary, the CAD increased over time at the low and medium elevations but decreased at the high and top elevations (Figures S10 and S11, Table S13).

The covariate beech mast score 3 years prior had a strong positive effect on the CAD (0.100 per class, 95% CI = 0.060– 0.139; Figure S10, Table S13). Increasing the beech mast score from 1 (poor mast) to 5 (full mast) increased the CAD by 150.4% at each of the four elevation sites on Chaumont Mountain (Figure S11).

Over the 15-year study period, beech trees produced 6 years of good or full mast scores (2004, 2006, 2009, 2011, 2014, and 2016), where high CAD years were expected to occur three years later (2007, 2009, 2012, 2014, 2017, and 2019, respectively). At the low, medium, high, and top site, these 5 good mast years (e.g. no CAD data for 2019) produced 4 (2017, 2007,

2014, and 2012), 4 (2017, 2014, 2007, and 2012), 2 (2007 and 2017), and 3 (2007, 2012, and 2014) of the 5 highest CAD values three years later (Figure S10).

In summary, the CAD increased significantly over time at the low and medium elevations but decreased at the high and top elevations. The CAD increased with beech tree seed production three years earlier (Table S13).

Table S11. Model selection results are shown for the linear models with normal errors of the log10-transformed CAD response variable. The explanatory variables were elevation site, year, tree masting variables obtained from MASTREE, and the climate variables obtained from the Climap-net and collected in the field. Shown for each model are the model rank (Rank), model structure (see below for explanation of explanatory variables), model degrees of freedom (Df), log-likelihood (logLik), Akaike information criterion (AIC), difference in the AIC value from the top model (ΔAIC), model weight (Weight1), cumulative weight (Weight2), and adjusted r-squared (r^2).

Rank	Model structure	Df	logLik	AIC	ΔAIC	Weight1	Weight2	r^2
1	CAD ~ S+Y+S:Y+B	10	8.8	7.3	0.0	14.0	14.0	64.6
2	CAD ~ S+Y+S:Y+B+RH2	11	10.2	7.5	0.2	12.0	26.0	65.7
3	CAD ~ S+Y+S:Y+B+PR_{y-1}	11	10.1	7.9	0.6	10.0	36.0	65.4
4	CAD ~ S+Y+S:Y+B+$SD2_{y-1}$	11	10.0	7.9	0.6	10.0	46.0	65.4
5	CAD ~ S+Y+S:Y+B+PR	11	10.0	8.1	0.7	9.0	55.0	65.3
6	CAD ~ S+Y+S:Y+B+$RH2_{y-1}$	11	9.9	8.2	0.9	9.0	64.0	65.2
7	CAD ~ S+Y+S:Y+B+SD2	11	9.3	9.4	2.1	5.0	69.0	64.5
8	CAD ~ S+Y+S:Y+B+$RH1_{y-1}$	11	9.3	9.5	2.2	5.0	74.0	64.4
9	CAD ~ S+Y+S:Y+B+T1	11	9.2	9.6	2.3	4.0	78.0	64.4
10	CAD ~ S+Y+S:Y+B+$T2_{y-1}$	11	9.1	9.7	2.4	4.0	82.0	64.3
11	CAD ~ S+Y+S:Y+B+SD1	11	9.0	9.9	2.6	4.0	86.0	64.2
12	CAD ~ S+Y+S:Y+B+$T1_{y-1}$	11	8.8	10.4	3.1	3.0	89.0	63.9
13	CAD ~ S+Y+S:Y+B+T2	11	8.8	10.4	3.1	3.0	92.0	63.8
14	CAD ~ S+Y+S:Y+B+$SD1_{y-1}$	11	8.8	10.4	3.1	3.0	95.0	63.8
15	CAD ~ S+Y+S:Y+B+RH1	11	8.8	10.4	3.1	3.0	98.0	63.8
16	CAD ~ S+Y+S:Y+B +S:B	13	10.6	13.4	6.1	1.0	99.0	64.6
17	CAD ~ S+B	6	-0.4	14.5	7.1	0.0	99.0	54.8
18	CAD ~ S+B+T1+S:T1	10	4.8	15.2	7.9	0.0	99.0	59.2
19	CAD ~ S+Y+B	7	-0.3	16.9	9.5	0.0	99.0	54.0
20	CAD ~ S+Y+B+PR_{y-1}	8	0.9	17.2	9.9	0.0	99.0	55.1
21	CAD ~ S+Y+B+PR	8	0.9	17.2	9.9	0.0	99.0	55.0
22	CAD ~ S+B+$T1_{y-1}$+S:$T1_{y-1}$	10	3.5	17.8	10.5	0.0	99.0	57.3
23	CAD ~ S+Y+B+$RH1_{y-1}$	8	0.5	18.0	10.7	0.0	99.0	54.4
24	CAD ~ S+Y+B+RH2	8	0.5	18.2	10.8	0.0	99.0	54.3
25	CAD ~ S+Y+B+$SD2_{y-1}$	8	0.3	18.5	11.2	0.0	99.0	54.0
26	CAD ~ S+Y+B+$RH2_{y-1}$	8	0.2	18.6	11.3	0.0	99.0	53.9
27	CAD ~ S+B+RH2+S:RH2	10	3.1	18.6	11.3	0.0	99.0	56.7
28	CAD ~ S+Y+B+T1	8	0.1	18.9	11.5	0.0	99.0	53.7
29	CAD ~ S+Y+B+SD2	8	0.0	19.1	11.7	0.0	99.0	53.6
30	CAD ~ S+Y+B+$T2_{y-1}$	8	0.0	19.1	11.8	0.0	99.0	53.5

31	CAD ~ S+B+T2+S:T2	10	2.8	19.2	11.9	0.0	99.0	56.2
32	CAD ~ S+Y+B+SD1	8	-0.1	19.3	12.0	0.0	99.0	53.3
33	CAD ~ S+Y+B+$T1_{y-1}$	8	-0.2	19.5	12.2	0.0	99.0	53.2
34	CAD ~ S+Y+B+T2	8	-0.2	19.5	12.2	0.0	99.0	53.2
35	CAD ~ S+Y+B+$SD1_{y-1}$	8	-0.3	19.6	12.3	0.0	99.0	53.1
36	CAD ~ S+Y+B+RH1	8	-0.3	19.6	12.3	0.0	99.0	53.1
37	CAD ~ S+B+$SD2_{y-1}$+S:$SD2_{y-1}$	10	2.6	19.7	12.4	0.0	99.0	55.9
38	CAD ~ S+B+SD1+S:SD1	10	2.5	19.9	12.6	0.0	99.0	55.7
39	CAD ~ S+B+$RH2_{y-1}$+S:$RH2_{y-1}$	10	2.4	20.2	12.9	0.0	99.0	55.5
40	CAD ~ S+B+SD2+S:SD2	10	2.1	20.7	13.4	0.0	99.0	55.0
41	CAD ~ S+B+$SD1_{y-1}$+S:$SD1_{y-1}$	10	2.1	20.7	13.4	0.0	99.0	55.0
42	CAD ~ S+B+S:B	9	0.3	21.3	14.0	0.0	99.0	53.1
43	CAD ~ S+B+PR_{y-1}+S:PR_{y-1}	10	1.3	22.2	14.9	0.0	99.0	53.8
44	CAD ~ S+B+PR+S:PR	10	1.3	22.3	14.9	0.0	99.0	53.8
45	CAD ~ S+B+RH1+S:RH1	10	0.9	23.2	15.9	0.0	99.0	53.0
46	CAD ~ S+B+$RH1_{y-1}$+S:$RH1_{y-1}$	10	0.7	23.6	16.2	0.0	99.0	52.7
47	CAD ~ S+Y+B+S:B	10	0.4	24.0	16.7	0.0	99.0	52.3
48	CAD ~ S+B+$T2_{y-1}$+S:$T2_{y-1}$	10	0.3	24.4	17.0	0.0	99.0	52.0
49	CAD ~ S+Y+S:Y	9	-4.6	31.2	23.8	0.0	99.0	44.1
50	CAD ~ S+Y	6	-10.6	34.8	27.5	0.0	99.0	34.9
51	CAD ~ B	3	-18.5	43.5	36.2	0.0	99.0	18.3
52	CAD ~ P	3	-21.8	50.1	42.7	0.0	99.0	8.2

The acronyms for the explanatory variables are as follows: S = site, Y = year, B = beech tree mast score, P = spruce tree mast score, T1 = temperature from the Climap-net data, $T1_{y-1}$ = temperature in year y-1 from the Climap-net data, RH1 = relative humidity from the Climap-net data, $RH1_{y-1}$ = relative humidity in year y-1 from the Climap-net data, SD1 = saturation deficit from the Climap-net data, $SD1_{y-1}$ = saturation deficit in year y-1 from the Climap-net data, PR = precipitation from the Climap-net data, and PR_{y-1} = precipitation in year y-1 from the Climap-net data, T2 = temperature from the field-collected data, $T2_{y-1}$ = temperature in year y-1 from the field-collected data, RH2 = relative humidity from the field-collected data, $RH2_{y-1}$ = relative humidity in year y-1 from the field-collected data, SD2 = saturation deficit from the field-collected data, $SD2_{y-1}$ = saturation deficit in year y-1 from the field-collected data.

Table S12. The support for each individual explanatory variable is shown for the CAD. This support is calculated as the sum of the Akaike weights for all the models in the set that include that particular explanatory variable.

Rank	Explanatory variable of interest	Support (%)
1	Site	100.0
2	Beech tree mast score	100.0
3	Year	99.1
4	Site:Year	98.2
5	RH2	12.5
6	PRy-1	10.4
7	SD2y-1	10.1
8	PR	9.5
9	RH2y-1	8.7
10	SD2	4.9
11	T1	4.7
12	RH1y-1	4.7
13	T2y-1	4.1
14	SD1	3.8
15	T1y-1	3.0
16	T2	3.0
17	SD1y-1	2.9
18	RH1	2.9
19	Site:T1	< 1.0
20	Site:T1y-1	< 1.0
21	Site:RH2	< 1.0
22	Site:T2	< 1.0
23	Site:SD2y-1	< 1.0
24	Site:SD1	< 1.0
25	Site:RH2y-1	< 1.0
26	Site:SD2	< 1.0
27	Site:SD1y-1	< 1.0
28	Site:PRy-1	< 1.0
29	Site:PR	< 1.0
30	Site:RH1	< 1.0
31	Site:RH1y-1	< 1.0
32	Site:T2y-1	< 1.0
33	Spruce tree mast score	< 1.0
34	Site:Beech tree mast score	< 1.0

The acronyms for the explanatory variables are as follows: T1 = temperature from the Climap-net data, $T1_{y-1}$ = temperature in year y-1 from the Climap-net data, RH1 = relative humidity

from the Climap-net data, $RH1_{y-1}$ = relative humidity in year y-1 from the Climap-net data, SD1 = saturation deficit from the Climap-net data, $SD1_{y-1}$ = saturation deficit in year y-1 from the Climap-net data, PR = precipitation from the Climap-net data, and PR_{y-1} = precipitation in year y-1 from the Climap-net data, T2 = temperature from the field-collected data, $T2_{y-1}$ = temperature in year y-1 from the field-collected data, RH2 = relative humidity from the field-collected data, $RH2_{y-1}$ = relative humidity in year y-1 from the field-collected data, SD2 = saturation deficit from the field-collected data, $SD2_{y-1}$ = saturation deficit in year y-1 from the field-collected data.

Table S13. Model-averaged parameter estimates are shown for the linear models of the log10-transformed CAD response variable. Shown are the parameter types, the parameter names, the parameter estimates, and the 95% confidence limits (LL = lower limit and UL = upper limit). Estimate 1 is averaged over all the models in the set. Estimate 2 is averaged over the subset of models with a cumulative support of 95%. The 95% confidence limits are for estimate 2. Statistically significant parameter estimates are shown in bold-face type.

Type	Name	Estimate 1	Estimate 2	95% LL	95% UL
Intercept	Low site	2.818	2.818	2.483	3.153
Contrast 1	Medium site	0.583	0.583	0.177	0.990
Contrast 2	High site	0.567	0.567	0.134	1.001
Contrast 3	Top site	0.404	0.404	-0.094	0.903
Slope 1	Year	0.041	0.041	0.010	0.073
Slope 2	Beech tree mast score	0.100	0.100	0.060	0.139
Slope 3	Spruce tree mast score	0.000	0.095	0.017	0.173
Slope 4	T1	-0.002	-0.050	-0.223	0.123
Slope 5	RH1	0.000	0.002	-0.081	0.084
Slope 6	SD1	-0.001	-0.035	-0.146	0.075
Slope 7	PR	0.005	0.049	-0.021	0.119
Slope 8	$T1_{y-1}$	0.000	-0.008	-0.172	0.157
Slope 9	$RH1_{y-1}$	0.002	0.040	-0.051	0.131
Slope 10	$SD1_{y-1}$	0.000	-0.003	-0.126	0.121
Slope 11	PR_{y-1}	0.005	0.052	-0.020	0.123
Slope 12	T2	0.000	-0.004	-0.101	0.092
Slope 13	RH2	-0.007	-0.055	-0.126	0.017
Slope 14	SD2	0.002	0.040	-0.048	0.127
Slope 15	$T2_{y-1}$	0.001	0.034	-0.058	0.126
Slope 16	$RH2_{y-1}$	-0.004	-0.048	-0.121	0.025
Slope 17	$SD2_{y-1}$	0.006	0.064	-0.027	0.155
Contrast 4	Medium site:Year	-0.031	-0.031	-0.074	0.011
Contrast 5	High site:Year	-0.055	-0.056	-0.099	-0.014
Contrast 6	Top site:Year	-0.085	-0.086	-0.129	-0.044
Contrast 7	Medium site:Beech tree mast score	0.000	0.010	-0.098	0.118
Contrast 8	High site:Beech tree mast score	0.000	-0.068	-0.176	0.040
Contrast 9	High site:Beech tree mast score	0.000	-0.046	-0.155	0.062
Contrast 10	Medium site:T1	0.000	-0.050	-0.412	0.312
Contrast 11	High site:T1	0.000	-0.144	-0.498	0.211
Contrast 12	Top site:T1	-0.001	-0.451	-0.799	-0.103
Contrast 13	Medium site:RH1	0.000	0.006	-0.257	0.269
Contrast 14	High site:RH1	0.000	-0.078	-0.340	0.183

Contrast 15	Top site:RH1	0.000	0.103	-0.151	0.356
Contrast 16	Medium site:SD1	0.000	-0.023	-0.300	0.254
Contrast 17	High site:SD1	0.000	0.006	-0.283	0.295
Contrast 18	Top site:SD1	0.000	-0.283	-0.583	0.018
Contrast 19	Medium site:PR	0.000	0.015	-0.193	0.222
Contrast 20	High site:PR	0.000	0.016	-0.191	0.223
Contrast 21	Top site:PR	0.000	0.077	-0.128	0.282
Contrast 22	Medium site:$T1_{y-1}$	0.000	-0.173	-0.569	0.223
Contrast 23	High site:$T1_{y-1}$	0.000	-0.298	-0.684	0.089
Contrast 24	Top site:$T1_{y-1}$	0.000	-0.471	-0.848	-0.093
Contrast 25	Medium site:$RH1_{y-1}$	0.000	0.009	-0.286	0.305
Contrast 26	High site:$RH1_{y-1}$	0.000	0.046	-0.246	0.339
Contrast 27	Top site:$RH1_{y-1}$	0.000	0.072	-0.210	0.354
Contrast 28	Medium site:$SD1_{y-1}$	0.000	-0.075	-0.406	0.256
Contrast 29	High site:$SD1_{y-1}$	0.000	-0.222	-0.564	0.119
Contrast 30	Top site:$SD1_{y-1}$	0.000	-0.323	-0.672	0.026
Contrast 31	Medium site:PR_{y-1}	0.000	-0.026	-0.240	0.188
Contrast 32	High site:PR_{y-1}	0.000	-0.023	-0.236	0.191
Contrast 33	Top site:PR_{y-1}	0.000	0.052	-0.160	0.264
Contrast 34	Medium site:T2	0.000	0.179	-0.119	0.478
Contrast 35	High site:T2	0.000	0.091	-0.206	0.387
Contrast 36	Top site:T2	0.000	-0.122	-0.418	0.174
Contrast 37	Medium site:RH2	0.000	-0.137	-0.344	0.070
Contrast 38	High site:RH2	0.000	-0.097	-0.321	0.127
Contrast 39	Top site:RH2	0.000	0.081	-0.147	0.310
Contrast 40	Medium site:SD2	0.000	0.166	-0.065	0.398
Contrast 41	High site:SD2	0.000	0.135	-0.128	0.398
Contrast 42	Top site:SD2	0.000	-0.067	-0.375	0.241
Contrast 43	Medium site:$T2_{y-1}$	0.000	0.092	-0.230	0.415
Contrast 44	High site:$T2_{y-1}$	0.000	0.086	-0.234	0.406
Contrast 45	Top site:$T2_{y-1}$	0.000	0.013	-0.307	0.333
Contrast 46	Medium site:$RH2_{y-1}$	0.000	-0.149	-0.358	0.061
Contrast 47	High site:$RH2_{y-1}$	0.000	-0.135	-0.359	0.090
Contrast 48	Top site:$RH2_{y-1}$	0.000	0.011	-0.215	0.237
Contrast 49	Medium site:$SD2_{y-1}$	0.000	0.200	-0.031	0.432
Contrast 50	High site:$SD2_{y-1}$	0.000	0.221	-0.038	0.480
Contrast 51	Top site:$SD2_{y-1}$	0.000	0.115	-0.178	0.408

The acronyms for the explanatory variables are as follows: T1 = temperature from the Climap-net data, $T1_{y-1}$ = temperature in year y-1 from the Climap-net data, RH1 = relative humidity from the Climap-net data, $RH1_{y-1}$ = relative humidity in year y-1 from the Climap-net data, SD1

= saturation deficit from the Climap-net data, $SD1_{y-1}$ = saturation deficit in year y-1 from the Climap-net data, PR = precipitation from the Climap-net data, and PR_{y-1} = precipitation in year y-1 from the Climap-net data, T2 = temperature from the field-collected data, $T2_{y-1}$ = temperature in year y-1 from the field-collected data, RH2 = relative humidity from the field-collected data, $RH2_{y-1}$ = relative humidity in year y-1 from the field-collected data, SD2 = saturation deficit from the field-collected data, $SD2_{y-1}$ = saturation deficit in year y-1 from the field-collected data.

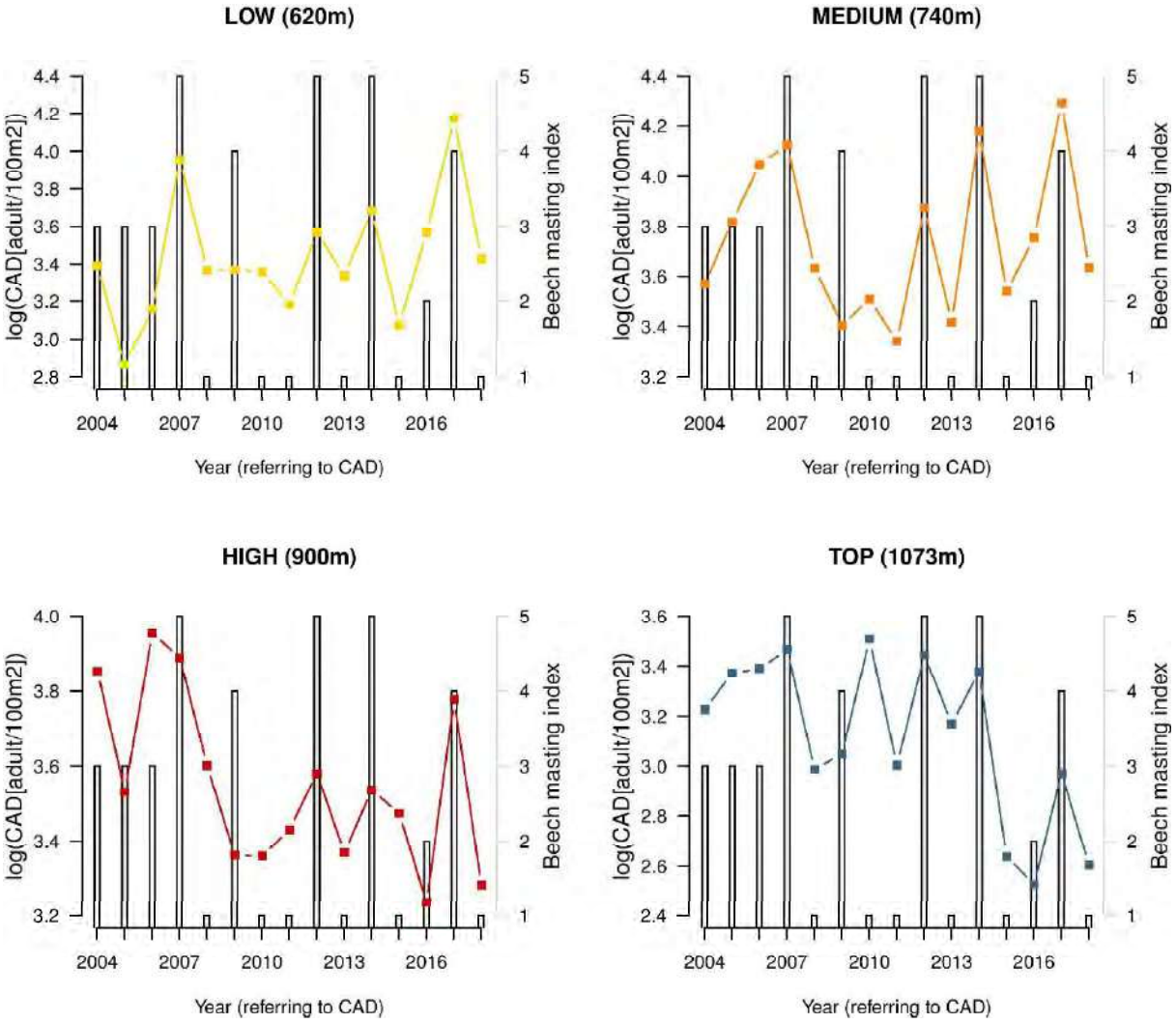

Figure S10. The log10-transformed cumulative adult density (CAD; points and solid lines) and the beech tree mast score (grey bars) are shown over time for each of the four elevations on Chaumont Mountain. The CAD increased significantly over the 15-year study period (2004 – 2018) at the low elevation site, but it decreased significantly at the high and top elevation. Years of high seed production by beech trees cause high CAD three years later. The CAD is the total number of questing *I. ricinus* adults sampled by the dragging method each year. Beech tree mast score ranges from 1 to 5 (class 1 = very poor, 2 = poor, 3 = moderate, 4 = good, and class 5 = full mast year).

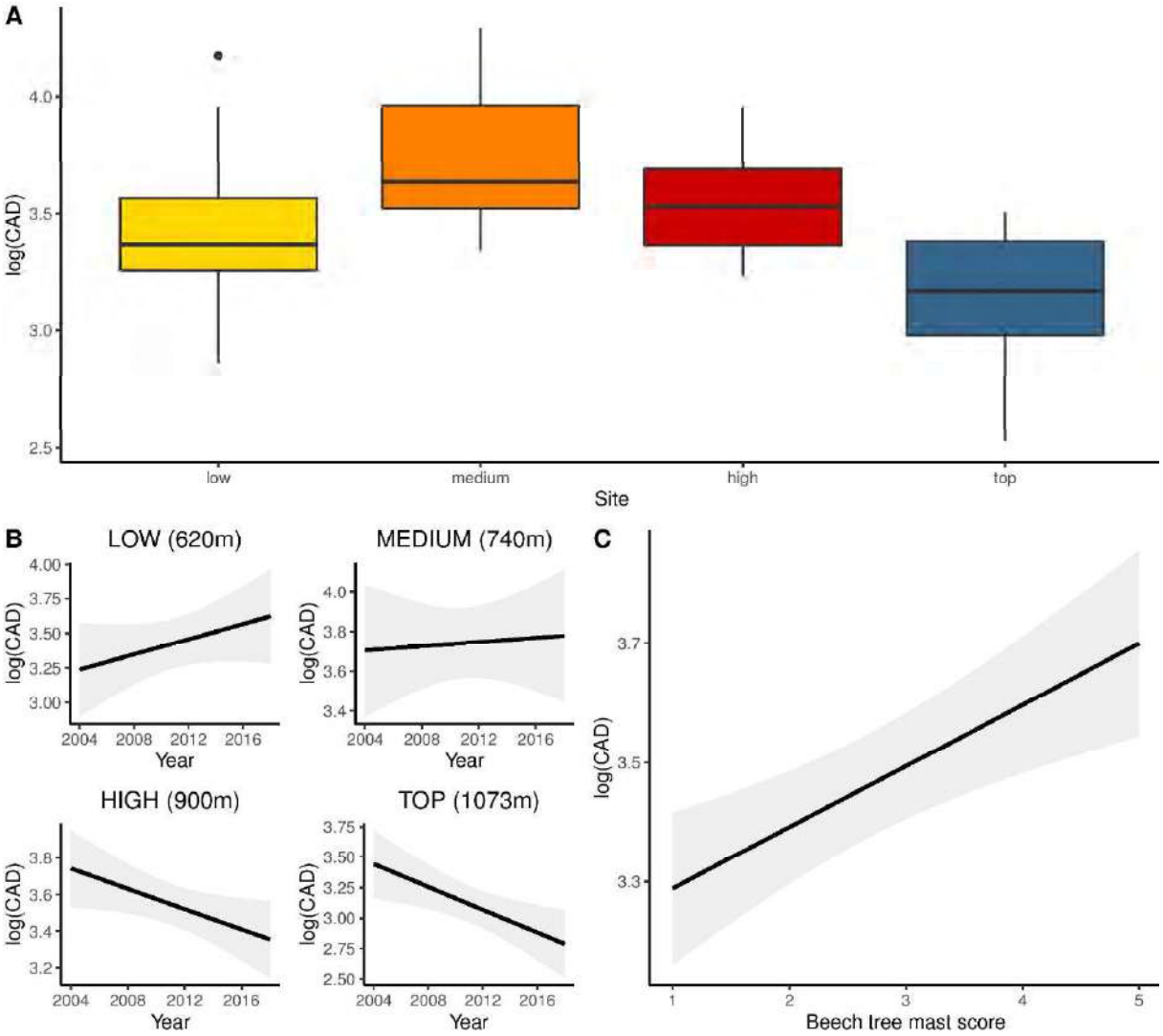

Figure S11. Effect sizes of the explanatory variables (elevation, year, site:year interaction, and beech mast score 2 years prior) on the log10-transformed cumulative adult density (CAD). The parameter estimates used to calculate the effect sizes were taken from the model-averaged in Table S13. (A) Effect of elevation on the CAD. The CAD at the medium, high, and top elevation was 256.6%, 224.6%, and 108.0% higher than the low elevation, respectively (partial r^2 = 47.7%). (B) Effect of year (e.g. time) on the CAD. The CAD increased by 280.3% at the low elevation and by 38.9% at the medium elevation, but decreased by 37.7% at the high elevation and by 76.5% at the top elevation (partial r2 = 9.8%). (C) Effect of beech mast score on the CAD. Increasing the beech mast score from 1 (poor mast) to 5 (full mast) increased the CAD by 150.4% (partial r2 = 21.0%).

SECTION 6 – Full model selection table, support of each individual explanatory variable, and model-averaged parameter estimates of the nymph abundance for the three lowest elevation sites

Methods: We used a model selection approach based on the Akaike information criterion (AIC) to find the most parsimonious model. Models were ranked according to their AIC values and the Akaike weights were calculated for each model. We used the Akaike weights to calculate the model-averaged parameter estimates and their 95% confidence intervals (CIs). The support for a given explanatory variable of interest was calculated as the sum of the Akaike weights of all the models in the set that included that particular explanatory variable. The support for a given explanatory variable ranged from low (0.0%) to high (100%).

Results: For the CND, the best six models had a combined support of 95.0% (Table S14). The other 46 models had a combined support of 5% (Table S14). The best six models all contained the explanatory variables of elevation site, year, and beech mast score, but they differed with respect to the identity of the climate variable. The best model had 76.0% of the support, explained 73.2% of the variation in the CND, and contained the explanatory variables of elevation site (partial r^2 = 26.6%), year (partial r^2 = 14.8%), beech tree mast score from 2 years prior (partial r^2 = 26.9%), and the field-collected relative humidity from the same year (partial r^2 = 7.6%) (Table S14). For the individual explanatory variables, there was strong support for the main effects of site (100.0%), beech tree mast score from 2 years prior (100.0%), year (99.9%), and field-collected relative humidity from the same year (81.6%; Table S15). None of the other explanatory variables had a support > 7.0% (Table S15).

We calculated the model-averaged parameter estimates to make robust inferences about the relationships between the explanatory variables and the CND (Table S16). We calculated the effect sizes with respect to the following baseline: the site was low elevation, the year was 2004, the beech tree mast was 1, and the field-collected relative humidity from the same year was 50.0% (Table S17).

The CND was significantly different between the three elevation sites (Figure S12). The CND at the low elevation was 10.3% higher than the medium elevation (Medium – Low contrast = -0.047, 95% CI = -0.159 – 0.065; Figure S13, Tables S18 and S19). The CND at the low elevation was 41.9% higher than the high elevation (High – Low = -0.236, 95% CI = -0.363 – 0.109; Figure S13, Tables S18 and S19). In summary, the CND was inversely related to

altitude; it was highest at the low elevation and lowest at the high elevation (Figure S12 and Figure S13).

The slope of the covariate year was positive (0.020 per year; Table S16) and the 95% CI did not overlap zero (0.009– 0.031), indicating that the CND was increasing over time at Chaumont Mountain (Figure S12). Over the 15-year period of the study (2004 – 2018), the CND increased by 90.5% at the low site (slope = 0.020, 95% CI = 0.009 – 0.031), at the medium site (slope = -0.006, 95% CI = -0.030 – 0.017), and at the high site (slope = -0.011, 95% CI = -0.035 – 0.012) (Figure S13).

The covariate beech mast score had a strong positive effect on the CND two years later (0.067 per class; Table S16) and the 95% CI did not overlap zero (0.045– 0.089), indicating that the CND increased with masting 2 years prior (Figure S12). Increasing the beech mast score from 1 (poor mast) to 5 (full mast) increased the CND by 85.6% at each of the three elevation sites on Chaumont Mountain (Figure S13; Table 19).

The slope of the field-collected relative humidity from the same year was negative (-0.074 per standard deviation; Table S16) and the 95% CI did not overlap zero (-0.117– -0.032), indicating that the CND decreased with the field-collected relative humidity in the same year. Increasing the field-collected relative humidity from 50.0% to 75.0% decreased the CND from the same year by 46.4% at each of the three elevation sites on Chaumont Mountain (Figure S13; Table S17). Temperature had a positive effect on the CND (slope = 0.077 per standard deviation, 95% CI = 0.018 – 0.137; Table S16) and saturation deficit had a positive effect on the CND (slope = 0.068 per standard deviation, 95% CI = 0.015 – 0.120; Table S16). In summary, our study found that years with higher temperatures and lower relative humidity have higher annual estimates of the CND compared to years with lower temperatures and high relative humidity. According to our model selection table, the level of support for relative humidity (81.6% in Table S15) is 14.3 and 14.1 times higher than that of temperature (5.7% in Table S15) and saturation deficit (5.8% in Table S15), respectively.

In summary, the CND increased significantly over time at the three lower elevations. The CND increased with beech tree seed production two years earlier while it decreased significantly with the field-collected relative humidity in the same year (Table S17).

Table S14. Model selection results are shown for the linear models with normal errors of the log10-transformed CND response variable. The explanatory variables were elevation site, year, tree masting variables obtained from MASTREE, and the climate variables obtained from the Climap-net and collected in the field. Shown for each model are the model rank (Rank), model structure (see below for explanation of explanatory variables), model degrees of freedom (Df), log-likelihood (logLik), Akaike information criterion (AIC), difference in the AIC value from the top model (ΔAIC), model weight (Weight1), cumulative weight (Weight2), and adjusted r-squared (r^2).

Rank	Model structure	Df	logLik	AIC	ΔAIC	Weight1	Weight2	r^2
1	CND ~ S+Y+B+RH2	7	33.0	-48.7	0.0	76.0	76.0	73.2
2	CND ~ S+Y+B+RH2+S:Y	9	33.6	-43.6	5.2	6.0	82.0	72.4
3	CND ~ S+Y+B+SD2	7	30.4	-43.5	5.3	5.0	87.0	69.7
4	CND ~ S+Y+B+T2	7	30.4	-43.4	5.3	5.0	92.0	69.6
5	CND ~ S+Y+B+$RH2_{y-1}$	7	29.4	-41.4	7.3	2.0	94.0	68.1
6	CND ~ S+Y+B+$SD2_{y-1}$	7	29.1	-40.8	7.9	1.0	95.0	67.7
7	CND ~ S+Y+B	6	26.6	-38.9	9.8	1.0	96.0	64.7
8	CND ~ S+Y+B+T1	7	28.0	-38.6	10.1	0.0	96.0	65.9
9	CND ~ S+Y+B+PR	7	27.9	-38.6	10.1	0.0	96.0	65.9
10	CND ~ S+Y+B+T2+S:Y	9	30.9	-38.3	10.5	0.0	96.0	68.7
11	CND ~ S+Y+B+SD2+S:Y	9	30.8	-38.0	10.7	0.0	96.0	68.5
12	CND ~ S+Y+B+$T2_{y-1}$	7	27.2	-37.1	11.6	0.0	96.0	64.7
13	CND ~ S+Y+B+S:B	8	28.6	-36.8	11.9	0.0	96.0	66.0
14	CND ~ S+Y+B+SD1	7	26.9	-36.6	12.2	0.0	96.0	64.2
15	CND ~ S+Y+B+$RH1_{y-1}$	7	26.9	-36.5	12.2	0.0	96.0	64.2
16	CND ~ S+Y+B+$T1_{y-1}$	7	26.9	-36.4	12.3	0.0	96.0	64.1
17	CND ~ S+Y+B+$RH2_{y-1}$+S:Y	9	30.0	-36.4	12.3	0.0	96.0	67.3
18	CND ~ S+Y+B+Pr_{y-1}	7	26.8	-36.3	12.4	0.0	96.0	64.0
19	CND ~ S+Y+B+$SD1_{y-1}$	7	26.7	-36.2	12.6	0.0	96.0	63.9
20	CND ~ S+Y+B+RH1	7	26.7	-36.1	12.7	0.0	96.0	63.8
21	CND ~ S+Y+B+$SD2_{y-1}$+S:Y	9	29.7	-35.7	13.0	0.0	96.0	66.7
22	CND ~ S+Y+B+S:Y	8	27.2	-34.0	14.7	0.0	96.0	63.6
23	CND ~ S+Y+B+T1+S:Y	9	28.5	-33.5	15.3	0.0	96.0	64.9
24	CND ~ S+Y+B+PR+S:Y	9	28.4	-33.2	15.5	0.0	96.0	64.8
25	CND ~ S+B+T1+S:T1	8	26.5	-32.7	16.0	0.0	96.0	62.5
26	CND ~ S+Y+B+$T2_{y-1}$+S:Y	9	27.7	-31.9	16.9	0.0	96.0	63.6
27	CND ~ S+B+RH2+S:RH2	8	25.9	-31.5	17.2	0.0	96.0	61.4
28	CND ~ S+Y+B+S:Y+S:B	10	29.2	-31.3	17.4	0.0	96.0	65.0
29	CND ~ S+Y+B+SD1+S:Y	9	27.4	-31.3	17.5	0.0	96.0	63.1
30	CND ~ S+Y+B+$T1_{y-1}$+S:Y	9	27.4	-31.2	17.5	0.0	96.0	63.0

31	CND ~ S+Y+B+$RH1_{y-1}$+S:Y	9	27.4	-31.1	17.6	0.0	96.0	62.9
32	CND ~ S+Y+B+PR_{y-1}+S:Y	9	27.3	-31.1	17.7	0.0	96.0	62.9
33	CND ~ S+Y+B+$SD1_{y-1}$+S:Y	9	27.3	-30.9	17.8	0.0	96.0	62.7
34	CND ~ S+B	5	21.3	-30.8	17.9	0.0	96.0	55.6
35	CND ~ S+Y+B+RH1+S:Y	9	27.2	-30.8	17.9	0.0	96.0	62.6
36	CND ~ S+B+$T1_{y-1}$+S:$T1_{y-1}$	8	25.2	-30.1	18.7	0.0	96.0	60.1
37	CND ~ S+B+SD2+S:SD2	8	24.7	-29.0	19.8	0.0	96.0	59.0
38	CND ~ S+B+T2+S:T2	8	24.4	-28.4	20.4	0.0	96.0	58.4
39	CND ~ S+B+S:B	7	22.7	-28.2	20.5	0.0	96.0	56.4
40	CND ~ S+B+SD1+S:SD1	8	24.0	-27.6	21.1	0.0	96.0	57.7
41	CND ~ S+B+$SD1_{y-1}$+S:$SD1_{y-1}$	8	22.6	-24.9	23.9	0.0	96.0	54.8
42	CND ~ S+B+Pr_{y-1}+S:Pr_{y-1}	8	22.4	-24.5	24.2	0.0	96.0	54.4
43	CND ~ S+B+$RH2_{y-1}$+S:$RH2_{y-1}$	8	22.3	-24.3	24.5	0.0	96.0	54.2
44	CND ~ S+B+RH1+S:RH1	8	22.1	-23.8	24.9	0.0	96.0	53.7
45	CND ~ S+B+PR+S:PR	8	22.1	-23.8	25.0	0.0	96.0	53.6
46	CND ~ S+B+$RH1_{y-1}$+S:$RH1_{y-1}$	8	21.6	-22.9	25.9	0.0	96.0	52.6
47	CND ~ S+B+$SD2_{y-1}$+S:$SD2_{y-1}$	8	21.6	-22.8	25.9	0.0	96.0	52.6
48	CND ~ S+B+$T2_{y-1}$+S:$T2_{y-1}$	8	21.4	-22.3	26.4	0.0	96.0	52.0
49	CND ~ S+Y	5	13.3	-15.0	33.7	0.0	96.0	35.3
50	CND ~ B	3	9.7	-12.8	36.0	0.0	96.0	26.9
51	CND ~ S+Y+S:Y	7	13.6	-9.9	38.8	0.0	96.0	32.6
52	CND ~ P	3	2.8	0.9	49.7	0.0	96.0	0.0

The acronyms for the explanatory variables are as follows: S = site, Y = year, B = beech tree mast score, P = spruce tree mast score, T1 = temperature from the Climap-net data, $T1_{y-1}$ = temperature in year y-1 from the Climap-net data, RH1 = relative humidity from the Climap-net data, $RH1_{y-1}$ = relative humidity in year y-1 from the Climap-net data, SD1 = saturation deficit from the Climap-net data, $SD1_{y-1}$ = saturation deficit in year y-1 from the Climap-net data, PR = precipitation from the Climap-net data, and PR_{y-1} = precipitation in year y-1 from the Climap-net data, T2 = temperature from the field-collected data, $T2_{y-1}$ = temperature in year y-1 from the field-collected data, RH2 = relative humidity from the field-collected data, $RH2_{y-1}$ = relative humidity in year y-1 from the field-collected data, SD2 = saturation deficit from the field-collected data, $SD2_{y-1}$ = saturation deficit in year y-1 from the field-collected data.

Table S15. The support for each individual explanatory variable is shown for the CND. This support is calculated as the sum of the Akaike weights for all the models in the set that include that particular explanatory variable.

Rank	Explanatory variable of interest	Support (%)
1	Site	100.0
2	Beech tree mast score	100.0
3	Year	99.9
4	RH2	81.6
5	Site:Year	7.0
6	SD2	5.8
7	T2	5.7
8	$RH2_{y-1}$	2.1
9	$SD2_{y-1}$	1.6
10	Spruce tree mast score	< 1.0
11	T1	< 1.0
12	RH1	< 1.0
13	SD1	< 1.0
14	PR	< 1.0
15	$T1_{y-1}$	< 1.0
16	$RH1_{y-1}$	< 1.0
17	$SD1_{y-1}$	< 1.0
18	PR_{y-1}	< 1.0
19	$T2_{y-1}$	< 1.0
20	Site:Beech tree mast score	< 1.0
21	Site:T1	< 1.0
22	Site:RH1	< 1.0
23	Site:SD1	< 1.0
24	Site:PR	< 1.0
25	Site:$T1_{y-1}$	< 1.0
26	Site:$RH1_{y-1}$	< 1.0
27	Site:$SD1_{y-1}$	< 1.0
28	Site:PR_{y-1}	< 1.0
29	Site:T2	< 1.0
30	Site:RH2	< 1.0
31	Site:SD2	< 1.0
32	Site:$T2_{y-1}$	< 1.0
33	Site:$RH2_{y-1}$	< 1.0
34	Site:$SD2_{y-1}$	< 1.0

The acronyms for the explanatory variables are as follows: T1 = temperature from the Climap-net data, $T1_{y-1}$ = temperature in year y-1 from the Climap-net data, RH1 = relative humidity

from the Climap-net data, $RH1_{y-1}$ = relative humidity in year y-1 from the Climap-net data, SD1 = saturation deficit from the Climap-net data, $SD1_{y-1}$ = saturation deficit in year y-1 from the Climap-net data, PR = precipitation from the Climap-net data, and PR_{y-1} = precipitation in year y-1 from the Climap-net data, T2 = temperature from the field-collected data, $T2_{y-1}$ = temperature in year y-1 from the field-collected data, RH2 = relative humidity from the field-collected data, $RH2_{y-1}$ = relative humidity in year y-1 from the field-collected data, SD2 = saturation deficit from the field-collected data, $SD2_{y-1}$ = saturation deficit in year y-1 from the field-collected data.

Table S16. Model-averaged parameter estimates are shown for the linear models of the log10-transformed CND response variable. Shown are the parameter types, the parameter names, the parameter estimates, and the 95% confidence limits (LL = lower limit and UL = upper limit). Estimate 1 is averaged over all the models in the set. Estimate 2 is averaged over the subset of models with a cumulative support of 95%. The 95% confidence limits are for estimate 2.

Type	Name	Estimate 1	Estimate 2	95% LL	95% UL
Intercept	Low site	3.934	3.934	3.802	4.067
Contrast 1	Medium site	-0.047	-0.047	-0.159	0.065
Contrast 2	High site	-0.236	-0.236	-0.363	-0.109
Slope 1	Year	0.020	0.020	0.009	0.031
Slope 2	Beech tree mast score	0.067	0.067	0.045	0.089
Slope 3	Spruce tree mast score	0.000	0.019	-0.038	0.075
Slope 4	T1	0.000	0.080	-0.032	0.193
Slope 5	RH1	0.000	-0.007	-0.066	0.052
Slope 6	SD1	0.000	0.026	-0.049	0.101
Slope 7	PR	0.000	0.035	-0.012	0.082
Slope 8	$T1_{y-1}$	0.000	0.039	-0.089	0.166
Slope 9	$RH1_{y-1}$	0.000	0.024	-0.050	0.098
Slope 10	$SD1_{y-1}$	0.000	0.016	-0.072	0.105
Slope 11	PR_{y-1}	0.000	-0.013	-0.064	0.039
Slope 12	T2	0.004	0.077	0.018	0.137
Slope 13	RH2	-0.061	-0.074	-0.117	-0.032
Slope 14	SD2	0.004	0.068	0.015	0.120
Slope 15	$T2_{y-1}$	0.000	0.032	-0.034	0.099
Slope 16	$RH2_{y-1}$	-0.001	-0.055	-0.105	-0.005
Slope 17	$SD2_{y-1}$	0.001	0.062	0.002	0.123
Contrast 3	Medium site:Year	0.000	-0.006	-0.030	0.017
Contrast 4	High site:Year	-0.001	-0.011	-0.035	0.012
Contrast 5	Medium site:Beech tree mast score	0.000	0.016	-0.044	0.075
Contrast 6	High site: Beech tree mast score	0.000	0.053	-0.007	0.112
Contrast 7	Medium site:T1	0.000	-0.080	-0.292	0.133
Contrast 8	High site:T1	0.000	-0.073	-0.281	0.135
Contrast 9	Medium site:RH1	0.000	0.075	-0.084	0.235
Contrast 10	High site:RH1	0.000	0.005	-0.154	0.164
Contrast 11	Medium site:SD1	0.000	-0.065	-0.231	0.101
Contrast 12	High site:SD1	0.000	0.004	-0.169	0.176
Contrast 13	Medium site:PR	0.000	0.050	-0.077	0.177
Contrast 14	High site:PR	0.000	-0.018	-0.145	0.109
Contrast 15	Medium site:$T1_{y-1}$	0.000	-0.136	-0.370	0.099
Contrast 16	High site:$T1_{y-1}$	0.000	-0.177	-0.406	0.051

Contrast 17	Medium site:$RH1_{y-1}$	0.000	0.013	-0.168	0.194
Contrast 18	High site:$RH1_{y-1}$	0.000	-0.043	-0.223	0.136
Contrast 19	Medium site:$SD1_{y-1}$	0.000	-0.038	-0.241	0.165
Contrast 20	High site:$SD1_{y-1}$	0.000	-0.008	-0.218	0.201
Contrast 21	Medium site:PR_{y-1}	0.000	-0.001	-0.131	0.129
Contrast 22	High site:PR_{y-1}	0.000	-0.002	-0.132	0.127
Contrast 23	Medium site:T2	0.000	-0.064	-0.242	0.115
Contrast 24	High site:T2	0.000	0.047	-0.130	0.224
Contrast 25	Medium site:RH2	0.000	-0.051	-0.171	0.069
Contrast 26	High site:RH2	0.000	-0.102	-0.232	0.027
Contrast 27	Medium site:SD2	0.000	0.045	-0.091	0.180
Contrast 28	High site:SD2	0.000	0.144	-0.010	0.297
Contrast 29	Medium site:$T2_{y-1}$	0.000	0.018	-0.179	0.215
Contrast 30	High site:$T2_{y-1}$	0.000	0.016	-0.179	0.212
Contrast 31	Medium site:$RH2_{y-1}$	0.000	0.013	-0.117	0.143
Contrast 32	High site:$RH2_{y-1}$	0.000	-0.058	-0.197	0.081
Contrast 33	Medium site:$SD2_{y-1}$	0.000	0.008	-0.139	0.156
Contrast 34	High site:$SD2_{y-1}$	0.000	0.054	-0.111	0.218

The acronyms for the explanatory variables are as follows: T1 = temperature from the Climap-net data, $T1_{y-1}$ = temperature in year y-1 from the Climap-net data, RH1 = relative humidity from the Climap-net data, $RH1_{y-1}$ = relative humidity in year y-1 from the Climap-net data, SD1 = saturation deficit from the Climap-net data, $SD1_{y-1}$ = saturation deficit in year y-1 from the Climap-net data, PR = precipitation from the Climap-net data, and PR_{y-1} = precipitation in year y-1 from the Climap-net data, T2 = temperature from the field-collected data, $T2_{y-1}$ = temperature in year y-1 from the field-collected data, RH2 = relative humidity from the field-collected data, $RH2_{y-1}$ = relative humidity in year y-1 from the field-collected data, SD2 = saturation deficit from the field-collected data, $SD2_{y-1}$ = saturation deficit in year y-1 from the field-collected data.

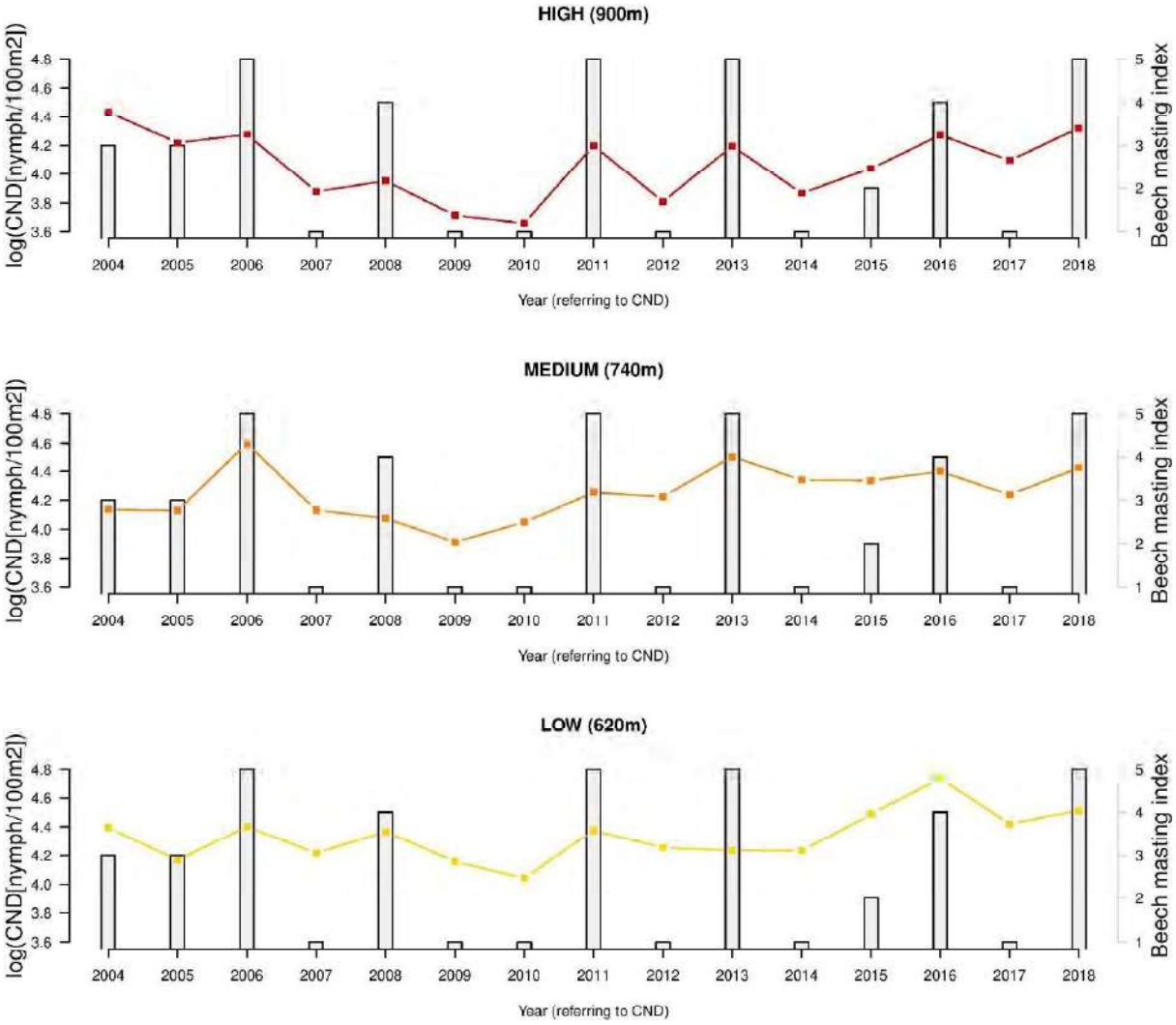

Figure S12. The log10-transformed cumulative nymphal density (CND) and the beech tree mast score over time is shown for each of the three elevations on Chaumont Mountain. The CND increased significantly over the 15-year study period (2004–2018). Years of high seed production by beech trees are strongly positively associated with high CND two years later. The CND is the total number of questing *I. ricinus* nymphs sampled by the dragging method each year. Beech tree mast scores range from 1 to 5 (1 = very poor mast; 2 = poor; 3 = moderate; 4 = good; and 5 = full mast year). The solid lines and barplots represent the CND and the beech tree mast score, respectively.

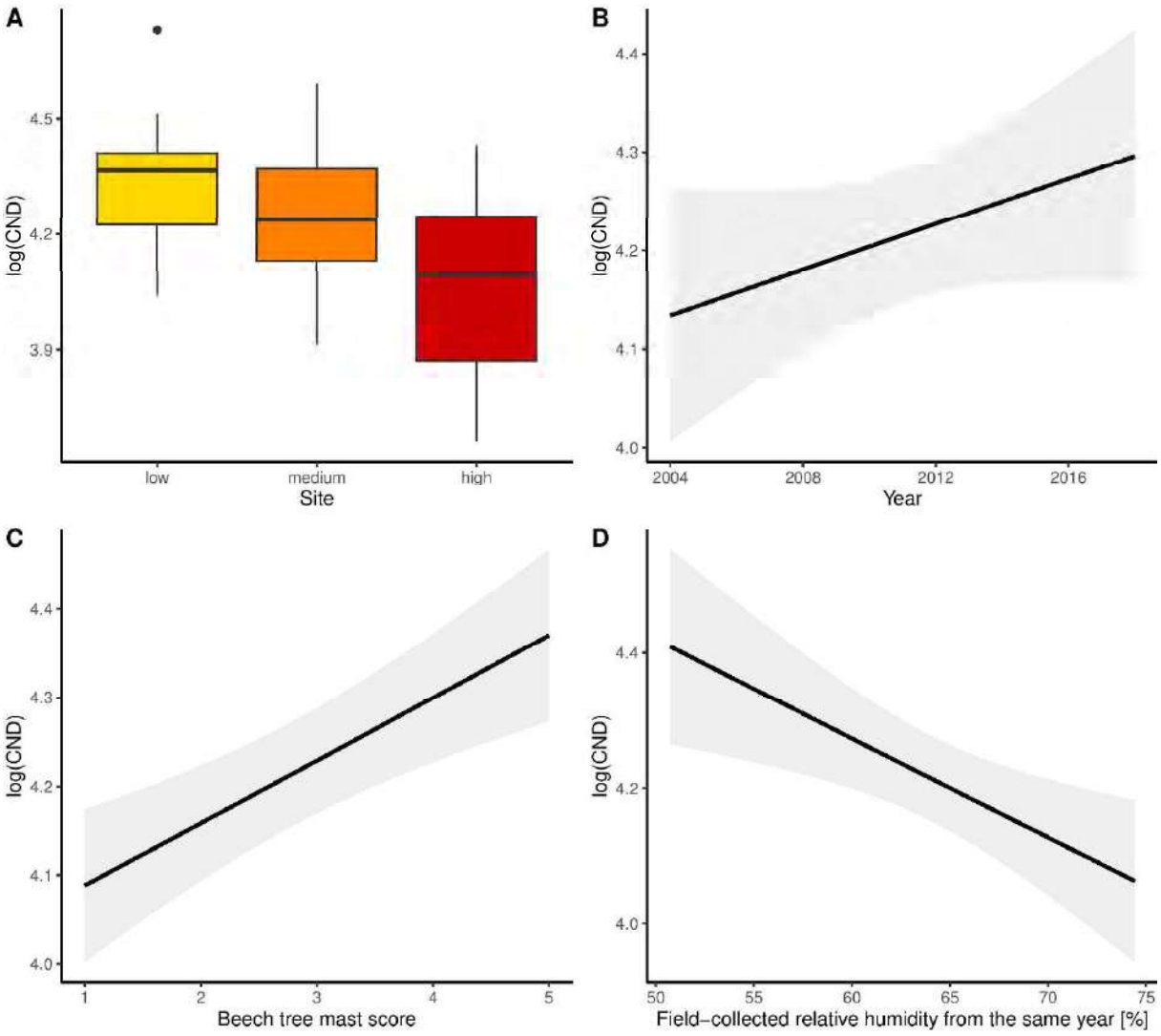

Figure S13. Effect sizes of the explanatory variables (elevation, year, beech mast score 2 years prior, and mean annual relative humidity in the same year) on the log10-transformed cumulative nymphal density (CND). The parameter estimates used to calculate the effect sizes were taken from the model-averaged in Table S16. (A) Effect of elevation on the CND. The CND at the low elevation was 10.3% higher than the medium elevation and 41.9% higher than the high elevation (partial r^2 = 26.6%). (B) Effect of year (e.g. time) on the CND. The CND increased by 90.5% over the 15-year study period (partial r^2 = 14.8%). (C) Effect of beech mast score on the CND. Increasing the beech mast score from 1 (poor mast) to 5 (full mast) increased the CND by 85.6% (partial r^2 = 26.9%). (D) Effect of the mean annual field-collected relative humidity on the CND in the same year. Increasing the field-collected relative humidity from 50.0% to 75.0% decreased the CND by 46.4% (partial r^2 = 7.6%).

SECTION 7 – Assumptions of the linear models for the best models from the AIC-based model selection approach of the nymph and adult abundance for the three lowest elevation sites

Methods: Linear models assume that the residuals follow a normal distribution and that the variance of the residuals is the same over the range of predicted values (or between groups). We used the Shapiro-Wilk normality test to test the assumption of normality for the log10-transformed CND residuals. We used a Bartlett's K-squared test to test whether the variance of the residuals was the same between the three sites.

Results for nymphal abundance: For the nymphal abundance, the residuals of the best model (model 1 in Table S8) followed a normal distribution (Shapiro-Wilk normality test: $W = 0.985$, $p = 0.843$) and these residuals had the same variance between the three elevation sites (Bartlett's K-squared = 0.664, df = 2, $p = 0.717$).

Results for adult tick abundance: For the adult tick abundance, the residuals of the best model (model 1 in Table S11) followed a normal distribution (Shapiro-Wilk normality test: $W = 0.985$, $p = 0.705$) and these residuals had the same variance between the three elevation sites (Bartlett's K-squared = 2.594, df = 2, $p = 0.273$).

SECTION 8 – Parameter estimates of the top model in the model selection table of the nymph abundance for the three lowest elevation sites

Table S17. The parameter estimates from the top model in the model selection table (Table S14) are shown. In this top model, the log10-transformed CND response variable was modelled as a function of elevation site, year, beech tree mast score 2 years prior, and the field-collected mean annual relative humidity in the same year. Shown are the parameter types, parameter names, parameter estimates on the log10-transformed scale, standard errors (s.e.), t-statistic (t), and p-values (p).

Type	Name	Estimate	s.e	t	p
Intercept	Low site	3.939	0.059	66.209	< 0.001
Contrast 1	Medium site	-0.053	0.045	-1.162	0.253
Contrast 2	High site	-0.245	0.047	-5.217	< 0.001
Slope 1	Year	0.020	0.005	4.262	< 0.001
Slope 2	Beech tree mast score	0.067	0.011	6.378	< 0.001
Slope 3	Relative humidity (field-collected)	-0.074	0.021	-3.570	0.001

SECTION 9 – Time lag between the nymph abundance and beech masting

Methods – Relationship between beech masting and CND with different time lags: To test the relationship between beech masting and CND across years, we used linear models to model the log10-transformed CND as a function of the beech mast score but with different time lags. We analyzed 9 different beech mast score explanatory variables ($beech_{y-4}$, $beech_{y-3}$, $beech_{y-2}$, $beech_{y-1}$, beech, $beech_{y+1}$, $beech_{y+2}$, $beech_{y+3}$, $beech_{y+4}$) where the time lag was allowed to shift from – 4 years to +4 years relative to the CND, which was always the same. Each CND was modelled as an ANCOVA of the beech mast score, site, and their interaction (Table S18).

Results – Relationship between beech masting and CND with different time lags: For all models, the interaction between the beech mast score and site was not significant (Table S18). We therefore ran all models without the interaction and tested the main effects (models 10 to 18 in Table S19). As expected from the biological chain reported firstly in the USA (Ostfeld et al. 2006), the coefficient of determination between the CND and beech mast score was maximal for the y-2 time lag (Table S19).

Methods – Variation in CND explained by time lag: The previous analysis led us to determine how much of the variation was explained by the time lag. We modeled the log10-transformed CND as a function of 9 different times lagged beech mast score alone, and as a function of site alone (Table S20). We performed a variance partitioning of the main effects model (Table S19) to evaluate how much variation could be attributed to the time lag. In this approach, we compared the multiple r^2 values between the main effect models (Table S19) and the models with a single explanatory factor (Table S20) to calculate the % variation in CND explained by the time lag (Table S21).

Results – Variation in CND explained by time lag: As expected, the best model had a two-year time lag between nymphs and beech mast score (model 12 in Table S19). This model had an r^2 value of 50.2%, and the main effects of the $beech_{y-2}$ ($F_{41, 45} = 24.687$, $p < 0.001$) and site ($F_{41, 43} = 11.306$, $p < 0.001$) were both highly significant. According to the variance partitioning method, $beech_{y-2}$ and site accounted for a minimum of 25.6% and 2.4% of the variation in CND, respectively (Table S21). The parameter estimates for model 12 showed the expected positive relationship between $beech_{y-2}$ and CND (slope = 0.070, s.e. of slope = 0.014; Table S22).

Altogether, these results show that the emphasize of the 2-year biological correlation of our study is accurate and not overinterpreted.

Table S18. The log10-transformed CND was modeled as an ANCOVA of the beech mast score with different time lags, site, and their interaction. Shown are the time lags (Lag), sample size (N), F-statistic of the interaction (Finter), and p-value of the interaction (pinter).

Model No.	Model Structure	Lag	N	F_{inter}	p_{inter}
1	$\log(CND) \sim beech_{y-4} + site + beech_{y-4}:site$	-4	45	0.201	0.819
2	$\log(CND) \sim beech_{y-3} + site + beech_{y-3}:site$	-3	45	0.144	0.866
3	$\log(CND) \sim beech_{y-2} + site + beech_{y-2}:site$	-2	45	1.310	0.281
4	$\log(CND) \sim beech_{y-1} + site + beech_{y-1}:site$	-1	42	0.003	0.997
5	$\log(CND) \sim beech + site + beech:site$	0	39	0.350	0.707
6	$\log(CND) \sim beech_{y+1} + site + beech_{y+1}:site$	+1	36	0.048	0.953
7	$\log(CND) \sim beech_{y+2} + site + beech_{y+2}:site$	+2	33	0.398	0.676
8	$\log(CND) \sim beech_{y+3} + site + beech_{y+3}:site$	+3	30	0.354	0.706
9	$\log(CND) \sim beech_{y+4} + site + beech_{y+4}:site$	+4	27	0.347	0.711

Table S19. The log10-transformed CND was modeled as a linear model of the beech mast score with different time lags and site. Shown are the time lag (Lag), sample size (N), F-statistic of the model (F), p-value of the model (p), and the multiple r^2 value of the model (expressed as a percent).

Model No.	Model Structure	Lag	N	F	p	r^2 (%)
10	$\log(CND) \sim beech_{y-4} + site$	-4	45	4.723	0.006	25.7
11	$\log(CND) \sim beech_{y-3} + site$	-3	45	6.222	0.001	31.3
12	$\log(CND) \sim beech_{y-2} + site$	-2	45	15.770	< 0.001	53.6
13	$\log(CND) \sim beech_{y-1} + site$	-1	42	6.322	0.001	33.3
14	$\log(CND) \sim beech + site$	0	39	5.722	0.003	32.9
15	$\log(CND) \sim beech_{y+1} + site$	1	36	3.950	0.017	27.0
16	$\log(CND) \sim beech_{y+2} + site$	2	33	3.878	0.019	28.6
17	$\log(CND) \sim beech_{y+3} + site$	3	30	4.771	0.009	35.5
18	$\log(CND) \sim beech_{y+4} + site$	4	27	4.263	0.016	35.7

Table S20. The log10-transformed CND is modeled as a linear function of (A) the lagged beech mast score and (B) site. Shown are the time lag (Lag), sample size (N), the F-statistic (F), p-value (p), and multiple r^2 (expressed as a %).

Model No.	(A) Model Structure	Lag	N	F	p	r^2 (%)
19	log(CND) ~ $beech_{y-4}$	-4	45	0.032	0.859	0.0
20	log(CND) ~ $beech_{y-3}$	-3	45	2.588	0.115	5.7
21	log(CND) ~ $beech_{y-2}$	-2	45	16.690	< 0.001	28.0
22	log(CND) ~ $beech_{y-1}$	-1	42	2.763	0.104	6.5
23	log(CND) ~ beech	0	39	3.047	0.089	7.6
24	log(CND) ~ $beech_{y+1}$	1	36	0.285	0.597	0.8
25	log(CND) ~ $beech_{y+2}$	2	33	1.777	0.192	5.4
26	log(CND) ~ $beech_{y+3}$	3	30	5.311	0.029	15.9
27	log(CND) ~ $beech_{y+4}$	4	27	4.044	0.055	13.9
Model No.	(B) Model Structure	Lag	N	F	p	r^2 (%)
28	log(CND) ~ site	-4	45	7.229	0.002	25.6
29	log(CND) ~ site	-3	45	7.229	0.002	25.6
30	log(CND) ~ site	-2	45	7.229	0.002	25.6
31	log(CND) ~ site	-1	42	7.151	0.002	26.8
32	log(CND) ~ site	0	39	6.096	0.005	25.3
33	log(CND) ~ site	1	36	5.856	0.007	26.2
34	log(CND) ~ site	2	33	4.534	0.019	23.2
35	log(CND) ~ site	3	30	3.282	0.053	19.6
36	log(CND) ~ site	4	27	3.347	0.052	21.8

Table S21. Variance partitioning to determine how much variation in the CND could be attributed to the time lag between nymphs and beech mast score. Shown are the r^2 values for the full models (models 10 to 18 models in Table S19) and the models containing site only (models 28 to 36 in Table S20). The difference between these two r^2 values (Δr^2) indicates the variation that is caused by the time lag between nymphs and beech mast score.

Model comparison	Full model	Site model	Δr^2 (%)
10 vs 28	25.7	25.6	0.1
11 vs 29	31.3	25.6	5.7
12 vs 30	53.6	25.6	28.0
13 vs 31	33.3	26.8	6.5
14 vs 32	32.9	25.3	7.6
15 vs 33	27.0	26.2	0.8
16 vs 34	28.6	23.2	5.4
17 vs 35	35.5	19.6	15.9
18 vs 36	35.7	21.8	13.9

Table S22. The parameter estimates of the best model in Table S19 are shown. The best model (model 12 in Table S19) had the expected two-year time lag between high nymph abundance (CND) and high beech mast score ($beech_{y-2}$). Shown are the parameter types, parameter names, parameter estimates on the logit scale, standard errors (s.e.), t-statistics (t), and p-values (p).

Type	Name	Estimates	s.e.	t	p
Intercept	Low site	4.136	0.057	72.164	< 0.001
Contrast 1	Medium site	-0.083	0.058	-1.418	0.164
Contrast 2	High site	-0.271	0.058	-4.640	< 0.001
Slope 1	$Beech_{y-2}$	0.070	0.014	4.969	< 0.001

SECTION 10 – Climate change over the 15-year study period

Methods: We tested for climate change in the mean annual temperature over the 15-year study period for the field-collected data at each of the four elevation sites (low site, medium site, high site, top site) and for the Climap-net data for each of the two weather stations (Neuchâtel at 485 m ASL and Chaumont at 1136 m ASL) that are close to our study location. The mean annual temperature (n = 15) was modelled as a simple linear regression of the covariate year (rescaled as 1, 2, 3, … 15). We then used Pearson's correlation test to determine whether the mean annual temperature was correlated between the field-collected data and the Climap-net data. The same approach was used to analyze the mean annual relative humidity, and the mean annual saturation deficit.

Results – Climate change in field-collected variables and Climap-net variables: The mean annual field-collected temperature decreased over the 15-year study period at the low elevation ($F_{1, 13} = 0.057$, $p = 0.816$), at the medium elevation ($F_{1, 13} = 0.124$, $p = 0.731$), at the high elevation ($F_{1, 13} = 0.068$, $p = 0.799$), and at the top elevation ($F_{1, 13} = 0.007$, $p = 0.935$), but these changes were not significant (Figure S14; Table S23). The mean annual field-collected relative humidity increased over the 15-year study period at the low elevation ($F_{1, 13} = 0.677$, $p = 0.425$), at the medium elevation ($F_{1, 13} = 0.698$, $p = 0.419$), at the high elevation ($F_{1, 13} = 1.024$, $p = 0.330$), and at the top elevation ($F_{1, 13} = 0.116$, $p = 0.738$), but these changes were not significant (Figure S15; Table S23). The mean annual field-collected saturation deficit decreased over the 15-year study period at the low elevation ($F_{1, 13} = 0.455$, $p = 0.512$), at the medium elevation ($F_{1, 13} = 1.285$, $p = 0.277$), at the high elevation ($F_{1, 13} = 1.626$, $p = 0.225$), and at the top elevation ($F_{1, 13} = 0.462$, $p = 0.509$) but these changes were not significant (Figure S16; Table S23). These analyses suggest that no significant climate change occurred with respect to any of the field-collected climate variables over the 15-year study period.

The mean annual Climap-net temperature increased significantly over the 15-year study period at the Neuchâtel weather station ($F_{1, 13} = 8.332$, $p = 0.013$) and at the Chaumont weather station ($F_{1, 13} = 7.540$, $p = 0.017$) (Figure S17; Table S24). The mean annual Climap-net relative humidity increased over the 15-year study period at the Neuchâtel weather station ($F_{1, 13} = 0.017$, $p = 0.898$) and decreased at the Chaumont weather station ($F_{1, 13} = 0.875$, $p = 0.367$), but these changes were not significant (Figure S18; Table S24). The mean annual Climap-net saturation deficit increased over the 15-year study period at the Neuchâtel weather station ($F_{1, 13} = 2.942$, $p = 0.110$) and at the Chaumont weather station ($F_{1, 13} = 6.225$, $p = 0.027$), but these changes

were only significant at the Chaumont weather station (Figure S19; Table S24). The mean annual Climap-net precipitation decreased over the 15-year study period at the Neuchâtel weather station ($F_{1, 13}$ =0.949, p = 0.348) and at the Chaumont weather station ($F_{1, 13}$ = 2.886, p = 0.113), but these changes were not significant (Figure S20; Table S24). These analyses suggest that significant climate change occurred with respect to temperature and saturation deficit from the Climap-net data over the 15-year study period.

Results – Correlation between the field-collected and Climap-net annual temperature: Across all four elevation sites, the mean annual temperature was weakly correlated between the field-collected data and the Neuchâtel weather station data (Pearson's r = 0.318, n = 60, p = 0.013; Table S25). Taking each elevation site independently, the mean annual temperature was not correlated between the field-collected data and the Neuchâtel weather station data (Table S25).

Across all four elevation sites, the mean annual temperature was weakly correlated between the field-collected data and the Chaumont weather station data (Pearson's r = 0.306, n = 60, p = 0.017; Table S25). Taking each elevation site independently, the mean annual temperature was not correlated between the field-collected data and the Chaumont weather station (Table S25). These analyses suggest that the mean annual temperature differed between the field-collected data and the Climap-net data over the 15-year study at Chaumont Mountain.

Results – Correlation between the field-collected and Climap-net annual relative humidity:

Across all four elevation sites, the mean annual relative humidity was weakly correlated between the field-collected data and the Neuchâtel weather station data (Pearson's r = 0.367, n = 60, p = 0.004; Table S26). Taking each elevation site independently, the mean annual relative humidity was not correlated between the field-collected data and the Neuchâtel weather station data (Table S26).

Across all four elevation sites, the mean annual relative humidity was not correlated between the field-collected data and the Chaumont weather station data (Pearson's r = 0.005, n = 60, p = 0.971; Table S26). Taking each elevation site independently, the mean annual relative humidity was not correlated between the field-collected data and the Chaumont weather station data (Table S26). These analyses suggest that the mean annual relative humidity differed between the field-collected data and the Climap-net data over the 15-year study at Chaumont Mountain.

Results – Correlation between the field-collected and Climap-net annual saturation deficit:

Across all four elevation sites, the mean annual saturation deficit was weakly correlated between the field-collected data and the Neuchâtel weather station data (Pearson's r = 0.305, n = 60, p = 0.018; Table S27). Taking each elevation site independently, the mean annual saturation deficit was not correlated between the field-collected data and the Neuchâtel weather station data (Table S27).

Across all four elevation sites, the mean annual saturation deficit was not correlated between the field-collected data and the Chaumont weather station data (Pearson's r = 0.162, n = 60, p = 0.218; Table S27). Taking each elevation site independently, the mean annual saturation deficit was not correlated between the field-collected data and the Chaumont weather station data (Table S27). These analyses suggest that the mean annual relative humidity differed between the field-collected data and the Climap-net data over the 15-year study at Chaumont Mountain.

Table S23. The simple linear regression models of each climate variable versus the covariate year are shown for the field-collected data. Shown are the parameter estimates, standard errors (s.e.), t-statistics (t), degrees of freedom (df), p-values (p), and the adjusted r^2 values of the model (expressed as a percent).

Climate variable	Site	Parameters	Estimates	s.e.	t	df	p	r^2(%)
Temperature	Low	(Intercept)	15.553	0.673	23.097	13	< 0.001	0.0
		Year	-0.018	0.074	-0.238	1	0.816	
Temperature	Medium	(Intercept)	14.574	0.813	17.929	13	< 0.001	0.0
		Year	-0.031	0.089	-0.351	1	0.731	
Temperature	High	(Intercept)	13.418	0.827	16.230	13	< 0.001	0.0
		Year	-0.024	0.091	-0.260	1	0.799	
Temperature	Top	(Intercept)	11.438	0.843	13.571	13	< 0.001	0.0
		Year	-0.008	0.093	-0.084	1	0.935	
Relative humidity	Low	(Intercept)	59.385	3.473	17.101	13	< 0.001	0.0
		Year	0.314	0.382	0.823	1	0.425	
Relative humidity	Medium	(Intercept)	60.904	3.755	16.219	13	< 0.001	0.0
		Year	0.345	0.413	0.835	1	0.419	
Relative humidity	High	(Intercept)	63.598	3.199	19.880	13	< 0.001	0.0
		Year	0.356	0.352	1.012	1	0.330	
Relative humidity	Top	(Intercept)	69.385	3.317	20.918	13	< 0.001	0.0
		Year	0.125	0.365	0.341	1	0.738	
Saturation deficit	Low	(Intercept)	6.683	0.722	9.262	13	< 0.001	0.0
		Year	-0.054	0.079	-0.674	1	0.512	
Saturation deficit	Medium	(Intercept)	6.174	0.704	8.765	13	< 0.001	2.0
		Year	-0.088	0.077	-1.134	1	0.277	
Saturation deficit	High	(Intercept)	5.184	0.560	9.264	13	< 0.001	4.3
		Year	-0.078	0.062	-1.275	1	0.225	
Saturation deficit	Top	(Intercept)	3.793	0.488	7.775	13	< 0.001	0.0
		Year	-0.036	0.054	-0.680	1	0.509	

Table S24. The simple linear regression models of each climate variable versus the covariate year are shown for the field-collected data. Shown are the parameter estimates, standard errors (s.e.), t-statistics (t), degrees of freedom (df), p-values (p), and the adjusted r^2 values of the model (expressed as a percent).

Climate variable	Station	Parameters	Estimates	s.e.	t	df	p	r^2(%)
Temperature	Neuchâtel	(Intercept)	10.118	0.260	38.865	13	< 0.001	34.4
		Year	0.083	0.029	2.886	1	0.013	
Temperature	Chaumont	(Intercept)	6.177	0.315	19.607	13	< 0.001	31.8
		Year	0.095	0.035	2.746	1	0.017	
Relative humidity	Neuchâtel	(Intercept)	73.021	0.815	89.625	13	< 0.001	0.0
		Year	0.012	0.090	0.131	1	0.898	
Relative humidity	Chaumont	(Intercept)	78.126	0.796	98.185	13	< 0.001	0.0
		Year	-0.082	0.088	-0.936	1	0.367	
Saturation deficit	Neuchâtel	(Intercept)	2.962	0.146	20.244	13	< 0.001	12.2
		Year	0.028	0.016	1.715	1	0.110	
Saturation deficit	Chaumont	(Intercept)	1.887	0.103	18.263	13	< 0.001	27.2
		Year	0.028	0.011	2.495	1	0.027	
Precipitation	Neuchâtel	(Intercept)	2.823	0.293	9.626	13	< 0.001	0.0
		Year	-0.031	0.032	-0.974	1	0.348	
Precipitation	Chaumont	(Intercept)	3.674	0.275	13.371	13	< 0.001	11.9
		Year	-0.051	0.030	-1.699	1	0.113	

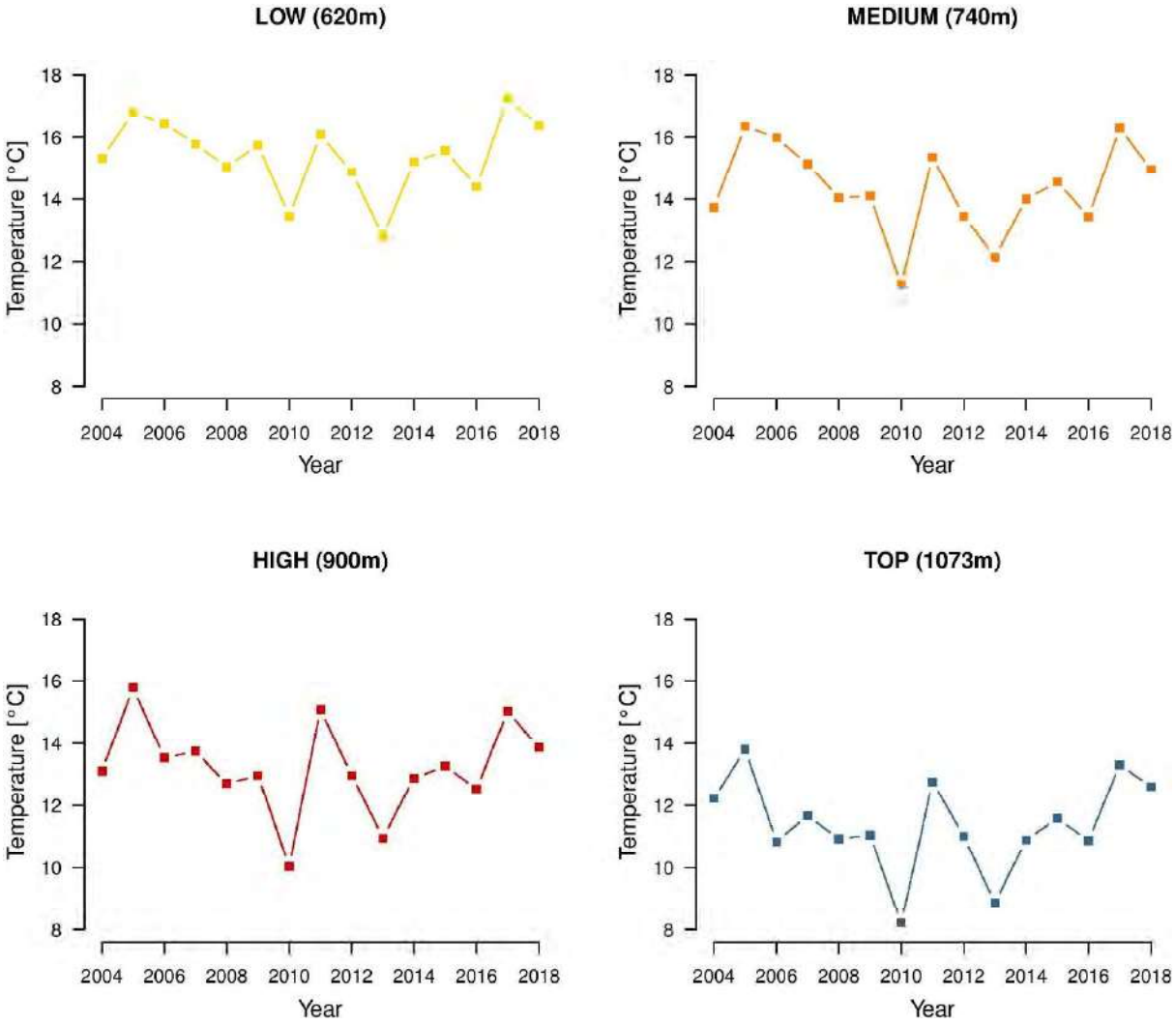

Figure S14. The change in the mean annual field-collected temperature over the 15-year study period is shown for each of the four elevations. Temperature decreased over time at each elevation but these changes were not significant.

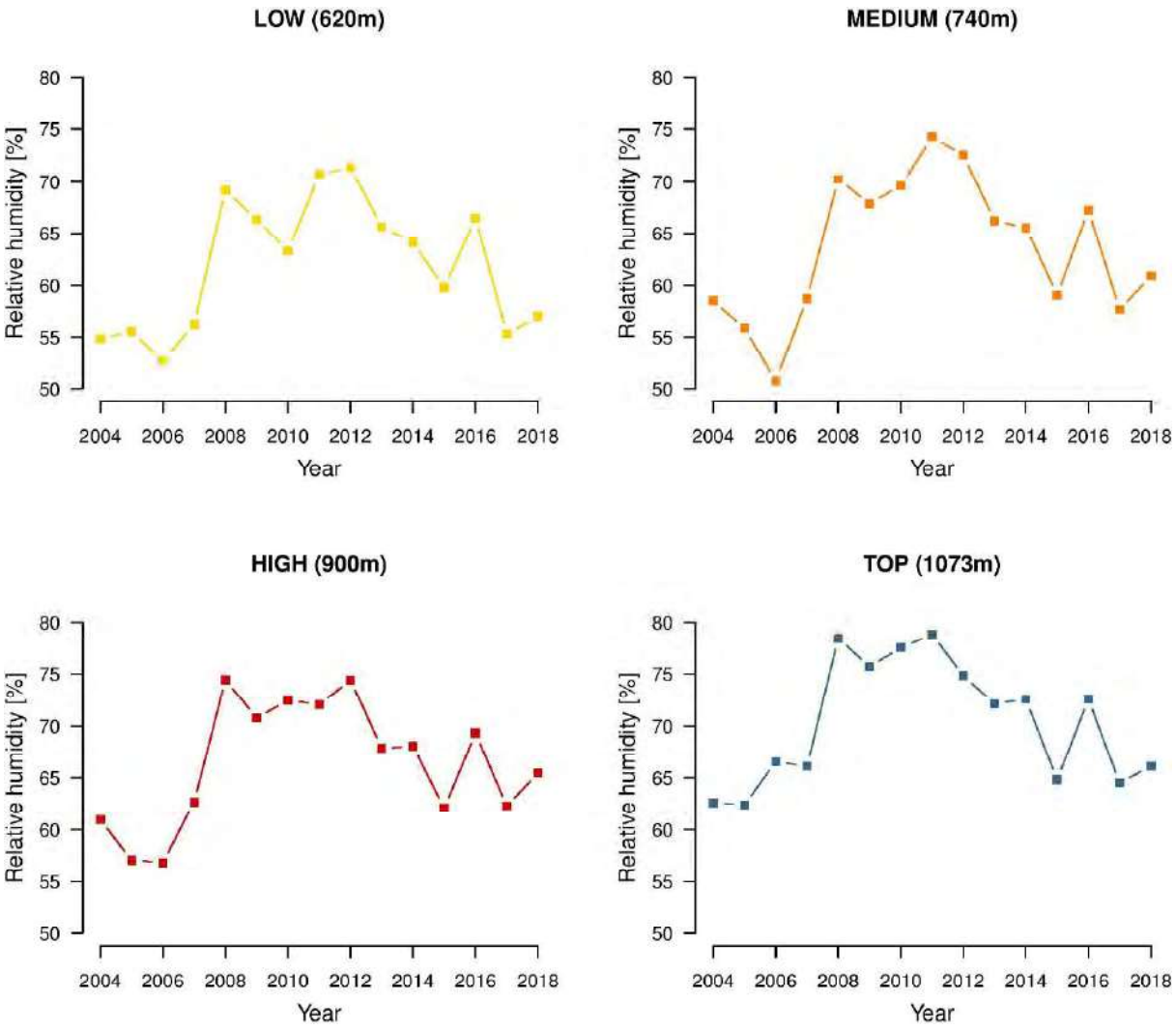

Figure S15. The change in the mean annual field-collected relative humidity over the 15-year study period is shown for each of the four elevations. Relative humidity increased over time at each elevation but these changes were not significant.

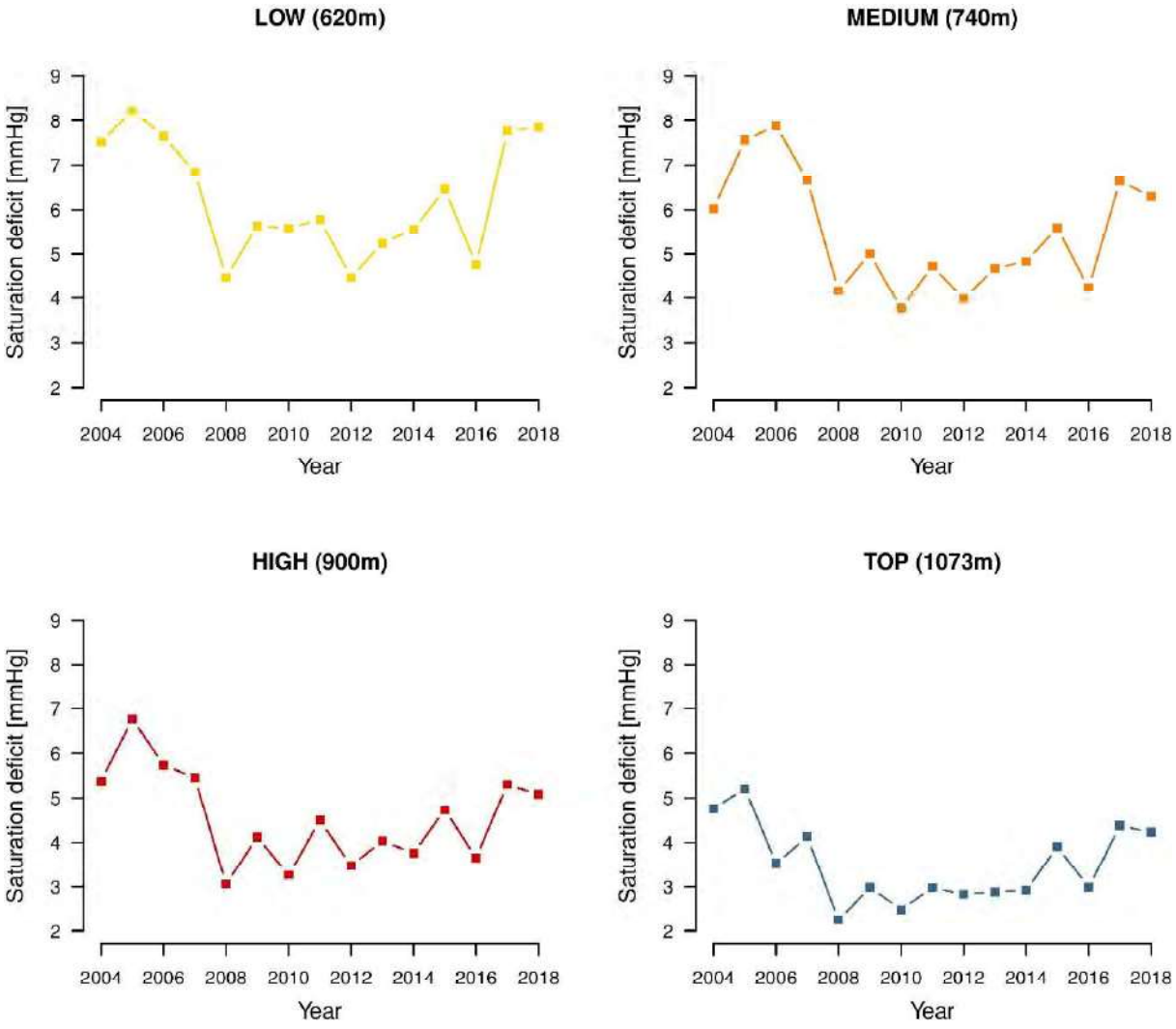

Figure S16. The change in the mean annual field-collected saturation deficit over the 15-year study period is shown for each of the four elevations. Saturation deficit decreased over time at each elevation but these changes were not significant.

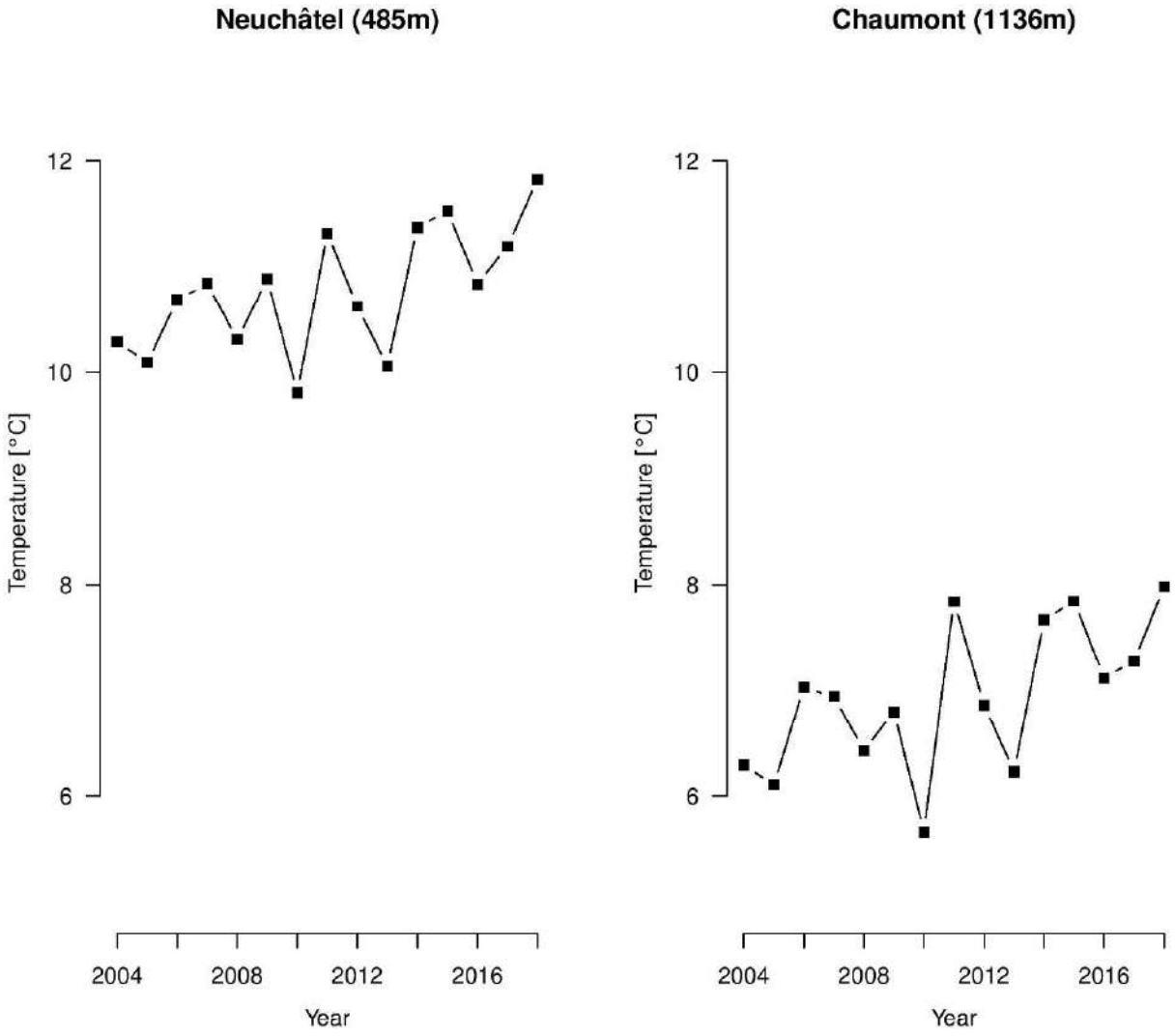

Figure S17. The change in the mean annual Climap-net temperature over the 15-year study period is shown for each of the two weather stations. Temperature increased significantly over time at each weather station.

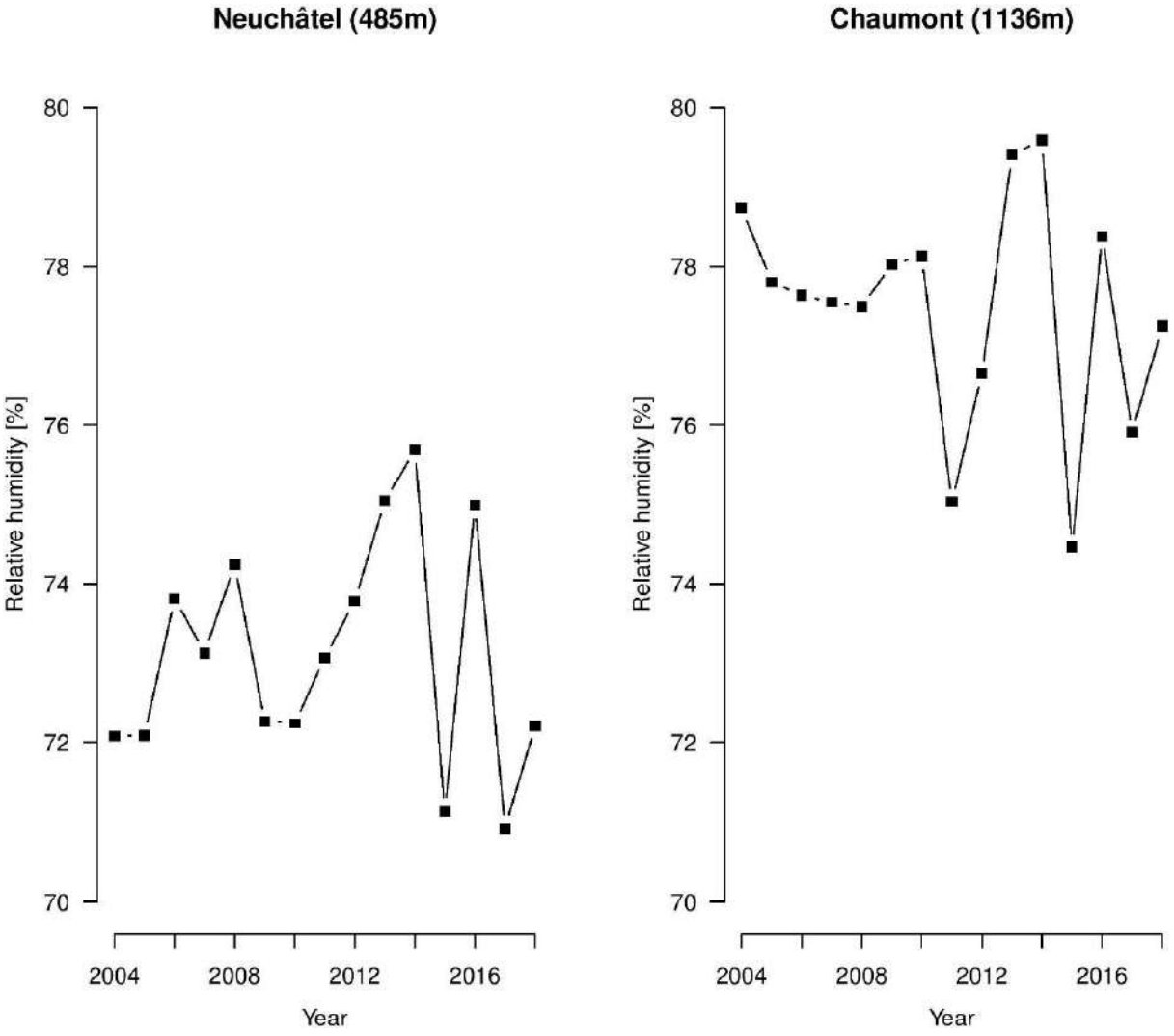

Figure S18. The change in the mean annual Climap-net relative humidity over the 15-year study period is shown for each of the two weather stations. Relative humidity increased over time at the Neuchatel weather station but decreased over time at the Chaumont weather station but this change was not significant.

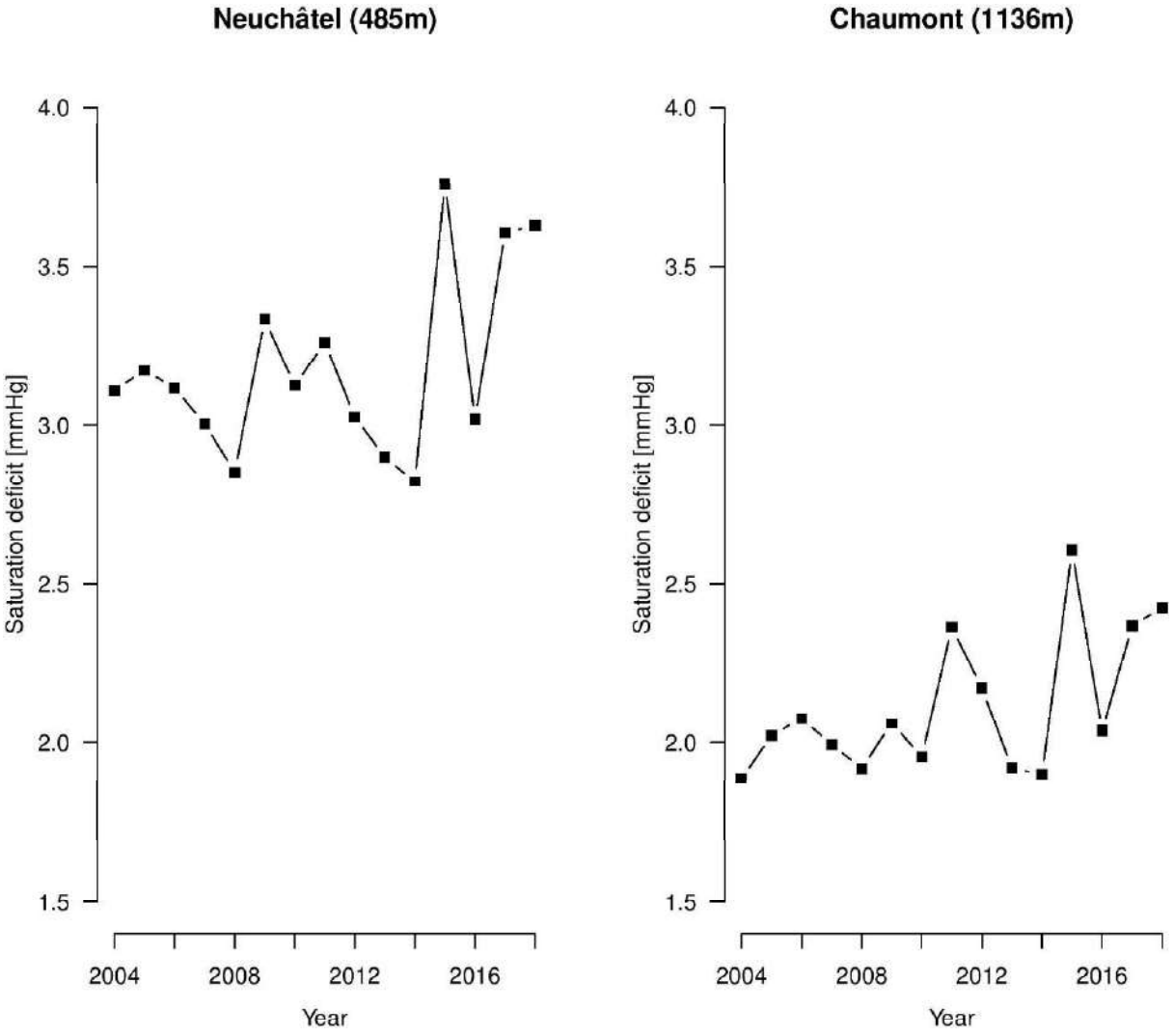

Figure S19. The change in the mean annual Climap-net saturation deficit over the 15-year study period is shown for each of the two weather stations. Saturation deficit increased over time, but this change was only significant for the Chaumont weather station.

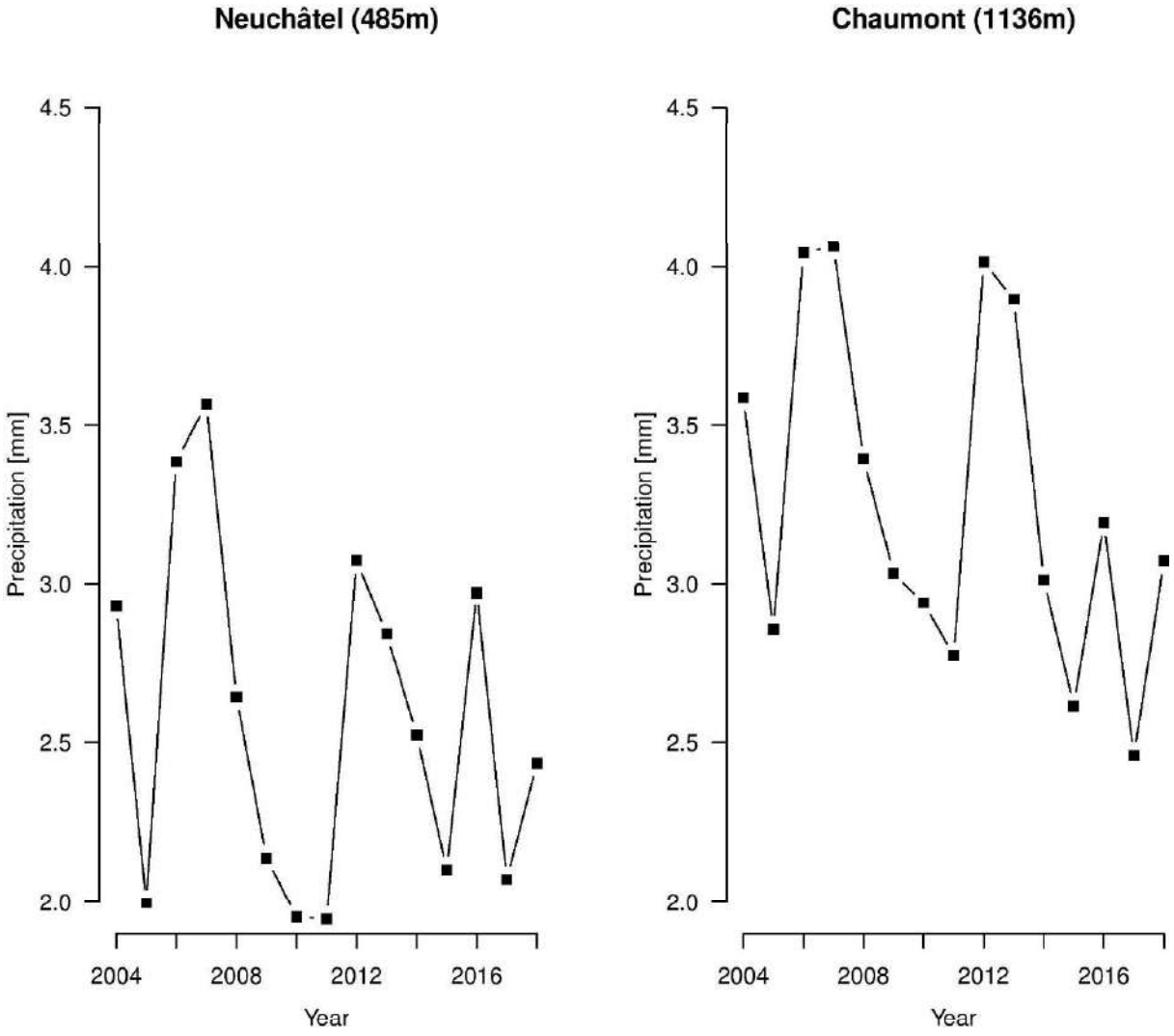

Figure S20. The change in the mean annual Climap-net precipitation over the 15-year study period is shown for each of the two weather stations. Precipitation decreased over time, but this change was not significant at either weather station.

Table S25. The correlation in the annual mean temperature between the field-collected data and the Climap-net data is shown for each of the eight combinations of the four elevation sites and the two weather stations. The four sites were located on the south side of Chaumont Mountain. The two weather stations in Neuchâtel and Chaumont were located at 485 m ASL and 1136 m ASL, respectively. The mean annual temperature for the field-collected data and the two weather stations were measured at 60 cm above ground and 200 cm above ground, respectively. Shown are Pearson's correlation coefficient (r), the sample size (n), and the statistical significance of the correlation (p).

	Neuchâtel[b]			Chaumont[c]		
Site	r	n	p	r	n	p
Low	0.520	15	0.047	0.472	15	0.075
Medium	0.464	15	0.081	0.464	15	0.081
High	0.451	15	0.092	0.454	15	0.089
Top	0.465	15	0.080	0.436	15	0.104
All[a]	0.318	60	0.013	0.306	60	0.017

[a] The daily mean temperatures were positively weakly correlated between the field-collected data and the Climap-net data from both weather stations.

Table S26. The correlation in the annual mean relative humidity between the field-collected data and the Climap-net data is shown for each of the eight combinations of the four elevation sites and the two weather stations. The four sites were located on the south side of Chaumont Mountain. The two weather stations in Neuchâtel and Chaumont were located at 485 m ASL and 1136 m ASL, respectively. The mean annual relative humidity for the field-collected data and the two weather stations were measured at 60 cm above ground and 200 cm above ground, respectively. Shown are Pearson's correlation coefficient (r), the sample size (n), and the statistical significance of the correlation (p).

	Neuchâtel[b]			Chaumont[c]		
Site	r	n	p	r	n	p
Low	0.475	15	0.074	0.037	15	0.895
Medium	0.359	15	0.189	0.017	15	0.953
High	0.375	15	0.169	0.026	15	0.928
Top	0.461	15	0.084	0.057	15	0.841
All[a]	0.367	60	0.004	0.005	60	0.971

[a] The daily mean relative humidity was positively weakly correlated between the field-collected data and the Climap-net data only from the Neuchâtel weather station.

Table S27. The correlation in the annual mean saturation deficit between the field-collected data and the Climap-net data is shown for each of the eight combinations of the four elevation sites and the two weather stations. The four sites were located on the south side of Chaumont Mountain. The two weather stations in Neuchâtel and Chaumont were located at 485 m ASL and 1136 m ASL, respectively. Shown are Pearson's correlation coefficient (r), the sample size (n), and the statistical significance of the correlation (p).

	Neuchâtel[b]			Chaumont[c]		
Site	r	n	p	r	n	p
Low	0.519	15	0.047	0.273	15	0.326
Medium	0.339	15	0.217	0.175	15	0.532
High	0.371	15	0.173	0.204	15	0.466
Top	0.459	15	0.086	0.242	15	0.384
All[a]	0.305	60	0.018	0.162	60	0.218

[a] The daily mean saturation deficit was positively weakly correlated between the field-collected data and the Climap-net data only from the Neuchâtel weather station.

SECTION 11 – Analysis of CND using Generalized Linear Models with Negative Binomial Errors

The cumulative nymphal density (CND) estimates the cumulative number of questing nymphs that were removed from each elevation site over the year. Each estimate of the CND is based on 12 sampling dates, and each sampling date is a mean of the tick counts that were obtained from 5 or 6 drags. In the main manuscript, we analyzed the log10-transformed CND (or CAD) using linear models with normal errors. In Section 7 of the Additional file 1, we showed that the residuals of these linear models met the assumptions of normality and equal variances. Here we present an alternative approach where we analyze the count data using generalized linear models (GLMs) with a Poisson error distribution or a negative binomial error distribution.

GLM with Poisson errors: To analyze the CND as a GLM with Poisson errors, we rounded each estimate of the CND to the nearest integer. We modelled the CND as a GLM with Poisson errors with the following fixed factors: elevation site, year, beech, and the field-collected relative humidity. A major problem with this approach was that the ratio of the residual deviance to the residual degrees of freedom (58778/36 = 1632.722) was highly overdispersed. In R, one can use the quasipoisson distribution to deal with overdispersed count data. However, the disadvantage of using the quasipoisson distribution to deal with overdispersion is that you can no longer use model selection because the model does not estimate an AIC value. For this reason, we decided to use a GLM with negative binomial errors to analyze our data.

GLM with negative binomial errors: To analyze the CND as a GLM with Poisson errors, we rounded each estimate of the CND to the nearest integer. For the GLM with negative binomial errors of the CND, we used the same AIC-based model selection approach that we used for the linear model with normal errors of the log10-transformed CND. We present the model selection table for the GLM with negative binomial errors of the CND in Table S28. For ease of comparison, we present the model selection table of the linear model of the log10-transformed CND in Table S29. For both approaches, the best model included the main effects of elevation site, year, beech masting index, and the field-collected relative humidity. This comparison shows that the two approaches returned the same model selection results. For the GLM with negative binomial errors of the CND, we present the parameter estimates of the best model (model 1 in Table S28) in Table S30. For the linear model of the log10-transformed CND, we present the parameter estimates of the best model (model 1 in Table S29) in Table S31. The

pattern of statistical significance is almost identical between the two tables. All the parameter estimates have the same sign. The magnitudes of the parameter estimates are not the same because the CNDs were log10-transformed for the linear model but not for the GLM. This comparison shows that these two approaches give the same results.

Table S28. Model selection results are shown for the negative binomial GLM of the cumulative nymph density response variable. The explanatory variables were site, year, tree masting variables obtained from MASTREE, and the climate variables obtained from the Climap-net database and collected from the field. The models are ranked according to their Akaike Information Criterion (AIC). Of the 52 models in the set, only the 6 top models are shown for which the cumulative support (Weight 2) is 95%. Shown for each model are the model rank (Rank), model structure (see below for explanation of explanatory variables), model degrees of freedom (Df), log-likelihood (logLik), Akaike information criterion (AIC), difference in the AIC value from the top model (ΔAIC), model weight (Weight1), cumulative weight (Weight2), and adjusted r-squared value (r^2). Additional file 1: Section 6 shows the results from the full model selection. The acronyms for the explanatory variables are as follows: S = site, Y = year, B = beech mast score, S:Y = interaction between site and year, RH2 = relative humidity from the field data, SD2 = saturation deficit from the field data, T2 = temperature from the field data, $RH2_{y-1}$ = relative humidity from the field data in year y-1, and $SD2_{y-1}$ = saturation deficit from the field data in year y-1.

Rank	Model structure	Df	logLik	AIC	ΔAIC	Weight1	Weight2	r^2
1	CND ~ S+Y+B+RH2	7	-409.4	836.2	0.0	75.0	75.0	NA
2	CND ~ S+Y+B+RH2+S:Y	9	-408.4	840.4	4.2	9.0	84.0	NA
3	CND ~ S+Y+B+SD2	7	-412.2	841.6	5.5	5.0	89.0	NA
4	CND ~ S+Y+B+T2	7	-412.3	841.9	5.8	4.0	93.0	NA
5	CND ~ S+Y+B+$RH2_{y-1}$	7	-413.3	843.9	7.7	2.0	95.0	NA
6	CND ~ S+Y+B+$SD2_{y-1}$	7	-413.4	844.1	7.9	1.0	96.0	NA

Table S29. Model selection results are shown for the linear models with normal errors of the log10-transformed CND response variable. The explanatory variables were site, year, tree masting variables obtained from MASTREE, and the climate variables obtained from the Climap-net database and collected from the field. The models are ranked according to their Akaike Information Criterion (AIC). Of the 52 models in the set, only the 6 top models are shown for which the cumulative support (Weight 2) is 95%. Shown for each model are the model rank (Rank), model structure (see below for explanation of explanatory variables), model degrees of freedom (Df), log-likelihood (logLik), Akaike information criterion (AIC), difference in the AIC value from the top model (ΔAIC), model weight (Weight1), cumulative weight (Weight2), and adjusted r-squared value (r^2). Additional file 1: Section 6 shows the results from the full model selection. The acronyms for the explanatory variables are as follows: S = site, Y = year, B = beech mast score, S:Y = interaction between site and year, RH2 = relative humidity from the field data, SD2 = saturation deficit from the field data, T2 = temperature from the field data, $RH2_{y-1}$ = relative humidity from the field data in year y-1, and $SD2_{y-1}$ = saturation deficit from the field data in year y-1.

Rank	Model structure	Df	logLik	AIC	ΔAIC	Weight1	Weight2	r^2
1	CND ~ S+Y+B+RH2	7	33.0	-48.7	0.0	76.0	76.0	73.2
2	CND ~ S+Y+B+RH2+S:Y	9	33.6	-43.6	5.2	6.0	82.0	72.4
3	CND ~ S+Y+B+SD2	7	30.4	-43.5	5.3	5.0	87.0	69.7
4	CND ~ S+Y+B+T2	7	30.4	-43.4	5.3	5.0	92.0	69.6
5	CND ~ S+Y+B+$RH2_{y-1}$	7	29.4	-41.4	7.3	2.0	94.0	68.1
6	CND ~ S+Y+B+$SD2_{y-1}$	7	29.1	-40.8	7.9	1.0	95.0	67.7

Table S30. The parameter estimates from the top model in the model selection table from negative binomial GLM are shown. In this top model, the CND response variable was modelled as a function of elevation site, year, beech tree mast score 2 years prior, and the field-collected mean annual relative humidity in the same year. Shown are the parameter types, parameter names, parameter estimates on the log10-transformed scale, standard errors (s.e.), t-statistic (t), and p-values (p).

Type	Name	Estimate	s.e	t	p
Intercept	Low site	9.102	0.127	71.645	< 0.001
Contrast 1	Medium site	-0.136	0.097	-1.403	0.161
Contrast 2	High site	-0.590	0.100	-5.878	< 0.001
Slope 1	Year	0.046	0.010	4.641	< 0.001
Slope 2	Beech tree mast score	0.159	0.023	7.053	< 0.001
Slope 3	Relative humidity (field-collected)	-0.170	0.045	-3.814	< 0.001

Table S31. The parameter estimates from the top model in the model selection table from linear models are shown. In this top model, the log10-transformed CND response variable was modelled as a function of elevation site, year, beech tree mast score 2 years prior, and the field-collected mean annual relative humidity in the same year. Shown are the parameter types, parameter names, parameter estimates on the log10-transformed scale, standard errors (s.e.), t-statistic (t), and p-values (p).

Type	Name	Estimate	s.e	t	p
Intercept	Low site	3.939	0.059	66.209	< 0.001
Contrast 1	Medium site	-0.053	0.045	-1.162	0.253
Contrast 2	High site	-0.245	0.047	-5.217	< 0.001
Slope 1	Year	0.020	0.005	4.262	< 0.001
Slope 2	Beech tree mast score	0.067	0.011	6.378	< 0.001
Slope 3	Relative humidity (field-collected)	-0.074	0.021	-3.570	0.001

REFERENCES

1. BikeAttitude: BikeAttitude, The World of Freeride. www.neuchbikepark.ch (2003). Accessed October 28 2019.
2. Neuchâtel LVd: Fête de Chaumont. www.neuchatelville.ch/fileadmin/sites/ne_ville/fichiers/presse/communiques_presse/imported/2011/Fete_20de_20Chaumont.pdf (2011). Accessed October 28 2019.
3. Tack W, Madder M, Baeten L, Vanhellemont M, Verheyen K. Shrub clearing adversely affects the abundance of Ixodes ricinus ticks. Exp Appl Acarol. 2013;60:411-20.

ADDITIONAL FILE – Chapter 2

Masting by beech trees predicts the risk of Lyme disease

Authors: Cindy Bregnard, Olivier Rais, and Maarten J. Voordouw

Table of Contents

SECTION 1 – Interpolation of the climap-net climate data..... 321
SECTION 2 – Correlation between two measures of nymph density..... 323
SECTION 3 – Assumptions of the statistical methods 325
SECTION 4 – Full statistical analysis of the adult infection prevalence (aip) and density of infected adults (dia) for the restricted 13-year period of the study (2006 – 2018) 327
SECTION 5 – Full statistical analysis of the nymphal infection prevalence (nip) for the restricted 13-year period of the study (2006 – 2018)..... 355
SECTION 6 – Full statistical analysis of the density of infected nymphs (din) for the restricted 13-year period of the study (2006 – 2018)..... 365

SECTION 1 – Interpolation of the Climap-net climate data

Methods: Climap-net data were obtained from two weather stations that are located at 485 m ASL in Neuchâtel and at 1136 m ASL in Chaumont and that are close to our four elevation sites. To create a climate profile that was specific for each of the four elevation sites, we interpolated the values between the two weather stations using the relative elevation distance of each elevation site to the two weather stations. For example, the total elevation distance between the Neuchâtel and Chaumont weather stations is 651 meters, and the elevation distance between the top site and the Neuchâtel weather station is 620 meters, which represents 95.2% of the elevation distance. Thus, the climate at the top site is expected to be more similar to the Chaumont weather station (95.2%) compared to the Neuchâtel weather station (4.8%), whereas the reverse would be true for the low site. For each elevation site, the mean daily temperature, relative humidity, saturation deficit, and precipitation were calculated based on the interpolating percentages (Table S1).

Table S1. Climap-net data interpolation. Shown are the site, elevation, elevation distance with the Neuchâtel weather station (Dist 1), elevation distance between Neuchâtel and Chaumont weather station (Dist 2), the interpolating percentage from the Neuchâtel weather station (Neuchâtel), and the interpolating percentage from the Chaumont weather station (Chaumont).

Site	Elevation (m ASL)	Dist 1 (m)	Dist 2 (m)	Neuchâtel	Chaumont
Top	1073	620	651	4.80%	95.20%
High	900	447	651	31.30%	68.70%
Medium	740	287	651	55.90%	44.10%
Low	620	167	651	74.30%	25.70%

SECTION 2 – Correlation between two measures of nymph density

Methods: We can estimate the mean daily density of nymphs (DON) per 100 m^2 by taking the arithmetic average of the ~12 annual sampling occasions, hereafter referred to as mean daily DON1. Over a 15-year study with 12 sampling occasions per year at 4 elevation sites, it is inevitable that some sampling occasions are missed due to bad weather or other reasons. Depending on whether these missing values are from months with low or high nymphal density, the estimate of the DON will be biased high or low, respectively. To lessen the bias caused by missing data, we estimated the cumulative nymph density (CND), which is an estimate of the total annual abundance of questing nymphs per 100 m^2. The CND was estimated by integrating the area under the curve (AUC) of the monthly questing nymph densities for each year (Perret et al. 2000, Eisen et al. 2003). The interpretation of the CND is the theoretical number of questing nymphs per 100 m^2 that would have been collected if we had sampled ticks daily over the course of a year (this assumes that the removal sampling has no effect on the tick density at the site). If the CND is divided by 365 or 366, we obtain an estimate of the mean DON collected per 100 m^2, hereafter referred to as the mean daily DON2. To validate our use of the mean daily DON2, we compared this value to the mean daily DON1. We used Pearson's correlation test to show that the mean daily DON1 and the mean daily DON2 were highly correlated (which was expected). We also used a paired samples t-test to determine the difference between the mean daily DON1 and the mean daily DON2.

Results: Across all four elevation sites, the mean daily DON1 and the mean daily DON2 were positively correlated (Pearson's $r = 0.971$, $n = 60$, $p < 0.001$; Figure S1). The mean daily DON2 was 20.9% lower than the mean daily DON1 (mean difference ± standard error: 8.4 ± 3.8 nymphs per 100 m^2), and this difference was significant (Paired sample t-test: $df = 58$, $t = 6.611$, $p < 0.001$). This result was expected; the mean daily DON1 is biased high because most of the missing data were from the winter months when the nymphal density is lowest at our field site. In contrast, the DON2 integrates the area under the curve over the entire calendar year and therefore includes these winter months with low nymphal density.

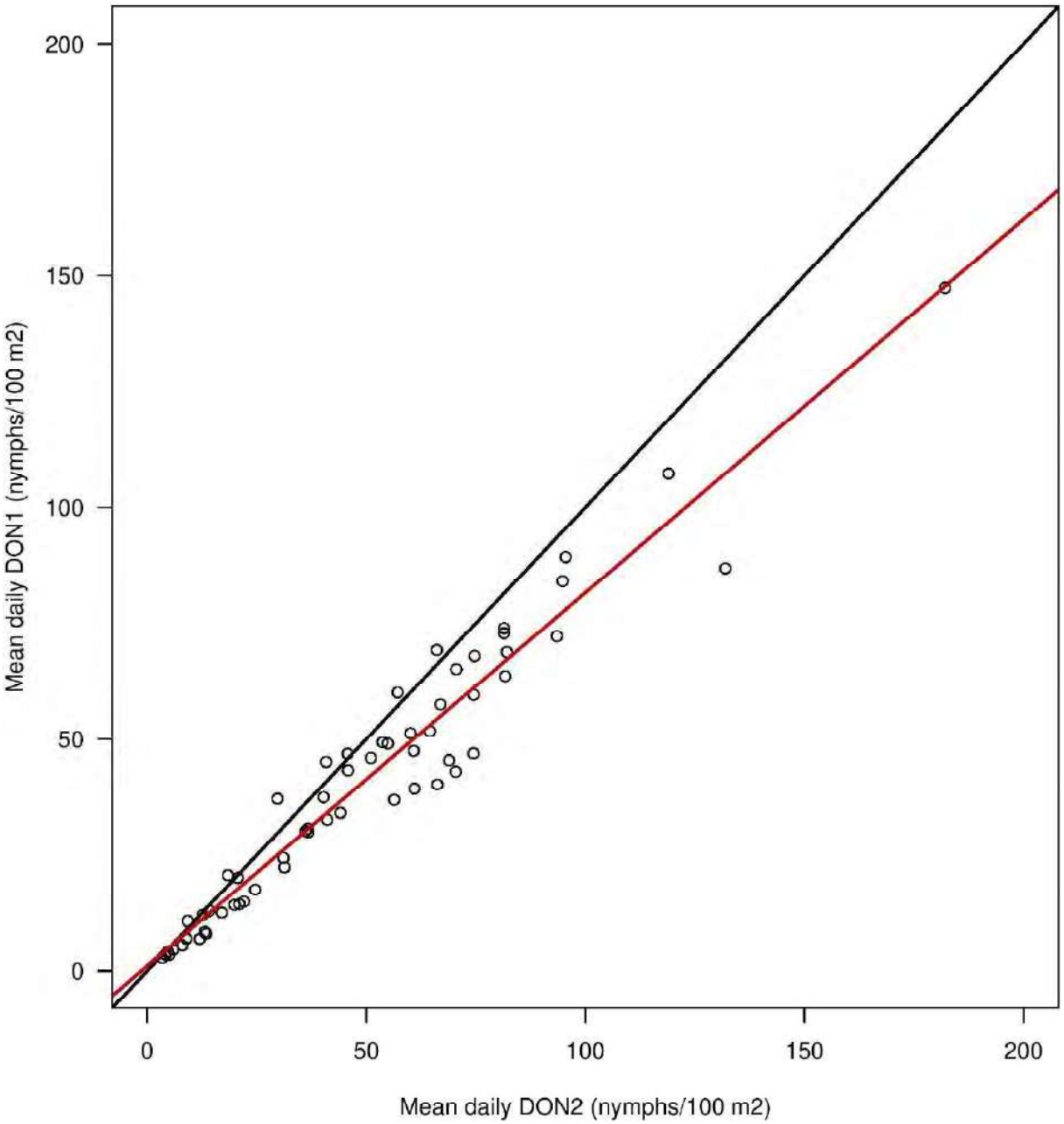

Figure S1. Relationship between the mean daily DON2 (i.e., CND divided by 365 or 366) and the mean daily DON1 (i.e., arithmetic average of the ~12 sampling occasions per year) is shown. The black line represents the 1:1 slope, whereas the red line represents the line of best fit from the linear regression.

SECTION 3 – Assumptions of the statistical methods

Assumptions of the generalized linear mixed effects models (GLMMs): Generalized linear mixed effects models (GLMMs) with binomial errors assume that the ratio between the residual variance and the residual degree of freedom should be close to 1. For the nymphal infection prevalence (NIP) and the adult infection prevalence (AIP), we examined this ratio for the best model in the AIC-based model selection table.

Results for the NIP: For the NIP, the ratio between the residual deviance (4726.2) and the residual degree of freedom (6918.0) of the best model (model 1 in Table S9) was 0.683, indicating that the data were not overdispersed.

Results for the AIP: For the AIP, the ratio between the residual deviance (4208.0) and the residual degree of freedom (4565.0) of the best model (model 1 in Table S3) was 0.922, indicating that the data were not overdispersed.

Assumptions of the linear mixed effects models (LMs): Linear models assume that the residuals follow a normal distribution and that the variance of the residuals is the same over the range of predicted values (or between groups). We used the Shapiro-Wilk normality test to test the assumption of normality for the residuals of the log10-transformed DIN (or DIA). We used a Bartlett's K-squared test to test whether the variance of the residuals was the same between the four elevation sites. For the density of infected nymphs (DIN) and the density of infected adults (DIA), we examined these two assumptions for the best model in the AIC-based model selection table.

Results for the DIN: For the DIN, the residuals of the best model (model 1 in Table S9) followed a normal distribution (Shapiro-Wilk normality test: $W = 0.963$, $p = 0.110$) and the residual variance was not different between the four elevation sites (Bartlett's K-squared = 1.925, df = 3, $p = 0.588$).

Results for the DIA: For the DIA, the residuals of the best model (model 1 in Table S6) followed a normal distribution (Shapiro-Wilk normality test: $W = 0.962$, $p = 0.096$) and the residual variance was not different between the four elevation sites (Bartlett's K-squared = 2.943, df = 3, $p = 0.401$).

SECTION 4 – Full statistical analysis of the adult infection prevalence (AIP) and density of infected adults (DIA) for the restricted 13-year period of the study (2006 – 2018)

Adult infection prevalence: Adults that tested negative or positive on the RLB were defined as being uninfected or infected with *B. burgdorferi* sl, respectively. The adult infection status is a binomial variable (uninfected and infected adults were coded as 0 and 1, respectively) that was used to calculate the annual infection prevalence (AIP), which is the percentage of adults infected with *B. burgdorferi* sl for a given combination of elevation site and year.

Annual density of infected adults: The annual density of infected adults (DIA) is a measure of the total annual abundance of questing infected adults per 100 m^2 and was estimated by multiplying our annual estimates of the DOA by our annual estimates of the AIP (separately for each of the four elevation sites). The interpretation of the DIA is the theoretical number of questing infected adults per 100 m^2 that would have been collected if we had sampled ticks daily over the course of a year.

Annual mean climate variables: To investigate the relationship between climate and the AIP and DIA, we collapsed our monthly or daily weather data into a set of annual means. For the field-collected data, the annual means were calculated over the 12 measurements (a single measurement for each month). For the weather station data, the annual means were calculated over 365 daily means (i.e., a total of 365 days*24 measurements/day = 8760 hourly measurements). Thus, the weather station annual means were based on 730 times more data than the field-collected annual means. However, an important advantage of the field-collected data was that they were specific for each of the four elevation sites. In contrast, the Climap-net data came from two weather stations that were located at some distance from the four elevation sites. To facilitate comparison between the slopes of the climate variables, we standardized the climate variables to z-scores (mean of 0 and a standard deviation of 1).

Annual tree masting variables: Previous studies (Ostfeld et al. 2006, Brugger et al. 2018, Bregnard et al. 2020) have shown that there is a two-year time lag between masting events and the DON and a three-year time lag between masting events and the DOA. Our recent analysis of tick abundance at our study location showed that annual variation in the DON and the DOA was strongly associated with the mast index of European beech trees but not with the mast index of Norway spruce (Bregnard et al. 2020). These studies validate our decision to model the DIN

and the DIA as a function of the European beech mast index two years previously (year y-2) and three years previously (year y-3), respectively. For example, we expect that beech mast index from the year 2001 predict the DIN in year 2003 (2 years later) and the DIA in year 2004 (three years later). The same approach was used to model the NIP and the AIP.

RLB time lag: As mentioned in the molecular methods of the main manuscript, there was considerable variation in the RLB time lag (range = 4 to 5,025 days), which is the time interval between the date of tick collection (and tick DNA extraction) versus the date of the RLB. The ammonium hydroxide solution used to extract the whole tick DNA is not optimal for long-term DNA storage, and we were concerned that the DNA would degrade over time and that our ability to detect *B. burgdorferi* sl would decrease with the duration of the RBL time lag. We therefore included the RLB time lag as an explanatory variable (standardized to z-score) in our statistical analyses. As the RLB time lag information was missing for the first two years of our study (2004 and 2005), we excluded these years from our statistical analysis.

Analysis of the AIP: The AIP was modelled using generalized linear mixed effects models (GLMMs) with binomial errors. The fixed effects structure included elevation site (4 levels: low, medium, high, top), the covariate year (rescaled as 1, 2, 3, … 15), the covariate beech mast index 3 years prior (range: 1 to 5), the covariate RLB time lag, and the mean annual climate variables of temperature, relative humidity, SD, and precipitation. As time lags are important in tick ecology, we modelled the AIP as a function of the mean climate variables in the present year, the previous year, or two years prior. As we did not measure the field-collected climate variables in the two years prior to the start of our study (e.g., 2002 and 2003), we had to exclude the years 2004 and 2005 from our statistical analysis. The unique drag identification number for the 720 combinations of site, year, and month (4*15*12) was included as the random factor. All variable acronyms can be found in Table S2.

Analysis of the DIA: Count data follow a Poisson distribution and aggregated count data follow a negative binomial distribution. However, our estimates of the DOA, and by extent the DIA, are summary statistics (sums or integrals) that are based on the counts of ~60 drags (12 dates*5 drags per date). According to the central limit theorem of statistics, summary statistics will follow a normal distribution even if the observations on which they are based are sampled from a non-normal distribution. We therefore assumed that the residuals of our DIA values follow a normal distribution. The annual DIA values were log10-transformed to further improve their fit

to the normal distribution. The log10-transformed DIA values (n = 60) were analysed using linear models (LM) with normal errors. The DIA was analysed as a function of the same explanatory variables as the AIP.

Model selection approach: To identify the best model, we used a model selection approach based on the Akaike information criterion (AIC). A big conceptual advantage of model selection is that it reminds the user that there are competing models with different parameter estimates and that some of these models have more support (i.e., are better at explaining the data) than other models. Another advantage is that you can compare non-nested models containing different explanatory variables, which is not possible with a more traditional approach like stepwise multiple regression. Models were ranked according to their AIC values and the Akaike weights, which indicate the percent support, were calculated for each model. We used the Akaike weights to calculate the model-averaged parameter estimates and their 95% confidence intervals (CIs). For the generalized linear mixed effects models that analysed the NIP and AIP, we assessed the goodness of fit of the binomial distribution for the best model from the model selection table. Similarly, for the linear models that analysed the DIN and DIA, the assumptions of normally distributed residuals and equal variances were assessed for the best model from the model selection table (Additional file 1: Section 3). We used R version 4.0.3 for all statistical analyses (Team 2013). We used the lm() function in the base package to run the LMs with normal errors. We used the glmer() functions in the lme4 package to run the GLMMs with binomial errors. We used the mod.sel() function and the model.av() function in the MuMIn package to create the model selection tables and the model-averaged parameter estimates.

Model selection analysis of the AIP

The model selection table for the 30 best out of 182 models is presented in Table S3. For the AIP, the best two models had a combined support of 96.0% (Table S3). The first- and second-best models had 76.0% and 20.0% of the support (Table S3), respectively, and contained the explanatory variables of beech mast score 3 years prior, RLB time lag, and field-collected mean annual relative humidity from 2 years prior. The only difference between these two models was that the second model contained site, whereas the first model did not (Table S3).

For the individual explanatory variables, there was strong support for RLB time lag (99.8%), beech mast score 3 years prior year (99.3%), and field-collected mean annual relative

humidity from 2 years prior (95.7%), and moderate support for site (20.5%; Table S4). None of the other explanatory variables had a support > 1.4% (Table S4).

Model-averaged parameter estimates for the AIP

To determine the direction and statistical significance of the explanatory variables on the AIP, we present the model-averaged parameter estimates (and their 95% confidence intervals) on the logit scale (Table S5). We also back-calculated the effect sizes of the explanatory variables on the AIP on the original scale with respect to the following baseline: the site was low elevation, the beech mast score 3 years prior was set to 1, and the covariates of RLB time lag and field-collected mean annual relative humidity from 2 years prior were set to 0 (i.e., the mean values on the z-score scale).

The AIP was not significantly different between the four elevation sites (Figure S2, Table S5).

The beech mast score 3 years prior had a negative and significant effect on the AIP (Figures S3; slope = -0.202 per class; 95% CI = -0.280 – -0.123). Increasing the beech mast score 3 years prior from 1 (poor mast) to 5 (full mast) decreased the AIP by 34.9% to 48.9% at the four elevation sites on Chaumont Mountain (Figure S3).

The RLB time lag had a positive effect on the NIP (Figure S4; slope = 0.054 per standard deviation, 95% CI = -0.063 – 0.170). Increasing the RLB time lag by one standard deviation (e.g., 925 days) increased the AIP on the original scale by 4.2% to 28.1% at the four elevation sites (Figure S4).

The field-collected mean annual relative humidity 2 years prior had a negative and significant effect on the AIP (Figure S5; slope = -0.311 per standard deviation, 95% CI = -0.457 – -0.165). Increasing the field-collected mean annual relative humidity 2 years prior by one standard deviation (e.g., 7.1% of relative humidity) decreased the AIP on the original scale by 2.4% to 22.0% at the four elevation sites (Figure S5).

In summary, the explanatory variables of beech mast score 3 years prior and relative humidity 2 years prior both had significant negative effects on the AIP.

Model selection analysis of the DIA

The model selection table for the 30 best out of 314 models is presented in Table S6. For the annual DIA, the top eleven models had a combined support of 80.0% (Table S6). The best model had 35.0% of the support (Table S6), explained 62.7% of the variation in the annual DIA, and contained the explanatory variables of elevation site (partial r^2 = 31.3%), year (partial

r^2 = 8.0%), site:year interaction (partial r^2 = 8.6%), RLB time lag (partial r^2 = 0.8%), and field-collected mean annual relative humidity 2 years prior (partial r^2 = 29.8%).

The support for the individual explanatory variables was as follows: site (99.9%), year (85.4%), field-collected mean annual relative humidity 2 years prior (74.0%), site:year interaction (69.6%), RLB time lag (63.8%), and beech mast score 3 years prior (37.3%; Table S7). None of the other explanatory variables had a support > 7.0% (Table S7).

Model-averaged parameter estimates for the DIA

To determine the effects of the explanatory variables on the DIA, we present the model-averaged parameter estimates on the log10-transformed scale. We also back-calculated the effect sizes of the explanatory variables on the DIA on the original scale with respect to the following baseline: the site was low elevation, the year was 2006, the beech mast score was set to 1, and the other covariates were set to 0 (i.e., the mean values on the z-score scale).

The interaction between site and year indicated that the change in the DIA over time differed between the four elevation sites (Figure S7, Table S8). Over the 13-year period (2006 – 2018), the DIA increased at the low (slope = 0.017 per year, 95% CI = -0.038 – 0.072), but decreased at the medium (Medium – Low contrast of the slope = -0.011, 95% CI = -0.064 – 0.042), high (High – Low contrast of the slope = -0.058, 95% CI = -0.111 – -0.004), and top (Top – Low contrast of the slope = -0.079, 95% CI = -0.133 – -0.026) elevation sites. Over the 13-year period (2006 – 2018), the DIA increased by 60.1% at the low elevation site, but decreased by 17.1%, 67.5%, and 82.1% at the medium, high, and top elevation sites, respectively (Figure S7). Due to the significant interaction between site and year, it does not make sense to interpret the differences in intercept between the four elevation sites (Table S8).

The RLB time lag had a positive effect on the DIA (slope = 0.047 95% CI = -0.054 – 0.148). Increasing the RLB time lag by one standard deviation (e.g., 925 days) increased the DIA on the original scale by 11.4% at each of the four elevation sites (Figure S8).

The field-collected mean annual relative humidity 2 years prior had a negative and significant effect on the DIA (slope = -0.173 per standard deviation, 95% CI = -0.289 – -0.057). Increasing the field-collected mean annual relative humidity 2 years prior by one standard deviation (e.g., 7.0% of relative humidity) decreased the DIA on the original scale by 32.9% at each of the four elevation sites (Figure S9).

In summary, the DIA remained stable over time at the two lower elevations but decreased significantly at the high and top elevations. The DIA increased with RLB time lag and decreased significantly with the field-collected relative humidity 2 years prior.

Table S2. Acronyms and definitions of the variables used in the main manuscript and additional file 1

Acronym	Description
DIN	Annual density of infected nymphs per 100 m^2
NIP	Annual nymphal infection prevalence
DIA	Annual density of infected adults per 100 m^2
AIP	Annual adult infection prevalence
S	Site name (factor with 4 levels: low, medium, high, top)
Y	Year of the study (covariate: 1, 2, …, 15)
B	Beech mast score in year y-2 (covariate: 1, 2, 3, 4, 5)
B3	Beech mast score in year y-3 (covariate: 1, 2, 3, 4, 5)
RLB	Time lag between tick sampling and RLB procedure (days)
DIN_{y-1}	Annual density of infected nymphs in year y-1 per 100 m^2
T1	Mean temperature in year y from the weather station data (°C)
$T1_{y-1}$	Mean temperature in year y-1 from the weather station data (°C)
$T1_{y-2}$	Mean temperature in year y-2 from the weather station data (°C)
RH1	Mean relative humidity in year y from the weather station data (%)
$RH1_{y-1}$	Mean relative humidity in year y-1 from the weather station data (%)
$RH1_{y-2}$	Mean relative humidity in year y-2 from the weather station data (%)
SD1	Mean saturation deficit in year y from the weather station data (mmHg)
$SD1_{y-1}$	Mean saturation deficit in year y-1 from the weather station data (mmHg)
$SD1_{y-2}$	Mean saturation deficit in year y-2 from the weather station data (mmHg)
PR1	Mean precipitation in year y from the weather station data (mm)
$PR1_{y-1}$	Mean precipitation in year y-1 from the weather station data (mm)
$PR1_{y-2}$	Mean precipitation in year y-2 from the weather station data (mm)
T2	Mean temperature in year y from the field-collected data (°C)
$T2_{y-1}$	Mean temperature in year y-1 from the field-collected data (°C)
$T2_{y-2}$	Mean temperature in year y-2 from the field-collected data (°C)
RH2	Mean relative humidity in year y from the field-collected data (%)
$RH2_{y-1}$	Mean relative humidity in year y-1 from the field-collected data (%)
$RH2_{y-2}$	Mean relative humidity in year y-2 from the field-collected data (%)
SD2	Mean saturation deficit in year y from the field-collected data (mmHg)
$SD2_{y-1}$	Mean saturation deficit in year y-1 from the field-collected data (mmHg)
$SD2_{y-2}$	Mean saturation deficit in year y-2 from the field-collected data (mmHg)

Table S3. Model selection results are shown for the generalized linear mixed effects model with binomial errors of the adult infection prevalence (AIP) response variable. The explanatory variables were site, year, beech masting index 3 years prior, RLB time lag, and the climate variables obtained from the weather stations and collected from the field. The models are ranked according to their Akaike Information Criterion (AIC). Shown for each model are the model rank (Rank), model structure (see below for explanation of explanatory variables), model degrees of freedom (Df), log-likelihood (logLik), Akaike information criterion (AIC), difference in the AIC value from the top model (ΔAIC), model weight (Weight1), and cumulative weight (Weight2).

Rank	Model structure	Df	logLik	AIC	ΔAIC	Weight1	Weight2
1	AIP ~ B3+RLB+$RH2_{y-2}$	5	-2104.0	4218.0	0.0	76.0	76.0
2	AIP ~ S+B3+RLB+$RH2_{y-2}$	8	-2102.3	4220.7	2.7	20.0	96.0
3	AIP ~ B3+RLB+$SD2_{y-2}$	5	-2108.3	4226.7	8.7	1.0	97.0
4	AIP ~ Y+B3+RLB	5	-2108.5	4227.1	9.1	1.0	98.0
5	AIP ~ Y+RLB+PR	5	-2109.1	4228.3	10.3	0.0	100.0
6	AIP ~ B3+RLB+$SD2_{y-2}$	8	-2106.3	4228.7	10.7	0.0	100.0
7	AIP ~ B3+RLB+PR_{y-2}	5	-2109.7	4229.4	11.4	0.0	100.0
8	AIP ~ B3	3	-2112.2	4230.4	12.4	0.0	100.0
9	AIP ~ B3+RLB+T2	5	-2110.6	4231.3	13.3	0.0	100.0
10	AIP ~ S+Y+B3+RLB	8	-2107.8	4231.6	13.6	0.0	100.0
11	AIP ~ B3+RLB+RH1	5	-2110.8	4231.7	13.7	0.0	100.0
12	AIP ~ B3+RLB	4	-2112.1	4232.2	14.2	0.0	100.0
13	AIP ~ B3+RLB+PR_{y-1}	5	-2111.1	4232.3	14.3	0.0	100.0
14	AIP ~ B3+RLB+PR	5	-2111.4	4232.9	14.9	0.0	100.0
15	AIP ~ B3+RLB+RH2	5	-2111.4	4232.9	14.9	0.0	100.0
16	AIP ~ S+Y+RLB+PR	8	-2108.4	4232.9	14.9	0.0	100.0
17	AIP ~ B3+RLB+$T2_{y-2}$	5	-2111.5	4232.9	14.9	0.0	100.0
18	AIP ~ B3+RLB+$RH1_{y-1}$	5	-2111.5	4232.9	14.9	0.0	100.0
19	AIP ~ S+B+PR_{y-2}	8	-2108.5	4233.0	15.0	0.0	100.0
20	AIP ~ B3+RLB+$T2_{y-1}$	5	-2111.7	4233.5	15.5	0.0	100.0
21	AIP ~ B3+RLB+$RH2_{y-1}$	5	-2111.7	4233.5	15.5	0.0	100.0
22	AIP ~ B3+RLB+$SD2_{y-1}$	5	-2111.8	4233.6	15.7	0.0	100.0
23	AIP ~ B3+RLB+SD1	5	-2111.8	4233.7	15.7	0.0	100.0

24	AIP ~ B3+RLB+$RH1_{y-2}$	5	-2111.9	4233.7	15.7	0.0	100.0
25	AIP ~ B3+RLB+$SD1_{y-2}$	5	-2111.9	4233.9	15.9	0.0	100.0
26	AIP ~ B3+RLB+T1	5	-2112.0	4234.1	16.1	0.0	100.0
27	AIP ~ B3+RLB+$T1_{y-2}$	5	-2112.0	4234.1	16.1	0.0	100.0
28	AIP ~ B3+RLB+$T1_{y-1}$	5	-2112.0	4234.1	16.1	0.0	100.0
29	AIP ~ B3+RLB+$SD1_{y-1}$	5	-2112.1	4234.2	16.2	0.0	100.0
30	AIP ~ B3+RLB+SD2	5	-2112.1	4234.2	16.2	0.0	100.0

Table S4. The support for each explanatory variable is shown from the AIC-based model selection table of the adult infection prevalence. This support is calculated as the sum of the Akaike weights for all the models in the set that include that explanatory variable.

Rank	Explanatory variable of interest	Support (%)
1	RLB	99.8
2	$Beech_{y-3}$	99.3
3	$RH2_{y-2}$	95.7
4	Site	20.5
5	Year	1.4
6	$SD2_{y-2}$	1.3
7	T1	< 1.0
8	RH1	< 1.0
9	SD1	< 1.0
10	PR	< 1.0
11	$T1_{y-1}$	< 1.0
12	$RH1_{y-1}$	< 1.0
13	$SD1_{y-1}$	< 1.0
14	PR_{y-1}	< 1.0
15	$T1_{y-2}$	< 1.0
16	$RH1_{y-2}$	< 1.0
17	$SD1_{y-2}$	< 1.0
18	PR_{y-2}	< 1.0
19	T2	< 1.0
20	RH2	< 1.0
21	SD2	< 1.0
22	$T2_{y-1}$	< 1.0
23	$RH2_{y-1}$	< 1.0
24	$SD2_{y-1}$	< 1.0
25	$T2_{y-2}$	< 1.0
26	Site:Year	< 1.0
27	$Site:Beech_{y-3}$	< 1.0
28	Site:RLB	< 1.0
29	Site:T1	< 1.0
30	Site:RH1	< 1.0
31	Site:SD1	< 1.0
32	Site:PR	< 1.0
33	$Site:T1_{y-1}$	< 1.0
34	$Site:RH1_{y-1}$	< 1.0
35	$Site:SD1_{y-1}$	< 1.0
36	$Site:PR_{y-1}$	< 1.0

37	Site:$T1_{y-2}$	< 1.0
38	Site:$RH1_{y-2}$	< 1.0
39	Site:$SD1_{y-2}$	< 1.0
40	Site:PR_{y-2}	< 1.0
41	Site:T2	< 1.0
42	Site:RH2	< 1.0
43	Site:SD2	< 1.0
44	Site:$T2_{y-1}$	< 1.0
45	Site:$RH2_{y-1}$	< 1.0
46	Site:$SD2_{y-1}$	< 1.0
47	Site:$T2_{y-2}$	< 1.0
48	Site:$RH2_{y-2}$	< 1.0
49	Site:$SD2_{y-2}$	< 1.0

Table S5. Model-averaged parameter estimates are shown for the generalized linear mixed effects model with binomial errors of the adult infection prevalence (AIP) response variable. Shown are the parameter types, the parameter names, the parameter estimates, and the 95% confidence limits (LL = lower limit and UL = upper limit). Estimate 1 is averaged over all the models in the set. Estimate 2 is averaged over the subset of models with a cumulative support of 95%. The 95% confidence limits are for estimate 2.

Type	Name	Estimate 1	Estimate 2	95% LL	95% UL
Intercept	Low site	-1.021	-1.021	-1.307	-0.736
Contrast 1	Medium site	0.007	0.033	-0.296	0.362
Contrast 2	High site	0.052	0.255	-0.093	0.604
Contrast 3	Top site	0.058	0.280	-0.147	0.708
Slope 1	Year	-0.001	-0.062	-0.111	-0.013
Slope 2	$Beech_{y-3}$	-0.200	-0.202	-0.280	-0.123
Slope 3	RLB	0.053	0.054	-0.063	0.170
Contrast 4	T1	0.000	0.017	-0.143	0.176
Contrast 5	RH1	0.000	-0.130	-0.291	0.031
Contrast 6	SD1	0.000	0.073	-0.120	0.266
Contrast 7	PR	-0.002	-0.299	-0.510	-0.089
Contrast 8	$T1_{y-1}$	0.000	-0.046	-0.260	0.168
Contrast 9	$RH1_{y-1}$	0.000	-0.088	-0.241	0.064
Contrast 10	$SD1_{y-1}$	0.000	0.000	-0.158	0.158
Contrast 11	PR_{y-1}	0.000	-0.129	-0.303	0.045
Contrast 12	$T1_{y-2}$	0.000	0.024	-0.162	0.209
Contrast 13	$RH1_{y-2}$	0.000	0.081	-0.106	0.267
Contrast 14	$SD1_{y-2}$	0.000	-0.073	-0.277	0.131
Contrast 15	PR_{y-2}	0.001	0.165	0.023	0.307
Contrast 16	Medium site:Year	0.000	0.027	-0.088	0.142
Contrast 17	High site:Year	0.000	-0.007	-0.122	0.109
Contrast 18	Top site:Year	0.000	0.006	-0.125	0.136
Contrast 19	Medium site:$Beech_{y-3}$	0.000	-0.009	-0.244	0.225
Contrast 20	High site:$Beech_{y-3}$	0.000	0.049	-0.188	0.286
Contrast 21	Top site:$Beech_{y-3}$	0.000	-0.017	-0.271	0.238
Contrast 22	Medium site:RLB	0.000	0.075	-0.270	0.420
Contrast 23	High site: RLB	0.000	0.169	-0.145	0.482
Contrast 24	Top site: RLB	0.000	0.134	-0.280	0.547
Contrast 25	Medium site:T1	0.000	0.240	-0.601	1.081
Contrast 26	High site:T1	0.000	0.045	-0.786	0.877
Contrast 27	Top site:T1	0.000	-0.131	-0.988	0.726
Contrast 28	Medium site:RH1	0.000	0.011	-0.534	0.557

Contrast 29	High site:RH1	0.000	0.026	-0.524	0.575
Contrast 30	Top site:RH1	0.000	-0.209	-0.789	0.370
Contrast 31	Medium site:SD1	0.000	0.037	-0.555	0.628
Contrast 32	High site:SD1	0.000	-0.025	-0.650	0.600
Contrast 33	Top site:SD1	0.000	0.239	-0.500	0.979
Contrast 34	Medium site:PR	0.000	0.047	-0.424	0.518
Contrast 35	High site:PR	0.000	0.271	-0.197	0.739
Contrast 36	Top site:PR	0.000	-0.032	-0.526	0.462
Contrast 37	Medium site:T_{y-1}	0.000	0.160	-0.712	1.032
Contrast 38	High site:T_{y-1}	0.000	-0.045	-0.907	0.816
Contrast 39	Top site:T_{y-1}	0.000	-0.074	-0.974	0.825
Contrast 40	Medium site:$RH1_{y-1}$	0.000	0.034	-0.512	0.581
Contrast 41	High site:$RH1_{y-1}$	0.000	-0.041	-0.597	0.515
Contrast 42	Top site:$RH1_{y-1}$	0.000	0.098	-0.514	0.709
Contrast 43	Medium site:$SD1_{y-1}$	0.000	0.036	-0.587	0.660
Contrast 44	High site:$SD1_{y-1}$	0.000	0.148	-0.517	0.813
Contrast 45	Top site:$SD1_{y-1}$	0.000	-0.096	-0.930	0.739
Contrast 46	Medium site:PR_{y-1}	0.000	0.102	-0.348	0.551
Contrast 47	High site:PR_{y-1}	0.000	-0.031	-0.484	0.423
Contrast 48	Top site:PR_{y-1}	0.000	-0.179	-0.676	0.319
Contrast 49	Medium site:$T1_{y-2}$	0.000	0.042	-0.871	0.955
Contrast 50	High site:$T1_{y-2}$	0.000	-0.071	-0.965	0.824
Contrast 51	Top site:$T1_{y-2}$	0.000	-0.056	-0.987	0.874
Contrast 52	Medium site:$RH1_{y-2}$	0.000	0.184	-0.363	0.731
Contrast 53	High site:$RH1_{y-2}$	0.000	0.027	-0.515	0.570
Contrast 54	Top site:$RH1_{y-2}$	0.000	-0.054	-0.633	0.524
Contrast 55	Medium site:$SD1_{y-2}$	0.000	-0.137	-0.809	0.535
Contrast 56	High site:$SD1_{y-2}$	0.000	-0.064	-0.752	0.623
Contrast 57	Top site:$SD1_{y-2}$	0.000	-0.035	-0.810	0.740
Contrast 58	Medium site:PR_{y-2}	0.000	-0.028	-0.453	0.396
Contrast 59	High site:PR_{y-2}	0.000	-0.276	-0.706	0.154
Contrast 60	Top site:PR_{y-2}	0.000	-0.360	-0.834	0.114
Contrast 61	T2	0.000	0.140	-0.037	0.317
Contrast 62	RH2	0.000	0.113	-0.062	0.289
Contrast 63	SD2	0.000	-0.011	-0.182	0.159
Contrast 64	$T2_{y-1}$	0.000	0.058	-0.092	0.208
Contrast 65	$RH2_{y-1}$	0.000	-0.062	-0.222	0.098
Contrast 66	$SD2_{y-1}$	0.000	0.051	-0.102	0.204
Contrast 67	$T2_{y-2}$	0.000	0.080	-0.068	0.227
Contrast 68	$RH2_{y-2}$	-0.298	-0.311	-0.457	-0.165
Contrast 69	$SD2_{y-2}$	0.003	0.231	0.052	0.410

Contrast 70	Medium site:T2	0.000	-0.111	-0.821	0.599
Contrast 71	High site:T2	0.000	-0.033	-0.752	0.686
Contrast 72	Top site:T2	0.000	-0.099	-0.837	0.638
Contrast 73	Medium site:RH2	0.000	-0.040	-0.497	0.417
Contrast 74	High site:RH2	0.000	-0.286	-0.793	0.221
Contrast 75	Top site:RH2	0.000	0.125	-0.444	0.694
Contrast 76	Medium site:SD2	0.000	0.007	-0.517	0.531
Contrast 77	High site:SD2	0.000	0.350	-0.286	0.987
Contrast 78	Top site:SD2	0.000	-0.039	-0.915	0.836
Contrast 79	Medium site:$T2_{y-1}$	0.000	-0.059	-0.741	0.623
Contrast 80	High site:$T2_{y-1}$	0.000	0.093	-0.586	0.772
Contrast 81	Top site:$T2_{y-1}$	0.000	-0.053	-0.763	0.658
Contrast 82	Medium site:$RH2_{y-1}$	0.000	-0.004	-0.489	0.482
Contrast 83	High site:$RH2_{y-1}$	0.000	-0.112	-0.631	0.408
Contrast 84	Top site:$RH2_{y-1}$	0.000	0.300	-0.284	0.885
Contrast 85	Medium site:$SD2_{y-1}$	0.000	-0.016	-0.538	0.505
Contrast 86	High site:$SD2_{y-1}$	0.000	0.187	-0.392	0.766
Contrast 87	Top site:$SD2_{y-1}$	0.000	-0.208	-0.962	0.547
Contrast 88	Medium site:$T2_{y-2}$	0.000	0.101	-0.611	0.813
Contrast 89	High site:$T2_{y-2}$	0.000	0.025	-0.684	0.734
Contrast 90	Top site:$T2_{y-2}$	0.000	-0.112	-0.857	0.634
Contrast 91	Medium site:$RH2_{y-2}$	0.000	0.064	-0.394	0.522
Contrast 92	High site:$RH2_{y-2}$	0.000	0.049	-0.439	0.537
Contrast 93	Top site:$RH2_{y-2}$	0.000	0.275	-0.248	0.798
Contrast 94	Medium site:$SD2_{y-2}$	0.000	0.116	-0.390	0.622
Contrast 95	High site:$SD2_{y-2}$	0.000	0.096	-0.466	0.658
Contrast 96	Top site:$SD2_{y-2}$	0.000	-0.178	-0.855	0.500

Table S6. Model selection results are shown for the linear models with normal errors of the log10-trasnformed density of infected adults (DIA) response variable. The explanatory variables were site, year, beech masting index 3 years prior, RLB time lag, and the climate variables obtained from the weather stations and collected from the field. The models are ranked according to their Akaike Information Criterion (AIC). Shown for each model are the model rank (Rank), model structure (see below for explanation of explanatory variables), model degrees of freedom (Df), log-likelihood (logLik), Akaike information criterion (AIC), difference in the AIC value from the top model (ΔAIC), model weight (Weight1), and cumulative weight (Weight2), and adjusted r-squared (r^2).

Rank	Model structure	Df	logLik	AIC	ΔAIC	Weight1	Weight2	r^2
1	DIA ~ S+Y+RLB+$RH2_{y-2}$+S:Y	11	5.1	18.5	0.0	35.0	35.0	62.7
2	DIA ~ S+Y+B3+$RH2_{y-2}$+S:Y	11	4.4	19.8	1.3	18.0	53.0	61.8
3	DIA ~ S+RLB+$RH2_{y-2}$	7	-2.3	21.2	2.7	9.0	62.0	54.7
4	DIA ~ S+Y+B3+T2+S:Y	11	2.6	23.4	5.0	3.0	65.0	58.9
5	DIA ~ S+Y+RLB+$RH2_{y-2}$	8	-2.1	23.5	5.1	3.0	68.0	54.1
6	DIA ~ S+Y+RLB+$RH2_{y-2}$	8	-2.1	23.5	5.1	3.0	71.0	54.1
7	DIA ~ S+Y+RLB+T2+S:Y	11	2.5	23.6	5.1	3.0	74.0	58.8
8	DIA ~ S+B3+RLB+$RH2_{y-2}$	8	-2.2	23.7	5.3	2.0	76.0	53.9
9	DIA ~ S+Y+B3+$RH2_{y-2}$	8	-2.2	23.8	5.4	2.0	78.0	53.9
10	DIA ~ S+Y+B3+$SD2_{y-2}$+S:Y	11	1.9	24.8	6.3	1.0	79.0	57.9
11	DIA ~ S+Y+RLB+$SD2_{y-2}$+S:Y	11	1.5	25.6	7.1	1.0	80.0	57.2
12	DIA ~ S+Y+B3+RH1+S:Y	11	1.5	25.7	7.2	1.0	81.0	57.1
13	DIA ~ S+$RH2_{y-2}$	9	-1.8	25.8	7.4	1.0	82.0	53.7
14	DIA ~ S+Y+S:Y	9	-1.9	26.1	7.7	1.0	83.0	53.4
15	DIA ~ S+Y+B3+SD2+S:Y	11	1.1	26.3	7.9	1.0	84.0	56.6
16	DIA ~ S+RLB+$RH2_{y-2}$	10	-0.6	26.5	8.0	1.0	85.0	54.8
17	DIA ~ S+Y+B3+RH1	8	-3.7	26.8	8.3	1.0	86.0	51.2
18	DIA ~ S+Y+B3+T2	8	-3.7	26.8	8.3	1.0	87.0	51.2
19	DIA ~ S+Y+B3+S:Y	10	-0.8	27.1	8.6	0.0	100.0	54.3
20	DIA ~ S+RLB+$SD2_{y-2}$	10	-0.8	27.1	8.6	0.0	100.0	54.3
21	DIA ~ S+Y+RLB+T2	7	-5.3	27.2	8.8	0.0	100.0	49.2
22	DIA ~ S+Y+RLB+$SD1_{y-2}$+S:Y	8	-3.9	27.2	8.8	0.0	100.0	50.8
23	DIA ~ S+B3+$RH2_{y-2}$+S:$RH2_{y-2}$	11	0.6	27.3	8.9	0.0	100.0	55.8
24	DIA ~ S+Y+B3+S:Y+$RH2_{y-1}$	10	-1.1	27.5	9.1	0.0	100.0	53.8
25	DIA ~ S+Y+RLB+SD2+S:Y	11	0.5	27.5	9.1	0.0	100.0	55.6
26	DIA ~ S+Y+B3+$SD1_{y-2}$+S:Y	11	0.5	27.6	9.1	0.0	100.0	55.6
27	DIA ~ S+Y+B3+SD1+S:Y	11	0.5	27.6	9.1	0.0	100.0	55.5
28	DIA ~ S+Y+RLB+$RH1_{y-2}$+S:Y	11	0.5	27.6	9.2	0.0	100.0	55.5
29	DIA ~ S+Y+B3+SD2	11	0.4	27.8	9.4	0.0	100.0	55.3

30	DIA ~ S+Y+B3+S:Y+$SD2_{y-1}$	8	-4.3	28.0	9.5	0.0	100.0	50.0

Table S7. The support for each explanatory variable is shown from the AIC-based model selection table of the density of infected adults. This support is calculated as the sum of the Akaike weights for all the models in the set that include that explanatory variable.

Rank	Explanatory variable of interest	Support (%)
1	Site	99.9
2	Year	85.4
3	$RH2_{y-2}$	74.0
4	Site:Year	69.6
5	RLB	63.8
6	$Beech_{y-3}$	37.3
7	T2	7.0
8	$SD2_{y-2}$	3.7
9	Site:$RH2_{y-2}$	1.9
10	RH1	1.9
11	SD2	1.7
12	$SD1_{y-2}$	1.3
13	PR_{y-1}	< 1.0
14	SD1	< 1.0
15	$T1_{y-1}$	< 1.0
16	PR	< 1.0
17	T1	< 1.0
18	$RH1_{y-1}$	< 1.0
19	$SD1_{y-1}$	< 1.0
20	$T1_{y-2}$	< 1.0
21	$RH1_{y-2}$	< 1.0
22	PR_{y-2}	< 1.0
23	RH2	< 1.0
24	$T2_{y-1}$	< 1.0
25	$RH2_{y-1}$	< 1.0
26	$SD2_{y-1}$	< 1.0
27	$T2_{y-2}$	< 1.0
28	Site:$Beech_{y-3}$	< 1.0
29	Site:RLB	< 1.0
30	Site:T1	< 1.0
31	Site:RH1	< 1.0
32	Site:SD1	< 1.0
33	Site:PR	< 1.0
34	Site:$T1_{y-1}$	< 1.0
35	Site:$RH1_{y-1}$	< 1.0
36	Site:$SD1_{y-1}$	< 1.0

37	Site:PR_{y-1}	< 1.0
38	Site:$T1_{y-2}$	< 1.0
39	Site:$RH1_{y-2}$	< 1.0
40	Site:$SD1_{y-2}$	< 1.0
41	Site:PR_{y-2}	< 1.0
42	Site:T2	< 1.0
43	Site:RH2	< 1.0
44	Site:SD2	< 1.0
45	Site:$T2_{y-1}$	< 1.0
46	Site:$RH2_{y-1}$	< 1.0
47	Site:$SD2_{y-1}$	< 1.0
48	Site:$T2_{y-2}$	< 1.0
49	Site:$SD2_{y-2}$	< 1.0

Table S8. Model-averaged parameter estimates are shown for the linear model with normal errors of the density of infected adults (DIA) response variable. Shown are the parameter types, the parameter names, the parameter estimates, and the 95% confidence limits (LL = lower limit and UL = upper limit). Estimate 1 is averaged over all the models in the set. Estimate 2 is averaged over the subset of models with a cumulative support of 95%. The 95% confidence limits are for estimate 2.

Type	Name	Estimate 1	Estimate 2	95% LL	95% UL
Intercept	Low site	2.474	2.474	1.964	2.983
Contrast 1	Medium site	0.381	0.381	-0.078	0.841
Contrast 2	High site	0.544	0.544	-0.122	1.210
Contrast 3	Top site	0.243	0.243	-0.594	1.080
Slope 1	Year	0.015	0.017	-0.038	0.072
Slope 2	$Beech_{y-3}$	0.008	0.021	-0.025	0.068
Slope 3	RLB	0.030	0.047	-0.054	0.148
Contrast 4	T1	0.000	-0.032	-0.274	0.209
Contrast 5	RH1	-0.002	-0.092	-0.196	0.012
Contrast 6	SD1	0.001	0.094	-0.054	0.243
Contrast 7	PR	0.000	-0.034	-0.139	0.070
Contrast 8	$T1_{y-1}$	0.000	-0.005	-0.203	0.193
Contrast 9	$RH1_{y-1}$	0.000	-0.017	-0.122	0.087
Contrast 10	$SD1_{y-1}$	0.000	0.037	-0.100	0.174
Contrast 11	PR_{y-1}	0.000	-0.026	-0.117	0.066
Contrast 12	$T1_{y-2}$	0.000	0.077	-0.114	0.267
Contrast 13	$RH1_{y-2}$	-0.001	-0.073	-0.196	0.050
Contrast 14	$SD1_{y-2}$	0.001	0.109	-0.031	0.248
Contrast 15	PR_{y-2}	0.000	-0.030	-0.119	0.060
Contrast 16	Medium site:Year	-0.008	-0.011	-0.064	0.042
Contrast 17	High site:Year	-0.040	-0.058	-0.111	-0.004
Contrast 18	Top site:Year	-0.055	-0.079	-0.133	-0.026
Contrast 19	Medium site:$Beech_{y-3}$	0.000	0.005	-0.129	0.139
Contrast 20	High site:$Beech_{y-3}$	0.000	-0.055	-0.191	0.080
Contrast 21	Top site:$Beech_{y-3}$	0.000	-0.052	-0.189	0.085
Contrast 22	Medium site:RLB	0.000	-0.102	-0.322	0.118
Contrast 23	High site: RLB	0.000	-0.112	-0.331	0.106
Contrast 24	Top site: RLB	0.000	0.142	-0.078	0.362
Contrast 25	Medium site:T1	0.000	0.125	-0.331	0.581
Contrast 26	High site:T1	0.000	-0.066	-0.514	0.381
Contrast 27	Top site:T1	0.000	-0.428	-0.867	0.011
Contrast 28	Medium site:RH1	0.000	0.052	-0.266	0.371

Contrast 29	High site:RH1	0.000	-0.043	-0.359	0.274
Contrast 30	Top site:RH1	0.000	0.080	-0.228	0.387
Contrast 31	Medium site:SD1	0.000	-0.018	-0.368	0.332
Contrast 32	High site:SD1	0.000	0.003	-0.361	0.368
Contrast 33	Top site:SD1	0.000	-0.200	-0.580	0.180
Contrast 34	Medium site:PR	0.000	0.074	-0.191	0.338
Contrast 35	High site:PR	0.000	0.143	-0.120	0.406
Contrast 36	Top site:PR	0.000	0.157	-0.103	0.417
Contrast 37	Medium site:T_{y-1}	0.000	-0.045	-0.552	0.463
Contrast 38	High site:T_{y-1}	0.000	-0.186	-0.682	0.310
Contrast 39	Top site:T_{y-1}	0.000	-0.307	-0.791	0.178
Contrast 40	Medium site:$RH1_{y-1}$	0.000	0.036	-0.293	0.366
Contrast 41	High site:$RH1_{y-1}$	0.000	-0.003	-0.331	0.324
Contrast 42	Top site:$RH1_{y-1}$	0.000	-0.002	-0.321	0.316
Contrast 43	Medium site:$SD1_{y-1}$	0.000	-0.031	-0.403	0.341
Contrast 44	High site:$SD1_{y-1}$	0.000	-0.088	-0.474	0.297
Contrast 45	Top site:$SD1_{y-1}$	0.000	-0.169	-0.568	0.229
Contrast 46	Medium site:PR_{y-1}	0.000	-0.011	-0.280	0.258
Contrast 47	High site:PR_{y-1}	0.000	-0.063	-0.332	0.205
Contrast 48	Top site:PR_{y-1}	0.000	-0.040	-0.306	0.225
Contrast 49	Medium site:$T1_{y-2}$	0.000	-0.203	-0.708	0.302
Contrast 50	High site:$T1_{y-2}$	0.000	-0.317	-0.808	0.175
Contrast 51	Top site:$T1_{y-2}$	0.000	-0.440	-0.919	0.039
Contrast 52	Medium site:$RH1_{y-2}$	0.000	0.106	-0.243	0.455
Contrast 53	High site:$RH1_{y-2}$	0.000	0.112	-0.229	0.454
Contrast 54	Top site:$RH1_{y-2}$	0.000	0.033	-0.293	0.360
Contrast 55	Medium site:$SD1_{y-2}$	0.000	-0.138	-0.535	0.260
Contrast 56	High site:$SD1_{y-2}$	0.000	-0.190	-0.597	0.216
Contrast 57	Top site:$SD1_{y-2}$	0.000	-0.255	-0.665	0.156
Contrast 58	Medium site:PR_{y-2}	0.000	0.055	-0.211	0.321
Contrast 59	High site:PR_{y-2}	0.000	-0.012	-0.280	0.255
Contrast 60	Top site:PR_{y-2}	0.000	-0.054	-0.322	0.214
Contrast 61	T2	0.011	0.152	0.020	0.284
Contrast 62	RH2	0.000	-0.052	-0.158	0.054
Contrast 63	SD2	0.002	0.101	-0.021	0.224
Contrast 64	$T2_{y-1}$	0.000	0.063	-0.059	0.184
Contrast 65	$RH2_{y-1}$	-0.001	-0.059	-0.172	0.054
Contrast 66	$SD2_{y-1}$	0.000	0.064	-0.063	0.190
Contrast 67	$T2_{y-2}$	0.000	0.056	-0.080	0.193
Contrast 68	$RH2_{y-2}$	-0.128	-0.173	-0.289	-0.057
Contrast 69	$SD2_{y-2}$	0.006	0.147	0.002	0.292

Contrast 70	Medium site:T2	0.000	0.006	-0.366	0.377
Contrast 71	High site:T2	0.000	-0.038	-0.414	0.338
Contrast 72	Top site:T2	0.000	-0.379	-0.754	-0.005
Contrast 73	Medium site:RH2	0.000	-0.087	-0.338	0.163
Contrast 74	High site:RH2	0.000	-0.140	-0.422	0.141
Contrast 75	Top site:RH2	0.000	0.205	-0.079	0.489
Contrast 76	Medium site:SD2	0.000	0.096	-0.191	0.383
Contrast 77	High site:SD2	0.000	0.232	-0.120	0.584
Contrast 78	Top site:SD2	0.000	-0.238	-0.657	0.182
Contrast 79	Medium site:$T2_{y-1}$	0.000	0.117	-0.274	0.508
Contrast 80	High site:$T2_{y-1}$	0.000	0.177	-0.211	0.564
Contrast 81	Top site:$T2_{y-1}$	0.000	0.093	-0.297	0.483
Contrast 82	Medium site:$RH2_{y-1}$	0.000	-0.115	-0.362	0.132
Contrast 83	High site:$RH2_{y-1}$	0.000	-0.158	-0.424	0.108
Contrast 84	Top site:$RH2_{y-1}$	0.000	0.180	-0.094	0.454
Contrast 85	Medium site:$SD2_{y-1}$	0.000	0.157	-0.125	0.439
Contrast 86	High site:$SD2_{y-1}$	0.000	0.263	-0.054	0.581
Contrast 87	Top site:$SD2_{y-1}$	0.000	-0.030	-0.406	0.347
Contrast 88	Medium site:$T2_{y-2}$	0.000	-0.100	-0.512	0.311
Contrast 89	High site:$T2_{y-2}$	0.000	-0.064	-0.471	0.343
Contrast 90	Top site:$T2_{y-2}$	0.000	-0.032	-0.441	0.377
Contrast 91	Medium site:$RH2_{y-2}$	0.000	-0.011	-0.245	0.223
Contrast 92	High site:$RH2_{y-2}$	-0.002	-0.117	-0.366	0.132
Contrast 93	Top site:$RH2_{y-2}$	0.002	0.103	-0.152	0.358
Contrast 94	Medium site:$SD2_{y-2}$	0.000	0.014	-0.263	0.291
Contrast 95	High site:$SD2_{y-2}$	0.000	0.167	-0.139	0.474
Contrast 96	Top site:$SD2_{y-2}$	0.000	0.034	-0.317	0.385

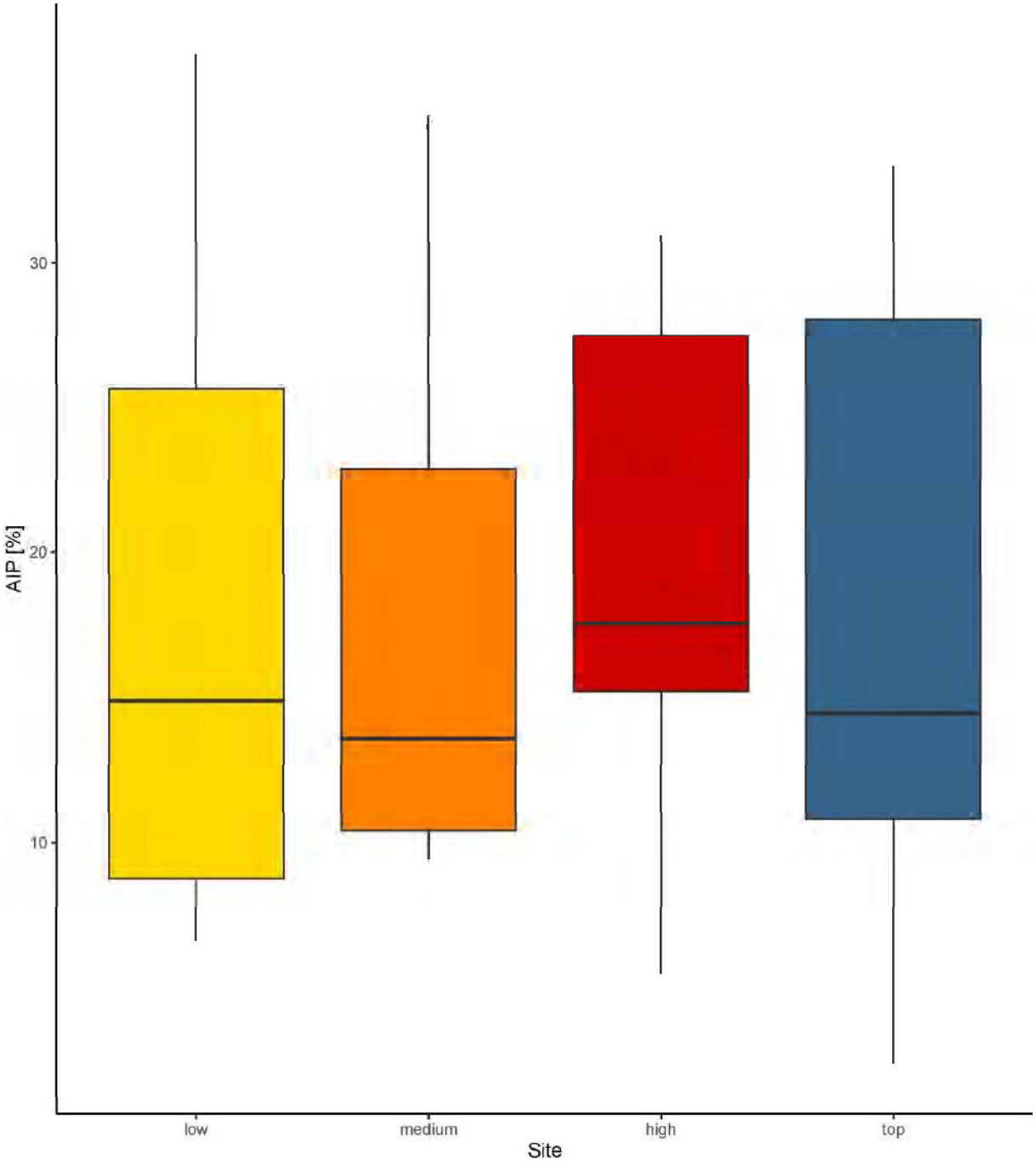

Figure S2. Effect of elevation on the adult infection prevalence (AIP), which is the percentage of *I. ricinus* nymphs infected with *B. burgdorferi* sl. For each of the four elevation sites, the mean NIP for the 15 years of the study is shown (2004–2018). Compared to the low elevation site, the AIP was 2.6% and 23.3% lower at the medium and top elevation sites, but 21.1% higher at the high elevation site. The boxplots show the median (black line), 25th and 75th percentiles (edges of the box), minimum and maximum values (whiskers), and outliers (solid circles).

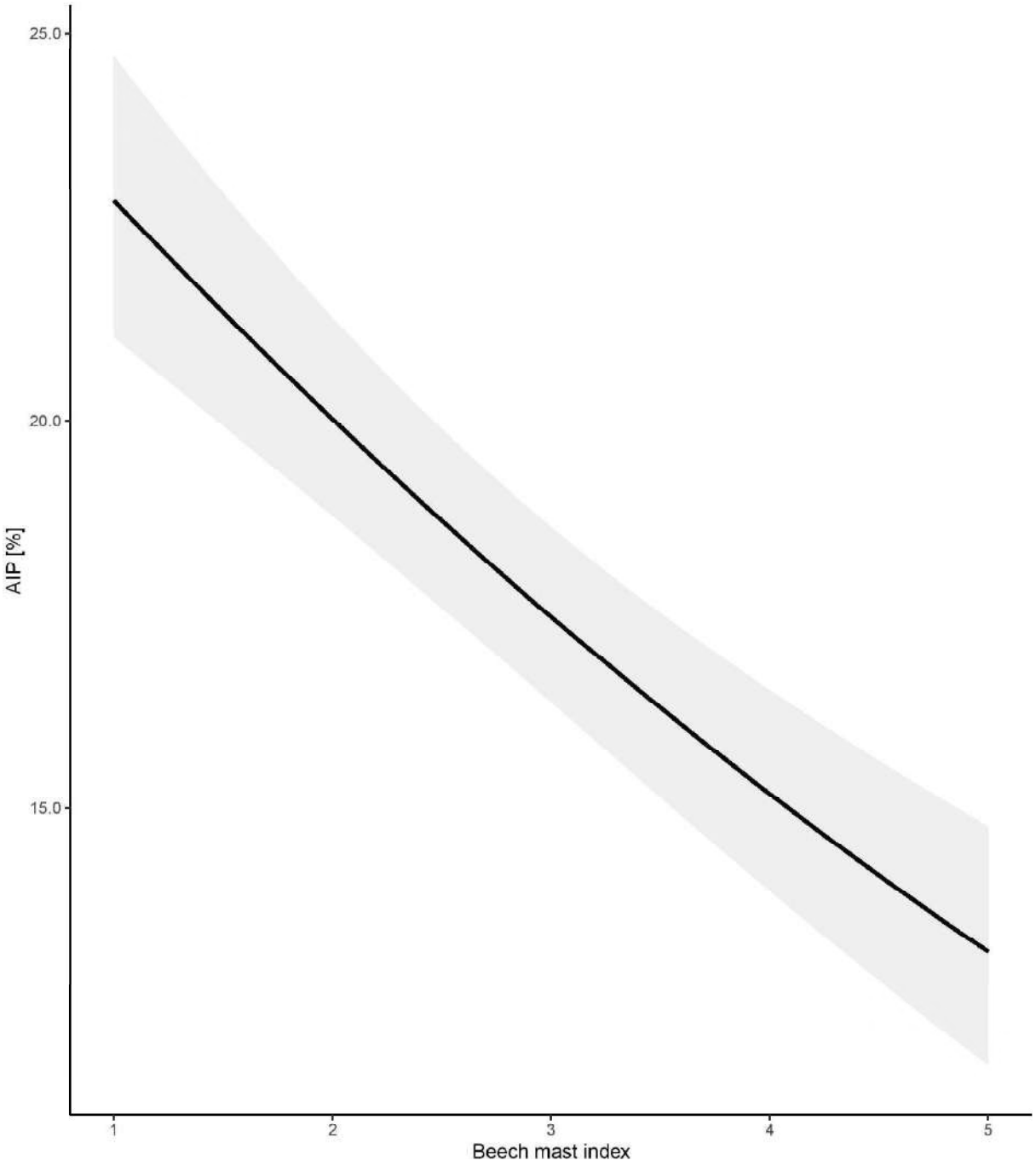

Figure S3. Effect of beech mast score 3 years prior on the adult infection prevalence (AIP), which is the the percentage of *I. ricinus* adults infected with *B. burgdorferi* sl. The beech tree mast score 3 years prior ranges from 1 (poor mast) to 5 (full mast) and was obtained from the MASTREE database.The parameter estimates used to calculate the effect sizes were taken from the model-averaged parameter estimates in Table S5 Increasing the beech mast score from 1 (poor mast) to 5 (full mast) decreased the AIP by 34.9% to 48.9% at the four elevation sites.

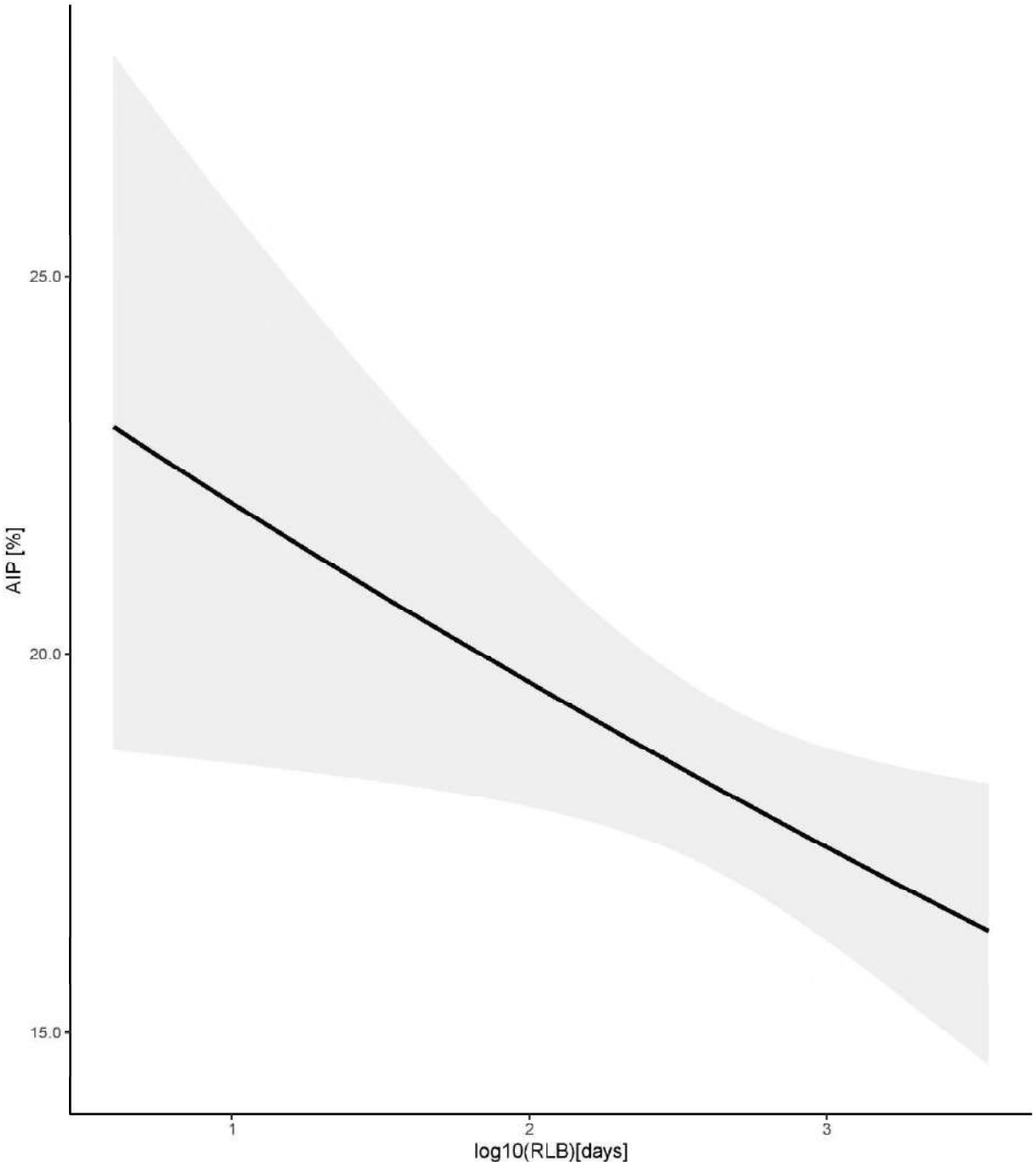

Figure S4. Effect of the reverse line blot (RLB) time lag on the adult infection prevalence (AIP), which is the percentage of *I. ricinus* adults infected with *B. burgdorferi* sl. The RLB time lag is the time interval between the date of collecting the ticks in the field and the date of testing the tick infection status using the RLB.. The parameter estimates used to calculate the effect sizes were taken from the model-averaged parameter estimates in Table S5. Increasing the RLB time lag by one standard deviation (e.g. 925 days) increased the AIP by 4.2% to 28.1% at the four elevation sites.

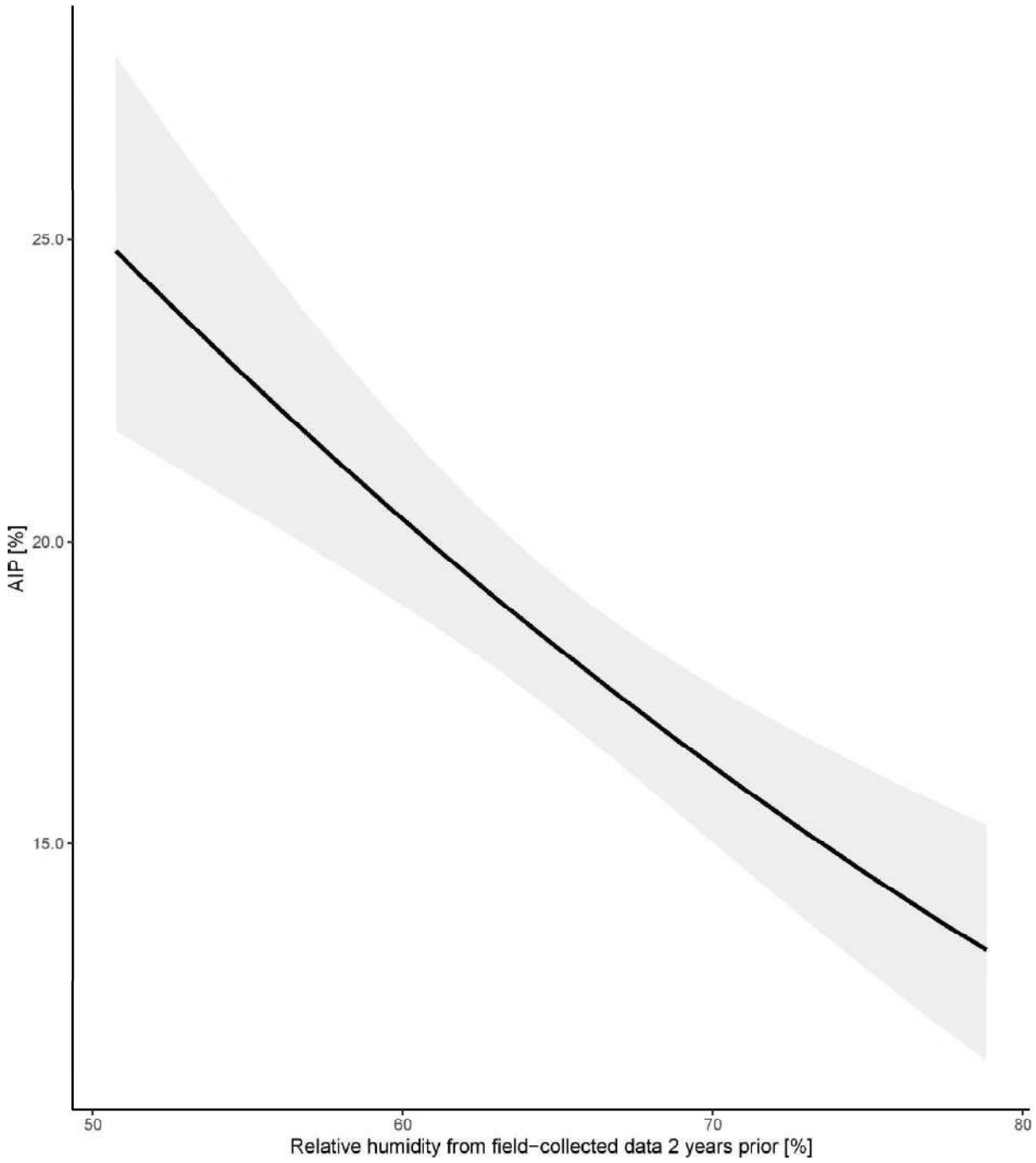

Figure S5. Effect of the mean annual field-collected relative humidity 2 years prior on the adult infection prevalence (AIP), which is the percentage of *I. ricinus* adults infected with *B. burgdorferi* sl. The mean annual relative humidity has units of % and was measured at 50 cm above ground on the day of sampling at the field site. The parameter estimates used to calculate the effect sizes were taken from the model-averaged parameter estimates in Table S5. Increasing the relative humidity 2 years prior by one standard deviation (e.g. 7.1% of relative humidity) decreased AIP by 2.4% to 22.0% at the four elevation sites.

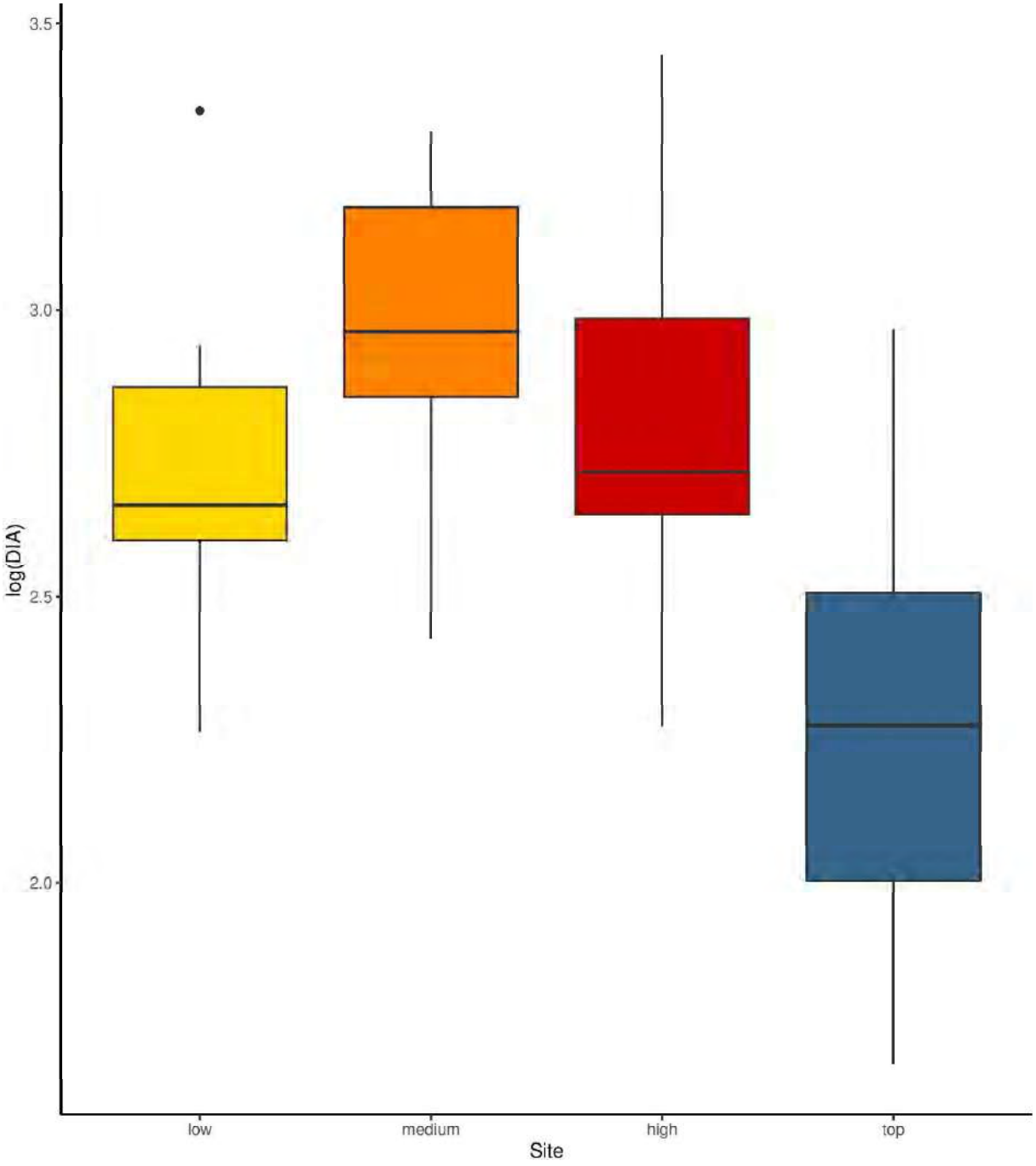

Figure S6. Effect of elevation on the density of infected adult (DIA). The DIA is an estimate of the number of infected questing *I. ricinus* nymphs per 100 m^2 sampled by the dragging method each year. For each of the four elevation sites, the mean DIA for the 15 years of the study is shown (2004–2018). Compared to the low elevation site, the mean DIA at the medium, high, and top elevation sites were 134.5%, 206.6%, and 45.8% lower, respectively. The boxplots show the median (black line), 25th and 75th percentiles (edges of the box), minimum and maximum values (whiskers), and outliers (solid circles).

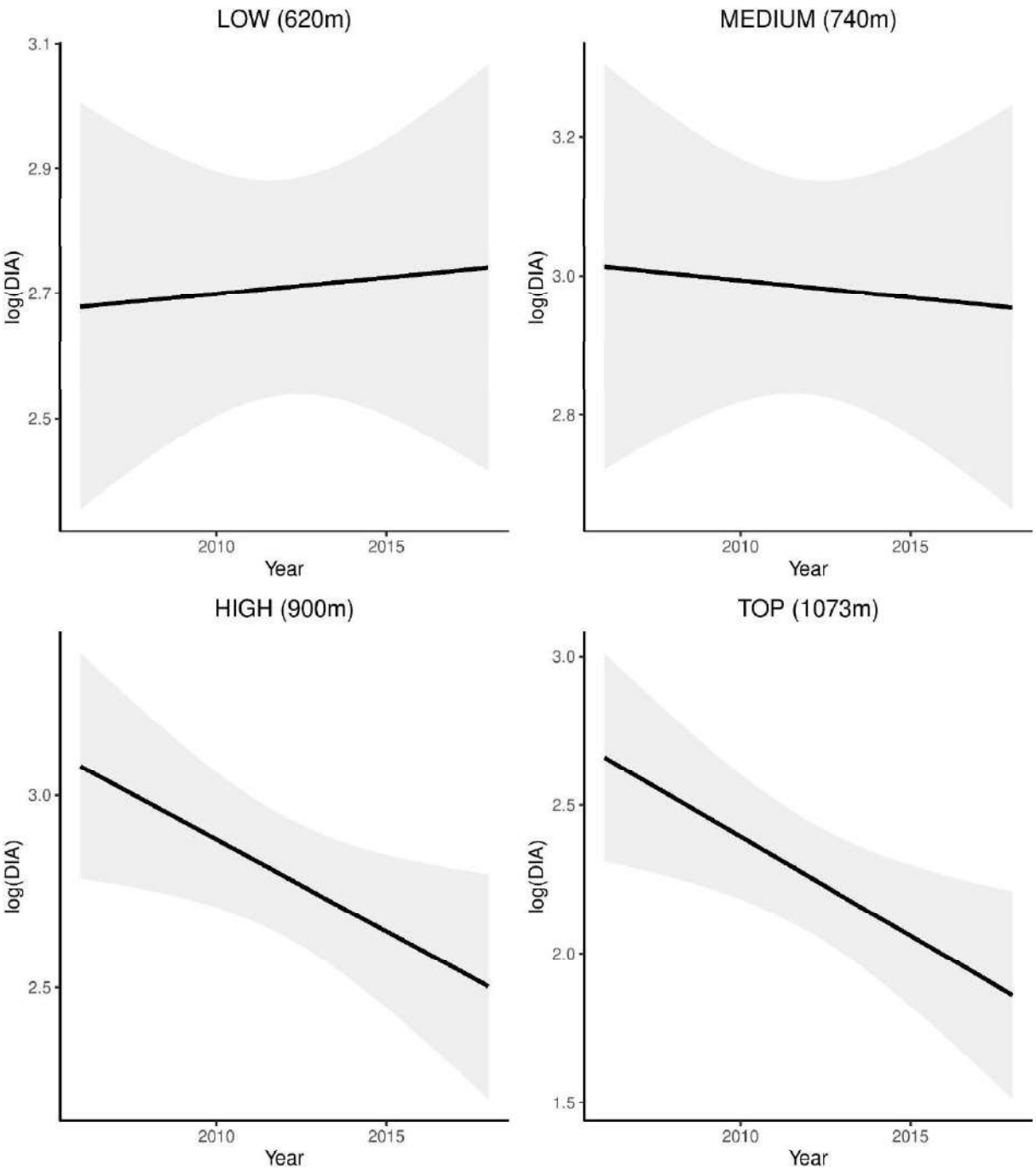

Figure S7. Effect of year on the density of infected adults (DIA). The DIA is an estimate of the number of infected questing *I. ricinus* adults per 100 m^2 sampled by the dragging method each year. The parameter estimates used to calculate the effect sizes were taken from the model-averaged parameter estimates in Table S8. The DIA increased by 60.1% at the low elevation site, but decreased by 17.1%, 67.5%, and 82.1% at the medium, high, and top elevation sites, respectively, over the 13-year study period.

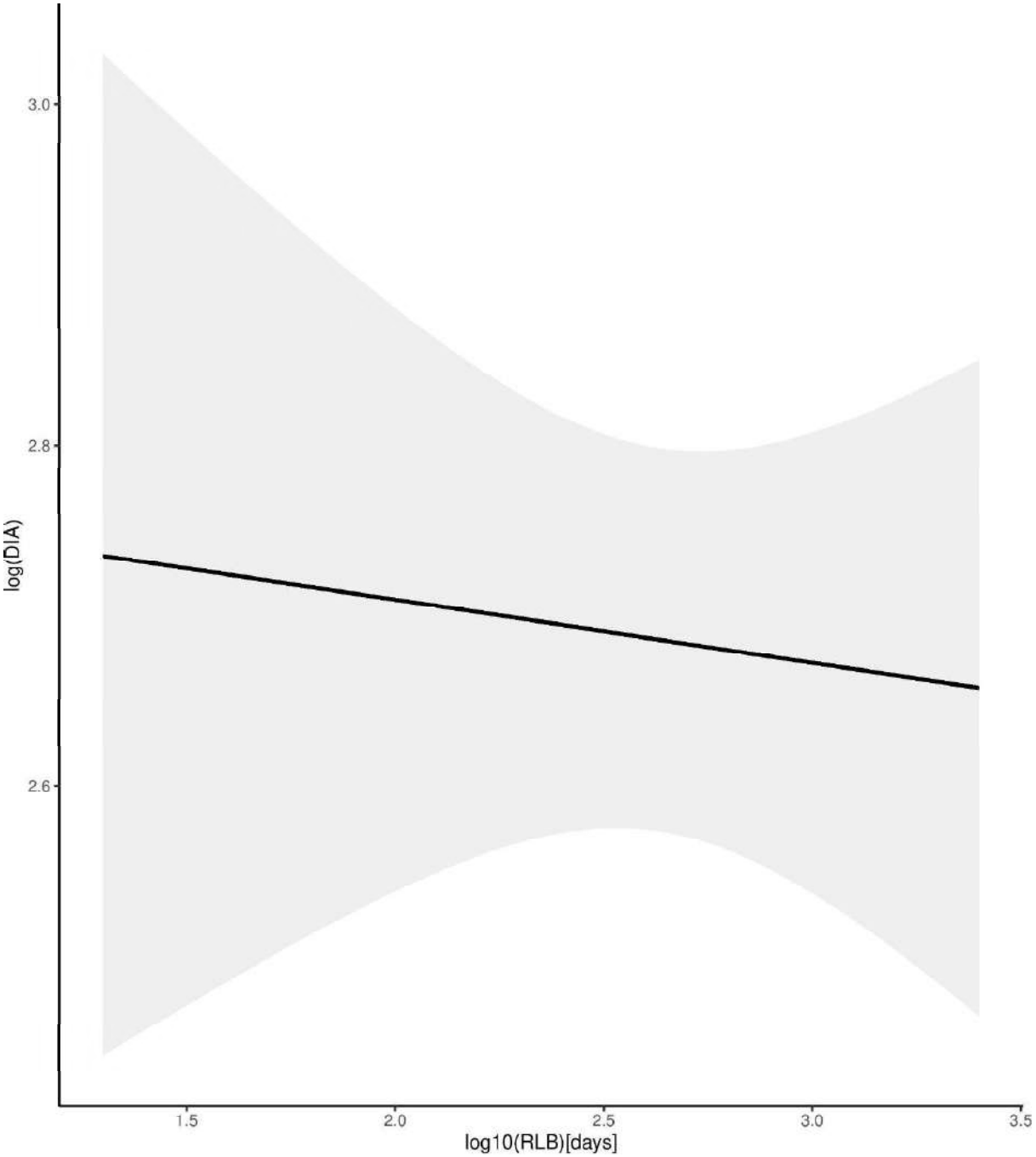

Figure S8. Effect of the reverse line blot (RLB) time lag on the density of infected adults (DIA), which is an estimate of the number of infected questing *I. ricinus* adults per 100 m^2 sampled by the dragging method each year. The RLB time lag is the time interval between the date of collecting the ticks in the field and the date of testing the tick infection status using the RLB. The parameter estimates used to calculate the effect sizes were taken from the model-averaged parameter estimates in Table S8. Increasing the RLB time lag by one standard deviation (e.g. 925 days) increased the DIA by 11.4% at each of the four elevation sites.

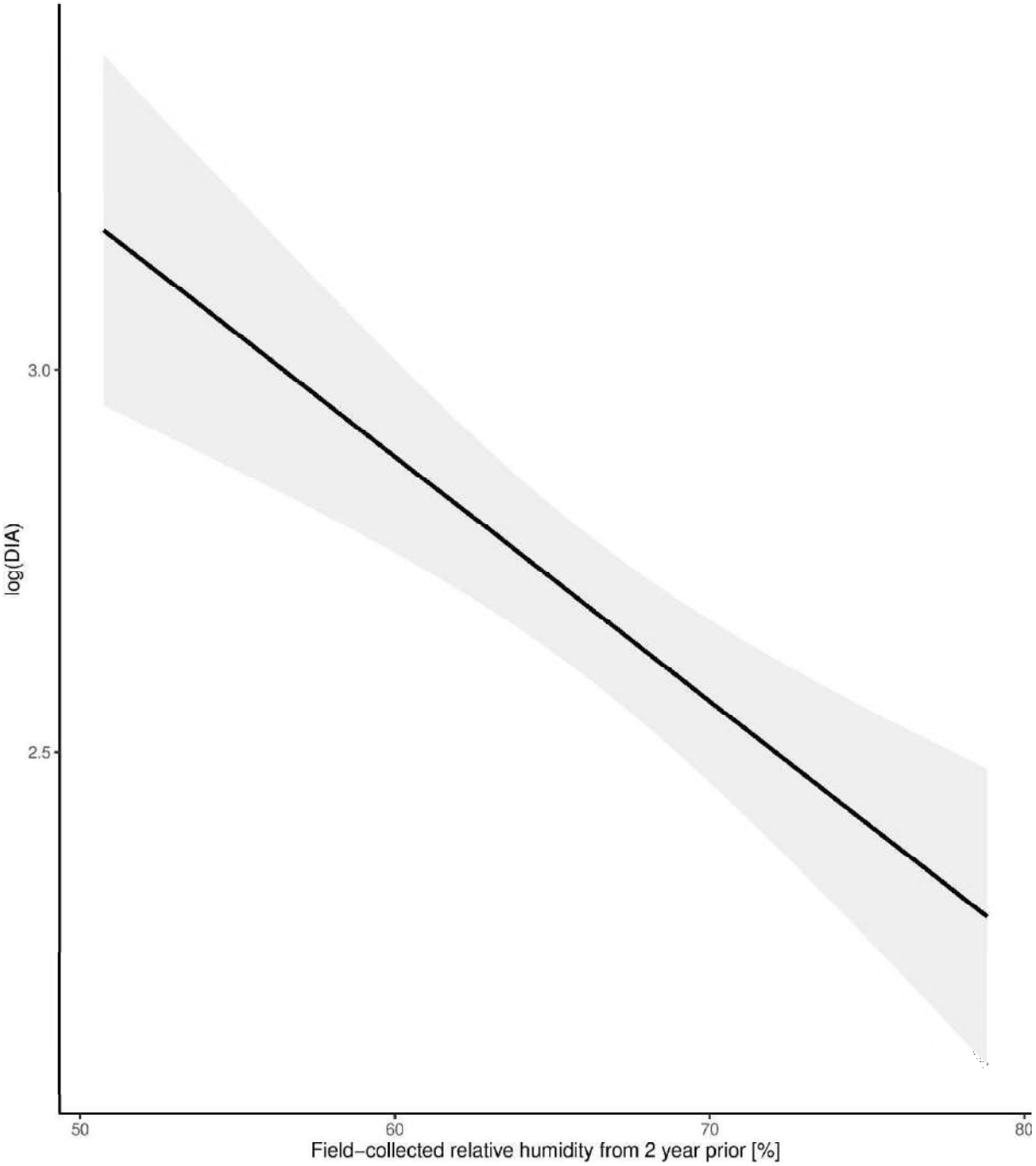

Figure S9. Effect of the field-collected relative humidity 2 years prior on the density of infected adults (DIA). The DIA is an estimate of the number of infected questing *I. ricinus* adults per 100 m^2 sampled by the dragging method each year. The mean annual relative humidity has units of % and was measured at 50 cm above ground on the day of sampling at the field site. The parameter estimates used to calculate the effect sizes were taken from the model-averaged parameter estimates in Table S8. Increasing mean annual relative humidity 2 years prior by one standard deviation (e.g. 7.0% of relative humidity) decreased the DIA by 32.9% at each of the four elevation sites.

SECTION 5 – Full statistical analysis of the nymphal infection prevalence (NIP) for the restricted 13-year period of the study (2006 – 2018)

Model selection approach: To identify the best model, we used a model selection approach based on the Akaike information criterion (AIC). A big conceptual advantage of model selection is that it reminds the user that there are competing models with different parameter estimates and that some of these models have more support (i.e., are better at explaining the data) than other models. Another advantage is that you can compare non-nested models containing different explanatory variables, which is not possible with a more traditional approach like stepwise multiple regression. Models were ranked according to their AIC values and the Akaike weights, which indicate the percent support, were calculated for each model. We used the Akaike weights to calculate the model-averaged parameter estimates and their 95% confidence intervals (CIs). For the generalized linear mixed effects models that analysed the NIP and AIP, we assessed the goodness of fit of the binomial distribution for the best model from the model selection table. Similarly, for the linear models that analysed the DIN and DIA, the assumptions of normally distributed residuals and equal variances were assessed for the best model from the model selection table (Additional file 1: Section 3). We used R version 4.0.3 for all statistical analyses (Team 2013). We used the lm() function in the base package to run the LMs with normal errors. We used the glmer() functions in the lme4 package to run the GLMMs with binomial errors. We used the mod.sel() function and the model.av() function in the MuMIn package to create the model selection tables and the model-averaged parameter estimates.

Model selection analysis of the NIP: The model selection table for the 30 best out of 232 models is presented in Table S9. For the NIP, the best two models had a combined support of 94.0% (Table S9). These two models each had 47.0% of the support (Table S9) and contained the explanatory variables year, RLB time lag, and weather station mean annual precipitation in the present year (e.g. no time lag). The only difference between these two models was that the second model contained elevation site, whereas the first model did not (Table S9).

For the individual explanatory variables, there was strong support for RLB time lag (100.0%), year (100.0%), and weather station mean annual precipitation in the present year (93.8%), moderate support for site (48.2%), and low support for weather station mean annual relative humidity in the present year (5.7%; Table S10). None of the other explanatory variables had a support > 1.0% (Table S10).

Model-averaged parameter estimates for the NIP: To determine the direction and statistical significance of the explanatory variables on the NIP, we present the model-averaged parameter estimates (and their 95% confidence intervals) on the logit scale (Table S11). We also back-calculated the effect sizes of the explanatory variables on the NIP on the original scale with respect to the following baseline: the site was low elevation, the year was 2006, and the covariates of RLB time lag and weather station precipitation in the present year were set to 0 (i.e., the mean values on the z-score scale).

The NIP was significantly different between the four elevation sites (Table S11). Compared to the low elevation site, the NIP was 13.4% lower at the medium (Medium – Low contrast = -0.195, 95% CI = -0.467 – 0.077), 23.6% lower at the high (High – Low contrast = -0.358, 95% CI = -0.653 – -0.063), and 9.4% lower at the top (Top – Low contrast = -0.135, 95% CI = -0.481 – 0.211) elevation sites.

Year had a negative and significant effect (slope = -0.145 per year, 95% CI = -0.181 – -0.108), indicating that the NIP was decreasing over time at Chaumont Mountain (Table S11). Over the 13-year period of the study (2006 – 2018), the NIP on the original scale decreased by 77.1% to 78.6% at the four elevation sites (Table S11).

The RLB time lag had a negative and significant effect on the NIP (Table S11; slope = -0.184 per standard deviation, 95% CI = -0.285 – -0.083). Increasing the RLB time lag by one standard deviation (e.g., 881 days) decreased the NIP on the original scale by 12.6% to 13.6% at the four elevation sites (Table S11).

The weather station mean annual precipitation in the present year had a negative and significant effect on the NIP (Table S11; slope = -0.311 per standard deviation, 95% CI = -0.447 – -0.174). Increasing the weather station mean annual precipitation in the present year by one standard deviation (e.g., 0.5 mm of precipitation) decreased the NIP on the original scale by 22.4% to 24.0% at the four elevation sites (Table S11).

In summary, the explanatory variables of year, RLB time lag, and precipitation in the same year all had significant negative effects on the NIP.

Table S9. Model selection results are shown for the generalized linear mixed effects model with binomial errors of the nymphal infection prevalence (NIP) response variable. The explanatory variables were site, year, beech masting index 2 years prior, RLB time lag, and the climate variables obtained from the weather stations and collected from the field. The models are ranked according to their Akaike Information Criterion (AIC). Shown for each model are the model rank (Rank), model structure (see below for explanation of explanatory variables), model degrees of freedom (Df), log-likelihood (logLik), Akaike information criterion (AIC), difference in the AIC value from the top model (ΔAIC), model weight (Weight1), and cumulative weight (Weight2).

Rank	Model structure	Df	logLik	AIC	ΔAIC	Weight1	Weight2
1	NIP ~ Y+RLB+PR	5	-2360.1	4736.2	0.0	47.0	47.0
2	NIP ~ S+Y+RLB+PR	8	-2363.1	4736.2	0.0	47.0	94.0
3	NIP ~ Y+RLB+RH1	5	-2365.4	4740.8	4.6	5.0	99.0
4	NIP ~ S+Y+RLB+RH1	8	-2363.9	4743.8	7.6	1.0	100.0
5	NIP ~ Y+RLB+SD1	5	-2368.3	4746.5	10.3	0.0	100.0
6	NIP ~ S+Y+RLB+SD1	8	-2366.8	4749.5	13.3	0.0	100.0
7	NIP ~ S+Y+RLB+RH2	8	-2367.7	4751.5	15.3	0.0	100.0
8	NIP ~ Y+RLB+$T2_{y-1}$	8	-2368.0	4752.1	15.9	0.0	100.0
9	NIP ~ Y+RLB+$T1_{y-2}$	5	-2371.1	4752.2	16.0	0.0	100.0
10	NIP ~ S+Y+RLB+$SD2_{y-1}$	8	-2368.5	4753.1	16.9	0.0	100.0
11	NIP ~ S+Y+RLB+PRy-1	8	-2368.6	4753.3	17.1	0.0	100.0
12	NIP ~ Y+DINy-1+RLB	5	-2371.9	4753.8	17.6	0.0	100.0
13	NIP ~ Y+RLB+PRy-1	5	-2371.9	4753.9	17.7	0.0	100.0
14	NIP ~ Y+RLB+T1	5	-2371.9	4753.9	17.7	0.0	100.0
15	NIP ~ Y+RLB+T2	5	-2372.0	4754.1	17.9	0.0	100.0
16	NIP ~ S+Y+RLB	7	-2370.2	4754.4	18.2	0.0	100.0
17	NIP ~ S+Y+RLB+RH1y-2	8	-2369.6	4755.2	19.0	0.0	100.0
18	NIP ~ S+Y+RLB+T1y-1	8	-2369.6	4755.3	19.1	0.0	100.0
19	NIP ~ S+Y+RLB+T1y-2	8	-2369.7	4755.3	19.1	0.0	100.0
20	NIP ~ S+Y+DINy-1+RLB	8	-2369.7	4755.4	19.2	0.0	100.0
21	NIP ~ Y+RLB+SD1y_1	5	-2372.7	4755.4	19.2	0.0	100.0
22	NIP ~ S+Y+RLB+SD2	8	-2369.7	4755.4	19.2	0.0	100.0
23	NIP ~ S+Y+RLB+RH2y-1	8	-2369.7	4755.5	19.3	0.0	100.0

24	NIP ~ S+Y+RLB+T2	8	-2369.9	4755.8	19.6	0.0	100.0
25	NIP ~ S+Y+RLB+RH2y-2	8	-2370.1	4756.2	20.0	0.0	100.0
26	NIP ~ Y+RLB+SD2y-2	5	-2373.1	4756.2	20.0	0.0	100.0
27	NIP ~ S+Y+RLB+PRy-2	8	-2370.1	4756.3	20.1	0.0	100.0
28	NIP ~ Y+RLB+SD1y-2	5	-2373.1	4756.3	20.1	0.0	100.0
29	NIP ~ S+Y+RLB+SD1y-2	8	-2370.1	4756.3	20.1	0.0	100.0
30	NIP ~ Y+RLB+RH1y-1	5	-2373.1	4756.3	20.1	0.0	100.0

Table S10. The support for each explanatory variable is shown from the AIC-based model selection table of the nymphal infection prevalence. This support is calculated as the sum of the Akaike weights for all the models in the set that include that explanatory variable.

Rank	Explanatory variable of interest	Support (%)
1	RLB	100.0
2	Year	100.0
3	PR	93.8
4	Site	48.2
5	RH1	5.7
6	SD1	< 1.0
7	Beech	< 1.0
8	DIN_{y-1}	< 1.0
9	T1	< 1.0
10	$T1_{y-1}$	< 1.0
11	$RH1_{y-1}$	< 1.0
12	$SD1_{y-1}$	< 1.0
13	PR_{y-1}	< 1.0
14	$T1_{y-2}$	< 1.0
15	$RH1_{y-2}$	< 1.0
16	$SD1_{y-2}$	< 1.0
17	PR_{y-2}	< 1.0
18	T2	< 1.0
19	RH2	< 1.0
20	SD2	< 1.0
21	$T2_{y-1}$	< 1.0
22	$RH2_{y-1}$	< 1.0
23	$SD2_{y-1}$	< 1.0
24	$T2_{y-2}$	< 1.0
25	$RH2_{y-2}$	< 1.0
26	$SD2_{y-2}$	< 1.0
27	Site:Year	< 1.0
28	Site:Beech	< 1.0
29	Site:DINy-1	< 1.0
30	Site:RLB	< 1.0
31	Site:T1	< 1.0
32	Site:RH1	< 1.0
33	Site:SD1	< 1.0
34	Site:PR	< 1.0
35	$Site:T1_{y-1}$	< 1.0
36	$Site:RH1_{y-1}$	< 1.0

37	Site:$SD1_{y-1}$	< 1.0
38	Site:PR_{y-1}	< 1.0
39	Site:$T1_{y-2}$	< 1.0
40	Site:$RH1_{y-2}$	< 1.0
41	Site:$SD1_{y-2}$	< 1.0
42	Site:PR_{y-2}	< 1.0
43	Site:T2	< 1.0
44	Site:RH2	< 1.0
45	Site:SD2	< 1.0
46	Site:$T2_{y-1}$	< 1.0
47	Site:$RH2_{y-1}$	< 1.0
48	Site:$SD2_{y-1}$	< 1.0
49	Site:$T2_{y-2}$	< 1.0
50	Site:$RH2_{y-2}$	< 1.0
51	Site:$SD2_{y-2}$	< 1.0

Table S11. Model-averaged parameter estimates are shown for the generalized linear mixed effects model with binomial errors of the nymphal infection prevalence (NIP) response variable. Shown are the parameter types, the parameter names, the parameter estimates, and the 95% confidence limits (LL = lower limit and UL = upper limit). Estimate 1 is averaged over all the models in the set. Estimate 2 is averaged over the subset of models with a cumulative support of 95%. The 95% confidence limits are for estimate 2.

Type	Name	Estimate 1	Estimate 2	95% LL	95% UL
Intercept	Low site	-0.783	-0.783	-1.161	-0.405
Contrast 1	Medium site	-0.094	-0.195	-0.467	0.077
Contrast 2	High site	-0.172	-0.358	-0.653	-0.063
Contrast 3	Top site	-0.065	-0.135	-0.481	0.211
Slope 1	Year	-0.145	-0.145	-0.181	-0.108
Slope 2	Beech	0.000	0.002	-0.073	0.077
Slope 3	DIN_{y-1}	0.000	0.155	-0.024	0.333
Slope 4	RLB	-0.184	-0.184	-0.285	-0.083
Contrast 4	T1	0.000	0.146	-0.069	0.361
Contrast 5	RH1	-0.018	-0.311	-0.447	-0.174
Contrast 6	SD1	0.001	0.282	0.119	0.446
Contrast 7	PR	-0.318	-0.339	-0.467	-0.211
Contrast 8	$T1_{y-1}$	0.000	-0.055	-0.426	0.316
Contrast 9	$RH1_{y-1}$	0.000	-0.080	-0.266	0.106
Contrast 10	$SD1_{y-1}$	0.000	0.098	-0.122	0.319
Contrast 11	PR_{y-1}	0.000	-0.149	-0.298	0.001
Contrast 12	$T1_{y-2}$	0.000	0.187	0.013	0.361
Contrast 13	$RH1_{y-2}$	0.000	0.078	-0.135	0.291
Contrast 14	$SD1_{y-2}$	0.000	0.044	-0.208	0.296
Contrast 15	PR_{y-2}	0.000	0.017	-0.133	0.168
Contrast 16	Medium site:Year	0.000	-0.037	-0.132	0.057
Contrast 17	High site:Year	0.000	-0.056	-0.154	0.042
Contrast 18	Top site:Year	0.000	-0.034	-0.145	0.076
Contrast 19	Medium site:Beech	0.000	-0.089	-0.349	0.172
Contrast 20	High site:Beech	0.000	-0.059	-0.324	0.206
Contrast 21	Top site:Beech	0.000	0.049	-0.226	0.324
Contrast 22	Medium site:DIN_{y-1}	0.000	0.499	-0.215	1.212
Contrast 23	High site:DIN_{y-1}	0.000	0.206	-0.425	0.838
Contrast 24	Top site:DIN_{y-1}	0.000	0.274	-0.350	0.898
Contrast 25	Medium site:RLB	0.000	0.141	-0.166	0.448
Contrast 26	High site: RLB	0.000	-0.133	-0.405	0.139
Contrast 27	Top site: RLB	0.000	-0.015	-0.385	0.354

Contrast 28	Medium site:T1	0.000	0.174	-0.697	1.046
Contrast 29	High site:T1	0.000	0.052	-0.813	0.916
Contrast 30	Top site:T1	0.000	0.321	-0.563	1.205
Contrast 31	Medium site:RH1	0.000	-0.003	-0.581	0.575
Contrast 32	High site:RH1	0.000	0.140	-0.442	0.722
Contrast 33	Top site:RH1	0.000	0.096	-0.498	0.689
Contrast 34	Medium site:SD1	0.000	-0.053	-0.702	0.596
Contrast 35	High site:SD1	0.000	-0.294	-0.987	0.400
Contrast 36	Top site:SD1	0.000	-0.133	-0.923	0.656
Contrast 37	Medium site:PR	0.000	-0.010	-0.505	0.485
Contrast 38	High site:PR	0.000	0.001	-0.501	0.503
Contrast 39	Top site:PR	0.000	0.164	-0.354	0.683
Contrast 40	Medium site:T_{y-1}	0.000	-0.325	-1.177	0.526
Contrast 41	High site:T_{y-1}	0.000	-0.532	-1.376	0.312
Contrast 42	Top site:T_{y-1}	0.000	-0.488	-1.351	0.374
Contrast 43	Medium site:$RH1_{y-1}$	0.000	0.000	-0.593	0.593
Contrast 44	High site:$RH1_{y-1}$	0.000	0.208	-0.393	0.810
Contrast 45	Top site:$RH1_{y-1}$	0.000	0.175	-0.453	0.803
Contrast 46	Medium site:$SD1_{y-1}$	0.000	-0.010	-0.666	0.646
Contrast 47	High site:$SD1_{y-1}$	0.000	-0.210	-0.908	0.488
Contrast 48	Top site:$SD1_{y-1}$	0.000	-0.298	-1.112	0.515
Contrast 49	Medium site:PR_{y-1}	0.000	-0.094	-0.582	0.395
Contrast 50	High site:PR_{y-1}	0.000	-0.003	-0.500	0.494
Contrast 51	Top site:PR_{y-1}	0.000	-0.076	-0.595	0.442
Contrast 52	Medium site:$T1_{y-2}$	0.000	-0.261	-1.154	0.632
Contrast 53	High site:$T1_{y-2}$	0.000	-0.264	-1.151	0.623
Contrast 54	Top site:$T1_{y-2}$	0.000	-0.280	-1.180	0.621
Contrast 55	Medium site:$RH1_{y-2}$	0.000	0.193	-0.431	0.816
Contrast 56	High site:$RH1_{y-2}$	0.000	0.291	-0.337	0.918
Contrast 57	Top site:$RH1_{y-2}$	0.000	0.251	-0.385	0.886
Contrast 58	Medium site:$SD1_{y-2}$	0.000	-0.352	-1.052	0.348
Contrast 59	High site:$SD1_{y-2}$	0.000	-0.459	-1.201	0.283
Contrast 60	Top site:$SD1_{y-2}$	0.000	-0.359	-1.177	0.460
Contrast 61	Medium site:PR_{y-2}	0.000	0.113	-0.362	0.588
Contrast 62	High site:PR_{y-2}	0.000	0.104	-0.385	0.593
Contrast 63	Top site:PR_{y-2}	0.000	0.059	-0.455	0.574
Contrast 64	T2	0.000	0.141	-0.036	0.318
Contrast 65	RH2	0.000	0.175	0.020	0.330
Contrast 66	SD2	0.000	-0.061	-0.293	0.171
Contrast 67	$T2_{y-1}$	0.000	-0.194	-0.388	0.000
Contrast 68	$RH2_{y-1}$	0.000	0.069	-0.113	0.250

Contrast 69	$SD2_{y-1}$	0.000	-0.169	-0.374	0.036
Contrast 70	$T2_{y-2}$	0.000	0.061	-0.158	0.279
Contrast 71	$RH2_{y-2}$	0.000	-0.080	-0.277	0.116
Contrast 72	$SD2_{y-2}$	0.000	0.072	-0.175	0.319
Contrast 73	Medium site:T2	0.000	0.051	-0.671	0.774
Contrast 74	High site:T2	0.000	-0.070	-0.808	0.668
Contrast 75	Top site:T2	0.000	-0.072	-0.836	0.692
Contrast 76	Medium site:RH2	0.000	0.035	-0.464	0.533
Contrast 77	High site:RH2	0.000	0.054	-0.516	0.624
Contrast 78	Top site:RH2	0.000	0.279	-0.336	0.893
Contrast 79	Medium site:SD2	0.000	0.069	-0.495	0.632
Contrast 80	High site:SD2	0.000	0.024	-0.681	0.730
Contrast 81	Top site:SD2	0.000	-0.426	-1.372	0.520
Contrast 82	Medium site:$T2_{y-1}$	0.000	-0.166	-0.867	0.534
Contrast 83	High site:$T2_{y-1}$	0.000	-0.527	-1.230	0.176
Contrast 84	Top site:$T2_{y-1}$	0.000	-0.331	-1.053	0.390
Contrast 85	Medium site:$RH2_{y-1}$	0.000	-0.060	-0.551	0.430
Contrast 86	High site:$RH2_{y-1}$	0.000	-0.031	-0.567	0.504
Contrast 87	Top site:$RH2_{y-1}$	0.000	0.217	-0.359	0.794
Contrast 88	Medium site:$SD2_{y-1}$	0.000	0.090	-0.451	0.631
Contrast 89	High site:$SD2_{y-1}$	0.000	0.025	-0.592	0.642
Contrast 90	Top site:$SD2_{y-1}$	0.000	-0.004	-0.771	0.764
Contrast 91	Medium site:$T2_{y-2}$	0.000	0.068	-0.600	0.736
Contrast 92	High site:$T2_{y-2}$	0.000	-0.014	-0.691	0.663
Contrast 93	Top site:$T2_{y-2}$	0.000	-0.298	-0.998	0.402
Contrast 94	Medium site:$RH2_{y-2}$	0.000	-0.023	-0.466	0.420
Contrast 95	High site:$RH2_{y-2}$	0.000	0.079	-0.398	0.555
Contrast 96	Top site:$RH2_{y-2}$	0.000	0.260	-0.248	0.768
Contrast 97	Medium site:$SD2_{y-2}$	0.000	0.067	-0.408	0.543
Contrast 98	High site:$SD2_{y-2}$	0.000	0.012	-0.525	0.549
Contrast 99	Top site:$SD2_{y-2}$	0.000	-0.146	-0.802	0.510

SECTION 6 – Full statistical analysis of the density of infected nymphs (DIN) for the restricted 13-year period of the study (2006 – 2018)

Model selection approach: To identify the best model, we used a model selection approach based on the Akaike information criterion (AIC). A big conceptual advantage of model selection is that it reminds the user that there are competing models with different parameter estimates and that some of these models have more support (i.e., are better at explaining the data) than other models. Another advantage is that you can compare non-nested models containing different explanatory variables, which is not possible with a more traditional approach like stepwise multiple regression. Models were ranked according to their AIC values and the Akaike weights, which indicate the percent support, were calculated for each model. We used the Akaike weights to calculate the model-averaged parameter estimates and their 95% confidence intervals (CIs). For the generalized linear mixed effects models that analysed the NIP and AIP, we assessed the goodness of fit of the binomial distribution for the best model from the model selection table. Similarly, for the linear models that analysed the DIN and DIA, the assumptions of normally distributed residuals and equal variances were assessed for the best model from the model selection table (Additional file 1: Section 3). We used R version 4.0.3 for all statistical analyses (Team 2013). We used the lm() function in the base package to run the LMs with normal errors. We used the glmer() functions in the lme4 package to run the GLMMs with binomial errors. We used the mod.sel() function and the model.av() function in the MuMIn package to create the model selection tables and the model-averaged parameter estimates.

Model selection analysis of the DIN: The model selection table for the best 30 out of 314 models is presented in Table S12. For the annual DIN, the top three models had a combined support of 80.0% (Table S12). The best model had 47.0% of the support (Table S12), explained 82.5% of the variation in the annual DIN, and contained the explanatory variables of elevation site (partial $r^2 = 28.3\%$), year (partial $r^2 = 14.8\%$), site:year interaction (partial $r^2 = 4.2\%$), beech mast score 2 years prior (partial $r^2 = 5.8\%$), and weather station mean annual relative humidity in the present year (partial $r^2 = 6.1\%$).

The support for the individual explanatory variables was as follows: site (100.0%), year (100.0%), site:year interaction (92.0%), beech mast score 2 year prior (69.1%), weather station mean annual relative humidity in the present year (50.8%), RLB time lag (31.2%), weather station mean annual precipitation in the previous year (20.0%), and weather station mean annual

saturation deficit in the present year (16.1%; Table S13). None of the other explanatory variables had a support > 2.5% (Table S13).

Model-averaged parameter estimates for the DIN: To determine the effects of the explanatory variables on the DIN, we present the model-averaged parameter estimates on the log10-transformed scale (Table S14). We also back-calculated the effect sizes of the explanatory variables on the DIN on the original scale with respect to the following baseline: the site was low elevation, the year was 2006, the beech mast score was set to 1, and the other covariates were set to 0 (i.e., the mean values on the z-score scale).

The interaction between site and year indicated that the change in the DIN over time differed between the four elevation sites (Table S14). Over the 13-year period (2006 – 2018), the DIN decreased at the low (slope = -0.018 per year, 95% CI = -0.059 – 0.023), medium (Medium – Low contrast of the slope = -0.023, 95% CI = -0.072 – 0.027), high (High – Low contrast of the slope = -0.027, 95% CI = -0.076 – 0.023), and top (Top – Low contrast of the slope = -0.088, 95% CI = -0.138 – -0.037) elevation sites. Over the 13-year period (2006 – 2018), the DIN decreased by 38.7%, 67.2%, 70.7% and 94.6% at the low, medium, high, and top elevation sites, respectively (Table S14). Due to the significant interaction between site and year, it does not make sense to interpret the differences in intercept between the four elevation sites (Table S14).

The beech mast score 2 years prior had a positive and significant effect on the annual DIN (Table S14; slope = 0.067 per class; 95% CI = 0.029 – 0.105). Increasing the beech mast score 2 years prior from 1 (poor mast) to 5 (full mast) increased the DIN by 85.5% at each of the four elevation sites on Chaumont Mountain (Table S14). The weather station mean annual relative humidity in the present year had a negative and significant effect on the DIN (Table S14; slope = -0.166 per standard deviation, 95% CI = -0.253 – -0.079). Increasing the weather station mean annual relative humidity in the present year by one standard deviation (1.8% of relative humidity) decreased the DIN by 31.8% at each of the four elevation sites on Chaumont Mountain (Table S14).

Other models contained other explanatory variables that had the following effects on the DIN. The RLB time lag had a negative and significant effect on the DIN (Table S14; slope = -0.131 per standard deviation, 95% CI = -0.215 – -0.047). The weather station mean annual precipitation in the previous year had a negative and significant effect on the DIN (Table S14; slope = -0.108 per standard deviation, 95% CI = -0.183 – -0.033). The weather station mean

annual saturation deficit in the present year had a positive and significant effect on the DIN (Table S14; slope = 0.205 per standard deviation, 95% CI = 0.079 – 0.330).

In summary, the DIN decreased over time at the four elevation sites and significantly so at the top elevation. The DIN increased significantly with tree seed production two years prior and decreased significantly with the relative humidity in the present year.

Table S12. Model selection results are shown for the linear models with normal errors of the log10-trasnformed density of infected nymphs (DIN) response variable. The explanatory variables were site, year, beech masting index 2 years prior, RLB time lag, and the climate variables obtained from the weather stations and collected from the field. The models are ranked according to their Akaike Information Criterion (AIC). Shown for each model are the model rank (Rank), model structure (see below for explanation of explanatory variables), model degrees of freedom (Df), log-likelihood (logLik), Akaike information criterion (AIC), difference in the AIC value from the top model (ΔAIC), model weight (Weight1), and cumulative weight (Weight2), and adjusted r-squared (r^2).

Rank	Model structure	Df	logLik	AIC	ΔAIC	Weight1	Weight2	r^2
1	DIN ~ S+Y+B+RH1+S:Y	11	8.1	12.3	0.0	47.0	47.0	82.5
2	DIN ~ S+Y+RLB+PR_{y-1}+S:Y	11	7.2	14.2	1.8	19.0	66.0	81.9
3	DIN ~ S+Y+B+SD1+S:Y	11	6.9	14.8	2.5	14.0	80.0	81.7
4	DIN ~ S+Y+B+RH1	8	0.7	17.9	5.6	3.0	83.0	78.3
5	DIN ~ S+Y+B+S:Y	11	4.9	18.8	6.5	2.0	85.0	80.2
6	DIN ~ Y+B+SD1	8	0.2	19.0	6.7	2.0	87.0	77.9
7	DIN ~ S+Y+RLB+$T1_{y-1}$+S:Y	11	4.6	19.3	7.0	1.0	88.0	80.0
8	DIN ~ S+Y+RLB+PR+S:Y	11	4.1	20.3	8.0	1.0	89.0	79.6
9	DIN ~ S+Y+RLB+$RH1_{y-1}$+S:Y	11	4.1	20.4	8.1	1.0	90.0	79.6
10	DIN ~ S+Y+RLB+S:Y	10	2.3	20.7	8.4	1.0	91.0	78.7
11	DIN ~ S+Y+RLB+SD1+S:Y	11	3.9	20.8	8.4	1.0	92.0	79.5
12	DIN ~ S+Y+RLB+$T1_{y-2}$	11	3.8	21.0	8.7	1.0	93.0	79.4
13	DIN ~ S+Y+RLB+S:Y+S:RLB	13	7.2	21.1	8.8	1.0	94.0	81.0
14	DIN ~ S+Y+RLB+RH1+S:Y	11	3.6	21.3	9.0	1.0	95.0	79.2
15	DIN ~ S+Y+RLB+T2+S:Y	11	3.6	21.4	9.1	0.0	100.0	79.2
16	DIN ~ S+Y+RLB+SD1y-1+S:Y	11	3.5	21.6	9.3	0.0	100.0	79.1
17	DIN ~ S+Y+RLB+PRy-1	8	-1.1	21.6	9.3	0.0	100.0	76.7
18	DIN ~ S+Y+RLB+PRy-1	8	-1.1	21.6	9.3	0.0	100.0	76.7
19	DIN ~ S+Y+B+RLB	8	-1.4	22.2	9.9	0.0	100.0	76.4
20	DIN ~ S+Y+RLB+RH2+S:Y	11	3.2	22.2	9.9	0.0	100.0	78.9
21	DIN ~ S+Y+B+RH2y-2+S:Y	11	3.2	22.3	9.9	0.0	100.0	78.9
22	DIN ~ S+Y+B+PRy-1+S:Y	11	2.9	22.9	10.5	0.0	100.0	78.6
23	DIN ~ S+Y+RLB+T2y-1+S:Y	11	2.8	23.0	10.6	0.0	100.0	78.6
24	DIN ~ S+Y+RLB+T1+S:Y	11	2.7	23.2	10.8	0.0	100.0	78.5
25	DIN ~ S+Y+RLB+RH1y-2+S:Y	11	2.6	23.4	11.1	0.0	100.0	78.4
26	DIN ~ S+Y+RLB+SD2y-2+S:Y	11	2.5	23.6	11.3	0.0	100.0	78.3
27	DIN ~ S+Y+B+PR+S:Y	11	2.4	23.7	11.4	0.0	100.0	78.3
28	DIN ~ S+Y+RLB+S:RLB	10	0.8	23.8	11.5	0.0	100.0	77.3
29	DIN ~ S+Y+RLB+T2y-2+S:Y	11	2.4	23.9	11.5	0.0	100.0	78.2

30	DIN ~ S+Y+B+T1+S:Y	11	2.4	23.9	11.6	0.0	100.0	78.2

Table S13. The support for each explanatory variable is shown from the AIC-based model selection table of the density of infected nymphs. This support is calculated as the sum of the Akaike weights for all the models in the set that include that explanatory variable.

Rank	Explanatory variable of interest	Support (%)
1	Site	100.0
2	Year	100.0
3	Site:Year	92.0
4	Beech	69.1
5	RH1	50.8
6	RLB	31.2
7	PR_{y-1}	20.0
8	SD1	16.1
9	T2	2.5
10	$T1_{y-1}$	1.7
11	PR	1.2
12	T1	< 1.0
13	$RH1_{y-1}$	< 1.0
14	$SD1_{y-1}$	< 1.0
15	$T1_{y-2}$	< 1.0
16	$RH1_{y-2}$	< 1.0
17	$SD1_{y-2}$	< 1.0
18	PR_{y-2}	< 1.0
19	RH2	< 1.0
20	SD2	< 1.0
21	$T2_{y-1}$	< 1.0
22	$RH2_{y-1}$	< 1.0
23	$SD2_{y-1}$	< 1.0
24	$T2_{y-2}$	< 1.0
25	$RH2_{y-2}$	< 1.0
26	$SD2_{y-2}$	< 1.0
27	Site:Beech	< 1.0
28	Site:RLB	< 1.0
29	Site:T1	< 1.0
30	Site:RH1	< 1.0
31	Site:SD1	< 1.0
32	Site:PR	< 1.0
33	Site:$T1_{y-1}$	< 1.0
34	Site:$RH1_{y-1}$	< 1.0
35	Site:$SD1_{y-1}$	< 1.0
36	Site:PR_{y-1}	< 1.0

37	Site:$T1_{y-2}$	< 1.0
38	Site:$RH1_{y-2}$	< 1.0
39	Site:$SD1_{y-2}$	< 1.0
40	Site:PR_{y-2}	< 1.0
41	Site:T2	< 1.0
42	Site:RH2	< 1.0
43	Site:SD2	< 1.0
44	Site:$T2_{y-1}$	< 1.0
45	Site:$RH2_{y-1}$	< 1.0
46	Site:$SD2_{y-1}$	< 1.0
47	Site:$T2_{y-2}$	< 1.0
48	Site:$RH2_{y-2}$	< 1.0
49	Site:$SD2_{y-2}$	< 1.0

Table S14. Model-averaged parameter estimates are shown for the linear model with normal errors of the density of infected nymphs (DIN) response variable. Shown are the parameter types, the parameter names, the parameter estimates, and the 95% confidence limits (LL = lower limit and UL = upper limit). Estimate 1 is averaged over all the models in the set. Estimate 2 is averaged over the subset of models with a cumulative support of 95%. The 95% confidence limits are for estimate 2.

Type	Name	Estimate 1	Estimate 2	95% LL	95% UL
Intercept	Low site	3.362	3.362	2.898	3.827
Contrast 1	Medium site	0.043	0.043	-0.442	0.529
Contrast 2	High site	-0.192	-0.192	-0.718	0.333
Contrast 3	Top site	-0.199	-0.199	-0.896	0.498
Slope 1	Year	-0.018	-0.018	-0.059	0.023
Slope 2	Beech	0.046	0.067	0.029	0.105
Slope 3	RLB	-0.041	-0.131	-0.215	-0.047
Contrast 4	T1	0.000	0.111	-0.088	0.311
Contrast 5	RH1	-0.084	-0.166	-0.253	-0.079
Contrast 6	SD1	0.033	0.205	0.079	0.330
Contrast 7	PR	-0.001	-0.077	-0.166	0.013
Contrast 8	$T1_{y-1}$	-0.003	-0.160	-0.335	0.015
Contrast 9	$RH1_{y-1}$	-0.001	-0.075	-0.168	0.019
Contrast 10	$SD1_{y-1}$	0.000	0.082	-0.042	0.206
Contrast 11	PR_{y-1}	-0.022	-0.108	-0.183	-0.033
Contrast 12	$T1_{y-2}$	0.001	0.120	-0.050	0.290
Contrast 13	$RH1_{y-2}$	0.000	0.050	-0.062	0.163
Contrast 14	$SD1_{y-2}$	0.000	-0.017	-0.147	0.114
Contrast 15	PR_{y-2}	0.000	-0.008	-0.090	0.074
Contrast 16	Medium site:Year	-0.021	-0.023	-0.072	0.027
Contrast 17	High site:Year	-0.025	-0.027	-0.076	0.023
Contrast 18	Top site:Year	-0.081	-0.088	-0.138	-0.037
Contrast 19	Medium site:Beech	0.000	-0.029	-0.154	0.095
Contrast 20	High site:Beech	0.000	0.016	-0.108	0.141
Contrast 21	Top site:Beech	0.000	-0.011	-0.136	0.113
Contrast 22	Medium site:RLB	0.000	0.049	-0.161	0.260
Contrast 23	High site: RLB	0.000	0.045	-0.162	0.252
Contrast 24	Top site: RLB	0.002	0.250	0.047	0.452
Contrast 25	Medium site:T1	0.000	0.054	-0.458	0.567
Contrast 26	High site:T1	0.000	0.052	-0.451	0.556
Contrast 27	Top site:T1	0.000	-0.283	-0.777	0.211
Contrast 28	Medium site:RH1	0.000	0.061	-0.270	0.391

Contrast 29	High site:RH1	0.000	0.081	-0.248	0.409
Contrast 30	Top site:RH1	0.000	0.179	-0.142	0.499
Contrast 31	Medium site:SD1	0.000	-0.076	-0.435	0.283
Contrast 32	High site:SD1	0.000	-0.115	-0.489	0.259
Contrast 33	Top site:SD1	0.000	-0.405	-0.800	-0.010
Contrast 34	Medium site:PR	0.000	0.049	-0.229	0.326
Contrast 35	High site:PR	0.000	-0.003	-0.278	0.273
Contrast 36	Top site:PR	0.000	0.222	-0.054	0.498
Contrast 37	Medium site:T_{y-1}	0.000	-0.258	-0.716	0.200
Contrast 38	High site:T_{y-1}	0.000	-0.379	-0.827	0.068
Contrast 39	Top site:T_{y-1}	0.000	-0.621	-1.058	-0.185
Contrast 40	Medium site:$RH1_{y-1}$	0.000	0.031	-0.317	0.379
Contrast 41	High site:$RH1_{y-1}$	0.000	0.099	-0.246	0.445
Contrast 42	Top site:$RH1_{y-1}$	0.000	0.147	-0.189	0.484
Contrast 43	Medium site:$SD1_{y-1}$	0.000	-0.042	-0.430	0.346
Contrast 44	High site:$SD1_{y-1}$	0.000	-0.111	-0.514	0.291
Contrast 45	Top site:$SD1_{y-1}$	0.000	-0.348	-0.764	0.068
Contrast 46	Medium site:PR_{y-1}	0.000	-0.060	-0.341	0.220
Contrast 47	High site:PR_{y-1}	0.000	-0.008	-0.288	0.272
Contrast 48	Top site:PR_{y-1}	0.000	0.130	-0.148	0.409
Contrast 49	Medium site:$T1_{y-2}$	0.000	-0.226	-0.757	0.305
Contrast 50	High site:$T1_{y-2}$	0.000	-0.050	-0.567	0.468
Contrast 51	Top site:$T1_{y-2}$	0.000	-0.371	-0.875	0.132
Contrast 52	Medium site:$RH1_{y-2}$	0.000	0.031	-0.344	0.406
Contrast 53	High site:$RH1_{y-2}$	0.000	0.061	-0.306	0.427
Contrast 54	Top site:$RH1_{y-2}$	0.000	-0.038	-0.389	0.313
Contrast 55	Medium site:$SD1_{y-2}$	0.000	-0.144	-0.568	0.280
Contrast 56	High site:$SD1_{y-2}$	0.000	-0.118	-0.551	0.315
Contrast 57	Top site:$SD1_{y-2}$	0.000	-0.189	-0.627	0.249
Contrast 58	Medium site:PR_{y-2}	0.000	0.034	-0.251	0.320
Contrast 59	High site:PR_{y-2}	0.000	0.020	-0.267	0.308
Contrast 60	Top site:PR_{y-2}	0.000	0.044	-0.244	0.332
Contrast 61	T2	0.004	0.147	0.017	0.277
Contrast 62	RH2	0.000	0.059	-0.058	0.176
Contrast 63	SD2	0.000	0.017	-0.132	0.166
Contrast 64	$T2_{y-1}$	0.000	-0.050	-0.167	0.066
Contrast 65	$RH2_{y-1}$	0.000	-0.026	-0.156	0.104
Contrast 66	$SD2_{y-1}$	0.000	0.002	-0.131	0.136
Contrast 67	$T2_{y-2}$	0.000	-0.018	-0.142	0.106
Contrast 68	$RH2_{y-2}$	0.000	-0.075	-0.219	0.069
Contrast 69	$SD2_{y-2}$	0.000	-0.025	-0.207	0.156

Contrast 70	Medium site:T2	0.000	0.006	-0.413	0.426
Contrast 71	High site:T2	0.000	0.005	-0.420	0.431
Contrast 72	Top site:T2	0.000	-0.269	-0.690	0.153
Contrast 73	Medium site:RH2	0.000	-0.046	-0.306	0.214
Contrast 74	High site:RH2	0.000	-0.029	-0.322	0.265
Contrast 75	Top site:RH2	0.000	0.316	0.018	0.614
Contrast 76	Medium site:SD2	0.000	0.076	-0.228	0.379
Contrast 77	High site:SD2	0.000	0.073	-0.305	0.451
Contrast 78	Top site:SD2	0.000	-0.484	-0.953	-0.015
Contrast 79	Medium site:$T2_{y-1}$	0.000	-0.070	-0.493	0.353
Contrast 80	High site:$T2_{y-1}$	0.000	-0.242	-0.663	0.180
Contrast 81	Top site:$T2_{y-1}$	0.000	-0.191	-0.617	0.235
Contrast 82	Medium site:$RH2_{y-1}$	0.000	-0.009	-0.286	0.267
Contrast 83	High site:$RH2_{y-1}$	0.000	-0.042	-0.339	0.255
Contrast 84	Top site:$RH2_{y-1}$	0.000	0.201	-0.106	0.508
Contrast 85	Medium site:$SD2_{y-1}$	0.000	0.029	-0.288	0.347
Contrast 86	High site:$SD2_{y-1}$	0.000	0.025	-0.331	0.381
Contrast 87	Top site:$SD2_{y-1}$	0.000	-0.062	-0.487	0.362
Contrast 88	Medium site:$T2_{y-2}$	0.000	-0.042	-0.492	0.407
Contrast 89	High site:$T2_{y-2}$	0.000	0.047	-0.399	0.493
Contrast 90	Top site:$T2_{y-2}$	0.000	0.105	-0.338	0.548
Contrast 91	Medium site:$RH2_{y-2}$	0.000	0.054	-0.211	0.319
Contrast 92	High site:$RH2_{y-2}$	0.000	0.017	-0.265	0.299
Contrast 93	Top site:$RH2_{y-2}$	0.000	0.070	-0.218	0.359
Contrast 94	Medium site:$SD2_{y-2}$	0.000	-0.046	-0.349	0.258
Contrast 95	High site:$SD2_{y-2}$	0.000	0.024	-0.311	0.360
Contrast 96	Top site:$SD2_{y-2}$	0.000	0.121	-0.263	0.504

REFERENCES

1. Perret JL, Guigoz E, Rais O, Gern L. Influence of saturation deficit and temperature on *Ixodes ricinus* tick questing activity in a Lyme borreliosis-endemic area (Switzerland). Parasitol Res. 2000;86:554-7.
2. Eisen RJ, Eisen L, Castro MB, Lane RS. Environmentally related variability in risk of exposure to Lyme disease spirochetes in northern California: effect of climatic conditions and habitat type. Environ Entomol. 2003;32:1010-8.
3. Brugger K, Walter M, Chitimia-Dobler L, Dobler G, Rubel F. Forecasting next season's *Ixodes ricinus* nymphal density: the example of southern Germany 2018. Exp Appl Acarol. 2018;75:281-8.
4. Ostfeld RS, Canham CD, Oggenfuss K, Winchcombe RJ, Keesing F. Climate, deer, rodents, and acorns as determinants of variation in Lyme-disease risk. PLoS Biol. 2006;4:e145.
5. Bregnard C, Rais O, Voordouw MJ. Climate and tree seed production predict the abundance of the European Lyme disease vector over a 15-year period. Parasit Vectors. 2020;13:408.
6. Team RC. R: A language and environment for statistical computing. 2013.

ADDITIONAL FILE – Chapter 3

Beech tree masting explains the inter-annual variation in the fall and spring peaks of *Ixodes ricinus* ticks with different time lags

Authors: Cindy Bregnard, Olivier Rais, Coralie Herrmann, Olaf Kahl, Katharina Brugger, and Maarten J. Voordouw

Table of Contents

SECTION 1 – Interpolation of the climate data from the weather stations 379
SECTION 2 – Goodness of fit for the best model 381
SECTION 3 – Effect of elevation site on the density of *i. ricinus* nymphs 383
SECTION 4 – Correlation plots between the fall peak and the spring peak with different time lags 385
SECTION 5 – Smoother function of calendar day predicts the bimodal phenology of *I. ricinus* nymphs at the four elevation sites. 389
SECTION 6 – Sequential modelling approach 391
SECTION 7 – Comparison of the beech masting variables with different time lags and the inter-annual variation in the spring and fall peaks of the don 395
SECTION 8 – Full aic-based model selection analysis 397

SECTION 1 – Interpolation of the climate data from the weather stations

Methods: We obtained climate data from the Federal Office of Meteorology and Climatology MeteoSwiss using the CLIMAP-net application. Climate data were obtained from two weather stations that are close to our four elevation sites and that are located at 485 m ASL in Neuchâtel and at 1136 m ASL in Chaumont. To create a climate profile that was specific for each of the four elevation sites, we interpolated the values between the two weather stations using the relative elevation distance of each elevation site to the two weather stations, as we have done previously [1, 2]. For example, the total elevation distance between the Neuchâtel and Chaumont weather stations is 651 meters, and the elevation distance between the top site and the Neuchâtel weather station is 620 meters, which represents 95.2% of the elevation distance. Thus, the climate at the top site is expected to be more similar to the Chaumont weather station (95.2%) compared to the Neuchâtel weather station (4.8%), whereas the reverse would be true for the low site. For each elevation site, the mean daily temperature, relative humidity, saturation deficit, precipitation and snowfall were calculated based on the interpolating percentages (Table S1).

Table S1. Interpolation of the climate data from the two weather stations. Shown are the site, elevation (in meters), elevation distance with the Neuchâtel weather station (Dist 1, in meters), elevation distance between Neuchâtel and Chaumont weather station (Dist 2, in meters), the interpolating percentage from the Neuchâtel weather station (Neuchâtel), and the interpolating percentage from the Chaumont weather station (Chaumont).

Site	Elevation	Dist 1	Dist 2	Neuchâtel	Chaumont
Top	1073	620	651	4.8%	95.2%
High	900	447	651	31.3%	68.7%
Medium	740	287	651	55.9%	44.1%
Low	620	167	651	74.3%	25.7%

SECTION 2 – Goodness of fit for the best model

Methods: We used the gam.check () function in R to assess the goodness of fit for the best GAM of the model selection table of the main manuscript (model 1 in Table 5 in the main manuscript).

Results for nymphal abundance: For the DON, the residuals of the best GAM (model 1 in Table 5 in the main manuscript) met the assumptions of the method (Figure S1) and therefore confirmed the goodness of fit.

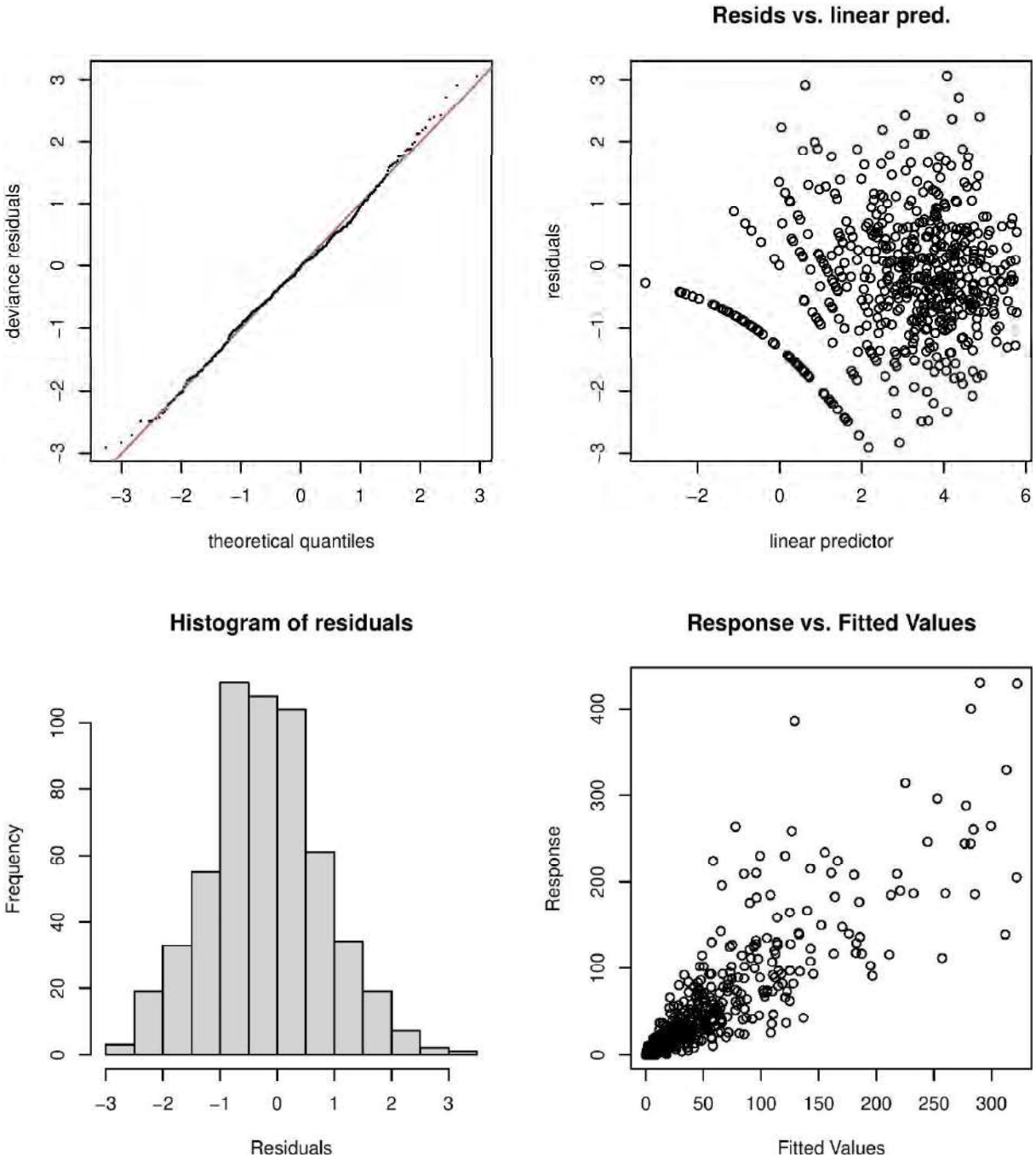

Figure S1. Goodness of fit assumptions for the best GAM in the model selection table of the main manuscript (model 1 in Table 5 in the main manuscript). The four plots generated by the gam.check() function confirmed that the residuals of the best model generally fit the assumptions of the GAM.

SECTION 3 – Effect of elevation site on the density of *I. ricinus* nymphs

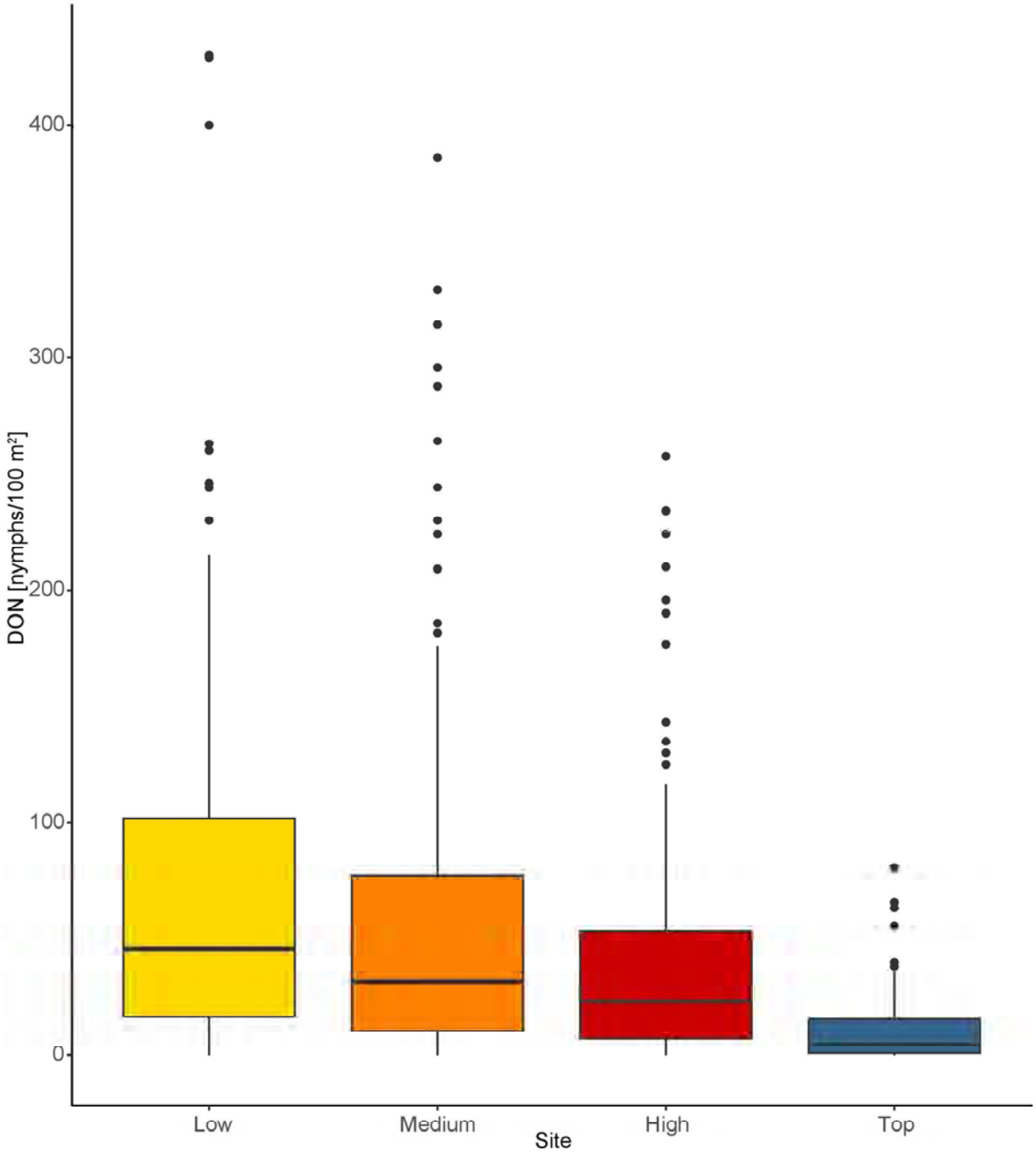

Figure S2. Effect of elevation on the density of nymphs (DON). The DON is an estimate of the number of questing *I. ricinus* nymphs per 100 m^2 sampled by the dragging method each month. The boxplot shows the medians (black line), the 25th and 75th percentiles (edges of the box), the minimum and maximum values (whiskers), and the outliers (solid circles).

SECTION 4 – Correlation plots between the fall peak and the spring peak with different time lags

Methods: Under the direct development hypothesis, the fall peak in year *y*-1 should be correlated with the spring peak in year *y*. In contrast, under the delayed diapause hypothesis, the fall peak in year *y* should be strongly correlated with the spring peak in year *y*. To compare these two competing hypotheses, we created scatter plots of the fall peak versus the spring peak with different time lags and calculated the Pearson correlation coefficient. As an additional control, we tested whether the fall peak in year y+1 was correlated with the spring peak in year y, even though this situation is not consistent with any particular hypothesis.

Results: The fall peak in year *y*-1 was strongly correlated with the spring peak in year *y* for the low and medium sites (Figure 5 in the main manuscript). In contrast, the fall peak and the spring peak in the same calendar year were not correlated (Figure S3). Similarly, the fall peak in year y+1 was not correlated with the spring peak in year y (Figure S4) and can be thought of as an additional negative control. Taken together, these correlation plots strongly provide strong evidence for the direct development hypothesis and that the tick year starts in the fall and ends the following summer. Most studies that analyse inter-annual variation in tick abundance calculate the total annual tick abundance over the calendar year. This approach is clearly wrong for our study location.

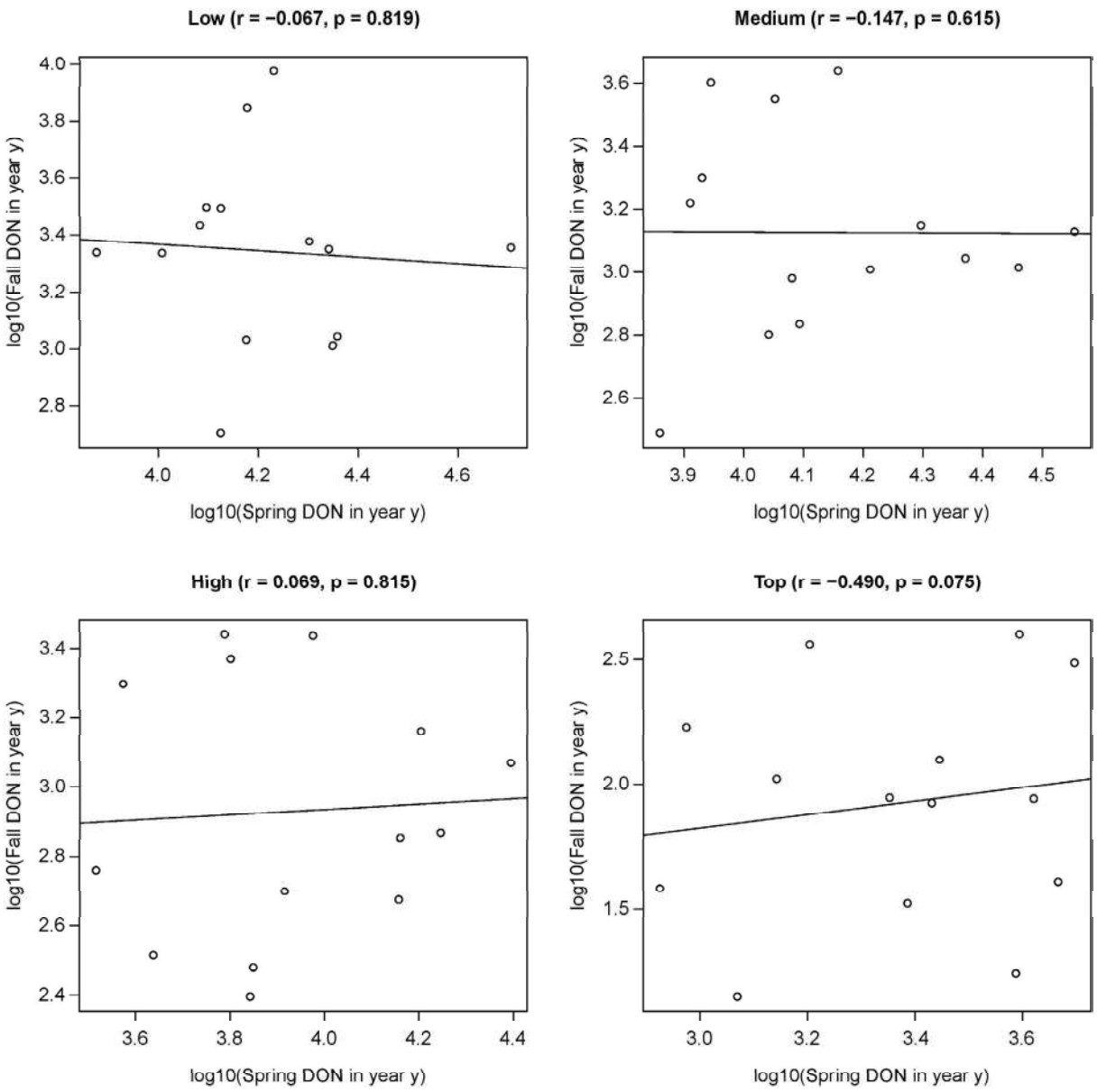

Figure S3. Correlation plot showing the relationship between the fall peak and the spring peak in the same calendar year for each of the four elevation sites. The fall peak in year *y* is not correlated with the spring peak in year *y*. The absence of significant correlations contradicts the delayed diapause hypothesis, which predicts that the fall peak in year *y* will be correlated with the spring peak in year *y*.

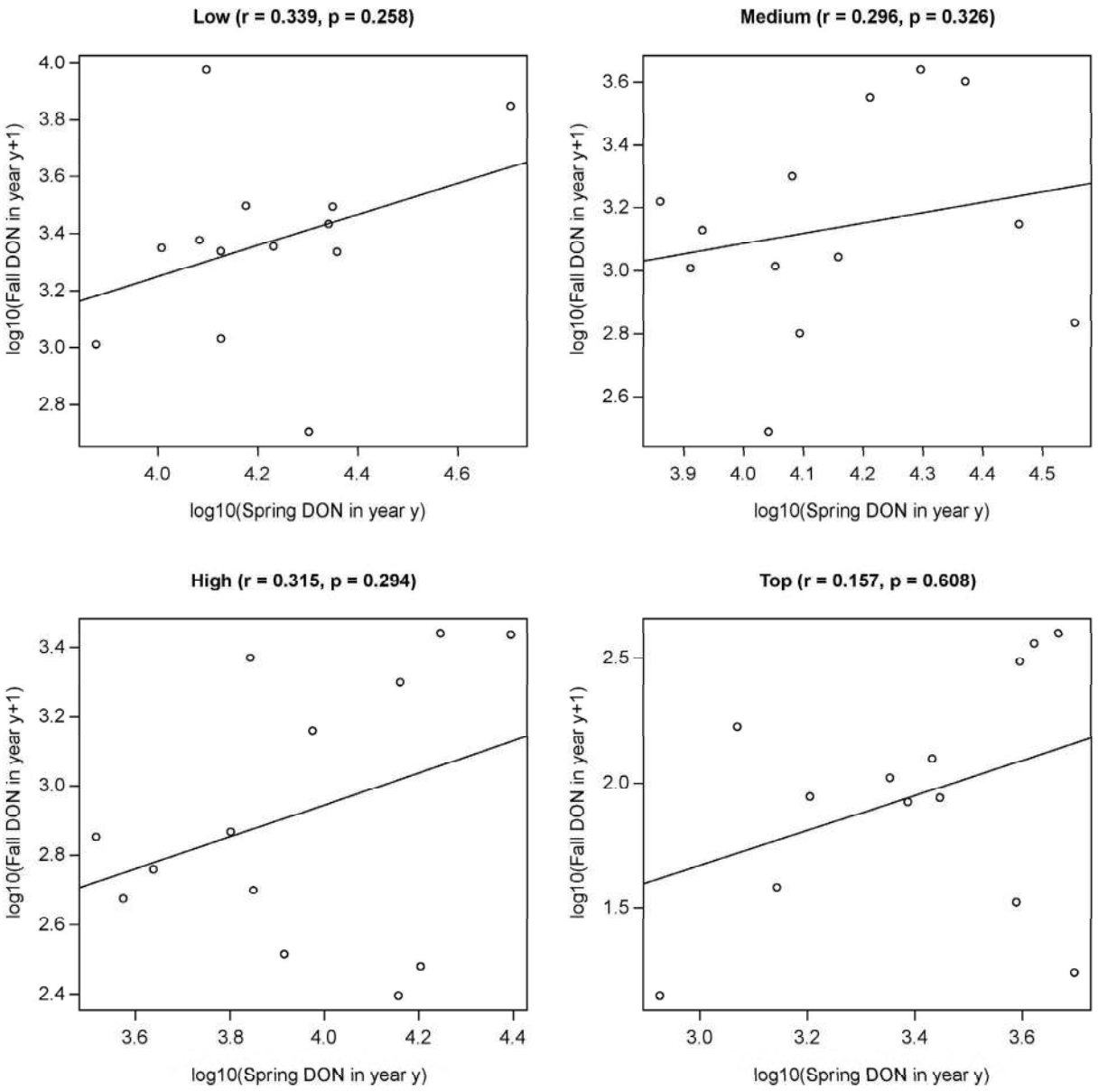

Figure S4. Correlation plot showing the relationship between the fall peak in year y+1 and the spring peak in year y for each of the four elevation sites. The fall peak in year y+1 is not correlated with the spring peak in year y. The correlation between the spring peak in year *y* and the fall peak in year *y*+1 is not predicted by any hypothesis about the diapause and phenology of *I. ricinus* nymphs. Figure S4 can be thought of as a control for Figure S3 and Figure 5 in the main manuscript.

SECTION 5 – Smoother function of calendar day predicts the bimodal phenology of *I. ricinus* nymphs at the four elevation sites.

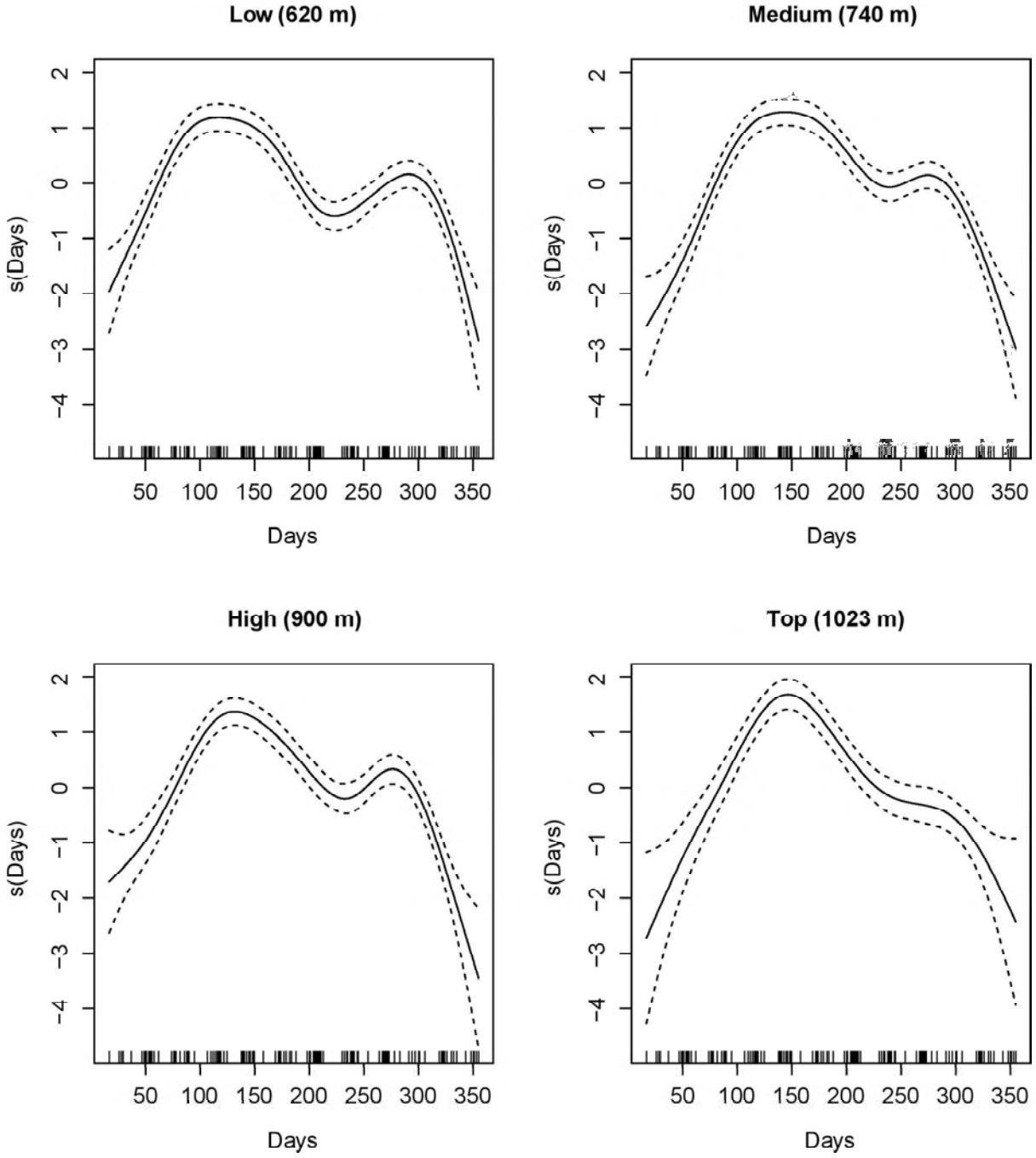

Figure S5. Visual interpretation of the smoother of the calendar day for each of the four elevation sites (partial r^2 = 32.1%). The smoother function of the calendar day recreates the bimodal phenology for the low, medium, and high elevation sites, whereas the top elevation site has a unimodal phenology.

SECTION 6 – Sequential modelling approach

To determine the best model for explaining variation in the monthly DON over the 14 years of the study (2004 to 2017) at the four elevation sites on Chaumont Mountain, we used a sequential modelling approach. We used our previous work on the same data set as starting point [1, 2]. This work had calculated the cumulative nymphal density (CND) for each calendar year (i.e., the CND values in Table 3 in the main manuscript) and found that the inter-annual variation in the CND was best explained by elevation site, year, site:year interaction, and the beech masting score 2 years prior. We therefore included these four explanatory variables in our set of starting models, as well as the previously mentioned smoother function of the calendar day to model the bimodal non-linear phenology of the DON (Figure S5). The original model set contained 23 models that were composed of different combinations of these 5 explanatory variables. We applied non-parametric smoother functions to all the explanatory variables (except site and site:year) and allowed for interactions with site. According to AIC-based model selection, the best model had an AIC score of 4422.1, 100% of the support, and an r^2 value of 76.7% (Table S2). As expected this best model (hereafter referred to as the base model 1) contained all 5 explanatory variables: site, smoothed function of year, site:year interaction, smoothed function of beech masting score, and smoothed function of calendar day. The relationship between the DON and year as well as the relationship between the DON and beech masting score both followed a linear relationship. We therefore removed the smoother functions for year and beech masting score, and all explanatory variables (except calendar day) were modelled as linear effects in base model 2. This base model 2 had an AIC score of 4482.1 and had an r^2 value of 68.3% (Table S2). The r^2 value of base model 1 (76.7%) is higher than that of base model 2 (68.3%) because non-parametric smoother functions of the explanatory variables always have better fit than the corresponding parametric functions. In summary, base model 2 confirmed our previous analyses [1, 2] and that we could model the complex bimodal non-linear phenology of the monthly DON using a smoother function of calendar day.

Using base model 2 as a starting point, we wanted to test which of the 66 climate variables explained additional variation in the DON over the 14 years of the study. As shown in Table 2 in the main manuscript, the 66 climate variables included 3 field-measured climate variables on the day of tick sampling, 15 annual means from the weather stations (5 climate variables * 3 time lags), and 48 seasonal means from the weather stations (4 climate variables * 4 seasons * 3 time lags). We compared a set of 66 models; each model included the base 2 model and one of the 66 climate variables. We applied non-parametric smoothers to each of the

66 climate variables to account for non-linear effects. According to AIC-based model selection, the best model (hereafter referred to as base model 3) had an AIC score of 4389.8, 100% of the support, and an r^2 value of 69.5% (Table S2). Base model 3 contained the base model 2 and the field-measured temperature on the day of tick sampling.

The DON had a quadratic relationship with the field-measured temperature on the day of tick sampling that did not appear to differ between the four elevation sites. In base model 4, we therefore replaced the non-parametric smoother function of the field-collected temperature with a parametric quadratic function. Base model 4 had an AIC score of 4386.8 and had an r^2 value of 67.1% (Table S2). Again, the r^2 value of base model 3 (69.5%) is higher than that of base model 4 (67.1%) because the site-specific non-parametric smoother function of the field-measured temperature always has a better fit than the site-invariant quadratic function. Using base model 4 as a starting point, we tested whether any of the 63 annual or seasonal climate variables explained additional variation in the DON over the 14 years of the study. We compared a set of 63 models; each model included base model 4 and one of the 63 annual or seasonal climate variables. We again applied non-parametric smoothers to each of these 63 climate variables to account for non-linear effects. According to AIC-based model selection, the three best models (hereafter referred to as base models 5a, 5b, and 5c) had AIC scores of 4344.1, 4347.6 and 4353.6, supports of 85.0%, 14.0%, and 1.0%, and r^2 values of 68.2%, 72.7%, and 70.7%, respectively (Table S2). Models 5a, 5b, and 5c each contained base model 4 and the annual snow fall in year *y*-1 (SN_{Y1}), mean saturation deficit of the summer in year *y* (SD_{S0}) and mean seasonal relative humidity of the summer in year *y* (RH_{S0}), respectively. We created base models 6a, 6b, and 6c, by replacing the site-specific non-parametric smoother functions in base models 5a, 5b, and 5c with an interaction between elevation site and a quadratic function of the respective climate variable (SN_{Y1}, SD_{S0}, and RH_{S0}). Base models 6a, 6b, and 6c had AIC scores of 4352.3, 4344.1 and 4355.2, supports of 2.0%, 98.0%, and 0.0%, and r^2 values of 67.7%, 71.4%, and 69.6%, respectively (Table S2). Again, the r^2 values of base models 5a, 5b, and 5c (68.2%, 72.7%, and 70.7%) were higher than that of base models 6a, 6b, and 6c (67.7%, 71.4%, and 69.6%) for the previously mentioned reasons.

In the main manuscript, base models 6b, 6a, and 6c were renamed as models 1, 2, and 3 in Table 5 in the main manuscript. We ran a final set of 13 models to determine whether these three climate variables (SN_{Y1}, SD_{S0}, and RH_{S0}) were best modelled using linear or quadratic terms (models 1, 2, and 3 in Table 5 in the main manuscript). Interestingly, there was no support for any of the annual climate variables, which had been important in our previous work on the inter-annual variation of the DON and the DIN [1, 2].

Table S2. Changes in the adjusted r^2 values for the best models during the sequential modelling approach. The explanatory variables were site (S), year (Y), site:year interaction (S:Y), calendar day, beech mast score with different time lags for spring and fall peak ($BM_{2/1}$), field-measured temperature on the day of tick sampling (t), Annual snowfall in the previous year (SN_{Y1}), mean seasonal SD of the summer in the present year (SD_{S0}), and mean seasonal RH of the summer in the present year (RH_{S0}). The explanatory variables were either modelled as non-parametric smoother functions or as parametric functions (e.g., linear effects or quadratic effects). To model the bimodal non-linear phenology of the DON, a site-specific smoother function was applied to the calendar day, s(day, by = S). Shown for each model are the explanatory variable compared between models (Var.), model identity (ID), model structure (see Table 2 in the main manuscript for the list of acronyms of the explanatory variables), and adjusted r^2 value (r^2).

Base	Type	Model structure	AIC	r^2 (%)
1	Smoother	DON ~ [a] + S + s(Y, by = S) + s($BM_{2/1}$, by = S)	4422.1	76.7
2	Parametric	DON ~ [a] + S + Y + S:Y + $BM_{2/1}$	4482.1	68.3
3	Smoother	DON ~ [b] + s(t, by = S)	4389.8	69.5
4	Parametric	DON ~ [b] + t + t^2	4386.8	67.1
5a	Smoother	DON ~ [c] + s(SN_{Y1}, by = S)	4344.1	68.3
6a	Parametric	DON ~ [c] + SN_{Y1} + SN_{Y1}^2 + S:SN_{Y1} + S: SN_{Y1}^2	4352.3	67.7
5b	Smoother	DON ~ [c] + s(SD_{S0}, by = S)	4347.6	72.7
6b	Parametric	DON ~ [c] + SD_{S0} + SD_{S0}^2 + S:SD_{S0} + S:SD_{S0}^2	4344.1	71.4
5c	Smoother	DON ~ [c] + s(RH_{S0}, by = S)	4353.6	70.7
6c	Parametric	DON ~ [c] + RH_{S0} + RH_{S0}^2 + S:RH_{S0} + S:RH_{S0}^2	4355.2	69.6

[a] All models contain the smoother function of calendar day: s(day, by = S)

[b] All models contain the following terms: s(day, by = S)+S+Y+S:Y+$BM_{2/1}$

[c] All models contain the following terms: s(day, by = S)+S+Y+S:Y+$BM_{2/1}$+t+t^2

SECTION 7 – Comparison of the beech masting variables with different time lags and the inter-annual variation in the spring and fall peaks of the DON

Methods: We created three different explanatory variables, $BM_{2/2}$, $BM_{1/1}$, and $BM_{2/1}$, for the beech masting (BM) score. $BM_{2/2}$ assumes there is a 2-year time lag between BM and the spring and fall peaks of nymphs. $BM_{1/1}$ assumes there is a 1-year time lag between BM and the spring and fall peaks of nymphs. $BM_{2/1}$ assumes there is a 2-year time lag and a 1-year time lag between BM and the spring and fall peak, respectively. $BM_{2/2}$ is consistent with the developmental diapause hypothesis, $BM_{2/1}$ is consistent with the direct development hypothesis, and $BM_{1/1}$ is not consistent with either hypothesis. To determine which of these three beech masting variables best explained the inter-annual variation in the spring and fall nymphal peaks, we re-ran the best model in the main manuscript (model 1 of Table 5 in the main manuscript), and included either $BM_{1/1}$, $BM_{2/2}$, or $BM_{2/1}$ as the explanatory variable for beech masting. As a side note, we conducted a similar comparison at the beginning of our sequential modelling approach (e.g., 639 different models), which we present in the results of this section as well.

Results: The best model had a support of 100.0%, explained 71.4% of the variation in the DON, and contained the masting explanatory variable $BM_{2/1}$ (Table S3). The two models containing $BM_{1/1}$ and $BM_{2/2}$ each had a support of 0.0%, explained 60.3% and 64.6% of the variation in the DON, and the model AIC value was 166.3 and 137.2 units higher, respectively (Table S3). When we conducted a similar analysis at the beginning of our sequential modelling approach (e.g., 639 different models), we found the same result. The best model had a support of 100.0%, explained 72.4% of the variation in the DON, and contained $BM_{2/1}$ (Table S3). The two models containing $BM_{1/1}$ and $BM_{2/2}$ each had a support of 0.0%, explained 66.6% and 76.2% of the variation in the DON, and the model AIC value was 175.0 and 84.0 units higher, respectively (Table S3). Based on these model comparisons, we are confident that the beech masting index with a 2-year time lag for the spring peak and a 1-year time lag for the fall peak best explained the inter-annual variation in the DON.

Table S3. Statistical analysis to test whether different time lags explain the inter-annual variation in the spring and fall peaks of *I. ricinus* nymphs. Model selection results are shown for the generalized additive model (GAM) with negative binomial errors of the monthly density of nymphs (DON). This analysis compared three different beech masting (BM) variables: $BM_{2/2}$, $BM_{1/1}$, and $BM_{2/1}$; the subscripts 'i/j' refer to the time lag (in years) for the spring nymphal peak and the fall nymphal peak, respectively. We compared these three BM variables on a common background model at the beginning and end of our sequential modelling approach. At the beginning, we used background model b, which contained site and the site-specific smoother function of the calendar day. At the end, we used background model a, which was the best model in the main text (model 1 in Table 5 in the main manuscript). In both analyses, the model with $BM_{2/1}$ had all of the support, whereas the models with $BM_{2/2}$ and $BM_{1/1}$ had no support. The models are ranked according to their Akaike Information Criterion (AIC). Shown for each model are the model rank (Rank), model structure (see below for explanation of explanatory variables), model degrees of freedom (Df), log-likelihood (logLik), Akaike information criterion (AIC), difference in the AIC value from the top model (ΔAIC), model weight (Weight1), cumulative weight (Weight2), and adjusted r-squared value (r^2).

Rank	Model structure	Df	logLik	AIC	ΔAIC	Weight1	Weight2	r^2
1	…[a] + $BM_{2/1}$	49	-2117.8	4344.1	0.0	100.0	100.0	71.4
2	…[a] + $BM_{2/2}$	49	-2186.4	4481.3	137.2	0.0	100.0	64.6
3	…[a] + $BM_{1/1}$	49	-2201.3	4510.4	166.3	0.0	100.0	60.3
1	…[b] + $BM_{2/1}$	47	-2204.3	4512.7	0.0	100.0	100.0	72.4
2	…[b] + $BM_{2/2}$	48	-2245.5	4596.7	84.0	0.0	100.0	76.2
3	…[b] + $BM_{1/1}$	40	-2299.6	4687.7	175.0	0.0	100.0	66.6

[a] The model structure of explanatory variables was $S+Y+S:Y+t+t^2+s(day, by = S)+SDS0+SD_{S0}^2+S:SD_{S0}+S:SD_{S0}^2$.

[b] The model structure of explanatory variables was S+s(day, by = S).

SECTION 8 – Full AIC-based model selection analysis

Methods: To identify the best model, we used a model selection approach based on the Akaike information criterion (AIC). Models were ranked according to their AIC values and the Akaike weights, which indicate the percent support, were calculated for each model. We used the Akaike weights to calculate the model-averaged parameter estimates and their 95% confidence intervals (CIs).

Results:

Full model selection table: The full model selection table for all 13 models is presented in Table S4. For the monthly DON, the best model had a support of 98.0%, and explained 71.4% of the variation in the DON. This model contained the explanatory variables of site, year, site:year interaction, beech mast score with different time lags for spring and fall peak ($BM_{2/1}$), quadratic function of the temperature on the day of tick sampling (t and t^2), quadratic function of the weather station mean seasonal SD of the summer in the present year (SD_{S0}, SD_{S0}^2, site:SD_{S0}, and site:SD_{S0}^2), and the site-specific smoother function of the calendar day (Table S4). The second-best and third-best model had 2% and 0% of the support respectively. The second-best and third-best model were identical to the top model except that it contained the annual snow fall (SN_{Y1}) in the previous year and the mean seasonal RH of the summer in the present year (RH_{S0}) instead of SD_{S0}.

Support for the individual explanatory variables: The supports for the 11 most important individual explanatory variables are shown in Table S5 and were as follows: site (100.0%), year (100.0%), site:year interaction (100.0%), beech mast score with different time lags for spring and fall peak ($BM_{2/1}$; 100.0%), temperature on the day of tick sampling (support is 100.0% for both t and t^2), smoothed function of the calendar day (100.0%), weather station mean seasonal SD of the summer in the present year (support is 97.8% – 97.9% for SD_{S0}, SD_{S0}^2, site:SD_{S0} interaction, and the site:SD_{S0}^2 interaction). None of the other explanatory variables had a support > 2.0% (Table S5).

Model-averaged parameter estimates: To determine the effect of the explanatory variables on the DON, we present the model-averaged parameter estimates on the log scale (and their 95% confidence intervals; Table S6). We also back calculated the effect sizes of the explanatory variables on the DON on the original scale with respect to the following reference conditions: the site was low elevation, the year was 2004, and the beech tree mast index ($BM_{2/1}$)

was given a value of 1. The model-averaged parameter estimates (Table S6) are virtually identical to the parameter estimates of the top model (Table 7 in the main manuscript) because the top model has 98.0% of the weight.

The interaction between elevation site and year indicated that the change in the DON over time differed between the four elevation sites (Table S6). Over the 14-year period (2004 – 2017), the DON increased at the low elevation site (slope = 0.056 per year, 95% CI = 0.029 to 0.083) and the medium elevation site (Medium – Low contrast of the slope = -0.034, 95% CI = -0.074 to 0.005), but the DON decreased at the high elevation site (High – Low contrast of the slope = -0.091, 95% CI = -0.128 to -0.053) and the top elevation site (Top – Low contrast of the slope = -0.142, 95% CI = -0.185 to -0.099). Over the 14-year period (2004 – 2017), the DON increased by 119.0% and 36.1% at the low and medium elevation sites but decreased by 38.7% and 70.0% at the high and top elevation sites, respectively.

The beech mast score with different time lags (2 years versus 1 year) for the spring and fall peak ($BM_{2/1}$) had a positive and significant effect on the DON (slope = 0.232 per class, 95% CI = 0.199 to 0.264; Table S6). Increasing the beech mast score from 1 (poor mast) to 5 (full mast) increased the DON by 152.9% at each of the four elevation sites on Chaumont Mountain.

The slope of the linear effect of the field-measured temperature (i.e., the temperature measured on the day of tick sampling) on the DON was positive and significant (slope = 9.608 per °C, 95% CI = 7.189 to 12.028; Table S6), indicating that the DON increased with temperature over the range of observed values (-5°C to 30°C). The slope of the quadratic effect of the field-measured temperature on the DON was negative and significant (slope = -8.828, 95% CI = -10.652 to -7.004; Table S6) indicating that the DON plateaued once the field-measured temperature reached ~ 30°C.

The SD_{S0} is the mean SD during the summer (1 June to 31 August) of the same year as the DON (i.e., no time lag). Thus, the SD_{S0} represents the saturation deficit during the last 3 months of the spring nymphal peak, just before the start of the fall peak. The significant interaction between elevation site and SD_{S0} indicates that the relationship between the DON and the SD_{S0} differed between the four elevation sites (Table S6). The relationship between the DON and the SD_{S0} was positive linear at the low and high elevation sites, and negative quadratic at the medium and top elevation sites. At the medium and top elevation sites, the DON decreased once the SD_{S0} reached ~ 5.5 mmHg and ~ 4.0 mmHg, respectively.

In summary, the DON had a bimodal phenology at the low, medium, and high elevation sites and a unimodal phenology at the top elevation site. The DON increased over time at the low and medium elevation sites, whereas it decreased at the high and top elevation sites. The

DON increased significantly with beech masting index and importantly, the time lag differed between the two nymphal peaks with a 2-year time lag for the spring peak and a 1-year time lag for the fall peak. This result provides strong evidence that the spring and fall nymphal peaks are distinct cohorts that were hatching as larvae in different years, which supports the direct development hypothesis and not the developmental diapause hypothesis. The DON increased with the field-measured temperature but reached a plateau at 30°C. Finally, the relationship between the DON and the seasonal SD of the summer in year y (SD_{S0}) was positive linear at the low and high elevation sites, and negative quadratic at the medium and top elevation sites.

Table S4. Full model selection results are shown for the generalized additive model (GAM) with negative binomial errors of the density of *I. ricinus* nymphs (DON) at the four elevation sites on Chaumont Mountain over 14 years (2004 to 2017). The explanatory variables were site, year, site:year interaction, day, beech mast score 2 years prior and 1 year prior for the spring and fall peak, respectively, field-measured temperature on the day of tick sampling, and 4 important weather station climate variables (see Overview of the preliminary analyses). All climate variables were coded as linear and quadratic fixed effects. A smoother function was applied to the covariate of calendar day. The models are ranked according to their Akaike Information Criterion (AIC). Shown for each model are the model rank (Rank), model structure (see below for explanation of explanatory variables), model degrees of freedom (Df), log-likelihood (logLik), Akaike information criterion (AIC), difference in the AIC value from the top model (ΔAIC), model weight (Weight1), cumulative weight (Weight2), and adjusted r-squared value (r^2).

Rank	Model structure	Df	logLik	AIC	ΔAIC	Weight 1	Weight 2	r^2
1	…[a]+SD_{S0}+SD_{S0}^2+S:SD_{S0}+S:SD_{S0}^2	49	-2117.8	4344.1	0.0	98.0	98.0	71.4
2	…[a]+SN_{Y1}+SN_{Y1}^2+S:SN_{Y1}+S:SN_{Y1}^2	49	-2122.3	4352.3	8.2	2.0	100.0	67.7
3	…[a]+RH_{S0}+RH_{S0}^2+S:RH_{S0}+S:RH_{S0}^2	49	-2123.4	4355.2	11.0	0.0	100.0	69.6
4	…[a]+SD_{S0}+S:SD_{S0}	45	-2128.8	4356.7	12.6	0.0	100.0	69.6
5	…[a]+RH_{S0}+S:RH_{S0}	45	-2130.4	4359.7	15.6	0.0	100.0	67.7
6	…[a]+SD_{S0}+SD_{S0}^2	43	-2138.7	4371.4	27.3	0.0	100.0	69.2
7	…[a]+RH_{S0}	42	-2140.8	4373.2	29.1	0.0	100.0	70.0
8	…[a]+SD_{S0}	42	-2141.0	4373.6	29.5	0.0	100.0	70.6
9	…[a]+RH_{S0}+RH_{S0}^2	43	-2140.6	4374.9	30.7	0.0	100.0	69.3
10	…[a]+SN_{Y1}+S:SN_{Y1}	44	-2142.5	4383.0	38.8	0.0	100.0	67.4
11	…[a]+SN_{Y1}	42	-2147.7	4386.4	42.3	0.0	100.0	66.8
12	…[a]	41	-2149.0	4386.8	42.6	0.0	100.0	67.1
13	…[a]+SN_{Y1}+SN_{Y1}^2	42	-2147.7	4388.8	44.7	0.0	100.0	66.7

[a] The model basic structure of explanatory variables were S+Y+S:Y+$BM_{2/1}$+t+t^2+s(day, by = S).

Table S5. The support for each of the 21 individual explanatory variables is shown for the GAMs of the DON. This support is calculated as the sum of the Akaike weights for all the models in the set that include that particular explanatory variable.

Rank	Explanatory variable of interest	Support (%)
1	Site	100.0
2	Year	100.0
3	Site:Year	100.0
4	$BM_{2/1}$	100.0
5	t	100.0
6	t^2	100.0
7	s(Day, by = Site)	100.0
8	SD_{S0}	97.9
9	SD_{S0}^2	97.8
10	$S:SD_{S0}$	97.9
11	$S:SD_{S0}^2$	97.8
12	SN_{Y1}	< 1.0
13	SN_{Y1}^2	< 1.0
14	RH_{S0}	< 1.0
15	RH_{S0}^2	< 1.0
18	$S:SN_{Y1}$	< 1.0
19	$S:SN_{Y1}^2$	< 1.0
20	$S:RH_{S0}$	< 1.0
21	$S:RH_{S0}^2$	< 1.0

Table S6. Model-averaged parameter estimates are shown for the GAMs with negative binomial errors of the DON. Shown are the parameter types, the parameter names, the parameter estimates, and the 95% confidence limits (LL = lower limit and UL = upper limit). Estimate 1 is averaged over all the models in the set. Estimate 2 is averaged over the subset of models with a cumulative support of 95%. The 95% confidence limits are for estimate 2.

Type	Name	Estimate 1	Estimate 2	95% LL	95% UL
Intercept	Low site	2.765	2.765	2.436	3.093
Contrast 1	Medium site	-0.496	-0.496	-0.878	-0.113
Contrast 2	High site	-0.149	-0.149	-0.655	0.357
Contrast 3	Top site	-1.894	-1.894	-2.674	-1.114
Slope 1	Year	0.056	0.056	0.029	0.083
Slope 2	$BM_{2/1}$	0.232	0.232	0.199	0.264
Slope 3	t	9.608	9.608	7.189	12.028
Slope 4	t^2	-8.828	-8.828	-10.652	-7.004
Slope 5	SD_{S0}	-1.890	-1.930	-7.492	3.633
Slope 6	SD_{S0}^2	2.892	2.959	-0.743	6.660
Slope 7	SN_{Y1}	-0.352	-21.692	-52.189	8.804
Slope 8	SN_{Y1}^2	-0.138	-8.525	-23.906	6.857
Slope 9	RH_{S0}	0.013	2.885	-2.853	8.622
Slope 10	RH_{S0}^2	0.015	3.785	0.247	7.322
Contrast 4	Medium site:Year	-0.034	-0.034	-0.074	0.005
Contrast 5	High site:Year	-0.091	-0.091	-0.128	-0.053
Contrast 6	Top site:Year	-0.142	-0.142	-0.185	-0.099
Contrast 7	Medium site:SD_{S0}	10.859	11.088	3.837	18.339
Contrast 8	High site:SD_{S0}	11.453	11.694	-4.210	27.598
Contrast 9	Top site:SD_{S0}	-22.966	-23.450	-43.662	-3.238
Contrast 10	Medium site:SD_{S0}^2	-14.676	-15.013	-22.600	-7.425
Contrast 11	High site:SD_{S0}^2	-10.329	-10.566	-28.823	7.692
Contrast 12	Top site:SD_{S0}^2	-18.642	-19.070	-32.112	-6.029
Contrast 13	Medium site:SN_{Y1}	0.126	7.771	-24.452	39.994
Contrast 14	High site:SN_{Y1}	0.336	20.702	-9.942	51.345
Contrast 15	Top site:SN_{Y1}	0.409	25.233	-5.712	56.177
Contrast 16	Medium site:SN_{Y1}^2	-0.127	-7.818	-25.709	10.072
Contrast 17	High site:SN_{Y1}^2	-0.102	-6.313	-22.481	9.856
Contrast 18	Top site:SN_{Y1}^2	0.143	8.785	-6.969	24.539
Contrast 19	Medium site: RH_{S0}	-0.052	-11.872	-19.761	-3.982
Contrast 20	High site: RH_{S0}	-0.066	-14.987	-26.128	-3.846
Contrast 21	Top site: RH_{S0}	0.041	9.308	-3.989	22.605
Contrast 22	Medium site:RH_{S0}^2	-0.041	-10.166	-17.398	-2.935
Contrast 23	High site:RH_{S0}^2	-0.018	-4.463	-18.465	9.539

Contrast 24	Top site:RH_{S0}^2	-0.053	-13.297	-21.843	-4.750
Contrast 25	s(Day, low 1)	0.537	0.537	-0.619	1.692
Contrast 26	s(Day, low 2)	-8.227	-8.227	-11.195	-5.258
Contrast 27	s(Day, low 3)	-2.464	-2.464	-3.258	-1.669
Contrast 28	s(Day, low 4)	4.359	4.359	2.209	6.510
Contrast 29	s(Day, low 5)	1.518	1.518	0.598	2.437
Contrast 30	s(Day, low 6)	3.358	3.358	1.449	5.266
Contrast 31	s(Day, low 7)	1.090	1.090	0.523	1.658
Contrast 32	s(Day, low 8)	12.083	12.083	7.203	16.963
Contrast 33	s(Day, low 9)	-1.737	-1.737	-3.746	0.272
Contrast 34	s(Day, medium 1)	0.093	0.093	-1.079	1.265
Contrast 35	s(Day, medium 2)	-3.908	-3.908	-6.942	-0.874
Contrast 36	s(Day, medium 3)	-1.806	-1.806	-2.597	-1.014
Contrast 37	s(Day, medium 4)	2.055	2.055	-0.122	4.231
Contrast 38	s(Day, medium 5)	0.871	0.871	-0.019	1.761
Contrast 39	s(Day, medium 6)	1.189	1.189	-0.699	3.076
Contrast 40	s(Day, medium 7)	0.417	0.417	-0.116	0.950
Contrast 41	s(Day, medium 8)	6.997	6.997	2.008	11.986
Contrast 42	s(Day, medium 9)	-1.136	-1.136	-3.195	0.923
Contrast 43	s(Day, high 1)	0.751	0.751	-0.805	2.307
Contrast 44	s(Day, high 2)	-4.324	-4.324	-8.055	-0.593
Contrast 45	s(Day, high 3)	-2.304	-2.304	-3.319	-1.289
Contrast 46	s(Day, high 4)	1.731	1.731	-0.939	4.401
Contrast 47	s(Day, high 5)	0.830	0.830	-0.284	1.945
Contrast 48	s(Day, high 6)	1.205	1.205	-1.095	3.506
Contrast 49	s(Day, high 7)	0.255	0.255	-0.384	0.893
Contrast 50	s(Day, high 8)	6.753	6.753	0.655	12.852
Contrast 51	s(Day, high 9)	-2.116	-2.116	-4.675	0.443
Contrast 52	s(Day, top 1)	-0.923	-0.923	-2.698	0.851
Contrast 53	s(Day, top 2)	-3.220	-3.220	-7.442	1.003
Contrast 54	s(Day, top 3)	-1.709	-1.709	-2.805	-0.613
Contrast 55	s(Day, top 4)	2.065	2.065	-0.828	4.957
Contrast 56	s(Day, top 5)	0.593	0.593	-0.514	1.700
Contrast 57	s(Day, top 6)	1.888	1.888	-0.483	4.259
Contrast 58	s(Day, top 7)	0.311	0.311	-0.303	0.925
Contrast 59	s(Day, top 8)	7.137	7.137	0.293	13.982
Contrast 60	s(Day, top 9)	0.138	0.138	-2.742	3.018

REFERENCES

1. Bregnard C, Rais O, Voordouw MJ. Climate and tree seed production predict the abundance of the European Lyme disease vector over a 15-year period. Parasit Vectors. 2020;13:408.
2. Bregnard C, Rais O, Voordouw MJ. Masting by beech trees predicts the risk of Lyme disease. Parasit Vectors. 2021;14:168.

ADDITIONAL FILE – Chapter 4

Experimental infections of mice and birds with Borrelia afzelii and Borrelia garinii

Authors: Cindy Bregnard[1*], Olivier Rais[2], Anouk Sarr[3], Kees van Oers[4], Peter Kraiczy[5], Ryan Rego[7], and Maarten J. Voordouw[1, 7]

BSK medium H

Cultures were maintained in 2X BSK-H medium (Bio&Sell, #BS 2.12OL.500) supplemented with warmed 200 ml of 7% gelatin (DIFCO 0143-17-9) and 6% of rabbit serum (Bio&Sell, #RAB.SE.0100) that has been decomplemented for 1 hour at 56°C. In addition, 0.023% L-Cysteine hydrochloride monohydrate (Sigma, # C-7880), 0.015% DL-Dithiothreitol (Sigma, #D-0632), 1µg L-Glutamine (GIBCO), 50 µg Rifampicin (Sigma, #R-3501), 25 µg Phosphomycin disodium salt (Sigma, #P-5396), and 2,5 µg Amphotericin B (GIBCO, #15290-026) were added per ml of solution. The medium was adjusted to pH 7.6 with NaOH 1N before being filtrated through VacuCap® 90 Filter 0.2 µm (Pall Corporation, #4622) into sterilized bottles which were stored in a fridge up to 2 months.

Table S1. Experimental design of the infection procedure.

Block	Host	Species	Strain
1	Mouse 1	*B. afzelii*	NE1827
1	Mouse 2	*B. afzelii*	NE1857
1	Mouse 3	*B. afzelii*	NE4556
1	Mouse 4	*B. afzelii*	NE4558
1	Mouse 5	*B. afzelii*	NE4779
1	Mouse 6	*B. afzelii*	NE4832
1	Mouse 7	*B. afzelii*	NE4049
1	Mouse 8	*B. afzelii*	S9 (FIN-A3)
1	Mouse 9	*B. afzelii*	NE4049
1	Mouse 10	*B. afzelii*	NE1857
1	Mouse 11	BSK medium H	BSK medium H
1	Canary 1	*B. afzelii*	NE1827
1	Canary 2	*B. afzelii*	NE1857
1	Canary 3	*B. afzelii*	NE4556
1	Canary 4	*B. afzelii*	NE4558
1	Canary 5	*B. afzelii*	NE4779
1	Canary 6	*B. afzelii*	NE4832
1	Canary 7	*B. afzelii*	NE4049
1	Canary 8	*B. afzelii*	S9 (FIN-A3)
1	Canary 9	*B. afzelii*	NE4049
1	Canary 10	*B. afzelii*	NE1857
1	Canary 11	BSK medium H	BSK medium H
2	Mouse 12	*B. garinii*	NE5308
2	Mouse 13	*B. garinii*	NE1883
2	Mouse 14	*B. garinii*	NE5158
2	Mouse 15	*B. garinii*	NE4907
2	Mouse 16	*B. garinii*	NE4891
2	Mouse 17	BSK medium H	BSK medium H
2	Mouse 18	*B. garinii*	NE1845
2	Mouse 19	*B. garinii*	NE1879
2	Mouse 20	*B. garinii*	NE4554
2	Mouse 21	*B. garinii*	NE5245
2	Mouse 22	*B. garinii*	NE5135
2	Canary 12	*B. garinii*	NE4907
2	Canary 13	*B. garinii*	NE5158
2	Canary 14	*B. garinii*	NE4891
2	Canary 15	*B. garinii*	NE1883
2	Canary 16	*B. garinii*	NE1879
2	Canary 17	*B. garinii*	NE4554
2	Canary 18	*B. garinii*	NE5245
2	Canary 19	*B. garinii*	NE1845
2	Canary 20	*B. garinii*	NE5135
2	Canary 21	*B. garinii*	NE5308
2	Canary 22	BSK medium H	BSK medium H

2	Great tit 1	*B. garinii*	NE5135
2	Great tit 2	*B. garinii*	NE4891
2	Great tit 3	*B. garinii*	NE1883
2	Great tit 4	*B. garinii*	NE5158
2	Great tit 5	*B. garinii*	NE1845
2	Great tit 6	*B. garinii*	NE5308
2	Great tit 7	*B. garinii*	NE4554
2	Great tit 8	*B. garinii*	NE4907